MICROMECHANISMS OF POLYMER SLIDING WEAR

A THESIS
SUBMITTED TO THE DEPARTMENT
OF MATERIALS ENGINEERING
AND THE FACULTY OF ENGINEERING
OF THE UNIVERSITY OF CAPE TOWN
IN FULFILLMENT OF THE REQUIREMENTS
FOR THE DEGREE OF DOCTOR OF PHILOSOPHY

By

KASHIF MARCUS

December 1992

ABSTRACT

A study has been made concerning the tribological behaviour of ultrahigh molecular weight polyethylene (UHMWPE) during water-lubricated reciprocating sliding wear. The experimental work has been extended to study also the effect of molecular weight, fillers, lubrication, counterface roughness and sliding configuration on the polymer's transfer characteristics. The wear behaviour of polytetrafluoroethylene (PTFE) has been included for comparative studies. The worn material was studied using stylus profilometry, optical microscopy, scanning electron microscopy (SEM), energy dispersive x-ray spectroscopy (EDS), Transmission electron microscopy (TEM), X-ray fluorescence (XRF), X-ray diffraction (XRD), differential scanning calorimetry (DSC), infrared spectroscopy (IR) and mass spectrometry.

The effect of two fillers, namely glass beads and a titanium-based inorganic filler on the friction and wear behaviour of UHMWPE has been investigated as a function of counterface roughness (R_a). It was found that the filled material exhibited lower wear rates than the unfilled material on the rougher counterface. The filled material was also found to be more sensitive to a change in R_a and showed higher wear rates than the unfilled polymer on the smooth counterface. A uniform and coherent transfer film is found on the rougher counterface but the transfer film for the titanium-based filler was patchy on the smooth counterface. No coherent transfer film was found when sliding was conducted parallel to the grinding direction on the steel counterface, resulting in relatively high wear rates. Polymer transfer was patchy, the amount increasing as the sliding distance increased. The observed phenomena are explained in terms of mechanical interlocking and chemical bonding of the polymeric material with the metal counterface.

An increase in molecular weight did not significantly improve the wear resistance of the UHMWPE. Small variations in counterface roughness values (R_a) were found to have a much greater effect on the wear rates than changes in molecular weight. The steady-state wear rate of the polymer was furthermore found to be more dependent on an adherent transfer film rather than a change in bulk morphology.

Although PTFE exhibited low friction coefficients, the high wear rates obtained by this polymer is explained by the polymer's inability to form a transfer film under water lubrication, while any film that forms under dry sliding wear is easily peeled off the surface. Significant improvements in wear are found when fillers are added to the polymer. The wear rates for PTFE under dry sliding are similar to those obtained for UHMWPE under water lubrication.

Transfer of UHMWPE material to the metal counterface during sliding wear involves interlamellar shear of the polymer and results in the development of a highly oriented transfer film. Significant differences have been found in the degree of crystallinity, crystallite size and orientation in the deformed surface layers of the polymer and debris compared with those of the bulk polymer. The worn surface of the polymer shows slightly increased crystallinity but the crystallinity of the debris is much higher than that of the bulk whilst the crystallite size is much reduced.

ACKNOWLEDGEMENTS

I would like to express my sincere appreciation to the following people who assisted me during this research project:

Professor Colin Allen, my supervisor, whose tireless dedication, encouragement and guidance helped to make this project a rewarding experience.

Professor Anthony Ball for advice and support.

Mr. Nicholas Dreze, Mr. Glen Newins and Mr. Dave Dean for their help in maintaining the test apparatus and preparing the test specimens.

Mr. Bernard Greeves and Mr. James Petersen for their photographic assistance.

Miss Feroza Mohammed, at Plastamid, for her help with the DSC scans.

Miss Nadia Isaacs for her patience in typing a large portion of this manuscript, and also Miss Tasneem Emeran for her able assistance.

My colleagues and the secretarial staff of the Department of Materials Engineering at the University of Cape Town for their assistance during the duration of this project.

The work described in this thesis was performed under a collaborative agreement between the Chamber of Mines Research Organization of South Africa (COMRO) and the University of Cape Town and formed part of the research programme of COMRO. I would also like to thank COMRO and the Foundation for Research and Development (FRD) for their financial support as well as Plastamid (Pty) Ltd. for the use of their equipment.

This thesis is dedicated to those striving for peace in South Africa and elsewhere and to those who believe that education is a right and not a privilege.

GLOSSARY OF TERMS

HDPE	High density polyethylene
LDPE	Low density polyethylene
VHMWPE	Very high molecular weight polyethylene
UHMWPE	Ultra-high molecular weight polyethylene
PTFE	Polytetrafluroethylene
POM	Polyoxymethylene
PMMA	Polymethylmethacrylate
PVC	Polyvinylchloride
PETP	Poly(ethylene)terepththalate
PCTFE	Polychlorotrifluoroethylene
PA6	Polyamide 6
P(A-I)/GR	Polyamide imide + 12%graphite & 3% PTFE
HCBD	Hexachlorobutadiene
KSCN	Potassium thiocyanate

μm	micrometer
nm	nanometer
pm	picometer

A_r	real area of contact
A_o	apparent area of contact
a	contact radius
CED	cohesive energy density
DSC	Differential Scanning Calorimetry
EDX	Energy Dispersive X-Ray Spectrometry
E	Young's modulus
ΔE_v	molar energy of vaporization
F	Frictional force
f_d	dynamic frictional force
f_s	static frictional force
f	frequency
H	hardness

ΔH_f	heat of fusion
ΔH_v	molar heat of vaporization
K_o	Specific wear rate
LVDT	Linear variable differential transducer
Mn	number average molecular weight
Mw	weight average molecular weight
P_o	yield pressure
P_m	mean contact pressure
Q	activation energy
R	universal gas constant
R_{av}	average radius of asperity curvature
R_a	centre-line-average surface roughness
S	breaking strength
SEM	Scanning electron microscopy
T	temperature
T_f	flow temperature
T_g	glass transition temperature
TEM	Transmission electron microscopy
V	volume
V_l	molar volume
v	velocity
W	load
XRD	X-ray diffraction
Y	yield stress
σ	mean deviation of asperity heights
β	asperity tip radius
ψ	plasticity index
ν	Poisson's ratio
τ	shear strength
μ	friction coefficient
ϵ	elongation to break
η	viscosity
ξ	solubility parameter
θ	angle
θ	temperature

CONTENTS

CHAPTER 1

INTRODUCTION

1.1 Chamber of Mines Research Overview

The unique and particularly harsh conditions under which South Africa's gold mining operations are being conducted has, as Wagner and Joughin pointed out, *"led to mining operations being conducted at the limits of existing knowledge and technology."* [1]

This situation has necessitated a collaborative programme of work between the mining industry and the Chamber of Mines Research Organization (COMRO), aimed at improving the technology and hence the overall efficiency of the mining industry.

Part of the research and development work has led to improved forms of mechanization for powering mining equipment. One such advance has been the replacement of electro-hydraulic pump systems for powering equipment such as hand operated rockdrills and impact hammers, by hydro-power. The simplicity, feasibility and economic viability of hydro-power has been shown with the successful operation of a pilot system at the Kloof gold mine [2].

In the hydro-power system, vast quantities of water are chilled on the surface in refrigeration plants and transported through insulated pipes to the working areas. The potential energy in the water column is manifested as hydrostatic pressure which is exploited to power stoping equipment directly and economically as well as assisting in cooling the working areas.

In figure 1.1, the typical water requirements for cooling and machine powering a working stope or face 35 m long is shown. It is seen that 1500 m below the surface, surplus power is available to drive additional types of equipment such as fans, scraper winches and mining machinery [2].

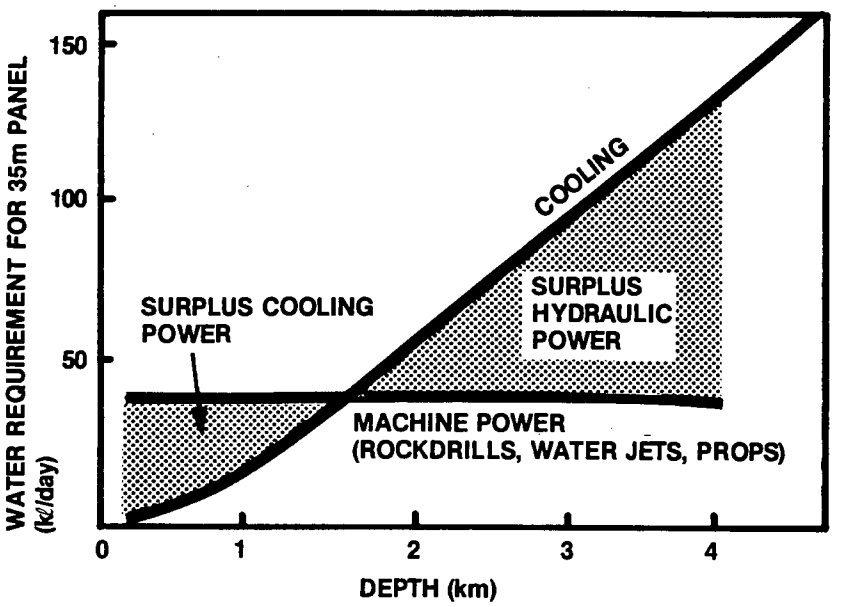

Figure 1.1: A graph showing the typical water requirements for both cooling and machine powering for one working stope 35 m long. [After ref. 2].

The hydro-power concept requires that water be recycled continuously to maintain the system. This recycling leads to contamination of the water through chloride- and nitrate salt pick-up, so that the mine water is particularly corrosive and has poor lubricating properties.

The implementation of water-powered machines has led to the identification, development and improvement of various engineering materials for use in these machines. The tribological behaviour of these materials forms a major part of this research programme.

An important part of the overall research programme has been to investigate the feasibility of using a range of tough, modern engineering polymeric materials in sliding wear applications. One such polymer, ultra-high molecular weight polyethylene (UHMWPE) has replaced the metal bearing sleeve in a hydraulic hammer because of the advantages of weight reduction, high mass production, corrosion and wear resistance. The excellent properties of UHMWPE have been its fortè as a high performance engineering material in the robust conditions of the mining and metallurgical industries. In this respect, UHMWPE has emerged as the best *"all-round"* material where low stress sliding wear applications are concerned such as experienced in rockdrills where hardened stainless steel reciprocates against polymer seals [3].

1.2 Aims of this Research Project

Although previous work has provided some information on UHMWPE under different operating variables, the mechanism by which this polymer wears against a metallic counterface is not very well understood [4]. The present work is thus an attempt to provide a further understanding of the polymer's transfer and excellent wear characteristics under water-lubricated reciprocating sliding wear.

The specific aims of the project were:

(i) to investigate the sliding wear behaviour of UHMWPE against stainless steel under simulated in-service testing conditions.

(ii) to use analytical and physical techniques to probe the atomic/molecular level of the interfacial layers to determine the structural transformations taking place and to correlate the polymer's frictional properties with its macro- and microstructure.

(iii) to determine the wear mechanisms responsible for the degradation of UHMWPE sliding components in mining equipment and how changing wear modes can be related to changing wear rates.

(iv) to investigate the influence of polymer morphology, molecular weight and fillers on the transfer and wear processes.

(v) to investigate the influence of counterface roughness, R_a and water-lubrication on the wear behaviour of UHMWPE.

(vi) to compare the tribology of UHMWPE with that of other commonly used bearing materials under similar operating conditions.

CHAPTER 2

LITERATURE REVIEW

THE MOLECULAR MORPHOLOGY OF SEMICRYSTALLINE POLYMERS

2.1 INTRODUCTION

Polymers are partially crystalline and are sometimes referred to as semicrystalline or just crystalline, the two terms being used interchangeably. It is well known that the physical, mechanical and chemical properties of crystalline polymers depend on the morphology of the crystals as well as the degree of crystallinity of the sample [5]. Many properties such as modulus, strength, elongation to break, impact strength, conductivity, solubility, and hardness are influenced by the degree of crystallinity [6,7].

In view of these factors, the molecular morphology of the polymer must therefore be considered if large scale irreversible processes are to take place during a deformation process, such as those occurring at the interface of polymer component sliding or rubbing against a metal counterface.

2.2 THE MOLECULAR ARRANGEMENT IN CRYSTALLITES

Physical investigations of the structure of polymeric solids by x-ray diffraction have revealed the presence of micro- heterogeneities. The discrete maxima observed arise from the scattering by small regions of three-dimensional order. These regions are called crystallites, and are separated from each other by material which gives an x-ray pattern of diffuse haloes or diffuse scattering typical of an amorphous material [8,9]. These crystallites are formed in the melt by a crystallization process similar to that depicted in figure 2.1. The sizes of these crystallites are small relative to the length of a fully extended polymer chain, but are found to be independent of molar mass, and their size rarely exceeds 100 nm.

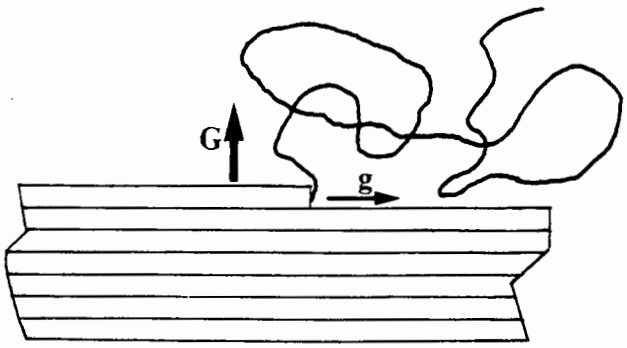

Figure 2.1: A Schematic representation of a lamellar crystallite in the process of growth on a face (*e.g.* 100 or 110) transverse to the chain axis. For an orthorhombic crystal such as polyethylene, the chain axes are normal to the diagram. Growth rates along the edge and normal to it are indicated by g and G, respectively. [After ref. 5].

Flory *et al.* have described the crystallization of a highly viscous and completely amorphous polymer chain from the molten state [5]. A point is reached where the section of the chain growing into a crystallite becomes strained as the rest of the molecule becomes tightly entangled. To incorporate more segments of the chain into the crystallite would require work to be done against the stress and a stage is quickly reached at which this work is equal to the decrease in free energy which would result from further crystallization. The crystallization process is thus inhibited by the work that would be required to be done against this stress. Widely separated sections of the same chain may become involved in the simultaneous development of two different crystallites. As a result each crystallite is surrounded by an amorphous band of polymer [5,8,9].

2.3 THE UNIT CELL

The basic molecular architecture or structure of a polymer may be described by the size and shape of its unit cell.

2.3.1 Polyethylene

The atomic arrangement within the unit cell for polyethylene has been obtained with some difficulty [10]. Polyethylene molecules crystallizing from the molten state assume their

lowest Gibbs free energy conformation state, a planar zig-zag arrangement along the single bonded carbon backbone as shown in figure 2.2 [7,8].

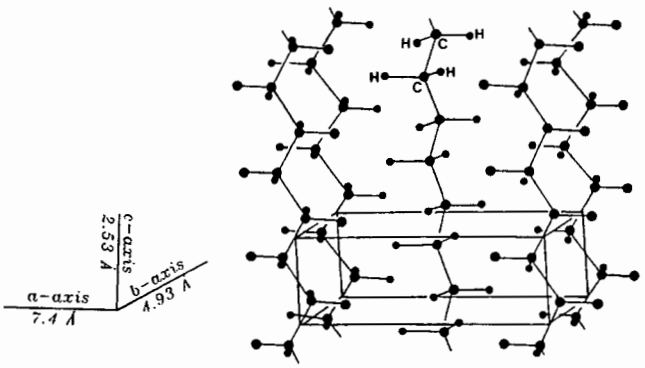

Figure 2.2a: A model of the packing in the crystal structure of polyethylene. The dimensions of the orthorhombic unit cell are shown. [After ref. 8].

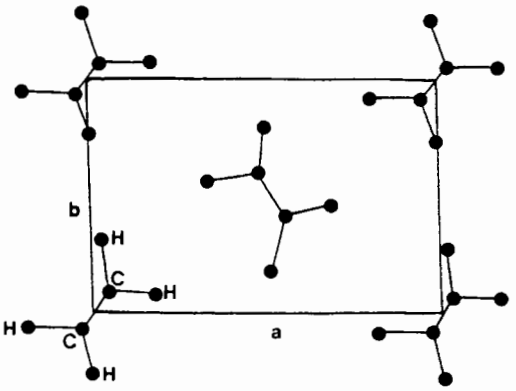

Figure 2.2b: A c-axis projection of the polyethylene unit cell. [After ref. 8].

The orthorhombic unit cell can be described by lattice vectors *a*, *b* and *c*. The *a* and *b* vectors characterize the side-by-side packing of the molecules, while the *c* vector is normal to these and parallel to the molecular axis. The length of the c-axis is determined by the crystallographic repeat unit. The diameter of the hydrogen atom (≈ 239 pm) is only slightly smaller than the |C| component and therefore the C-C backbone would have to be rotated if the hydrogen atoms are replaced by larger atoms as in helically twisted polytetrafluoroethylene (PTFE) [7,8].

2.3.2 Polytetrafluoroethylene

The van der Waals radius of 1.4 Å for the fluorine atom would cause overcrowding of the planar zig-zag conformation, hence the chains have to be twisted through 14° at each carbon atom in order to make room for the fluorine atoms [8,11]. This produces a molecular conformation, in the PTFE crystal, of a helix with a 180° twist and a repeat distance of 16.8 Å every 13 CF_2 units. The helical molecules then pack laterally to form the crystal [7,8]. The conformation of the PTFE molecule is shown in figure 2.3a. X-ray diffraction studies have shown that the PTFE unit cell is triclinic up to 20 °C. Above 20 °C

a slight untwisting of the spiral occurs and the molecular packing becomes hexagonal. The molecular conformation changes to a 15 CF_2 unit helix with a repeat distance of 19.5 Å [7]. Transmission electron micrographs indicate that PTFE has a banded structure due to 200 Å thick crystalline slices separated by thin amorphous regions, as shown in figure 2.3b [12]. The structure of PTFE is thus in marked contrast to the spherulitic structure of other crystalline polymers.

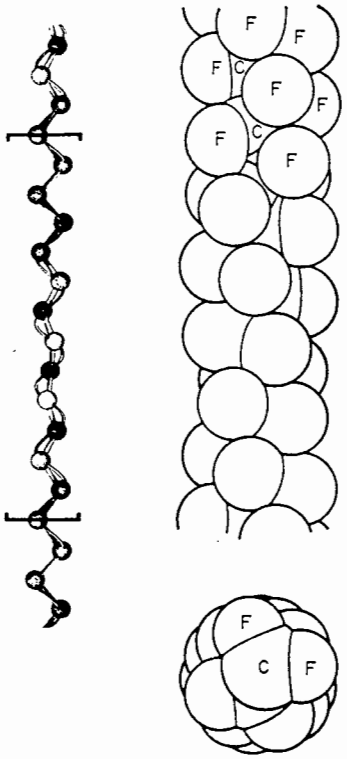

Figure 2.3a: The helical conformation of molecular chains in PTFE, showing both the side and end view. [After refs. 8 and 11].

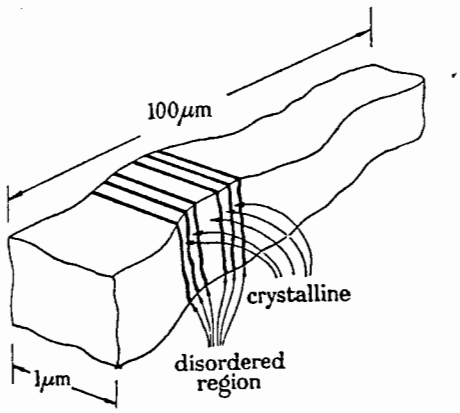

Figure 2.3b: The banded structure of PTFE. See also figure 3.51. [After ref. 12].

2.4 POLYMER SINGLE CRYSTALS

The most detailed information on polymer structure can be obtained from the study of single crystals. Single crystals of polymers have been obtained by crystallization from very dilute solutions. Their study is of great practical importance, since they may explain crystallization processes in molten polymer. The individual polymer molecules are not entangled and crystallize in a lozenge or diamond-shaped single crystal [8,13]. Figure 2.4 shows the fold packing in a single crystal of polyethylene. Electron diffraction patterns of

these crystals indicate that the polymer chains are oriented perpendicular to the flat faces of the single crystal. It is evident that, since the average length of the polyethylene molecule is several thousand Ångströms, the chains must fold back into the crystal many times [14,15]. In figure 2.4, the faces of these crystals are the (110) planes and the long- and short diagonals of these lozenges coincide with the *a* and *b* crystallographic axes respectively [8].

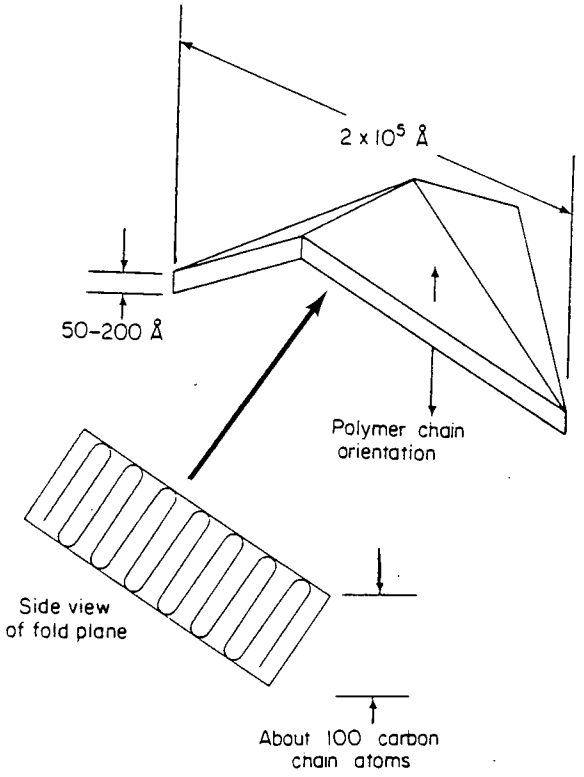

Figure 2.4a: Fold packing in a polyethylene single crystal. This single crystal may contain many individual molecules. The chain folding of a single polymer molecule within a fold plane is also shown. [Adapted from ref. 15].

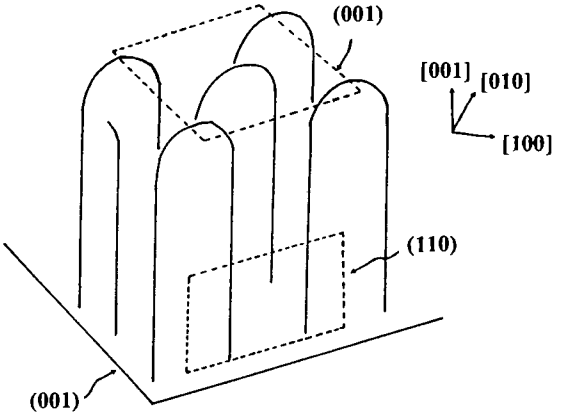

Figure 2.4b: A schematic showing the crystallographic planes and axes directions of the polyethylene crystal. [After ref. 13].

Although the atomic positions in the unit cell of these crystallites are known with good precision, much less is known about the sizes and distribution of crystallites in bulk polymer. Electron microscopy and x-ray diffraction techniques have shown, however, that even in bulk crystallized polymer, similar structures are present. Radiating lamellae of the order 50-150 Å thick are found, wherein the molecular orientations are perpendicular to their planes [8,14]. The extent to which entangled polymer chains from the bulk are able to form and orient themselves therefore needs further clarification.

2.5 THE POLYMER MORPHOLOGY CRYSTALLIZED FROM THE MELT

The predominant morphology of polyethylene and many other crystalline polymers, as observed through a polarizing microscope, is spherulitic in nature. This melt crystallized polymer forms chain-folded lamellae, similar to those grown from dilute solution. The structure of a typical spherulite is shown in figure 2.5.

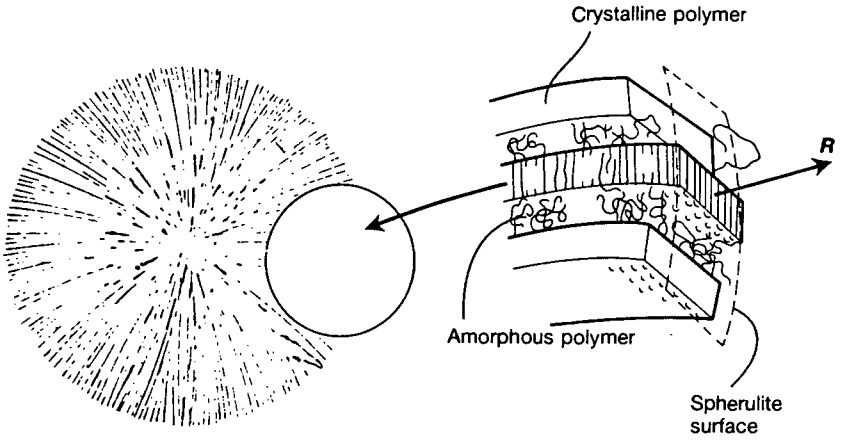

Figure 2.5: A typical spherulite, grown from the melt, showing a magnified view of the chain-folded lamellae. The direction of the spherulite radius, **R** or *b*-axis is shown, with the *a* and *c*-axes being perpendicular to the *b*-axis. [After ref. 7].

The spherulite is a polyhedral entity of helically twisted lamellae that radiate from a common centre of nucleation, leaving amorphous material trapped between their fold surfaces and also between the spherulites themselves. In polyethylene, accretion of polymer occurs on the (010) plane [7]. The unit cell is orthorhombic, the *b*-axis is the radial growth axis, while the *a* and *c*-axes are normal to the spherulite radius. When thin films of polyethylene are examined under the optical microscope, characteristic Maltese cross patterns are observed. These birefringent effects are associated with the molecular orientation resulting from the characteristic lamellar morphology. The number, size and fine structure of the spherulite depend on the temperature of crystallization. Spherulitic growth is limited by interference from neighbouring growing spherulites, so that crystallization at a high temperature, when there are relatively few initiating nuclei, produces large spherulites. Crystallization at a low temperature produces a very large number of small spherulites [8].

2.6 POLYMER CONCEPTS

2.6.1 Crystallinity and Factors Affecting Crystallinity

The crystallization of polymers into an ordered array and the formation of a crystalline lattice requires the long chain molecules of the polymer to pack neatly together. To achieve this, uniformity of the molecules is essential. Thus the intermolecular bond strength and the stereoregularity of side groups along the backbone affect the crystallization behaviour [6,9,16].

2.6.1.1 Intermolecular bond strength

For crystals to exist at a given temperature, the intermolecular forces must be sufficient to overcome the disordering tendency of thermal vibrations. In polyethylene crystallites, the close packing achieved by the chains allows the van der Waals forces to act co-operatively and provide additional stability to the crystallites [6,9].

2.6.1.2 Chain symmetry

In order for crystallites to form, the polymer molecules must have a regular, ordered structure. The presence of random short-chain branching in some polymers correlates with lower crystallinity. In low density polyethylene (LDPE) they are fairly numerous (15 to 25 branches per 1000 carbon atoms), whereas in high density polyethylene (HDPE) they are less frequent (0.5 branches per 1000 carbon atoms). HDPE molecules therefore align to a higher degree than LDPE molecules and exhibit a higher density (a measure of crystallinity) as shown in figure 2.6 [6,17].

The polyethylenes have a broad or narrow range of molecular sizes and the molecules contain few or many branch points, according to the method of polymerization. Large, bulky atoms or side groups can also interfere with the alignment process. Atactic polymers, which have an irregular spatial structure along the molecular chain, are generally unable to crystallize. In contrast, isotactic and syndiotactic structures, having a stereoregular arrangement of side groups, are generally able to form a crystalline lattice since the molecular uniformity makes close packing and accommodation of side groups possible

[6,16].

	LLDPE	HDPE	UHMWPE
Density (g/cm^3)	< 0.94	> 0.94	0.94
Melting point (°C)	123	135	137
Tensile strength (MPa)	4.1–15.9	21.4–37.9	44
Tensile modulus (MPa)	96.5–262	414–1250	232
Elongation to break (%)	90–800	20–1300	> 350
Hardness (Shore D)	41–50	60–70	66
No. of branches per 1000 C atoms	15–25	0.5	0
Molecular structure			

Figure 2.6: Typical properties and molecular structure of the polyethylenes. [Adapted from refs. 6, 17 and 18].

2.6.2 Density and Molecular Weight

The most important magnitudes which delineate the characteristic properties of polymers and especially a linear polymer such as polyethylene, are density and molecular weight. Many mechanical properties such as yield stress and stiffness depend particularly on the density value, while the length of the polymer molecules has a profound influence on properties such as toughness and wear resistance [6,18].

As the homologous series in the paraffinic structure is ascended, the properties that might be attributed to intermolecular forces of attraction should increase. The influence of chain length on properties such as modulus, tensile- and impact strength, glass-transition temperature and resistance to creep, for a given repeating unit is illustrated in figure 2.7. Initially, there is a large change in the property with increasing degree of polymerization until a critical stage is reached, at which the relative change in the property decreases substantially [6,14]. Eventually, even with linear polymers, the molecular weight becomes so high that the polymers cannot be dissolved, worked mechanically or be made to flow in

the molten state. This intractability usually sets in at a molecular weight above 10^7 g.mol^{-1} [14].

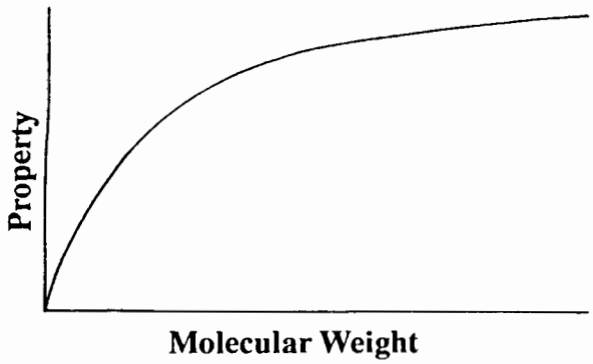

Figure 2.7: The variation in mechanical properties with degree of polymerization. [After ref. 6].

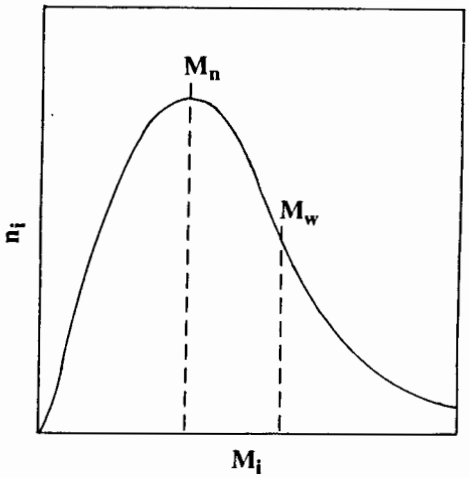

Figure 2.8: Typical distribution of molar masses for a synthetic polymer, where n_i is the number of molecules with molecular weight M_i. [After ref. 9].

The molecular weight is not a uniformly defined magnitude but an average value since individual polymer molecules generally possess different chain lengths *i.e.* a distribution of molecular lengths always occurs in bulk polymers [14,18]. A typical distribution of molar mass is shown in figure 2.8. A colligative method, such as osmotic pressure, effectively counts the number of molecules present and provides a number average molar mass M_n defined by: [6,9].

$$M_n = \sum_{i=1}^{n} n_i M_i / \sum_{i=1}^{n} n_i$$

where n_i is the number of molecules with molecular weight M_i. From light scattering measurements, a method depending on the size rather than the number of molecules, a weight average molar mass, M_w is obtained.

This is defined as:

$$M_w = \sum_{i=1}^{n} n_i M_i^2 / \sum_{i=1}^{n} n_i$$

For most bulk properties, M_w is a more informative average than M_n. The ratio M_w/M_n is

called the polydispersity index. The greater this ratio, the greater is the dispersity of the chain lengths [6]. The properties of a polymer sample are strongly dependent on the way in which the molecular weights of the individual molecules are distributed about the average [6,8].

2.6.3 The Cohesive Energy Density

An important property of ordinary liquids, is a measure of the strength of the secondary bonds, which is given by the cohesive energy density (CED) [14,15]. This quantity is determined from the properties of liquids through the relationship:

$$CED = \Delta E_v/V_l = (\Delta H_v\text{-}RT)/V_l$$

where ΔE_v is the molar energy of vaporization,
V_l is the molar volume of the liquid,
ΔH_v is the molar heat of vaporization, and
RT is the perfect gas volume of the molar work of expansion during vaporization [19].

The cohesive energy of polymers may be defined as the energy required to overcome all intermolecular contacts within one mole of material. The CED of a polymer can be estimated by determining the equilibrium swelling of a slightly cross-linked analogue in various solvents, the swelling being a maximum in solvents of the same CED.

The solubility parameter, ξ, is defined as the square root of the cohesive energy density,

$$\xi = (\Delta E_v/v_l)^{0.5}$$

Generally, the smaller the difference between the solubility parameter of two substances, the greater is their mutual solubility.

2.6.4 The Glass-Transition Temperature

For polymers in the molten state, the molecular chains are in relatively rapid motion, but as the temperature is lowered, the movement becomes progressively slower until eventually the available thermal energy is insufficient to overcome the rotational energy barriers in the chain. Within this region, the polymer will change from a soft, rubbery and flexible material to a hard, glass-like and inflexible material. This drastic transition in mechanical properties is referred to as the glass-transition and the temperature at which it occurs is called the glass-transition temperature, T_g [9,14]. The glass-transition temperature, therefore, has an important bearing on the potential application of the polymer. As the T_g depends largely on the amount of thermal energy required to keep the polymer chain moving, a number of factors which affect rotation about chain links will also influence T_g. These include: [9].

(i) Chain flexibility
(ii) Molecular structure (steric effects)
(iii) Molar mass, and
(iv) Branching and crystallinity

Generally, therefore, the glass-transition temperature tends to be lower for a polymer consisting of inherently flexible molecules than for those consisting of inherently stiff molecules [6].

2.6.5 Thermal Properties

The thermal conductivities of polymers are very low, of the order of one-hundredth that of steel, and the dissipation of frictional heat is therefore very poor [20]. For polymers, the low thermal conductivity of about 0.2 $W.m^{-1}.K^{-1}$ will give rise to large temperature gradients in the material and may cause a reduction in mechanical properties such as strength and stiffness or even degradation of the polymer. Heat conduction in polymers is affected by a number of variables, including the degree of crystallinity, molecular weight and the presence of fillers [6]. Another property which must be considered in the design of polymeric components when used in contact with other materials, is the coefficient of thermal expansion. Thermal expansion coefficients are relatively high, typically ten times that of steel, and this may introduce large dimensional changes in the polymer when

working temperatures are high [6,21].

2.6.6 Molecular Orientation

When a bulk polymer is crystallized in the absence of external forces, there is no preferred orientation of crystallites or molecules. When a linear polymer is subjected to mechanical deformation by means of cold work such as drawing, stretching or rolling or subjected to a wear process above the glass-transition temperature, the crystallites and molecular chains usually tend to align themselves parallel to the direction of deformation. If a polymer is highly crystalline, drawing will not affect the degree of crystallinity, but if the sample is of low crystallinity, the crystallinity is likely to increase during the process of cold drawing. Preferred orientation of linear polymers has great practical consequences, which arise from the fact that the primary bonds within the molecular chains are much stronger than the interchain forces. Preferential orientation of the chains parallel to the direction of the external stress can result in a great improvement in unidirectional mechanical properties [11,14,22].

Although a great deal of work has been published on both experimental and theoretical aspects of deformation mechanisms in crystalline polymers, the detailed morphological and crystallographic changes taking place during orientation remains unsolved [14,22-25]. A range of dimensional levels may be involved in the deformation of crystalline polymers. It is presumed that the lamellae-like character of the undrawn material is preserved when considering structural aspects of the deformation of spherulites, rotation of lamellae, deformation of the crystal lattice or the unfolding of chains in the crystal [14,26]. Concepts familiar in the plastic deformation of metals are also applicable to that of polymers. Thus, edge- and screw dislocations, as well as dislocation networks have been observed. Phase changes and twinning of crystal lattices, segmental tilt and chain slip have been found to be important features in the deformation processes of crystalline polymers [22-28]. Most work on the deformation of crystalline polymers has been confined to polyethylene, because of the ease of interpretation with respect to its simple molecular structure. Electron microscopy of bulk crystallized polymers with spherulitic structures such as polyethylene and of single crystals, show that the basic mechanism of plastic deformation contains, as the most important step, a discontinuous transformation from the unoriented material into a highly oriented fibre structure [23,29]. The spherulites tend to remain intact during the first stages of drawing, elongate to an ellipsoid, and finally rupture at the spherulitic

boundaries [30].

Figure 2.9 illustrates schematically Peterlin's ideas for the structural metamorphosis that occurs during deformation. A multilayer lamellar crystal is destroyed with chain tilting, slipping and breaking off of blocks of folded chains, with subsequent re-formation of folded chains in the fibre [30,31]. The molecules in the structure of semicrystalline polymers such as HDPE, PTFE and Polyoxymethylene (POM) are stretched and aligned during a wear process at temperatures above the glass-transition temperature [32]. In figure 2.10, the deformation of chain-folded domains in the surface layers is shown. Bulk PTFE is non-spherulitic and crystallizes in the form of thick lamella crystals up to 1 μm thick. Electron microscopic examination of replicas of the fracture surfaces of PTFE show that striations, which are parallel to the chain direction, become tilted in the direction of extension when the material is deformed. These observations have been taken as an indication of deformation by chain slip [22,33].

A host of quantitative techniques, including x-ray diffraction, optical birefringence and infrared dichroism can be used qualitatively to measure the preferred orientation that prevails in a polymer specimen [11,29,34-36].

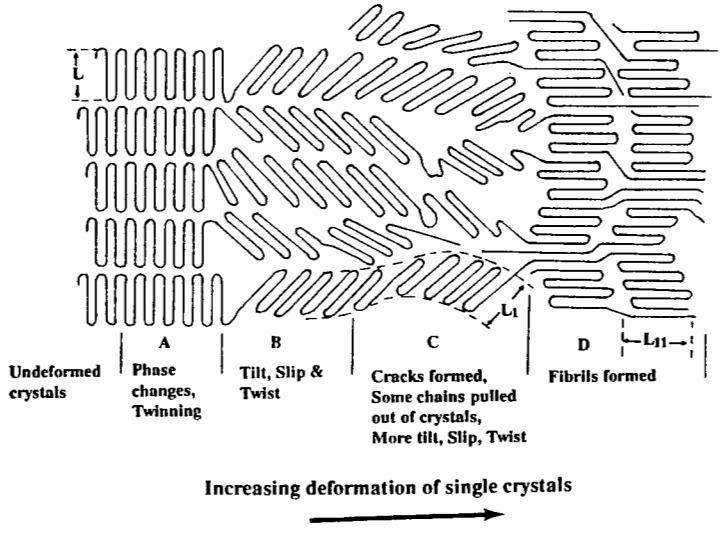

Figure 2.9: A suggested model for the fibre formation by mechanisms of chain tilting, slip and breaking off of blocks of lamellae. [After ref. 31].

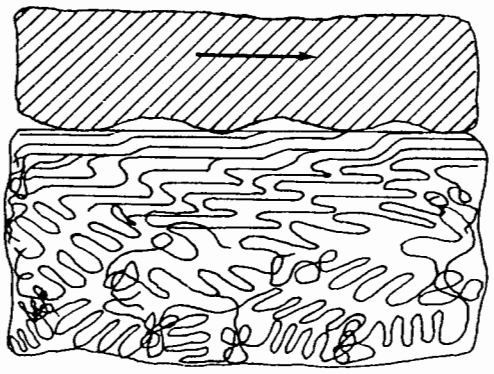

Figure 2.10: Stretching and reorientation of polymer molecules in semicrystalline polymers above their Tg during adhesive wear. [After ref. 32].

CHAPTER 3

LITERATURE REVIEW

THE FRICTION AND WEAR OF POLYMERIC MATERIALS

3.1 INTRODUCTION

3.1.1 Introduction To Friction And Wear

This chapter describes several fundamental areas in tribology such as the nature of friction, the mechanism and processes of wear, bulk mechanical and chemical properties of the polymer, lubrication, interfacial transfer and the operating parameters that affect the wear rates of polymers.

Friction is a central issue in tribology. An important concept in friction is the real area of contact. Most interfacial phenomena such as the generation and dissipation of frictional heat, adhesion, ploughing and film formation occur at the intimate contact between two surfaces. Many recent developments have been made in theoretical analysis of surface topography and the prediction of the real area of contact. However, there are no satisfactory experimental techniques for the determination of the real area of contact between two solid bodies [37]. Two main processes are generally regarded as being responsible for the frictional work dissipated when two solid bodies are moved over each other *viz.* the interfacial or adhesive mode and the ploughing or deformation mode. These contributions to friction are not independent and will interact, but it is useful to add their relative contributions [38].

The subject of wear cannot be treated with the same simplicity as friction. We can study each wear mechanism in isolation, but in most tribological applications they interact in a complex and unpredictable way. In addition, the surface topography of the counterface may be modified by transferred material which may change the relative importance of the separate mechanisms. The mechanical and chemical properties of the polymer play an

important role in the processes of wear [39]. A broad knowledge of the mechanical and chemical properties, coupled with an appreciation of the likely conditions existing in the contact region does not, however, enable us to predict accurately the level of wear as the interfacial deformations cannot be reproduced by bulk deformation studies [39,40].

In his introductory note to *"The Fundamentals of Friction and Wear"*, Briscoe makes the following comment:

"The central problem in tribology is that the zone of interest is an inaccessible and comparatively tiny region between two solid bodies. What happens here is very unlike anything which we can see in our common experiences. We have to deduce what is happening by means of clever experiments and speculations based upon science developed in other contexts. Because what is happening is so complex we make simplifications and approximations. We invoke model processes such as transfer wear and abrasion and then suppose that they operate in isolation. This is currently the essence of our approach to the fundamentals of polymer tribology." [38].

3.1.2 The Scope of Tribology

Tribology is the science and technology of contacting surfaces in relative motion. The word tribology is derived from the Greek word *tribos* meaning "the science of rubbing" [41].

Tribology is an interdisciplinary and complex subject involving friction, wear and lubrication. Since it is ultimately concerned with the properties of the surfaces exposed, an understanding of the basic principles of tribology requires an appreciation of the topographical, chemical, physical and crystallographic features of the interacting surfaces [41,42]. The interaction of surfaces in relative motion involves changes in the mechanical and chemical composition of the contacting surfaces. These changes arise from the induced deformations and temperature changes due to frictional loading. Some basic problems which need to be addressed are thus:

(i) the origin of the frictional resistance and the modes of energy dissipation due to sliding,

(ii) the properties of the interacting materials, the applied forces, speed, temperature and the presence of an interposed film or lubricant [42].

There has recently been an "upsurge" in tribology research at many academic institutions. Many industrial companies have come to realize the importance of tribology in their overall research and development programmes [37,43]. Quinn contends that for research to be fruitful and effective, an empirical approach is needed *i.e.* one would need a preconceived notion of what actually occurs on an "atomistic level" at the sliding interfaces. The application of modern physical and analytical techniques would play a vital role in order to get a microscopic insight of the interfacial mechanisms and for the formulation of a reliable mechanism and prediction [44].

3.2 FRICTION

3.2.1 The Nature of Friction

The frictional force is the resistive force which opposes motion when a solid body slides over another. When two surfaces are brought together, the first contact occurs at the asperity tips as shown in figure 3.1. The tangential force required to maintain relative motion is called the dynamic frictional force (f_d), while the static frictional force (f_s) is required to initiate motion from rest. The dynamic frictional force is generally lower than the static frictional force, the size of both being dependent on the area of real contact and on the system parameters such as the rubbing velocity, normal load, temperature and surface roughness [39].

Tabor noted that there are three basic elements involved in the friction of unlubricated solids: [45].

(i) the area of true contact between the sliding surfaces;

(ii) the strength of the bond that is formed at the interface where the contact occurs; and

(iii) the way in which the material in and around the contacting regions is sheared and ruptured during sliding.

3.2.2 The True Area of Contact

Real surfaces are rough on a microscopic scale and the true area of contact between two surfaces is determined by the surface topography as well as the deformation properties of the materials under loading. The asperities of the bodies in contact may be deformed elastically, plastically, viscoelastically or brittly [45,46].

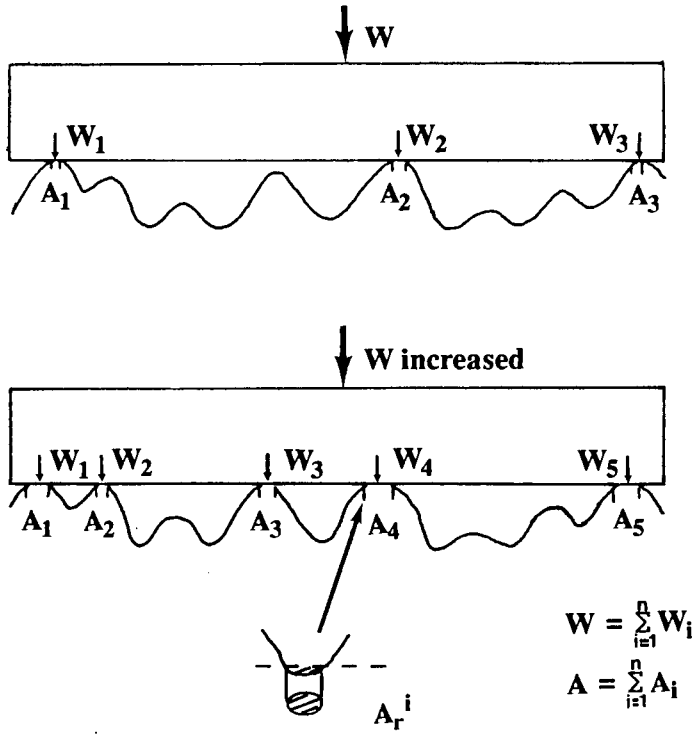

Figure 3.1: The effect of increasing the load on the contact of a smooth surface and a rough surface having asperities of varying heights. [After ref. 47].

Consider the contact between two surfaces, one flat, smooth and undeformable and the other rough and deformable as shown in figure 3.1 above. As the load is increased, the existing contacts will grow in size while new ones are formed as the lower asperities come into contact [47]. The contact between the two solid bodies is controlled by deformation properties such as the plane stress elastic modulus, the hardness and the yield stress as well as by topographical characteristics such as the surface density of the asperities, the standard deviation of their height distribution, the slopes of the asperities and their mean radii as summarized in figure 3.2. [48,49].

It has been shown by Greenwood and Williamson that for an exponential distribution of the asperities, the average size of the asperity contact remains constant, whether the asperity deformation is elastic, plastic or a mixture of both, *i.e.*, doubling the load, doubles the number of asperity contacts and doubles the area.

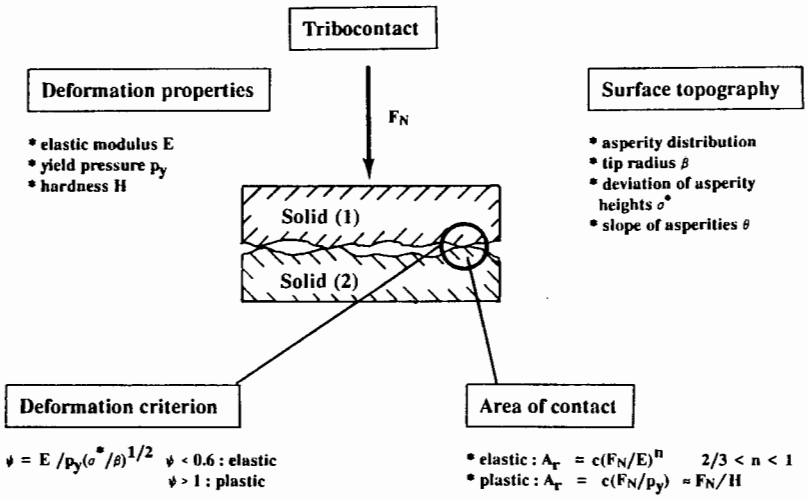

Figure 3.2: The characteristics of tribocontact between two solid bodies. [After ref. 50].

If we assume a Gaussian distribution of asperity heights, where σ is the mean deviation of asperity heights, β is the asperity tip radius, P_o is the plastic yield pressure and E is the elastic (Young's) modulus, we have the plasticity index or surface texture parameter:

$$\psi = (E/P_o)(\sigma/\beta)^{0.5} \qquad (3.1)$$

The first term describes the mechanical properties of the solid, while the second term describes the surface topography [48].

The elastic or plastic deformation behaviour of metals is governed by the plasticity index. For polymeric materials in contact, viscoelastic and relaxation phenomena lead to a time dependence of the contact area and to hysteresis losses during the loading and unloading cycles [50]. The summation of the individual contacts gives the real area of contact, Ar, which is much smaller than the apparent area of contact Ao, *i.e.*,

$$A_r = \sum_{i=1}^{n} A_r^i << A_o \qquad (3.2)$$

where A_n^i is the real area of contact at the ith location.

Consider the idealized single point contact between a hemispherically smooth asperity against a smooth flat surface or the case of two orthogonal cross cylinders of radii R_1 and R_2 made of softer material. When the asperity and the flat surface are brought into contact under a load W and the contact is elastic, the area of contact A is given by: [51]

$$A = \pi(kWR)^{2/3} \tag{3.3}$$

where $k = 3/4\ (1-\nu_1^2/E_1 + 1-\nu_2^2/E_2)$

R is the radius of the hemispherical asperity or the mutual radius of curvature, R_1R_2/R_1+R_2

ν and E are the Poisson's ratios and Young's moduli respectively.

For rough surfaces undergoing elastic deformation, A is generally proportional to the load W such that $A \propto W^m$ [48]. This multiple asperity elastic contact was modelled by Archard, who showed that for metals $A_r \propto W^m$, where m ranges from 2/3 to 1 [52].

It is conventional to define the hardness of a material (H) by the ratio of the load to the surface area of the permanent indentation, *i.e.*, by the mean contact pressure, for example between a ball and a plane where the mean contact of pressure

$$P_m = W/\pi a^2 = H \tag{3.4}$$

and a is the radius of the contact.

From this definition it is seen that the mean pressure is related to the load by:

$$P_m \propto W^{1/3} \tag{3.5}$$

for complete elastic deformation. Because of the constraining effects of the elastic material, plastic indentation does not materialize until the mean contact pressure has a value of three times the yield stress Y, of the material, *i.e.*

$$P_m = 3Y = H_v \qquad (3.6)$$

In other words, no significant permanent indentation of the surface will occur when spherical surfaces are loaded against a plane until the mean contact pressure is at least three times the yield strength of the material. This implies that any increase in the load at a point where P_m exceeds 3Y will only cause the contact area to increase and P_m is thus constant once full plasticity is obtained. For complete plastic behaviour then, $A_r = W/H$. For elastic deformation the total area of contact is proportional to $W^{2/3}$, whereas for plastic deformation it is proportional to W [47].

The following generalizations which can be made are summarized in figure 3.3. If the asperities are the same height and the load W is increased, the area of contact in the range where the asperities deform elastically will be proportional to $W^{2/3}$. If the number of asperity contacts increase with the load such that the average size of each asperity contact remains constant, *i.e.*, the total area of contact Ar divided by the number of contacts remains constant, the area of contact in the elastic region will be proportional to W. If plastic deformation takes place the area of contact will be proportional to W whatever the asperity distribution since the yield pressure for each asperity contact will be a material constant P_o [45,47].

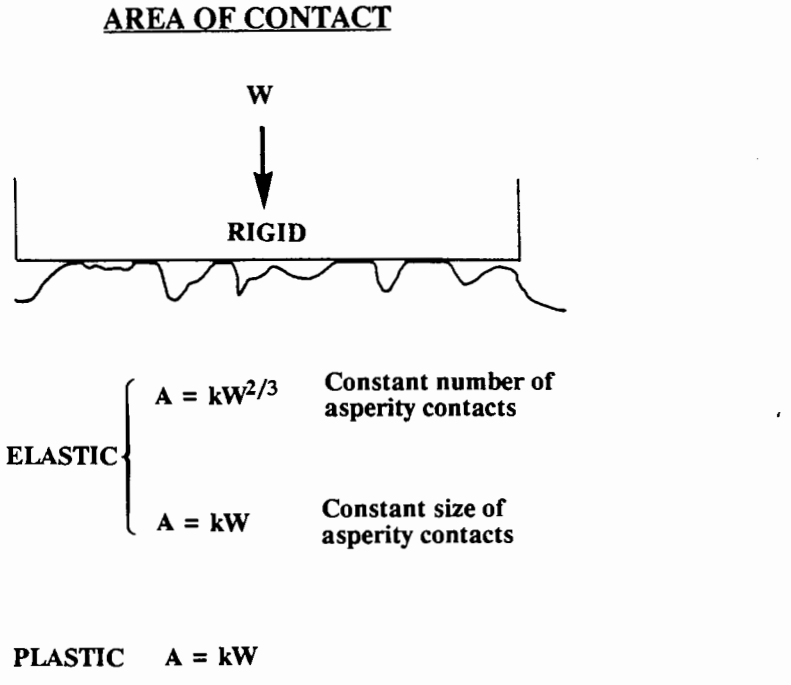

Figure 3.3: The area of contact between two surfaces in terms of asperity deformation. [After ref. 45].

3.2.3 The Two-Term Non-Interacting Friction Model

The two-term non-interacting friction model was introduced by Bowden and Tabor to describe the mechanism of polymer friction [39,46]. Although many mechanisms may be involved in the sliding friction of solids, the contributions of these two terms are regarded as being the most important. The two contributions are then conveniently and, perhaps, oversimplistically summed up to provide the total friction. This simplified model has gained wide acceptance in explaining polymer friction [45,46].

$$F_{total} = F_{adhesion} + F_{deformation}$$

The first component is the contribution due to the shearing of adhesive forces at the regions of real contact. The second component is due to the ploughing of the asperities of the harder solid through the surface of the softer polymer. Figure 3.4 shows an illustration of the two-term model of friction. Surface melting as a result of the polymer's poor thermal conductivity and low melting point, material transfer, reorientation and chemical degradation are some consequences due to the adhesive frictional component whereas viscoelastic ploughing and elastic tearing are associated with the deformation term. The two processes will therefore produce different damage modes [39,45].

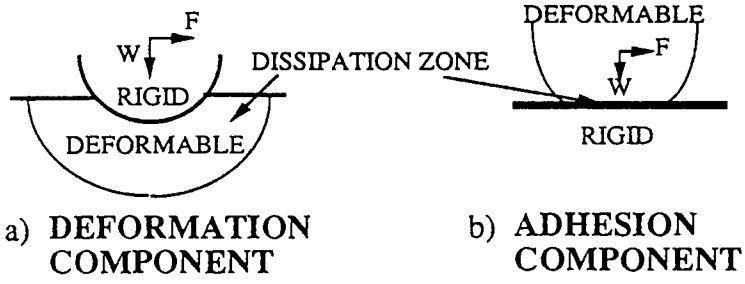

$$F_{TOTAL} = F_{DEFORMATION} + F_{ADHESION}$$

Figure 3.4: A schematic of the two-term model of friction, showing the two possible cases of solid contact where one body is rigid and the other deformable. [After ref. 53].

Virtually all the frictional work ultimately appears as heat which is conducted out of the boundaries of the system, some of this work being dissipated in inelastic deformations in

volumes adjacent to the contact. These volumes are commonly known as "primary energy dissipation zones" [45]. The way in which the energy may be introduced and dissipated into the contact zone is depicted in figure 3.5.

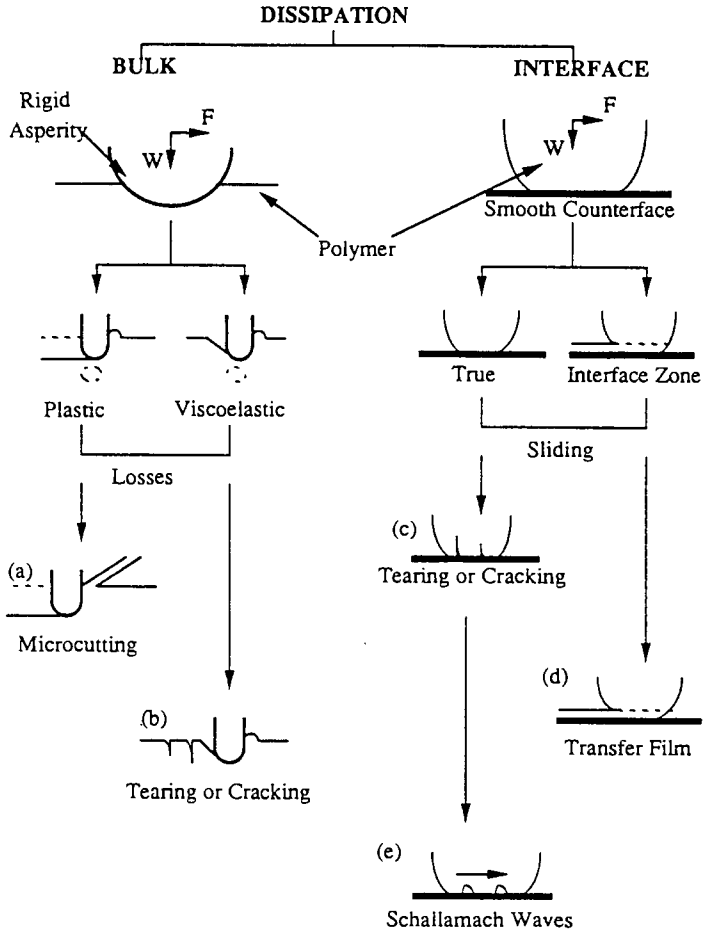

Figure 3.5: Polymeric frictional damage and energy dissipation processes, subdivided by adhesion and ploughing components. [After ref. 53].

When the friction is described by analogies with the bulk deformation behaviour, it must be borne in mind that the deformation behaviour of the polymer is sensitive to the temperature, pressure, strain, rate of strain and the chemistry of the polymer and environment. There are major differences in the conditions prevailing in each zone and for comparable energy dissipation levels the temperatures, strains and strain rates in the surface layers will be much greater than for the ploughing zone. The strains are presumed to be very high and may lead to appreciable reorientation of the polymer structure. The strain rates are obtained by dividing the sliding velocity by the film thickness and are thus

typically 10^6 s^{-1} [37,39,54]. Table 3.1 distinguishes the conditions prevailing in the two zones.

Variable	Cohesive zone*	Interfacial zone
Temperature	**Nearly ambient**	**Invariably high**
Contact pressure	**Close to ambient**	**Often high**
Strain	**Low**	**Sometimes very high**
Strain rate	**Moderate**	**Generally very high**
Contact time	**Similar**	**Similar**

Table 3.1: Notational deformation conditions in the two primary friction dissipation zones. (*) The conditions developed in the cohesive zone are comparable with the conditions produced in certain bulk deformation experiments. [After ref. 54].

3.2.4 The Adhesion Component of Friction

Adhesion may be defined by the physical strength of an interface, the failure strength depending on whether the energy is dissipated through a mechanism of plastic work, or for brittle polymers by fracture work [39].

It has been shown that when certain semicrystalline polymers such as HDPE and PTFE are rubbed against a relatively smooth and hard surface as shown in figure 3.5, that a very thin (about 10 nm) and highly oriented polymer film is laid onto the counterface [55]. In these instances the ploughing or deformation term is negligible and the interfacial bonding is largely due to the long range van der Waals forces, aided with a small amount of hydrogen bonding and electrostatic forces. These forces are comparable with those existing between the polymer chains themselves so that when sliding occurs there is a tendency for shear to occur within the bulk polymer. The shear strength of the adhesive junctions are conventionally assumed to be equivalent to the bulk strength of the polymer, hence cohesive failure and transfer during sliding. Pooley and Tabor have attributed the easy shear of PTFE to the "smooth molecular profile" of the polymer rather than the shear

amorphous units of the PTFE crystallites as suggested by Makinson and Tabor [55,56]. The high pressures at the interface are able to easily distort these linear molecules and orient the hydrocarbon chain in the direction of sliding [57].
Since the polymer shears a short distance within the polymer itself, microscopic plastic flow is envisaged [39]. If we ascribe a specific shear strength, τ, to the system, the interfacial frictional force F_a is given by:

$$F_a = A_r \tau \qquad (3.7)$$

where A_r is the real area of contact. The stresses are transmitted by adhesive forces which operate at a range less than 0.1 nm, the interface zone being up to 100 nm, as shown in figure 3.6 [39,40,54].

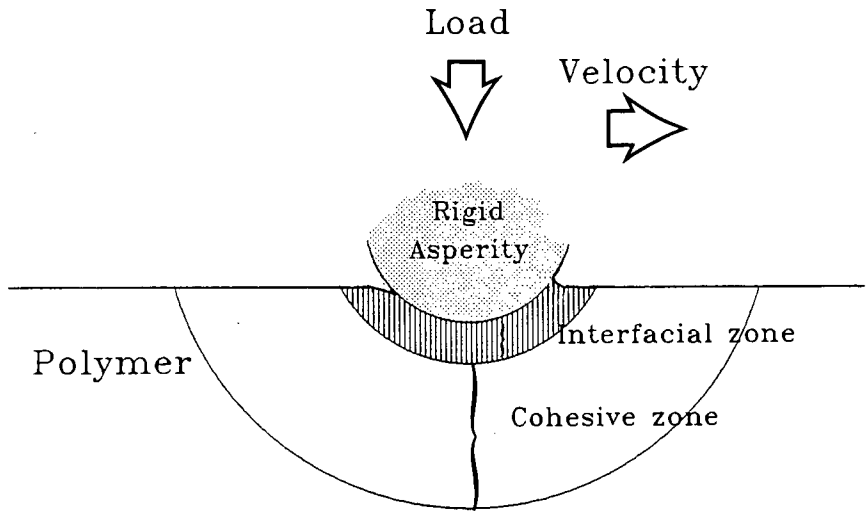

Figure 3.6: Two general categories of wear process *viz.* interfacial wear and cohesive wear. The thickness of the interfacial zone is of the order of a few nanometres while the cohesive zone is of the order of a contact radius. [After ref. 40].

Briscoe and Tabor noted that the shear properties of these thin films resemble those of the bulk polymer only if allowance is made for a high degree of molecular orientation produced in the film during sliding [58]. The reason for this will be clarified as follows. The apparatus and experimental technique used for the measurement of τ have been described and detailed in reference 57. Very thin films (*ca.* 20 nm) of the polymer are deposited on smooth glass plates either from solution or by rubbing the polymer on a heated glass surface. The films are then sheared by spherical glass sliders sliding on them

and the frictional force, F_a, is measured. The area of contact Ar, is estimated from the elastic properties of the sliding surfaces.

It is found that for a wide range of polymers, the shear strength τ, is generally a function of the temperature T, the contact pressure P and the sliding velocity v. The area of real contact cannot be measured directly and must be estimated by using a mathematical model for the contact. The important factors which must be taken into account are the mechanical properties of the polymer, the overall geometry of the contact, the surface roughness, the surface energy of the solids and the contact pressure [39,59].

(1) The Effect of Contact Pressure

If a smooth sphere of radius R is loaded against a smooth surface upon which a thin polymer film is deposited, then for high loads where the contact deformation is elastic, the area of contact A, is given by the Hertzian equation (3.3). The mean contact pressure P, is given by W/A. If a force F, parallel to the plate is required to maintain a velocity v, then the frictional force per unit contact area τ is F/A. In figure 3.7, τ is plotted against P for a range of different polymers.

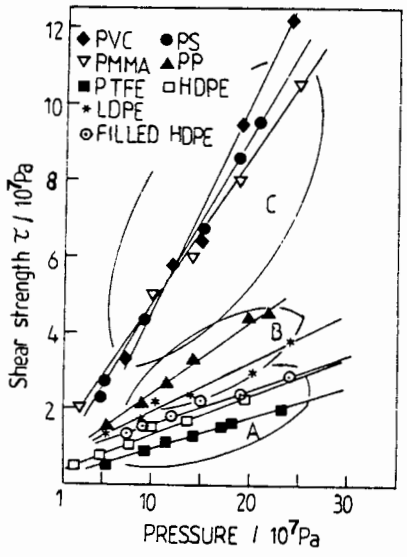

Figure 3.7: The interfacial strength, τ, as a function of mean contact pressure. The temperatures and sliding velocities were fixed at 20 °C and 0.2 mm.s^{-1} respectively. τ is a linear function of pressure. The data fall into the three general groups A, B and C as shown in table 3.2. [After ref. 60].

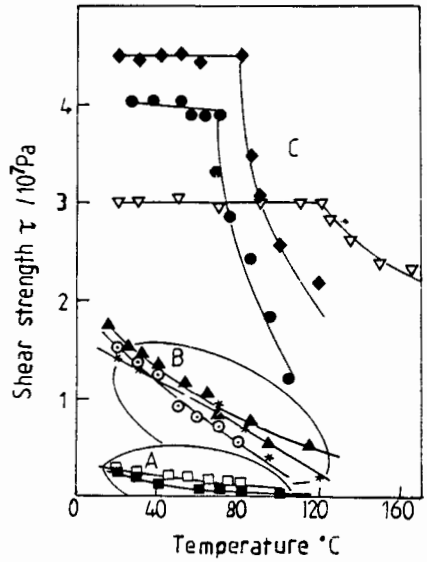

Figure 3.8: The interfacial shear strength, τ, as a function of temperature T, for polymers referred to in fig. 3.7, at a constant pressure of 7.2 x 10^7 Pa and a sliding velocity of 0.2 mm.s^{-1}. The polymers again fall into the three groups A, B and C. [After ref. 60].

The relationship between τ and P is given by: [57,60].

$$\tau = \tau_o + \alpha P \qquad \text{at constant T and v} \qquad (3.8)$$

where τ_o and α are constants for each polymer. The values of the parameter α are listed in table 3.2 for three different groups of polymers. The "smooth molecular profile" polymers show the lowest pressure dependence, while the amorphous polymers have the highest dependence [60]. This correlates with the view that the frictional properties of polymers are dependent on their molecular morphology and thus their film forming ability.

Polymer	Tg ℃	α Below Tg	α Above Tg	Q kJ/mole Below Tg	Q kJ/mole Above Tg	μ_c	μ_b	μ_g	Polymer transfer to glass at 20 ℃
Group A									
PTFE	−112	–	0.08	–	20	0.12	0.16	0.13	Yes
HDPE	−120	–	0.10	–	16	0.16	0.15	0.08	Yes
filled HDPE	–	–	0.09	–	14	–	–	–	Yes
Group B									
PP	−20	–	0.17	–	17	0.27	0.26	0.26	No
LDPE	−120	–	0.14	–	9–30	0.53	0.52	0.42	Yes
Group C									
PMMA	105–120	0.36	0.10	-0	14	0.39	0.36	0.41	No
PS	100–105	0.45	0.17	-0	26	0.48	0.42	0.45	No
PVC	87	0.57	0.18	-0	18	0.46	0.55	0.54	–

Table 3.2: A comparison between the coefficients of friction, deduced from thin film experiments, and those directly measured. The values of α and Q for the various groups are also shown; Q from $\tau = \tau' \exp(Q/RT)$, α from $\tau = \tau_o + \alpha P$

u_c = coefficient of friction calculated from $(\tau_o/P_o) + \alpha$
u_b = coefficient of friction obtained when the bulk polymer is slid on itself.
u_g = coefficient of friction obtained when the bulk polymer is slid over a flat glass substrate
Group A: "Smooth molecular profile" polymers
Group B: "Normal polymers
Group C: Amorphous polymers
[Adapted from refs. 54, 58 & 60].

It is also found that the values of τ_o lie between one tenth and one hundredth that of the isotropic bulk shear strength of the film material at atmospheric pressure. In this regard the following points have been noted: [58].

(i) τ does not depend on the nature of the hard solid provided it is hard and smooth.
(ii) τ for thin metal films agrees well with bulk values.
(iii) With regard to polymers that are not readily oriented, the discrepancy between τ and the bulk shear strength is small.
(iv) For bulk polymers that are heavily drawn, the modulus and shear strength could be as much as 10 times smaller in the direction of chain orientation than at right angles to it.

The low values of the shear stresses would then probably be due to extensive reorientation of the molecular chains in the interfacial layers as well as to the existence of a well defined shear plane during sliding [58]. When the contacting surfaces are loaded so that appreciable plastic deformation occurs on one or both substrates then: [39]

$$Ar = W/P_o \tag{3.9}$$

where P_o is the plastic yield stress of the polymer and W the normal load. The coefficient of friction μ, of such contacts is given by:

$$\begin{aligned} \mu &= F/W = A\tau/W = 1/P_o(\tau_o + \alpha P) \\ &= \tau_o/P + \alpha \approx \alpha \text{ at high loads; } (P > \tau_o) \end{aligned} \tag{3.10}$$

The limiting value of μ is approached for most polymer layers when P is greater than 10^9 Pa [58].

Equation (3.10) is found to accurately predict the coefficient of friction of the group A polymers (table 3.2) and to a first approximation is unaffected by the topography of the solids [39,60].

(2) The Effect of Temperature

The dependence of τ on the temperature of the polymer at a constant pressure has also been studied as shown in figure 3.8 [60]. It is found that for the amorphous polymers below their glass transition temperature T_g, that high values of α, corresponding to their high friction and inability to form transfer films, are obtained (table 3.2). Above the glass transition temperature, α is small and similar to the values obtained for the "normal" polymers. This confirms the observation that above T_g, polymers like PMMA form transfer

films similar to that obtained by LDPE at room temperature [60]. Polymers for which the T_g is below room temperature show a pronounced decrease in the shear force, the deformation resembling a viscous flow and is highly temperature-dependent. The activation energy Q, may be calculated from a log τ *vs.* 1/T plot and are given in table 3.2. When τ decreases with temperature the experimental data fit the equation: [58,60]

$$\tau = \tau_o' \exp(Q/RT) \text{ at constant P,v.} \qquad (3.11)$$

The value of Q is a measure of the temperature dependence of the mobility of the polymer chains, a low value indicating chains that are rigidly fixed, while higher Q values correspond to more mobile chain segments as envisaged in a viscous flow process [60].

The adhesion theory of friction developed by Bowden and Tabor takes into account the fact that the real area of contact is affected by the sliding process. When two surfaces are loaded together, the local pressure at the asperities may reach the yield stress of the softer material. This process will continue until the area of contact is sufficient to support the load, *i.e.*, the area of contact is proportional to the load (W) and inversely proportional to the yield pressure of the softer material (P_o) [46,61].

$$Ar = W/P_o \qquad (3.9)$$

Welds may occur at the contacts so that the friction force arises from the force required to shear these welds, the friction thus arising from macrojunctions and not from intermolecular forces. The total frictional force F_a is:

$$F_a = Ar\tau \qquad (3.7)$$

where Ar is the sum of the area of contacts. Substituting for Ar, we get the expression for the frictional force:

$$F_a = W\tau/P_o \qquad (3.12)$$

This simple picture gives a satisfactory description of the two laws of friction:
(i) The frictional force F_a is independent of the contact area.
(ii) The frictional force is proportional to the load.

If the difference in hardness of the two materials is big then the ploughing term cannot be ignored. The coefficient of friction is given by:

$$\mu = F/W = \tau/P_o \qquad (3.13)$$

The yield pressure is generally about five times the critical shear stress and for most materials this ratio is of the order of 0.2. For metals the junction growth may be considerable and the adhesion component of friction may increase by 10-100 times, but junction growth is not so extensive for polymers [50,62].

If the surfaces are separated by a film with an effective shear strength about half that of the parent metal then a friction coefficient of 0.1 may result. The simplified Bowden and Tabor model may be extended by including the surface energy of the contacting materials [50].

3.2.5 The Deformation or Ploughing Component of Friction

If the adhesion component is small, an appreciable part of the friction may be due to the asperities of the hard material ploughing out a groove, by plastic flow, into the softer polymer [41,45]. The ploughing term involves deformation in a relatively large volume of the polymer [39]. (See figures 3.4 and 3.6). Consider the simple case of a hard material composed of a large number of conical asperities of semi-apical angle θ, in contact with a soft material as shown in figure 3.9.

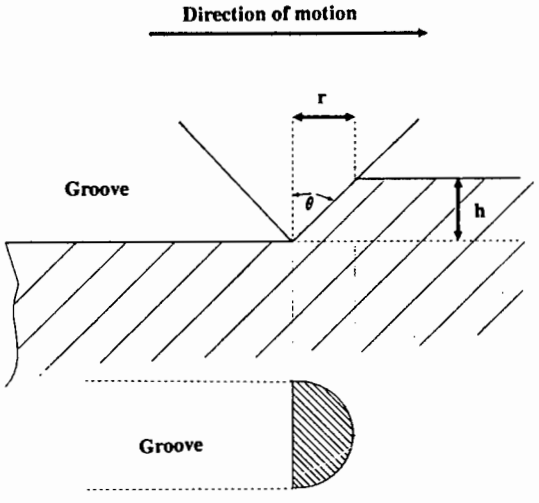

Figure 3.9: The ploughing of a soft surface due to a hard conical asperity of semi-apical angle, θ. [After ref. 45].

During sliding, the front surface of each conical asperity is in contact with the opposing material and the vertically projected area of contact is given by: [41]

$$A = n\pi r^2/2 \tag{3.14}$$

where n is the total number of asperities. The load W is given by:

$$W = AP_o = n\pi r^2 P_o/2 \tag{3.15}$$

where P_o is the yield pressure of the softer material.

The friction force F_d, is obtained by considering the total projected area of material displaced by plastic flow:

$$F_d = nrhP_o \tag{3.16}$$

and the coefficient of the friction due to ploughing alone is:

$$\mu_p = F_d/W = 2h/\pi r \tag{3.17}$$

and since $\cot\theta = h/r$,

$$\mu_p = (2/\pi)\cot\theta \tag{3.18}$$

Most asperities have slopes of the order of 5°-10° so that the equivalent values of θ lie between 85° and 80°. This gives μ_p lying between 0.07 and 0.14. These values may be regarded as the lower limit of μ_p as a pile-up of material ahead of the grooving path occurs, but this contribution may nevertheless be added arithmetically to that part of the friction due to adhesion [45].

The sharp asperity is then essentially a miniature cutting tool when it is slid over the surface of the ductile polymer. Energy is fed into the polymer ahead of the asperity (figure 3.10) and some of this energy is restored at the rear end of the slider because of elastic recovery, and urges it forward. The net energy lost in this process account for the force or work required to maintain sliding [38,63].

In figure 3.11, where μ is plotted as a function of θ, ($\theta' = \pi/2 - \theta$), μ increases with cot θ. The geometric properties of the asperities are clearly important as it has been shown that rough surfaces with rounded asperities favour a fatigue wear mechanism whereas smooth surfaces would favour interfacial transfer. Rough surfaces with sharp asperities would involve an abrasive wear mechanism [64,65].

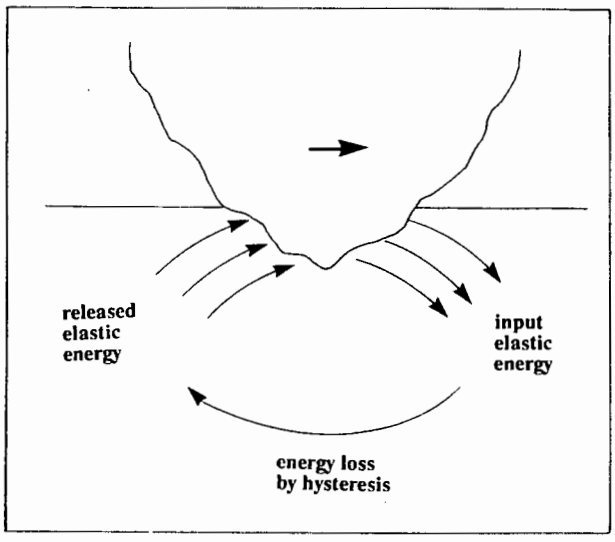

Figure 3.10: A model of the mechanism in the deformation of a polymer by a hard asperity. [After ref. 63].

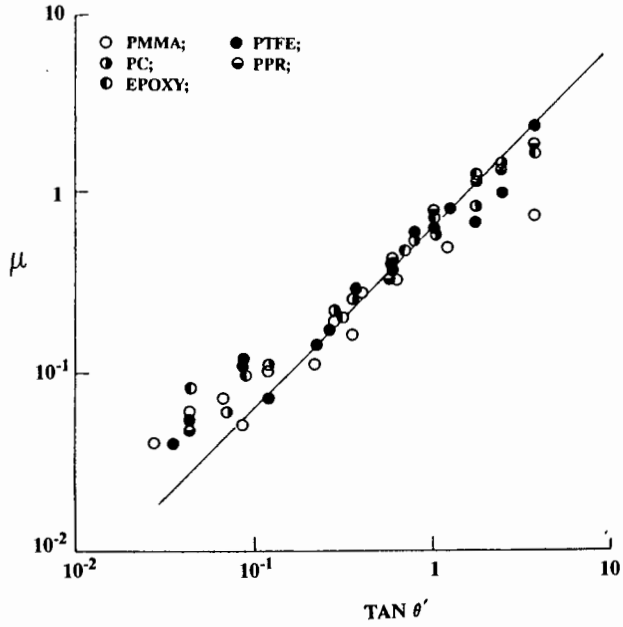

Figure 3.11: The coefficient, μ_d, as a function of θ', the cutting angle for various cones of semi-apical angle θ. The solid line has a gradient of $2/\pi$ (eqn. 3.18). The load is 1N, sliding speed 4.2×10^{-5} m.s^{-1} and the contact is unlubricated. Cutting occurs at tan$\theta > 1$. [After ref. 54].

3.3 WEAR MECHANISMS

Wear is the removal of material from one or both of two solid surfaces in solid state contact. It occurs when solid surfaces are in sliding, rolling or rubbing motion relative to one another [66]. A number of wear mechanisms have been categorized. According to Evans and Lancaster, the wear processes of polymers may be divided into four main groups, *viz.*, abrasion, adhesion, fatigue and thermal/oxidative degradation [20]. The difficulties which may arise from such a classification is that:

(a) The detailed mechanisms of surface failure leading to the removal of debris depend significantly on the mechanical properties of the material, *e.g.*, abrasive wear against rough surfaces may occur via tensile tearing for elastomers and cutting or shearing for high modulus polymer composites.

(b) There is a considerable amount of interrelationship among different processes that lead to failure [20].

Briscoe distinguished between two general classes of wear processes, *viz.*, cohesive wear and interfacial wear [40].

(i) Cohesive wear processes are governed by the cohesive strength of the polymer, and the frictional work is dissipated in relatively large volumes adjacent to the interface either through the interaction of surface forces or by the interlocking of asperity contacts. (See figure 3.6). The wear mechanisms rely upon an understanding of the mechanical properties of the polymer and their wear rates may be correlated with a strength, toughness or a fatigue property obtained from bulk deformation experiments.

(ii) Interfacial wear processes involve a dissipation of frictional work in a thinner region at the interface. The chemistry of the surfaces and the surface forces are the main influencing factors. These surface regions suffer from transient temperature rises of uncertain extent and duration.

Abrasion and fatigue wear fall within the first category, while transfer and chemical wear fall under interfacial wear processes. This subdivision of the wear processes into two classes provides a useful simplification of the complex wear mechanisms encountered. In practice wear processes are not monomechanistic and there are in most cases an overlap of interfacial and cohesive tribological processes [40].

In order to reduce wear in practical tribological devices, it is important to understand and appreciate the various wear mechanisms. If the mechanism of wear operating in a particular system can be identified, this can do much to assist in reducing wear [66].

3.3.1 Abrasive Wear

Abrasive wear is defined as *"wear by displacement of material from surfaces in relative motion caused by the presence of hard protuberances, or by the presence of hard particles either between the surfaces or embedded in one of them."* [67]. Abrasive wear can thus be characterized as a result of two or three body abrasive wear as shown in figure 3.12 [32,66,68]. Two body abrasive wear occurs when a rough surface or fixed abrasive particles cut or groove the softer surface with plastic flow of the softer surface occurring around the asperities of the harder surface, *e.g.*, when polymers slide against rough metal surfaces or abrasive papers [68,69]. In three body abrasive wear, the particles are loose and move relative to one another while sliding across the wearing surface. Lubricant films, either sufficiently thick to completely separate the surfaces or thicker than the size of the hard particles will greatly reduce the abrasive wear [70].

For rigid polymers, the abrasive wear of the hard surface asperities penetrating the surface and removing polymer by shearing or cutting, leads to the following relationship: [20,40].

$$z = k\,(W/H)\tan\theta \qquad (3.19)$$

z is the volume of material removed per unit sliding distance,
W is the normal load,
k is the probability of the formation of a wear particle, *i.e.*, expresses the fact that only a portion of the material undergoing deformation appears as a loose wear debris and
H is the hardness and θ is the base angle of the indenting asperity.

For these rigid polymers, the idealized case of two-body abrasive wear can be considered when a hard conical indentor penetrates and ploughs a groove into the softer material, removing polymer by shearing and cutting. (See section 3.2.5). The results for an amorphous polymer, PMMA and a soft material (tin) is shown in figure 3.13. With the metal, plastic deformation occurs at all angles but for the polymer, the relationship is linear only when θ exceeds 30°, *i.e.*, when the apex angle is small. It can be concluded that with polymers, plastic deformation only becomes the predominant mode when the indentor is very sharp.

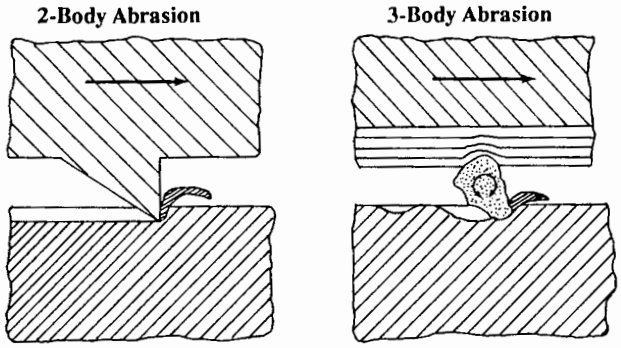

Figure 3.12: Two- and three body abrasive wear. [After ref. 32].

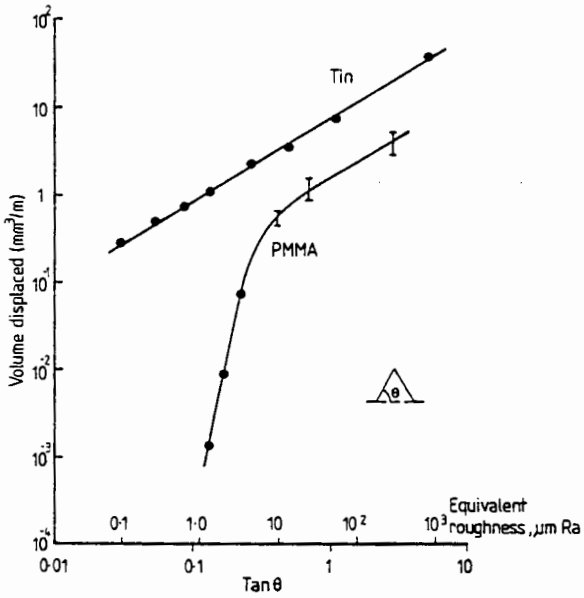

Figure 3.13: The relationship of volume of material displaced per unit sliding distance with the base angle of a conical indentor. [After ref. 20].

Generally, the deformation of polymers is partly elastic and partly plastic and the relative proportions will vary with roughness [69]. In abrasive wear, the product $S\epsilon$, which is essentially the area under the stress-strain curve, appears to become an important material parameter influencing the wear. The work of Lancaster and Ratner *et al.* show that for single traversals over relatively rough steel counterfaces, that the wear rates of various polymers are proportional to $1/S\epsilon$ where S is the rupture stress and ϵ is the elongation to break [71,72]. This linear relationship is shown in figure 3.14. The $S\epsilon$ values were obtained from conventional tensile tests carried out at relatively low strain rates of about 10^{-4} s^{-1}. The product $S\epsilon$, which is proportional to the work required to produce a wear fragment, may be fortuitous as a low strain rate tensile test cannot sense the approximate strength or roughness property of the polymeric matrix. This is so, because the rate of strain may be too low, the geometry of the stress system unrealistic and the damage process in a wear test may be of a fatigue rather than a unitary nature [40].

As the product $S\epsilon$ is some measure of the impact strength of the material, Ratner attempted to correlate the notched impact strength to the abrasive wear of polymers. This is in view of the fact that the high localized strain rates involved during the wear process approach that of the impact test, where the strain rates may be as high as 10^4 s^{-1} [69].

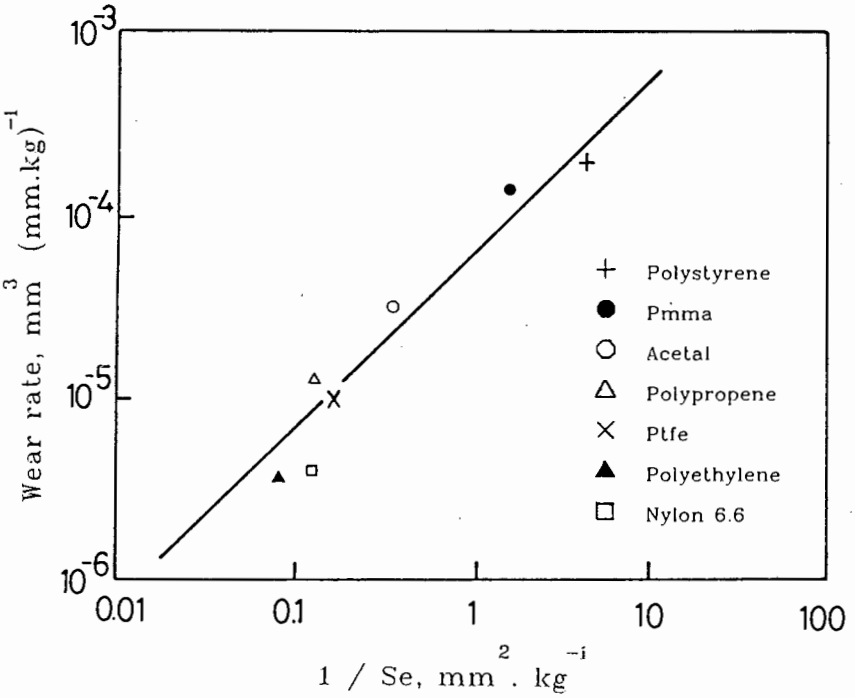

Figure 3.14: The Ratner-Lancaster correlation between wear rates of polymers and the reciprocal of the energy parameter $S\epsilon$. The wear rates refer to single traversals over a rough steel surface of 1.2 μm R_a. [After ref. 69].

Giltrow has shown that a correlation exists between the rate of abrasive wear of thermoplastic polymers and their cohesive energies, *i.e.*, the interaction energy between the chains [73]. The advantage of introducing the concept of cohesive energy is that it may be calculated on the basis of the chemical structure of the polymer and the opportunity therefore arises in principle, of being able to relate the wear properties of polymers to their chemical constitution. The rate of abrasive wear of thermoplastic polymers was shown to be inversely proportional to the square root of their cohesive energies as illustrated in figure 3.15. This non-linear relationship is attributed to the complex structure of polymers (degree of crystallinity, extent of chain branching, variations in molecular weight, *etc.*) and to the high rates of strain which occur during abrasion, with a consequent reduction in polymer chain mobility. Furthermore, the relationship is observed only when the predominant mode of deformation is plastic, leading to a microcutting type of wear process [73].

Lancaster described the abrasive wear as a combination of the two extreme processes of cutting and fatigue [69]. Cutting would be expected of rough surfaces with sharp asperities and fatigue of rough surfaces with rounded asperities.

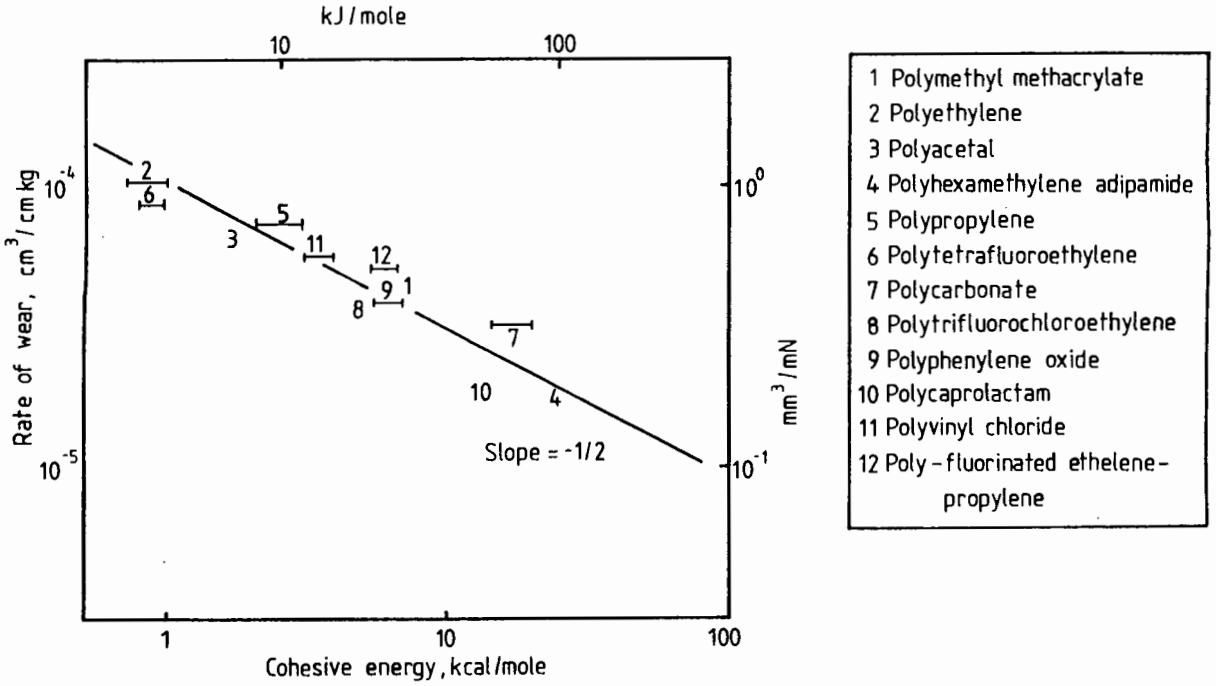

Figure 3.15: The relationship between abrasive wear and cohesive energy of thermoplastic polymers. The polymers in the inset refer to the numbers in the figure. [After ref. 73].

Hollander and Lancaster obtained a good relationship between the wear in a 'single pass' abrasion test and the ratio σ/R_{av}, where σ is the standard deviation of heights of the asperities and R_{av} is the average radius of curvature of asperities [74]. Tabor has shown that the asperity slope θ may be estimated from the relationship:

$$\tan\theta \approx (\sigma/2R_{av})^{0.5} \qquad (3.21)$$

The wear rate increases with an increase in the calculated mean slope as shown in figure 3.16 [75]. The experiments reviewed correspond to single pass abrasions and in steady-state conditions, modifications of the counterface by transfer leads to a reduction in roughness and wear, especially for ductile polymers [40].

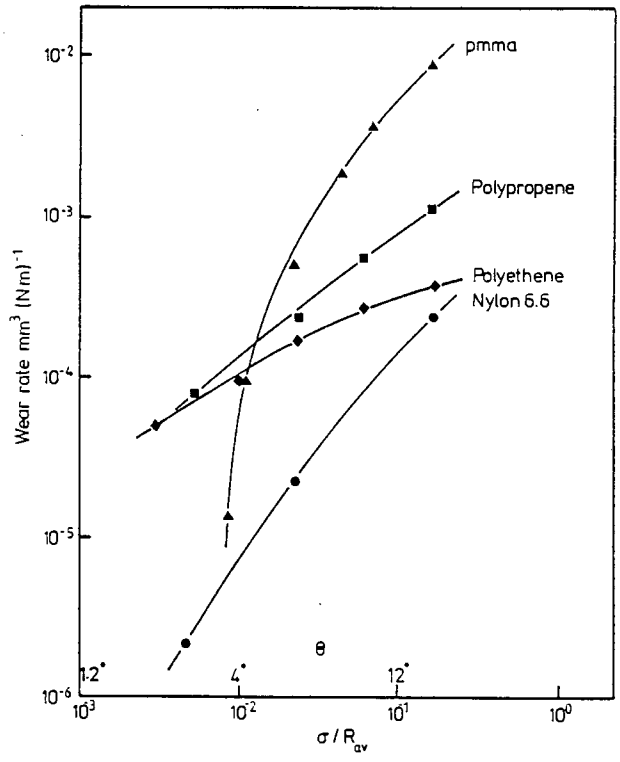

Figure 3.16: Single pass wear rates of various polymers plotted against σ/R_{av}, showing a pronounced increase in wear rates with the calculated mean asperity slope. The asperity slope θ is estimated from the relationship $\theta \approx (\sigma/2R_{av})^{0.5}$. R_{av} is the average radius of curvature of the asperities, and σ is the standard deviation of asperity heights. [Data from refs. 40 and 74].

3.3.2 Adhesive Wear

Of the principal forms of wear, adhesive wear is the most significant, since it plays a part in all wear processes, whereas other forms of wear such as abrasive wear only arise when hard, sharp particles are present at the sliding interface [76].

When two solid surfaces are placed in contact, bonding in the form of weak van der Waals attraction, electrostatic, hydrogen bonding, or stronger chemical bonding occurs at the interface. The likelihood of strong bonding is enhanced by increasing the applied load and extremely strong bonding may occur when the two surfaces are atomically clean. In order to accomplish tangential motion, shear must take place in order to rupture the adhesive bonds at the interface [66]. An intensive adhesive interaction is thus developed in the contact region during the shear process which may overcome the strength of individual structural elements in the surface layers of the material, causing it to fracture at the very

start of frictional interaction [66,77]. In practice, the bonds very seldom rupture at the interface and the bonds of the cohesively weaker of the two materials rupture. The fracture products, the character of which depends on the type of the material and the operating conditions, form a third body and a transferred layer is deposited on the surface of the cohesively stronger material. (See figure 3.5). The higher the surface free energy of the polymer, the greater will be the adhesive forces, although this is counterbalanced by the tendency of the high cohesive density solids to fail in a brittle manner with the result that the adhesive work, is reduced [68]. Frictional transfer is the most important characteristic of adhesive wear in polymers and this subject is dealt with in greater detail in section 3.5.

Some of the important features in adhesive wear include the following: (These are dealt with in section 3.5 and are only briefly mentioned here.)

(i) *The nature of the initial adhesion*

The initial junction strength will be a function of the interaction of the surface forces and the mechanical properties of the contact. Polymers above their glass transition temperature will adhere stronger than brittle polymers, and have the ability to conform to minor surface imperfections.

(ii) *The mode of failure at the junction and the criteria for film transfer*

During the wear process, brittle polymers normally fail at the original interface whereas the more ductile polymers transfer material to the counterface. An important aspect is the role of fillers and counterface roughness in the wear behaviour.

(iii) *The structure and thickness of the transfer layer*

Thin transfer films which develop during the sliding wear are restricted to what have been termed "smooth molecular profile" polymers. If bulky side groups are introduced into the polymer chain, the friction and transfer are high and transfer is in the form of lumpy polymer patches. The smooth profile implies that sliding of the polymer over the transferred film is easy and that friction values are low. Thin films approximately 50-100 Å thick may be transferred to the counterface [40].

In general, adhesion and transfer are likely to be most significant in wear when polymers

slide repeatedly over themselves or over relatively smooth metal surfaces. Under these circumstances, the specific wear rate almost invariably becomes constant after an initial period of "running-in" and it is then reasonable to assume that the sliding surfaces have reached steady-state conditions [20].

3.3.3 Fatigue Wear

Fatigue wear occurs in the presence of appreciable adhesion and several traversals of the same portion of the surface may be required before a fragment is finally detached [78]. These traversals over the same localized area involve a series of cycles of compression and recovery and are complicated by tensile stresses over the contact region arising from adhesion and tangential movement. In polymeric fatigue, tribo-cracking of the polymer molecules may be due to mechanical and thermal effects. Fatigue wear becomes increasingly important as the metal surface become smoother and the polymer more elastic. Direct microscopic evidence of fatigue failures is difficult to detect. Brown *et al.* and Atkinson *et al.* have attributed a sudden increase in the sliding wear of UHMWPE to fatigue [79,80]. Shallow pits and small cracks appear to align perpendicularly to the sliding direction in the UHMWPE surfaces after prolonged sliding. Ratner and Lure found that the addition of stabilizers to polymers to improve their resistance to oxidative degradation also improve their wear resistance in conditions where fatigue wear predominates [81].

3.3.4 Chemical Wear

Chemical wear is associated with a chemically active medium in the presence of an applied stress. An element of chemical degradation is almost always present in all wear processes. It can be in the form of mild chain scission. Even in the most favourable circumstances there is doubt as to the precise role played by the chemical reactions in the overall wear process. Invariably, bulk thermal decomposition or oxidation data are applied to reacting contacts without a detailed knowledge of the transient thermal conditions or the pressure at the contacts. Additional complications may arise from the uncertain effects of strain activation, the catalytic effect of clean metal surfaces and the part played by potentially active fillers [40].

3.4 PROPERTIES RELEVANT TO TRIBOLOGY

3.4.1 Chemical- and Structure Relations to Friction and Wear

The mechanical properties of a polymeric material are dependent on both the chemical and physical nature of the polymer as well as the environment in which it is used. Properties such as chain flexibility, intermolecular attractions, elastic modulus and crystallinity are ultimately linked to the basic constituent of the polymer. The mechanical properties are profoundly linked to the degree of chain branching and crosslinking, chain length and crystallinity of the polymer [82].

The low coefficient of friction of PTFE, for example, is generally ascribed to the intrinsically low adhesion between the molecules. The carbon atoms of the long, rigid PTFE molecules are effectively shielded by the surrounding fluorine atoms, thus reducing interchain forces and enabling the chains to slip easily over each other [20]. The tribological properties of the polyethylenes are not only dependent on their relatively simple structure, but also on the degree of chain branching and molecular weight. Figure 3.17 shows that the wear rate of polyethylene decreases significantly as the molecular weight increases [83].

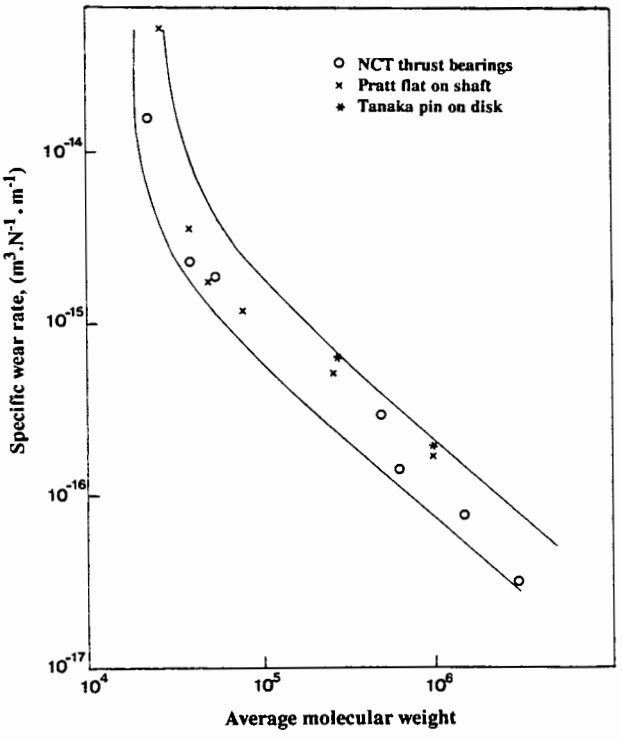

Figure 3.17: The variation of the wear rate of the polyethylenes with molecular weight. [After ref. 83].

Lancaster showed that the abrasive wear of a variety of polymers are inversely proportional to the product of the breaking strength and the elongation to break ($S\epsilon$) [69]. The product $S\epsilon$, is related to the energy of failure and hence the cohesion between the polymer chains *i.e.* the cohesive energy. The cohesive energy of the polymer may be calculated on the basis of the chemical constitution of the polymer. By using this concept, Giltrow showed that a non-linear relationship existed between the abrasive wear and the cohesive energies of thermoplastic polymers. (See figure 3.15). This non-linear relationship was attributed to the complex nature of thermoplastics [73].

The molecular mobility of the polymer molecules has a critical effect on the friction and wear processes. Crosslinking results in a more tightly bound network and this accounts for the decreased elongation to break and the increase in hardness. The presence of crosslinks would prevent the easy drawing out of the molecules to form a transfer film on the counterface [84-87]. Shen and Dumbleton studied the effects of high doses of γ-irradiation on the friction and wear properties of UHMWPE. The wear rates were higher than those of the unirradiated samples, and were ascribed to the inhibition of the formation of a transfer film on the counterface [84]. There are, however, reports that very low dosages of γ-irradiation improves the wear resistance of UHMWPE in a liquid environment [85].

Free solidified polymer melts are largely homogeneous and isotropic. Orientation caused by injection moulding cannot be prevented. Pressed sheets, on the other hand, are largely free from orientation. Brown *et al.* studied the effects of orientation in UHMWPE when the specimens were either hydrostatically extruded or tensile drawn. Their results show that, compared with the isotropic UHMWPE, wear rates are higher when the molecular chains are oriented perpendicular to the sliding direction. Furthermore, the wear rates were found to increase with an increase in draw ratio *i.e.* an increase in molecular orientation. It appears that orientation of the molecules perpendicular to the wear surface is less beneficial than when they are aligned parallel to it. The results show the importance of the method of production of a polymer bearing when molecular orientation at the wear interface is taken into account [88].

3.4.2 Mechanical Properties

3.4.2.1 Viscoelasticity

It is important to be aware of the mechanical and rheological properties of a polymer and understand the basic principles underlying its response to a stress [9]. The word *"viscoelastic"* is used to describe the mechanical response of materials exhibiting both the springiness associated with elastic solids and viscous flow characteristics associated with fluids [89]. The viscoelastic phenomena in polymers are associated with both long and short range rearrangements of the long-chain molecules, the rearrangements occurring on a continuous range of time scales [9,89]. This results in time-dependent shape and time-dependent force changes. Creep and stress relaxation are characteristic phenomena of a viscoelastic response. Since polymers are viscoelastic, their deformation is dependent on strain rate as well as temperature. McLaren and Tabor found that the friction of polymers on like material becomes less dependent on speed and temperature as the polymer structure becomes more rigid [90]. They reported that maxima occurred in the coefficient of friction *vs.* sliding speed curves and these could be correlated with the viscoelastic properties of the polymers. These curves closely resemble the dynamic loss characteristics (a measure of the internal friction) of the polymer as a function of frequency of deformation. The damping loss rises to a maximum at a characteristic frequency and then falls as the frequency is increased. Raising the temperature shifts the curve into the region of higher frequency. From the sliding speed v, at which the adhesion term reached its maximum and the corresponding frequency f, at which the viscoelastic losses in the polymer reached a maximum, the critical length involved in the sliding process ($l = v/f$) was found to be of the order of 50 Å. This is comparable with the length of a segment of the molecules. This suggests that the adhesion process of friction occurs on a molecular scale and the time- and temperature dependent properties of friction are closely connected with the viscoelastic properties of the polymer [90-92].

3.4.2.2 The role of mechanical properties in relation to the friction and wear of polymers

There are good indications that the friction and wear behaviour of polymers is largely governed by the mechanical properties of the polymer [39,69,72]. This is so because mechanical properties such as the hardness, elastic modulus, Poissons's ratio, yield stress and the elongation to break control the deformation of polymeric materials.

In the case of adhesive wear, the frictional force is the product of the shear stress τ and the real area of contact. The real area of contact is largely governed by the mechanical properties of the polymer. There is also evidence that it is the mechanical properties of the

polymer which govern the frictional losses when considering the ploughing component of friction [39].

Lancaster and Ratner *et al.* considered that in single pass abrasive wear, there is an approximately linear relationship between the wear rate and $1/S\epsilon$ for a number of polymers [69,72,93]. Since $S\epsilon$ is a measure of the toughness of the polymer, representing the work required to detach a particle from the wearing surface by tensile failure, this relationship again emphasizes the role of plastic deformation in the wear process [93]. Ratner *et al.* suggested that the wear rate is proportional to $\mu/HS\epsilon$, where μ is the coefficient of friction and H is the indentation hardness [72]. Lancaster, however, found that the correlation between wear rate and $1/S\epsilon$ becomes significantly worse if values of μ and H are incorporated [93]. It should be borne in mind that in conditions of repetitive sliding, the wear process is complicated by transfer of material to the counterface and the correlation between wear rates and specific mechanical properties, S and ϵ, may be unrealistic. For the case of adhesive wear, linear polymers such as PTFE and polyethylene which show relatively long elongations to rupture (*ca.* 450-500%), are able to transfer thin films onto the counterface. Brittle polymers such as PMMA and polystyrene, which exhibit smaller elongations to break (*ca.* 10%) do not form these layers on the counterface at room temperature [39].

As far as mechanical properties are concerned, Briscoe and Tabor noted that although the mechanical properties of the polymer play and important role in the wear processes, a detailed knowledge of the mechanical properties of the polymer does not enable us to predict accurately the level of wear [39].

3.4.3 Lubrication

3.4.3.1 Definition and modes

The tribological processes, *i.e.*, the contact, friction and wear processes are, in general, related to direct physical interaction between relatively moving surfaces [94]. By definition, any material that reduces friction and wear or surface damage of sliding components may be called a lubricant. In the absence of lubricant films, marked adhesion may occur at the regions of intimate contact, the friction is high and plucking of material from one surface to the other occur and result in wear. The purpose of lubrication is thus to separate surfaces

moving relative to each other with a film of a material which can be sheared with low resistance without causing damage to the surfaces [94,95].

For a lubricant film to be effective it should possess two main properties. First, it should prevent solid-solid contact thus reducing wear; secondly it should possess a low shear strength thus ensuring a relatively low friction. Sometimes solid lubricant films are used *e.g.* graphite or MoS_2 but these are worn away by repeated traversals. The best lubricant is basically a fluid since this may be sheared an infinite number of times without failing from wear or fatigue, though of course chemical degradation may take place [95]. Depending on the thickness of the lubricant film (ranging from 10^{-4}m to 10^{-9}m), the interfacial height distribution of the lubricant film and the degree of geometric conformity, three basic forms of fluid lubrication can be distinguished [94,95].

(i) Hydrodynamic lubrication (and Elastohydrodynamic lubrication)
(ii) Thin film or mixed lubrication
(iii) Boundary lubrication

(i) Hydrodynamic and Elastohydrodynamic lubrication

Within the hydrodynamic and elastohydrodynamic lubrication regimes, the mating surfaces are separated by a viscous fluid whose thickness is larger than the surface roughness measure (R_a) of the surfaces, as shown in figure 3.18a. The friction resistance is due to the internal friction (viscosity) of the lubricant. In this regime, the tribological behaviour of the system is determined by the rheology of the lubricant and can be calculated or estimated by the methods of fluid mechanics. If the lubricant system under consideration consists of non- conformal concentrated contacts, the elastic (Hertzian) deformation of the surfaces and the pressure dependence of the lubricant's viscosity must also be taken into account. This leads to the regime of elastohydrodynamic lubrication. Since in regime I, no direct physical contact interactions between the surfaces occur, wear processes cannot take place (except surface fatigue wear, cavitation wear or fluid erosion) [94].

(ii) Thin film or mixed lubrication

If under conditions of hydrodynamic or elastohydrodynamic lubrication, the lubricant viscosity or the velocity decreases as the load increases, the lubricant film gets "thinner" and the separation of the surfaces decreases. In thin film lubrication, surface asperities

penetrate and disturb the desirable laminar conditions of flow so that only part of the load is carried by hydrodynamic forces and the remainder by contacting surface asperities as shown in figure 3.18b. In this regime the friction resistance is due partly to the shearing of the lubricant film and partly to asperity interactions [94,96].

(iii) Boundary lubrication

True boundary lubrication occurs only when contact pressures are high enough and sliding velocities low enough for hydrodynamic effects to be completely absent and the entire load is then carried by an extremely thin (a few Ångströms), multi-molecular layer of boundary lubricant as shown in figure 3.18c. Within the boundary lubrication regime the physico-chemical interactions at the solid/lubricant solid/interface become of paramount importance and determine the friction and wear behaviour of the system. Today, the term boundary lubricant is usually extended to cover other types of lubricant that do not function hydrodynamically, such as chemical coatings, surface films and lamellar solids such as graphite. Whilst a good boundary lubricant may reduce the coefficient of friction, it is much more significant that the interfacial damage be reduced a thousand fold [97].

The main purpose of a boundary lubricant is to interpose a film between the moving surfaces that is able to reduce the amount of direct solid/solid interaction and that is itself easily sheared. This is best provided by an interfacial film consisting of long-chain molecules possessing the following properties:

(a) strong attraction between the chains to resist penetration by surface asperities (thus mitigating wear processes),
(b) low shear strength to give a low friction and a
(c) high melting point so that it provides solid-film protection to a high temperature [94].

In general, the lubrication regimes are highly complex. While the laws relating to hydrodynamic and elastohydrodynamic regimes may now be satisfactorily understood, the same cannot be said of mixed and boundary regimes, where all aspects of the materials involved can operate simultaneously (*e.g.* metallurgy, nature of oxide films, physico-chemical properties of the lubricant *etc.*) [98].

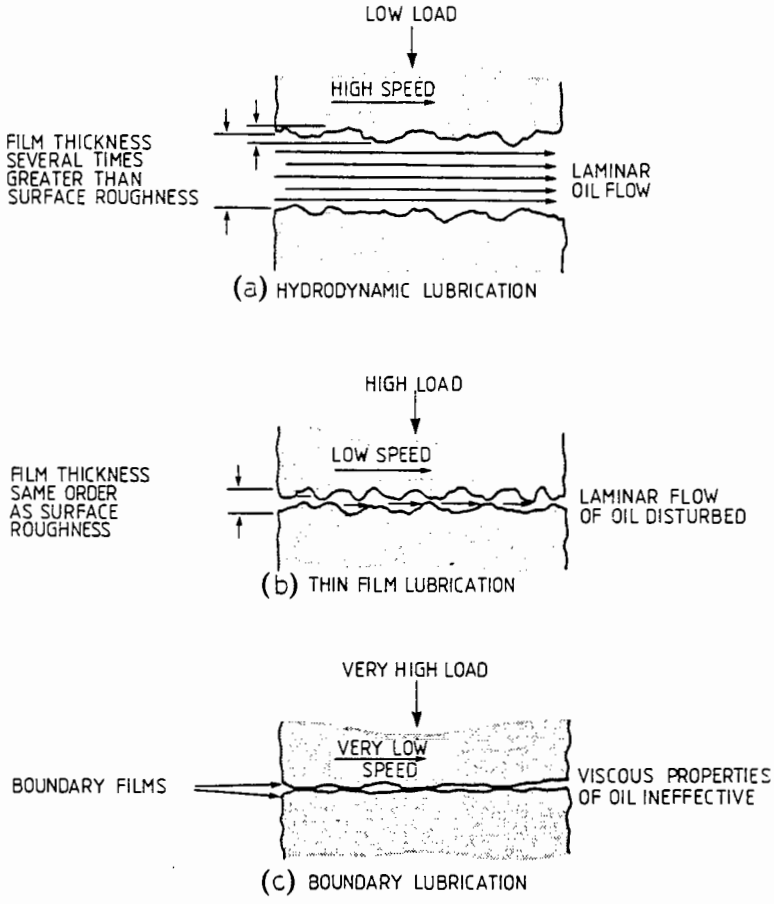

Figure 3.18: A schematic representation of the various modes of lubrication, hydrodynamic, thin-film and boundary lubrication. [After ref. 96].

3.4.3.2 Mechanism of self-lubrication

The two basic requirements of any solid lubricant are low shear strength and the ability to form a strongly adherent film on metal substrates [21,99]. Self-lubrication may be produced by:

(i) Interface sliding of structurally anisotropic components such as graphite, molybdenum disulphide or diselenides.
(ii) Interchain sliding in linear thermoplastics such as PTFE or polyolefins [100].

Typical inorganic solid lubricants include the element carbon in its graphitic form, lamellar compounds such as molybdenum disulphide (MoS_2) and tungsten disulphide (WS_2). These

materials reduce friction and wear by interposing between the rubbing surfaces a thin adherent layer of material that shears easily and prevents direct contact between the substrate materials. Unless the solid lubricants are bonded to the substrate, the powders are soon brushed away and the lubrication is lost. Some solids have the ability to self-bond to metal surfaces, apparently due to their chemical reactivity or to the presence of loosely bound electrons. Examples of lamellar solids that are capable of some degree of self-bonding to metals include graphite and molybdenum disulphide. In the case of MoS_2 on steel, strong metal to sulphur bonds are thought to form between the MoS_2 particles and the steel surface. To extend their wear lives and achieve other advantages *e.g.* to serve as protective coatings, lamellar solids are bonded to surfaces by various adhesives. These include thermoplastic resins such as acrylics, thermosetting resins such as alkyds and phenolics and inorganic binders such as phosphates and silicates. These powders can also be impregnated into the solid polymers for gears, bearings, seals and similar applications to form "self-lubricating" bearings. With such composites the sliding process continues to feed a thin film of MoS_2, for example, to the surfaces so that the friction remains low even after prolonged sliding [21,99,101].

3.4.3.3 The effect of water on the friction and wear of polymers

Although dry bearing materials do not always operate in dry conditions, it is important to emphasize that fluid lubrication is not always beneficial to all polymer composites. The work of Evans shows that when the relative solubility parameter ξ, which is a measure of the intermolecular cohesion within the fluid, is close to that of the polymer, high wear rates are obtained [102].

Fluids generally reduce the coefficient of friction but may either increase or decrease the rate of wear. Many fluids reduce the wear rates of amorphous polymers such as PPO and PMMA but high wear rates are obtained in those fluids that are strongly adsorbed into the polymer. For the more crystalline polymers which rely on transfer film formation on the counterface to achieve low wear in dry conditions for example PTFE composites, the introduction of a fluid disrupts the transfer film, exposes the original surface topography of the counterface and leads to an increase in the wear rate [21,102]. This effect is illustrated in figure 3.19. In these cases, it is particularly interesting to note that water is particularly deleterious in preventing transfer film formation and the effects of water on the wear of polymers constitutes a challenging problem [20,102,103].

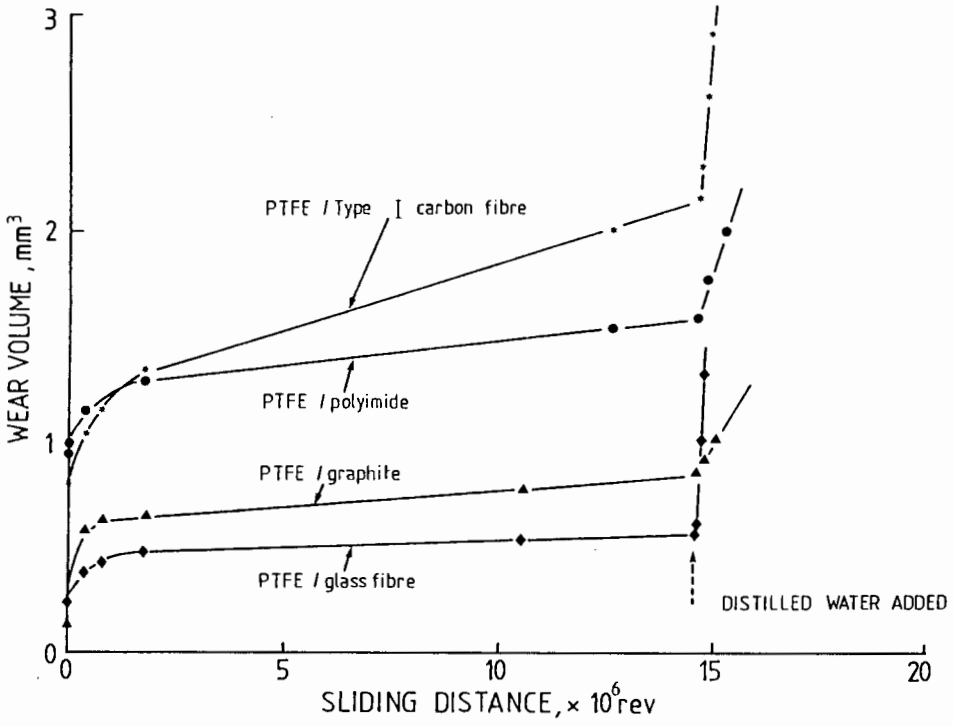

Figure 3.19: The effect of introducing water on the wear of four PTFE composites. [After ref. 21].

3.4.3.4 The boundary lubrication ability of water of polymers sliding against steel.

The study of the water lubrication ability of polymers under boundary lubrication conditions have been reported by several authors [103-109]. It has been shown that for good water lubrication, one of the two sliding surfaces must be hydrophilic. The friction of polymers sliding against steel will decrease under water lubrication because the hydrophilic nature of the steel surface allows the formation of a weakly held water film on these sliders [106].

Tanaka found that transfer occurs in water lubrication as well as under dry sliding conditions. The amount of transferred material is similar in both cases but the characteristics of the worn surfaces are different. The increase in wear under water lubrication may be due to a modification of the surface structure of polymers by water rather than the effect of modification of the counterface by polymer transfer [103].

3.4.4 The Effect of Bearing Pressure

For unfilled polymers, the wear rate is generally independent of the bearing pressure up to some critical value which is typically one third of the compressive strength of the polymer [110]. Anderson *et al.* found that for PTFE composites acting as thrust washers rubbing against mild steel counterfaces, the specific wear rate increases rapidly at stresses greater than 10 MPa as illustrated in figure 3.20. They accounted for the increase by a change in wear mechanism from stable transfer film formation to a mechanism which is likely to be abrasion by wear debris [111]. Data for UHMWPE as thrust bearings indicate that the wear rate is independent of the pressure over a smaller range as shown in figure 3.21 [110].

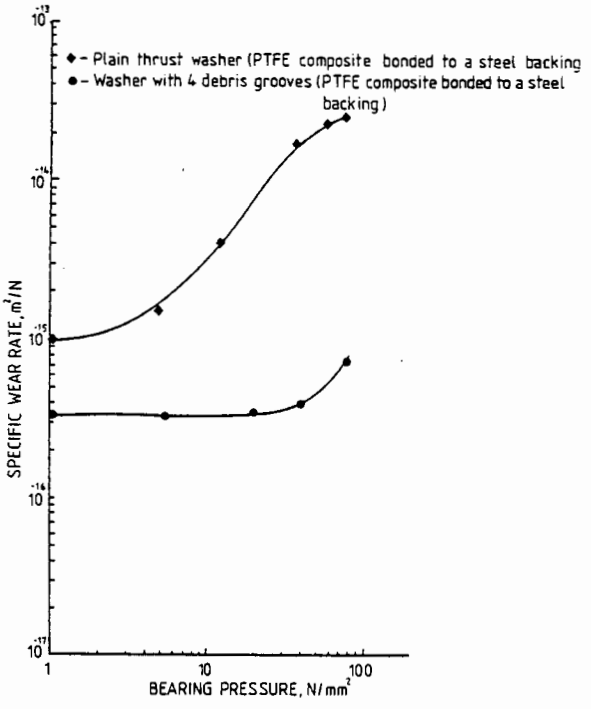

Figure 3.20: The variation of specific wear rate with bearing pressure for a PTFE composite. The wear rates are greatly reduced by grooves in the thrust bearing that permit the wear debris to escape rapidly. [After ref. 111].

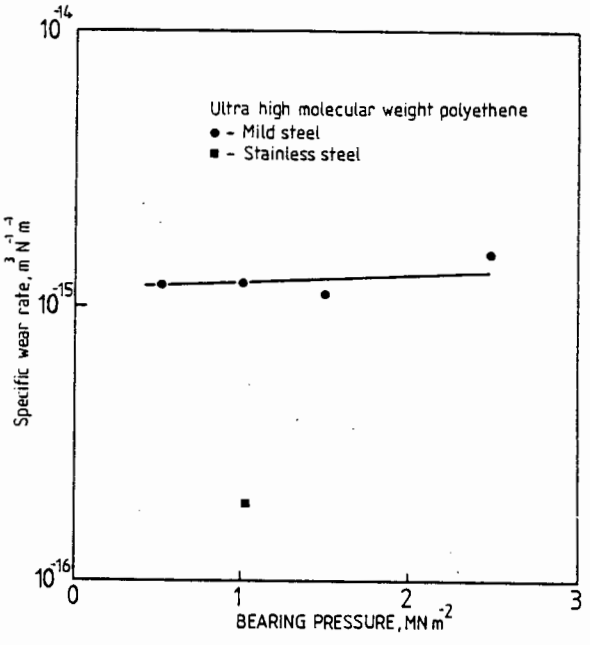

Figure 3.21: The variation of specific wear rate with bearing pressure of UHMWPE on a mild steel counterface. [After ref. 110].

By using a pin-on-disk configuration, Dowson *et al.* have reported increases in the wear rates by a factor of 2 to 4 after prolonged sliding [112,113]. Similar discontinuities of wear rate have been observed in thrust bearing tests at higher bearing loads [110,114]. In the pin-on-disk tests, this transition was concurrent with the appearance of small cracks in the

polymer surface perpendicular to the direction of sliding. However, for the thrust bearing tests, the transition was associated with the disruption of the third body film on the metal surface. Figure 3.22 shows that the sliding distance to the onset of the transition had a strong dependence on the applied load, a characteristic usual of fatigue.

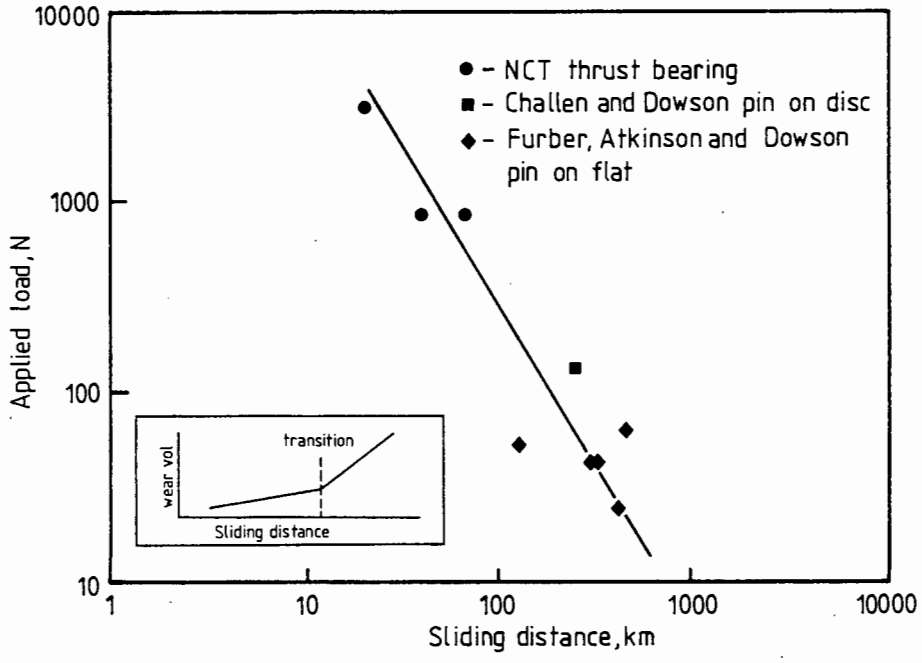

Figure 3.22: Load *vs.* sliding to the onset of a wear transition for UHMWPE sliding against mild steel. The inset shows the wear transition in a wear volume *vs.* sliding distance curve. [After refs. 110, 112 and 113].

3.4.4.1 The "pv" limit

The performance of polymer bearing composites depends on a complex mixture of parameters and wear processes and cannot be adequately described by a single index. The *"pv"* factor is frequently used and is the product of the load on the projected bearing area, p and the sliding velocity, v [115-117]. It is usually found that above a maximum combination of bearing pressure and velocity, that the wear rate increases dramatically as illustrated in figure 3.23. Since temperature is particularly important for thermoplastics whose melting points are relatively low, it seems reasonable to assume that the limiting *"pv"* values are those at which the total temperature rise at the surface (the flash temperatures at the asperity contacts superimposed on the mean surface temperature resulting from the

general dissipation of frictional heat) reaches a value near to the melting or softening point of the polymer [117].

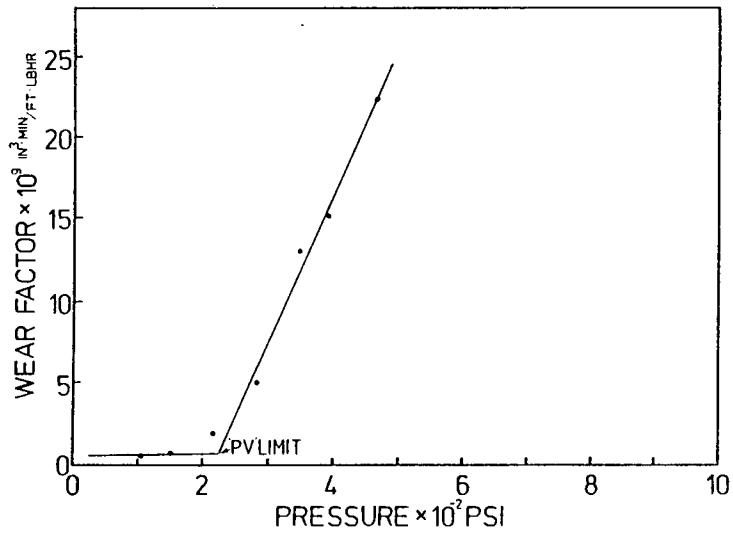

Figure 3.23: Wear rate *vs.* pressure for VHMWPE against stainless steel in a dry thrust washer wear test. [After ref. 84].

3.4.5 The Effect of Sliding Speed

The friction and wear behaviour of polymers as a function of sliding speed has been researched by several authors and it is of interest to report on some of their results [90,91,117-125]. The effect of speed in polymer wear plays a major role through its viscoelastic response to stress and the generation of frictional heat. Research workers have observed complex, non-monotonic relationships between the wear, frictional characteristics and the sliding speed. The complexity arises from the interaction of both the deformation and interfacial components of wear, the type of polymeric and counterface material as well as the effects of transfer to the counterface [118-120]. For these reasons, no unique relationship between wear rate and speed is expected and experiments show that the relationship may exhibit a maxima, minima or show little variation. By analyzing data on the effect of velocity on the frictional characteristics of polymeric materials, we should be able to distinguish between two conflicting tendencies: [118]

(i) the effect of the straining rate on the mechanical properties of the interacting materials (taking relaxation phenomena into account).

(ii) the effect of sliding velocity on frictional heating in the friction assembly which causes corresponding variations in its mechanical and adhesion properties.

According to Lancaster, the effect of velocity in wear is mainly due to surface temperature effects [117]. His results show that the wear rate of polymers increased rapidly above a critical velocity. This abrupt increase in wear rate (figure 3.24) was attributed to the softening or melting of the polymer due to the increased surface temperature at high velocities. By using modified forms of Jaeger's equations, he showed that flash temperatures are more sensitive to sliding speed than applied load [117,125]. In these tests, the period of sliding was kept relatively short so as to limit the mean surface temperature increase.

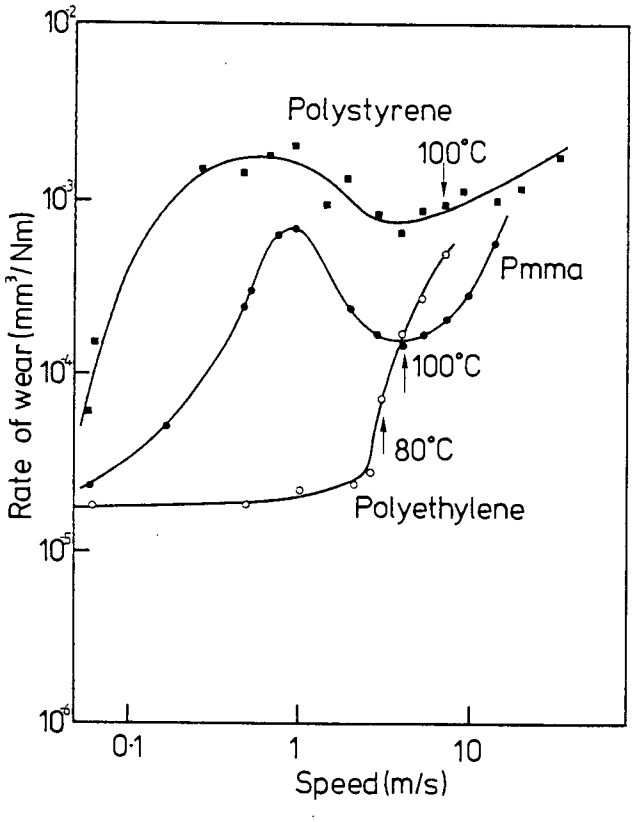

Figure 3.24: Variation of steady-state wear rates with sliding speed. † indicates the speed at which the calculated flash temperature reaches the melting/softening point of the polymer. Measurements were made on a pin-on-ring apparatus against mild steel of 0.15 μm R_a surface roughness. [After ref. 117].

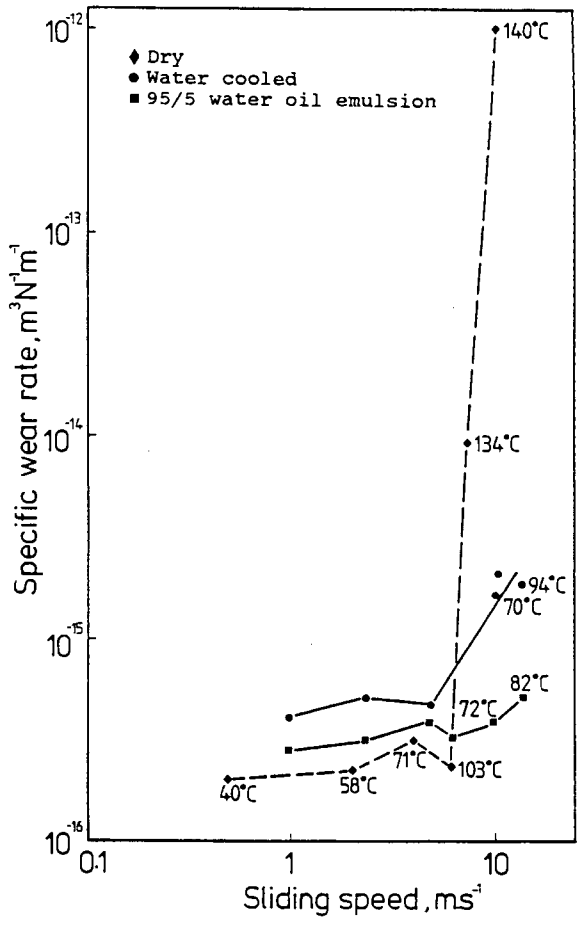

Figure 3.25: The variation of specific wear rate of an UHMWPE pin, on a steel disc, with speed. The temperatures plotted are the sum of the measured surface temperature and the calculated flash temperature at each velocity. [After ref. 110].

The maximum in the wear rate/speed curve can only be explained by postulating a direct effect of speed on wear, independent of associated temperature effects. As the sliding speed increases, the moderate increases in temperature increase the elongation to break, ϵ, to an extent which more than compensates for the breaking strength, S. It is suggested that the wear rate is directly proportional to $1/S\epsilon$ thus accounting for the observed minimum.

In pin-on-disk tests carried out by Anderson at NCT, such a dramatic increase was also observed for UHMWPE under dry conditions, but was absent under lubricated conditions using both water and a 95/5 water/oil emulsion as shown in figure 3.25 [110]. The temperature plotted are the sum of the measured mean pin temperature and the flash temperature obtained by Lancaster's formulae. The magnitude of the critical sliding speed is also strongly dependent on the thermal conductivity of the counterface against which the polymer slides, the critical sliding speed being shifted to higher values as the thermal conductivity of the counterface increases. (See figure 3.26).

3.4.6 The Effect of Temperature

The mechanical properties of all polymers are adversely affected by an increase in temperature, so that many of the temperature-dependent properties have a strong influence on the tribological behaviour of the polymer [84,110]. The temperature rise at the sliding interface affects the wear of the polymeric materials much more significantly than that of their metal counterparts because of their lower thermal conductivities and melting points as illustrated in figure 3.26. The reduction in strength results from the weakening of the intermolecular bonds between the polymer chains as the temperature is increased.

The temperature at the bearing surface can arise either due to a high environmental temperature or to the generation of frictional heat at the sliding interface. It is useful to consider the interfacial temperature as the summation of two parts, *viz.*: [84,110]

(i) The mean surface temperature immediately beneath the bearing surface, results from the ambient temperature and the overall efficiency with which the bearing assembly dissipates frictionally generated heat. The mean surface temperature may be measured by placing a thermocouple at a short distance below the surface.

(ii) The flash temperature, which is the local temperature rise at points of real contact.

The difficulty of estimating the flash temperature either theoretically or experimentally is well known and the reliability of the estimation is critically dependent on the assumptions made [84,110,126-128].

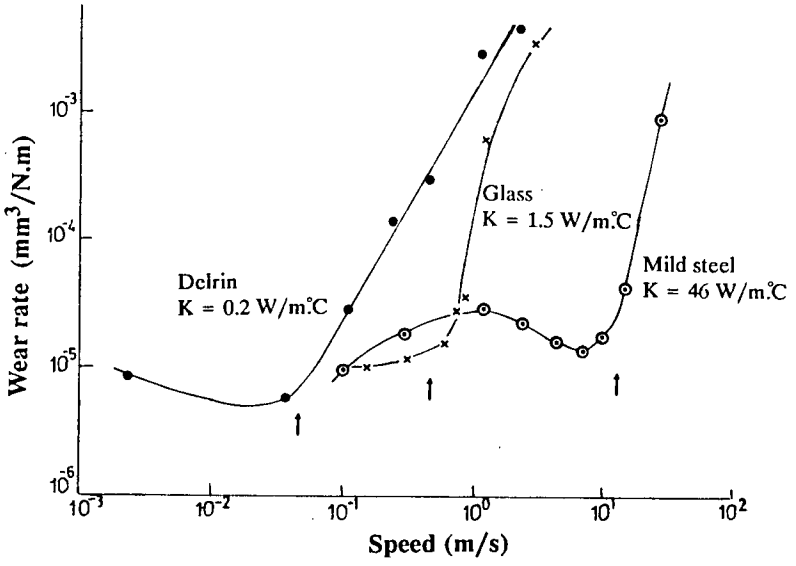

Figure 3.26: The effect of thermal conductivity (K) of the counterface on the wear rate-speed relationship for polyacetal. ↑ is the calculated speed at which asperity contact temperatures reach the melting point (175°C) of the polymer. For polyacetal K = 0.2 $W.m^{-1}.K^{-1}$; for glass K = 1.5 $W.m^{-1}.K^{-1}$ and for mild steel K = 46 $W.m^{-1}.K^{-1}$. [After ref. 130].

Many parameters influence the friction and wear characteristics of polymeric materials, making it difficult to isolate the effect of temperature alone. Lancaster, for example, found that the heat generated at the sliding interface depends more on speed than on load [71]. The results of Anderson and Robbins show that the wear rates of polymers is determined by the mean temperature of the counterface, whether generated by a high ambient temperature or by frictional heat [129]. It is also found that above a certain critical temperature there is a rapid increase in wear as a consequence of thermal softening, leading to extrusion and gross polymer flow [113,117,126]. If the input energy is not removed at a sufficient rate, the polymer will reach a temperature at which severe wear will

occur [110,131]. The steady state mean surface temperature attained will then depend on the heat transfer properties of the bearing assembly. The mean surface temperature at the sliding surface, θ, is given by:

$$\theta = R\mu pv \tag{3.27}$$

where the product μpv constitute the energy input into the sliding interface and,

μ is the coefficient of friction
p is the bearing pressure
v is the sliding velocity and
R is the thermal resistance of the bearing assembly.

Several authors have attempted to thermally model the temperature rise in a sliding pair, yet there appears to be no satisfactory model for the surface temperature in polymer sliding [71,84,126-132]. The first significant analytical contribution based on the assumption that the entire bearing load is supported on a single plastically deformed asperity, was obtained by Jaeger [125]. Since then, many authors have modified Jaeger's equation to calculate the interfacial temperatures. As yet, there is no general agreement on what the critical temperature for severe wear is. Lancaster calculated the critical speeds required to generate temperatures reaching the melting or softening points of several polymers and found them to be in good agreement with experimental measurements of the speeds corresponding to the *"pv"* limit of the polymer. The wear rates of HDPE and POM increased at the *"pv"* limit corresponding to temperatures of 80°C and 175°C respectively [117].

Several other authors have inferred similar conclusions. Kar and Badahur found that the temperature at the interface increased steadily and failure of HDPE and POM occurred because of thermal softening of the polymer [126]. They showed that a good agreement held between the steady state experimental temperature rise and those calculated by an equation they developed. Challen and Dowson presented an analytical thermal analysis for the calculation of the maximum interfacial temperature in a pin-on-disk wear tester for UHMWPE and showed that severe wear occurred when the temperature exceeded 125°C [113]. Rhee and Ludema, however, do not agree that the surface temperature can be taken as the melting point of the polymer at the point of severe wear [130,131]. Their analysis

show that for POM the sliding surface temperature was appreciably higher than the melting point of the polymer and may reach the decomposition temperature of the polymer [131].

These models are useful, but may not be realistic when a transfer film is formed on the metal counterface, as the temperature at the interface will change with time [131]. The transfer film is important because it is thicker than the expected height of the asperities and as such there are no asperities in contact. Furthermore, the transfer film will also lower the ability of the counterface to conduct heat away from the counterface. Rhee and Ludema assert that in order to develop good physical models of sliding surfaces, it is useful to measure surface temperatures experimentally and from these data develop good physical models [131]. Although the thermocouple is placed at a small distance from the sliding surface, the surface temperatures should give an idea of the temperatures existing at the interface as a function of the sliding conditions.

It is evident that the interfacial temperature plays an important role as far as the stability of the transfer film is concerned. Several researchers have looked at the effect of independently controlling the counterface temperature in dry oscillatory sliding. Evans *et al.* and Blanchet *et al.* have developed relationships between the temperature and the friction and wear characteristics of UHMWPE [133,134]. Their results indicate that for moderate temperatures between 15°C and 45°C, as the temperature of the counterface was raised there was an increase in coverage of the protective transfer film on the metallic counterface, with the result that the wear rates and friction coefficients decreased. A moderate increase in temperature aids the deformation process and a smoother film reduces the wear rates by limiting polymer/metal contact.

3.4.7 The Effect of Counterface Roughness

The counterface roughness has been shown to be one of the principal factors affecting the friction and wear behaviour of polymers. For sliding applications of polymeric materials, it is important to investigate the relationship between the wear rates and mechanisms of wear and counterface roughness. Recently, several researchers have studied the effect of counterface roughness on polymeric wear behaviour [134-142]. These workers have shown that for the polymers investigated, a minimum in wear rate existed at a certain counterface roughness. An examples of this minima is illustrated in figure 3.27. Dowson *et al.* found a minimum in wear rate at a roughness of about 0.03 μm R_a for UHMWPE against stainless

steel under dry sliding conditions (figure 3.27) [138]. Their very smooth counterfaces were prepared by polishing while the rougher surfaces were prepared by grinding.

Thus, the different machining process could account for the observed minimum. The minimum in wear rate at the optimum roughness is attributed to a low in both the lumpy transfer due to adhesion, and the ploughing effect of abrasion. The authors did, however, find that some of the specimens produced by lapping had R_a values which overlapped those produced by fine grinding. For these counterfaces, the wear rates were found to be similar at equal values of R_a [138]. In general, it would appear that an optimum counterface roughness for minimum wear may exist, but only for those polymers that rely on transfer film formation in order to exhibit low wear [20].

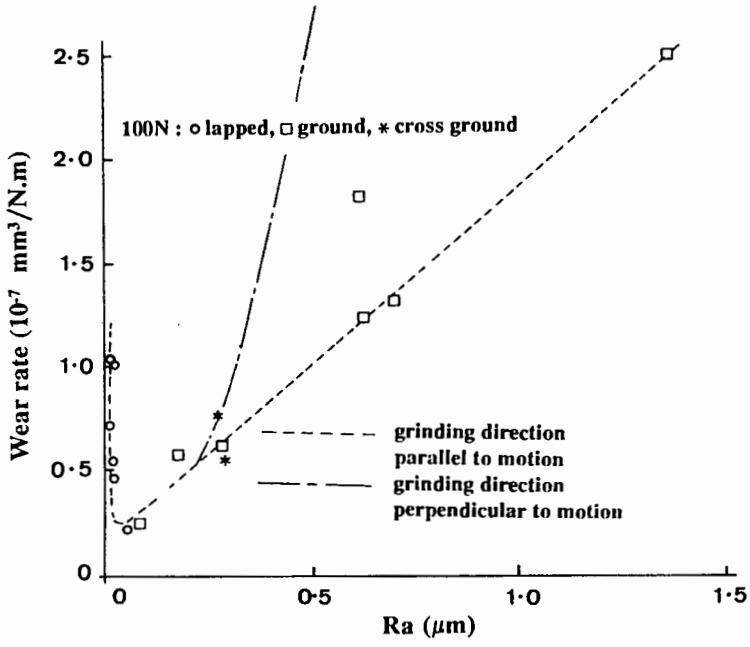

Figure 3.27: The effect of surface roughness on the wear rate of UHMWPE in dry reciprocating sliding on an austenitic stainless steel disk. A minimum in wear rate occurs at a roughness of 0.03 μm R_a. [After ref. 138].

The topography of the metal counterface also affects the mechanism and magnitude of wear. Many studies have been performed to identify the important topographical features and how they influence the wear mechanism [64,74,144-147]. Jain and Bahadur have studied the variation in topographical parameters of the metal surface such as the root-mean-square (r.m.s) and the centre-line-average (R_a) roughness, slopes and radii of

curvature of the asperities [146,147]. Their results indicate that a number of surface roughness parameters undergo a marked variation during the early part of sliding but that the variation is statistically insignificant during the steady-state wear. These parameters are important because the real areas of contact between the polymer and the metal counterface does not only depend on the modulus of elasticity of the contacting bodies and the normal load, but also on the shape, size, standard deviation and distribution of the heights and radii of curvature of the asperity peaks.

The work of Hollander and Lancaster involved a detailed topographical analysis of the metal counterface [74]. They showed that the wear rate decreased with increasing values of the average radius of the asperities. (See figure 3.16). Lancaster's results indicate that the wear rate in single pass experiments is directly proportional to the base angle of the cone of a hard indentor. (See figure 3.14) [69].

3.4.7.1 The effect of grinding direction on the metal counterface

There have been relatively few studies concerned with the effect of grinding direction on the wear of polymers. Dowson *et al.* found that the wear rates on cross-ground surfaces are much more sensitive to R_a than those obtained on parallel ground surfaces as illustrated in figure 3.27 [138]. This is clearly due to the increased abrasive effect when the surfaces are cross ground. The continuity in the curve of low R_a values for both types of counterfaces, suggest that the scale of the asperities measured in terms of R_a are more important than the grinding direction. In a later paper by Dowson *et al.*, a detailed account is given on the effect of single transverse and longitudinal scratches on a stainless steel counterface in linear reciprocating wear tests [148]. The study showed that a single shallow indentation in the form of a scratch transverse to the sliding direction can increase the wear rate of polyethylene by an order of magnitude, whereas longitudinal scratches increase the wear factor to a smaller extent. The results of these tests are shown in figure 3.28. The piled-up metallic material flanking each transverse scratch is primarily responsible for the increased wear rates. If remedial lapping is used to remove most of the piled-up edges, the wear rates return essentially to those recorded for the appropriate roughness of the unblemished surfaces. Friedrich *et al.*, however, found that the wear rates for unfilled PEEK was higher when the sliding direction was parallel to the grooves on the counterfaces [149]. This they attributed to a more pronounced formation of a transfer film when the sliding is conducted perpendicular to the grooves thus reducing the abrasive component of sliding wear. The R_a

and R_t values are much lower after the sliding for the perpendicular case than when the sliding direction is parallel to the grooves.

From the studies on the effect of grinding direction, it is clear that when the microploughing and microcutting effect of metal counterface is dominant, high wear rates will be obtained, while a smooth transfer film will ensure an adhesive character and lower wear rates.

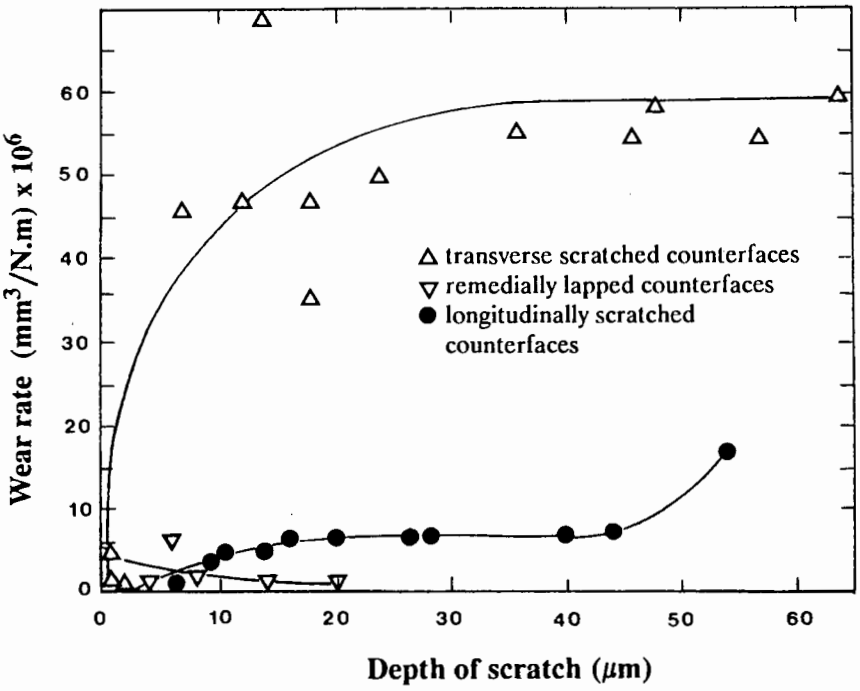

Figure 3.28: The variation of wear rate with depth of an imposed imperfection on the metal counterface. [After ref. 148].

3.4.8 The Effect of Type of Motion

The tribological behaviour of polymers in oscillatory or reciprocating motion can be quite different from that found in unidirectional sliding [88,133,134]. In the former case the direction of motion is not constant. In an oscillating test the wear track describes an arc while in a reciprocating test it follows a straight line [88].

The major difference between the two cases is that wear debris tends to remain trapped within the oscillatory/reciprocatory contacts, while the debris can easily escape from the interface during unidirectional sliding. In both cases, the tribological behaviour of the

polymer/metal couple is dictated by the build-up and maintenance of the transfer film formed on the metallic counterface. During continuous sliding wear, for example, in a pin-on-disc configuration, wear debris can be flung from the disc by the centrifugal force, while the entrapment of debris in a oscillating or reciprocating couple could either be beneficial or detrimental, depending on the nature of the debris [133,134].

The transfer film and wear debris (third bodies) can play a protective role and reduce wear by limiting the contact between the polymer and metal surfaces. Brown *et al.* found that the steady-state wear rate of UHMWPE against relatively smooth, dry stainless steel takes place by the same basic wear mechanisms, whether unidirectional or reciprocating motion is used. They found that the wear rates in reciprocating motion are about 2.5 times less than those in unidirectional tests. Streamer wear debris were produced in unidirectional motion, whereas the debris were in a roll or powdered form in reciprocating motion [88]. In typical engineering bearings of the journal and thrust type, the rubbing surfaces are highly conforming so that they are much less efficient in expelling wear debris compared with non-conforming geometries such as gears and cams [116].

3.4.9 The Effect of Fillers

Most commercial polymer-based materials used in industry as dry bearing materials commonly incorporate fillers and reinforcements, not only to improve the tribological, mechanical and thermal properties, but also to reduce material costs and to improve the processability of the polymer [6,20,110] A wide range of materials is added to polymers and these may broadly be classified as additives, reinforcing agents or fillers. Additives are solids or liquids used primarily as colourants, UV absorbers, plasticizers, flame retardants and lubricants. Besides additives, a variety of particulate and fibrous materials are also frequently mixed with polymers. Fibres normally increase the strength of the polymer and are termed reinforcing agents. Some of those that are frequently mixed with polymers include glass-, carbon- and metal fibres. Fillers are added for reasons other than increasing the strength of the polymer. These fillers include calcium carbonate, wood flour, carbon black, glass spheres, metallic powders and flakes, silicate materials such as clay, talc and mica, and other synthetic polymers [6]. Some of the most widely used fillers and reinforcing agents are listed in table 3.3.

Function	Filler
To improve mechanical properties	Asbestos, Carbon, Glass Silica, Metal Oxides Textile Fibres
To reduce friction	Graphite, MoS_2, PTFE Silicones, Mineral Oils
To improve thermal conductivity	Bronze, Graphite Powder

Table 3.3: Fillers and reinforcements of interest for tribological applications. [After ref. 20].

When the polymer composite is used in sliding wear, the particle size, aspect ratio, hardness, concentration, alignment as well as the nature of the interface between the polymer and the particles are important [6,40]. Most commercially available polymers usually contain around 15-25% by volume of filler [20]. The matrix determines the tribological performance at low (10%) inclusion volumes whilst at higher (50%) volumes, the reinforcement dominates [53]. Although fillers and reinforcing fibres significantly improve many mechanical properties of the polymer, it is not valid to assume that they always improve the friction and wear properties also [20]. Graphite, for example, when added to polymers to reduce friction may also improve mechanical properties but can result in greatly increased wear in vacuum. An increase in friction may occur when glass fibres are added to polymers in order to increase strength and stiffness.

The selection of suitable fillers is thus usually a compromise between the properties of the polymer and its friction and wear behaviour [20]. A composite such as filled PTFE shows a wear resistance of over 1000 times that of unfilled PTFE, but at the same time maintains approximately the same level of frictional work [150]. It would appear that the choice of filler content and concentration is purely empirical as the mechanism of filler action in reducing wear is not well understood [20].

3.4.9.1 The role of fillers in friction and wear of polymers.

There is a scientific and technological need to develop an understanding of the action of fillers in reducing wear. Lancaster studied the effect of carbon fibres incorporated in PTFE [20]. Two types of carbon fibres were used in the investigation, a high modulus (type I) and a high strength (type II) carbon fibre. Fibre orientation can play a part in the wear process and a minimum friction and wear were obtained with the fibres oriented normally to the sliding surface. The carbon fibres are exposed at the surface of the composite and support a significant part of the applied load. In addition, the high strength carbon fibres (type II) are considered more abrasive than the high modulus variety (type II). The abrasiveness of type II fibres is sufficient to modify the counterface topography of the steel during sliding so that the wear rates of these composites are much less sensitive to the magnitude of the initial roughness [150]. The abrasion process may produce an optimum surface roughness which facilitates good adhesion. Very abrasive fillers such as glass fibres may severely damage a soft counterface and increase the wear rate of the composite [69].

Glass-fibre reinforced PTFE is considerably more abrasive than carbon-, graphite- and bronze- filled versions [116]. The degree of surface damage to the counterface by the filler will also depend on the relative hardness of the counterface. Very soft counterfaces such as aluminium alloys are readily damaged by glass fibres, whereas harder counterfaces such as tool steels are merely polished [20]. It would generally appear that the improved wear rates by hard fillers are caused by intensive stresses at local points on the counterface. These points then provide suitable mechanical and chemical interactions to allow the polymer transfer film to adhere strongly to the counterface. Data by Briscoe and Steward shows that for carbon systems, the mean coefficient of friction is a maximum and the wear rate a minimum for an initial counterface roughness of 0.4 μm R_a. Thus it appears that the greater the frictional work dissipated in the contact, the lower the wear rate. If some of this energy is used to create good adhesion between the counterface and the transfer film, then the observation is consistent with the view that the filler particles act as stress intensifiers in the contact region leading to abrasion of the counterface [143].

There is evidence that chemical reactions take place between solid lubricants and metals during frictional loading [151]. Briscoe found that an inorganic mixture of 5% CuO and 30% Pb_3O_4 produced a marked reduction in the wear when added to HDPE [152]. It is suggested that these filler particles promote the formation of a strongly adhered film to the metal counterface while leaving the nature of the film unaltered. These fillers were

ineffective when glass or aluminium were used as counterfaces but strong adhesion occurred between the polymer and a steel counterface. Steel surfaces rougher than a few μm show no improvement with the filler as the abrasive component was dominant [152]. It would generally appear that chemical effects are important in the transfer process but that it is difficult to identify the precise mechanism which produces enhanced adhesion of the polymer film to the counterface [143].

3.5 POLYMER TRANSFER AND THE TRANSFER FILM

3.5.1 The Importance and Structure of the Transfer Film

It is generally considered that the formation of a stable polymer transfer film onto the metal counterface plays a crucial role in the friction and wear characteristics of the couple [80,134,153].

It would also appear that low wear rates are only obtained when a coherent transfer film is firmly established onto the counterface surface [20]. For ductile polymers such as polyethylene, the intensity of wear is reduced by 10 to 15 times by the formation of the transfer film [118]. Transfer films also show their beneficiality in that severe wear may be postponed to a 50 °C higher temperature than in a system without the film and that it can also act as a self-lubrication mechanism in metal-polymer pairs [103,153]. Pooley and Tabor have shown that the low frictional behaviour of PTFE and HDPE are due to this coherent and oriented film which may be only 100 Å thick and which need not be continuous over the entire surface [55].

Over the past few decades a great deal of research has gone into transfer wear studies, but it still seems that this mechanism is not well understood, because of the lack of understanding of the micro-processes occurring at the interface. The situation becomes very complex because of various correlations of wear with different properties [40,154]. Dumbleton and Shen make an important point about the difference between transfer and transfer films: [115]

"The transfer need not be in the form of a coherent oriented layer, but may be lumpy. It is generally agreed that formation of a transfer film is beneficial but transfer may or may not be beneficial. Lumpy transfer may increase the wear rate. It seems that the ability to form a

transfer film depends on the molecular architecture of the polymer and polyethylene satisfies the criteria in this respect."

As far the molecular organization of the transferred layer is concerned, Briscoe noted that for HDPE there are generally two types of transferred films formed [40]. When sliding commences against a smooth counterface, a relatively thick (*ca.* 0.1 μm) and highly drawn layer is deposited onto the counterface. As sliding progresses a thinner (*ca.* 10 nm) but patchy layer is transferred. LDPE, however, will form a thick and unoriented transfer film. This process is shown schematically in figure 3.29 [155]. Electron microscopic studies of the transferred films of polymers, *e.g.*, PTFE and HDPE indicates substantial orientation of the transfer film [55,154,156]. Using selected area electron diffraction patterns, it has been shown that the transfer films of polymers, PTFE, HDPE and POM, have their c-axis oriented in the direction of sliding [154].

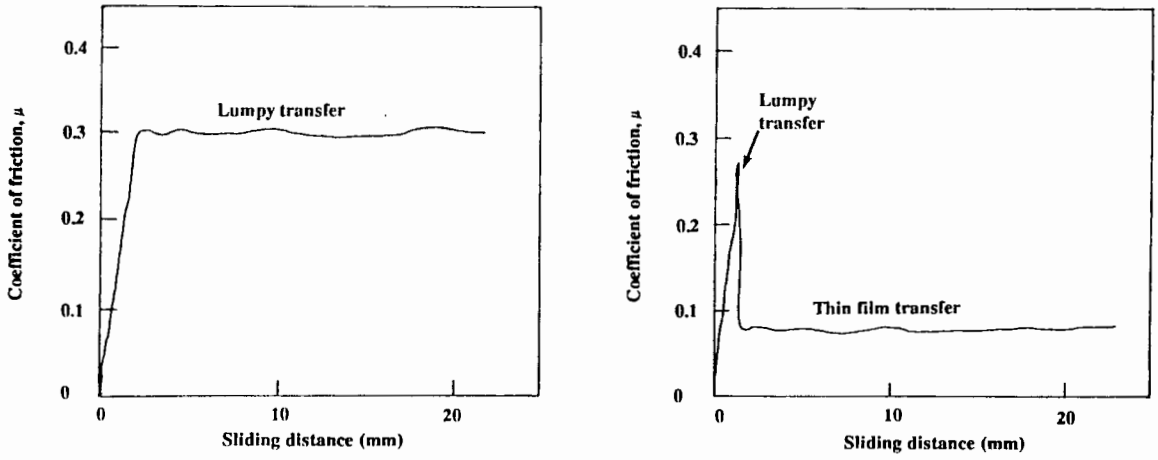

Figure 3.29: Coefficient of friction *vs.* sliding distance for a polyethylene slider over a smooth glass surface. (a) LDPE showing high friction throughout. (b) HDPE showing high initial (static) coefficient of friction falling to a low value as sliding commences, forming a thin, oriented film. [After ref. 155].

3.5.2 Mechanism of Formation of the Transfer Film

The mechanism of polymer transfer onto polymers, metals and other materials during sliding wear has been poorly investigated although it is of great scientific and practical

importance. Belyi *et al.* noted that the systematic research and development had been weak in this field [118]. Despite numerous studies in the field of frictional transfer, there is still not a common view on the mechanism of polymer transfer to metal, or how transfer influences wear [40].

The adhesion between crystalline thermoplastics sliding over clean and smooth metal counterfaces is large enough to inhibit sliding at the original interface. This causes *junctions* to rupture within the polymer and a coherent polymer layer is transferred to the counterface. The failure mode is cohesive (subsurface) since the interfacial shear strength of these clean junctures is assumed to be of the same order of magnitude of the bulk strength of the polymer [20,40]. The thickness of the transferred layer, which is considered to be between 10 nm to a few μm, gives an idea of the depth of this shear plane [40].

Briscoe considered the junction strength as a contact mechanical property as well as a surface force parameter [40]. These surface forces are a combination of van der Waals, Coulombic and hydrogen forces. Figure 3.30 shows an illustration of how a polymer may bond to the metal surface [157]. The surface forces of the couple play a big role in that the higher the ultimate surface tension of the polymer, the greater will be its adhesiveness to the counterface and hence the greater the wear. The development, thickness and strength of the transfer layer thus depends in part on the presence and polarity of the functional groups in the polymer structure [77].

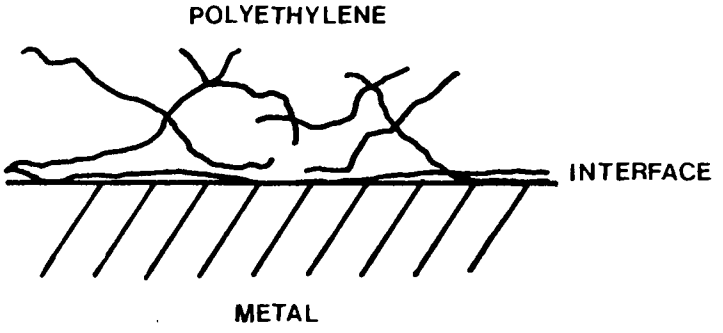

Figure 3.30: The "octopus effect". Formation of multiple van der Waals contacts in a polyethylene chain. [After ref. 157].

Kar and Bahadur used a model based on an energy criterion to investigate the nature of frictional transfer of polymers during sliding wear [158]. Their conditions for transfer are based on the adhesive forces operating between the interacting surfaces. Other workers

have considered softening of the polymer surface by heating as the criterion for initial transfer [153]. The energetics model, however, seems more plausible because the major part of the energy dissipation is in the thin interfacial zone [40]. In the energy model, the authors could estimate the thickness of the wear particles for different polymers. Wear particles trapped in between the sliding surfaces could form a strong bond to a steel surface because of the much higher surface energy compared with that of the polymer. This results in the formation of the transfer film on the steel surface [158].

Madakson's frictional model takes into account the surface energy of the contacting materials. The adhesion that occurs at asperity tips depends on the surface energy, the contacting materials and the environment amongst other factors. During sliding, the heavily deformed polymer surface layers accumulate energy, until a critical level is reached which leads to a periodic delamination of material. Energy is then built up again and this cyclic energy dissipative process leads to further layers being removed [159].

3.5.3 Factors Influencing the Formation of a Stable Transfer Film

The tribological behaviour of a polymer/metal oscillatory sliding system is not only dictated by the transfer film but also by the tenacity of this film adherence to the metallic counterface. The stability of the interfacial bonding between the transfer film and the counterface is determined by the intrinsic chemistry and molecular geometry of the polymer, as well as by the base metal and external parameters of the system.

3.5.3.1 Chemical effects

The most promising and effective way of improving the adhesion of the transfer film of the polymer to the counterface is through the addition of certain fillers [40,102,152]. In an excellent review, Evans and Lancaster found that the wear resistance of smooth molecular profile polymers such as PTFE can be increased by a factor of 100 or more when inorganic and organic fillers are added [20]. Briscoe *et al.* reports that there may be a chemical reaction between the fillers and the oxide of the metal base [152]. This dramatic effect of the filler on the polymer wear is shown in figure 3.31.

There is also evidence that certain transition metal oxide fillers could induce mild degradation of the polymer and that strong valence bonds between the transferred layer and the counterface are created [40]. The mechanical and chemical processes that take place at the interface during frictional loading, suggest that many complex interactions may occur. These include the formation of highly active free radicals, the activation of the metal surface, the reduction of the polymer molecular weight, oxidation of the polymer and the disintegration of the initial crystalline structure [40,126].

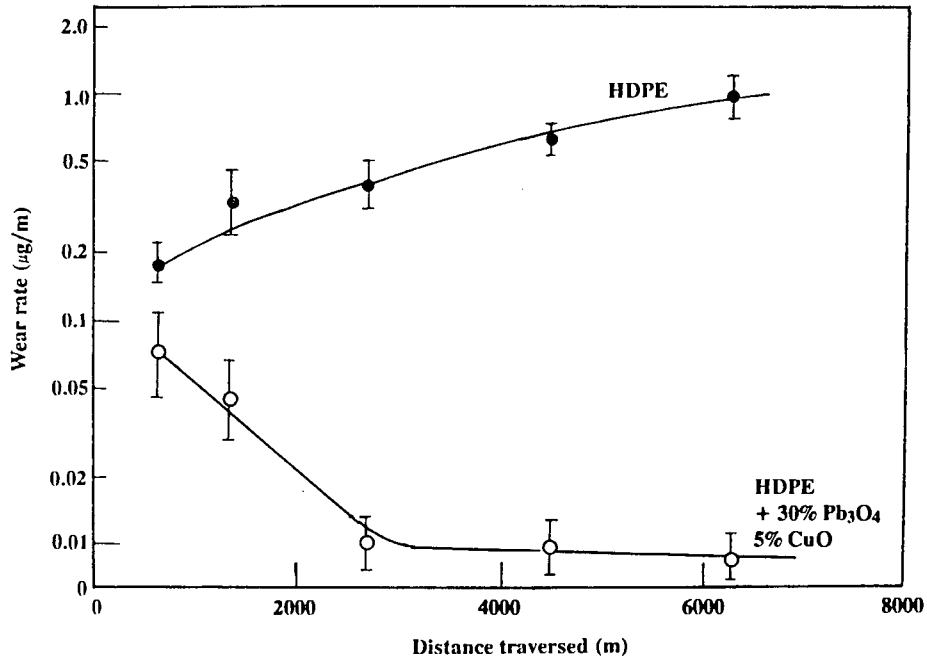

Figure 3.31: Wear rate as a function of sliding distance for filled and unfilled HDPE in air. [After ref. 152].

It has been suggested that an amorphous structure of a metal oxide film can increase the rate of the formation of the transfer film [160]. Some researchers have found that fillers are effective in promoting adhesion to surfaces such as steel but are ineffective against glass or aluminium [152,153]. Other workers have found that chemical surface treatment of the metal counterface gives a significant improvement in the wear by promoting adhesion [161].

The fact that cohesive failure occurs within the polymer, shows that the forces existing between the polymer chains are less than or at least comparable to those existing in the local regions of adhesive contact [40,77]. Whether metals or polymers are interacting, it is

found that material transfer takes place from a lower to a higher cohesive energy density material. Thus, in addition to the mechanical interlocking of the polymer with the interacting surface, the surface forces within the contacting region are important [40,45].

3.5.5.2 Lubrication

It is well known that lubricants, particularly water, can greatly influence the wear of some polymers through their effect of inhibiting the formation of stable transfer films on the metal counterface. Water and aqueous solutions generally increase the wear rates of those polymers that form transfer films in dry wear processes but do not significantly influence wear of polymers when transfer does not occur during dry sliding [20,102,103]. (See section 3.4.3). Table 3.4 shows how the wear rates may be significantly affected by the presence of water for polymers such as PTFE and UHMWPE [116].

The higher wear rates for semicrystalline polymers may be due to modification of the worn polymer surface by the water molecules or modification of the counterface by the absence of the transfer film [102,103]. The amount of polymer transfer in water lubrication may be similar to that found in dry sliding. Dowson *et al.* showed that the deleterious effect of water on the transfer film formation is particularly true for rough counterfaces. They found that the wear rates under lubrication exceeds that under dry conditions at a counterface roughness in excess of 0.01 μm. [139].

Material	Wear rate ($m^3 N^{-1} m^{-1} x10^{-15}$)	
	Dry	Wet
PTFE + graphite	1.3	14
PTFE / 25% glass fibre	7.7	330
PTFE / 25% asbestos	26	500
PTFE / mica	12.5	50
PTFE / graphite bronze	6.5	6
PTFE / carbon fibre	2	100
UHMWPE	0.048	4.5

Table 3.4: The deleterious effect of water on the wear rates of polymers that rely on a transfer film under dry conditions. [After ref. 116].

3.5.3.3 Counterface topography

The ability of the transfer film of smooth molecular profile polymers to adhere tenaciously to the counterface is influenced by the topography of the counterface [4,139,162]. With very smooth counterfaces the more intimate contact facilitates adhesion and the surface energies of the couple dominate the transfer process, whereas very rough surfaces may suppress the formation of a polymer transfer film [20,80,83]. Clarke reported very low wear rates for filled UHMWPE at steel counterface roughnesses between 0.25 and 0.6 μm R_a and attributed this to an extensive valley transfer film [162]. The increasing contribution of asperity fatigue also plays a greater role as the surface roughness increases [150].

3.5.3.4 Other factors

The stability of the transfer film may be affected by the polymer structure, load, temperature and type of motion [84,133,153]. Shen *et al.* found that a transfer film is formed for VHMWPE, whereas irradiated polyethylene does not form a transfer film. Irradiation causes crosslinking, which inhibits orientation and movement of the polymer molecules necessary to form a transfer film [84]. Brown *et al.* found that orientation of the polymer molecules perpendicular to the wear surface is less beneficial than orientation parallel to the counterface. The wear surface also appeared much rougher when sliding is perpendicular to the molecular orientation [88].

Rhee *et al.* and Tanaka found increases in thickness of the transfer film with increases in load which may suppress the onset of severe wear to a higher temperature [153,156]. Evans *et al.* used a pin-on-disc wear and friction tester which could allow independent temperature control of the polymer pin and the steel counterface. Their research found that the uniformity of the transfer film was temperature dependent and that uniformity had an effect on polymer wear [133]. Higher counterface temperatures aided the formation of a protective transfer film. Polymer debris influences the build-up and maintenance of the transferred polymer [163]. In oscillatory motion it is more difficult for wear debris to leave the contact zone and thus protective transfer films develop more easily [133]. The wear rate is usually lower in oscillatory motion than in unidirectional sliding.

CHAPTER 4

EXPERIMENTAL TECHNIQUES

4.1 TEST MATERIALS

4.1.1 The Polymer Wear Pins

The polymeric materials used in this study were ultra-high molecular weight polyethylene (UHMWPE) and polytetrafluoroethylene (PTFE). The materials were obtained from the supplier, Solidur Plastics SA (Pty) Ltd. and Chemplast Marc Etter (Pty) Ltd. The physical and mechanical properties of the materials are given in table 4.1. Further properties of the materials appear in Appendix A. The UHMWPE was compression moulded, while the PTFE was obtained from moulded billets.

The polymer wear samples used in the investigation were cut from the bulk material in the form of square pins, 10 mm x 10 mm x 25 mm in length. The UHMWPE was considered to be isotropic following sectioned optical microscopy. A small 45° chamfer was cut along the leading and trailing edge of the wear surface, to minimize rocking of the polymer pins during reciprocating wear testing. This gives an initial cross-sectional area of the polymer pin of approximately 90 mm^2 as shown in figure 4.1.

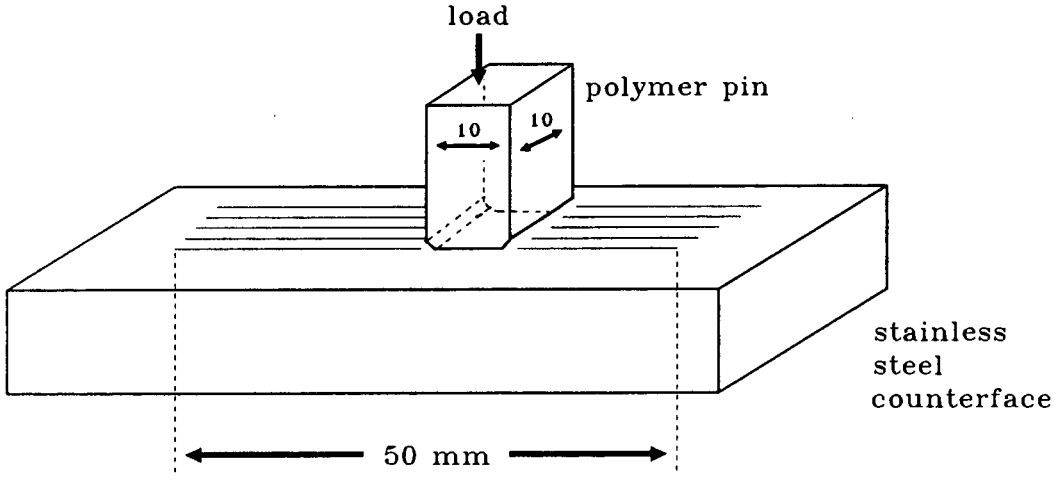

Figure 4.1: A schematic representation of the polymer wear pin and counterface.

Properties	Unit	Polymeric material							
		UHMWPE					PTFE		
		Special DS	Ceram P	10/100	B 15	GUR 416	unfilled	g/fibre	bronze
Physical properties									
density of homogeneous material (SG)	$g.cm^2$	0.96 *	0.98*	0.94	0.93	0.93	2.17	2.26	3.95
average molecular weight	$g.mol^{-1} \times 10^6$	6	6	4.5	7.3	8	7.4	—	—
Mechanical properties at 23 C, 50% RH									
tensile strength	MPa	23	21	22	22	20	28-35	18-22	
UTS	MPa	43	43	44	40	40	36	19	5-8
elongation to break	%	450	450	450	450	>350	250-400	200-300	10-15
shore D hardness		67	68	66	66	57	65	55-70	55
impact strength (notched)	MJ/mm^2	100	60	150	>100	>100			
elastic modulus	MPa	232					750	—	800
Thermal properties									
melting point	°C	139	139	137	137	136	327		
thermal conductivity at 20°C	W/m.K	0.42					0.25	0.38	1.25
Antifriction properties on polished steel	μ								
wet coefficient		0.05-0.08					0.04-0.25		
dry coefficient		0.11-0.22					0.07-0.13		

Table 4.1: The physical and mechanical properties of UHMWPE and PTFE. Data were obtained from Solidur Plastics, S.A. (Pty) Ltd and Chemplast Marc Etter (Pty) Ltd. * indicates the filled UHMWPE grades, while the other UHMWPE grades are unfilled.

4.1.2 The Stainless Steel Counterfaces

The stainless steel counterfaces were machined from grade AISI 431 material obtained from the suppliers, Böhler. These bars 70 mm in length, 12 mm wide and 10 mm deep, were then subjected to a heat treatment schedule used for AISI machine components such as rockdrills and impact hammers.

To prevent decarburization, the specimens were coated in a zirconia-based ceramic and dried in an oven. They were then soaked at 1000 °C for 45 minutes, oil quenched to room temperature and double tempered at 260 °C for one hour. The counterface hardness, as measured on an ESEWAY hardness tester, gave hardness values of approximately 450 ± 20 HV30. A mechanical surface grinder was used to obtain the final surface finish on the steel counterface. The grinding direction was either perpendicular or parallel to the sliding direction. Following machining, the plates were demagnetized to enable loose metallic particles to be removed. They were then degreased in a commercial degreasing agent, Arklone and finally ultrasonically cleaned in alcohol. Although this procedure was carefully carried out, optical microscopy revealed, as shown in figure 4.2 below, that in a few cases, loose metallic particles remained on the counterfaces and became embedded in the polymer during wear testing. These metallic particles can cause severe abrasive damage to both the metallic counterface and polymer pin, resulting in certain tests being abandoned.

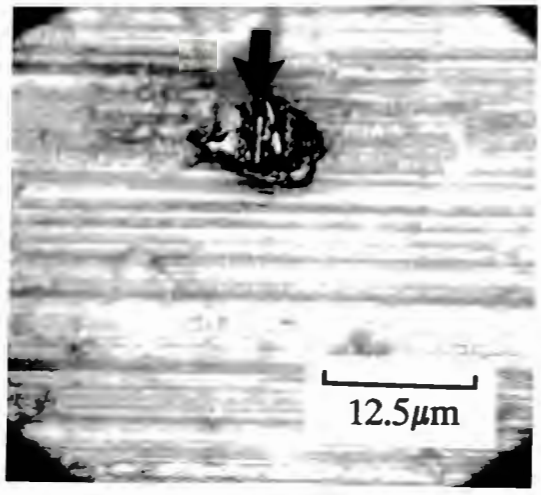

Figure 4.2: Loose metallic particles (arrowed) may be embedded in the polymer wear surface during wear testing and cause severe abrasive damage to both the polymer and metallic counterface.

A Taylor Hobson surface profilometer was used to measure the centre-line-average (R_a) surface roughnesses of the counterfaces. Between 10 and 15 traversals were taken at different positions on the metal counterfaces. Only sliders that conformed to a 5% tolerance in R_a for a particular test, were selected and used in the experiments shown in table 4.2.

4.2 LABORATORY WEAR TESTING

4.2.1 The Testing Rig

The reciprocating pin-on-plate wear rig used in this study, is able to simulate the sliding action of a steel piston against a polymer seal. It consists essentially of a wear pin sliding on a flat counterface as illustrated in figure 4.3.

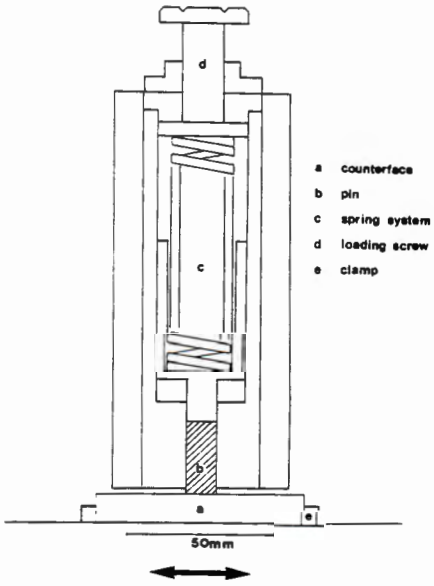

Figure 4.3: A schematic of the pin housing and counterface.

The wear tester has the facility to allow for the measurement of wear rates, frictional forces and surface temperatures of the sliding couple under different operating variables. Figure 4.4 shows the test rig and peripheral instrumentation. The rig consists of an aluminium housing, in which the pins are clamped in a holder such that they are able to reciprocate

continuously against the stationary metallic counterface. A force is applied to the pins via a pre-calibrated steel spring and a loading screw. The housing slides on two lubricated steel rods driven by a 0.72 kW D.C. electric motor. Figure 4.5 shows the aluminium housing and clamping system used to locate the counterface in greater detail. The sliding velocity can be controlled by a thyristor controller which regulates the speed of the motor. The sliding distances can be set on a preset counter which sends a signal to the control unit to stop the motor once the required distance has been traversed.

A safety shut-off mechanism may be triggered off by a signal from the LVDT when a set length loss on the wear pin is reached. Frictional forces can be measured by a friction transducer and the friction signal can be displayed and stored on an oscilloscope. A stainless steel bath enables the test to be carried under a suitable lubricant.

Figure 4.4: The laboratory wear apparatus and instrumentation.

The components in figure 4.4 are:

A) An aluminium housing in which the polymer pin is clamped. The housing is supported by four bearings and reciprocates on two metal shafts connected to the gear box.

B) A stainless steel bath which contains the lubricant.

C) A safety shut-off mechanism which operates on a feed-back signal from the LVDT.

D) A counter which can be set to stop the motor after a preset number of cycles.

E) A thyristor controller which regulates the speed of the motor.

F) An oscilloscope which converts the signal from the load cell to a wave form.

G) A chart recorder and thermocouples to measure and monitor the sub-surface temperatures during testing.

H) A Polaroid camera which can be used to photograph the friction trace.

I) A 0.72 kW D.C. electric motor and a 4:1 ratio gear box.

Figure 4.5: The pin holder assembly.

The components in figure 4.5 are:

A) The aluminium housing containing a pre-calibrated steel spring and pin holder.

B) An aluminium T-section used to clamp the specimen firmly in the holder.

C) The stationary metal counterface.

D) An aluminium clamping system for securing the stationary counterface.

E) A friction transducer which measures the friction forces generated at the interface during sliding.

F) A linear variable differential transducer (LVDT) which is mounted above the upper sliding specimens used to continuously monitor the (progressive decrease) length loss of the pin.

G) The cylinder lid and loading screw.

H) Two steel rods on which the housing slides.

4.2.2 The Test Parameters

The operating parameters chosen for this study had to take into account both the capabilities of the test rig as well as the objectives of the study. The actual conditions employed in the wear tests are shown in table 4.2. The typical conditions applicable to impact hammers and rockdrills are also shown.

4.2.2.1 Sliding velocity

The sliding velocity is sinusoidal with an average velocity of 0.25 $m.s^{-1}$. The maximum velocity of the pin, calculated to be 0.4 $m.s^{-1}$, is experienced at the mid-point of the counterface as shown in figure 4.6. From table 4.2, it can be seen that high velocities are reached on impact for both the rockdrill and impact hammer in the firing strokes where hydrodynamic lubrication is prominent, resulting in very little wear. It has been reported that boundary lubrication, which results in wear, prevails at relative velocities below 0.75 $m.s^{-1}$ [4]. Thus the test velocity employed simulates only the boundary lubrication conditions observed in practice.

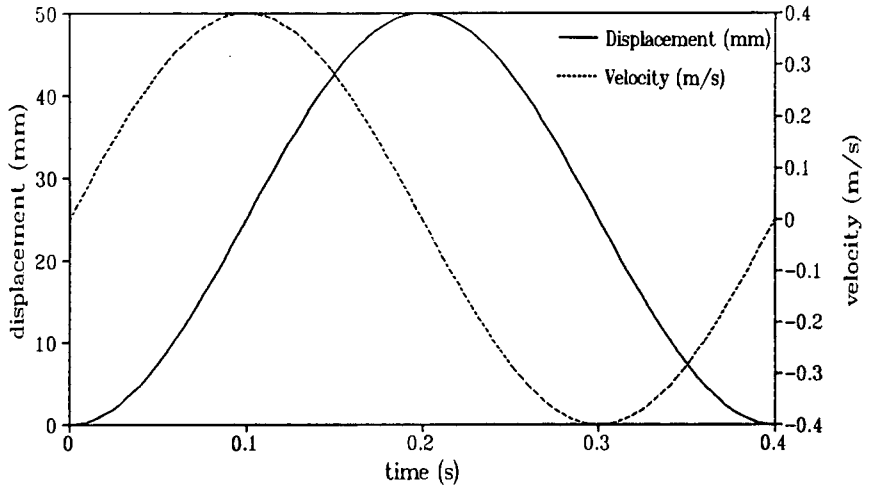

Figure 4.6: Velocity/time and displacement/time curves of the laboratory wear rig.

4.2.2.2 Pressure

The required operating pressures for a typical rockdrill were calculated to be between 14 and 18 MPa (table 4.2). With a maximum normal applied load of 100 kg and an initial contact area of about 90 mm^2, the test pin experiences an initial pressure of 11.11 MPa. The maximum operating pressure was used as a compromise between the rig's capability and the operating conditions encountered in mining machinery.

4.2.2.3 Counterface roughness

A slight variation in the counterface roughness is known to affect the transfer mechanism considerably, and it was decided that a surface roughness of 0.3 μm R_a would be appropriate for this particular study. Only counterfaces that conformed to 5% tolerance were used for the wear tests.

4.2.2.4 Lubricant

Distilled water was used in lubricated tests rather than mine water as employed in hydro-powered equipment [2,4].

4.2.2.5 Sliding distance

The sliding distances chosen had to take into the account the objectives of this study, *i.e.*, to study the development of the transfer films to steady-state, to investigate how the operative wear mechanisms change during the course of experimentation and to establish reliable wear rates for the various polymeric materials used in the sliding wear experiments.

variable	unit	testing value	rockdrill	impact hammer
stroke	mm	50	23	80
velocity	m/s	0.25 (ave.) 0.40 (max.)		
firing velocity return velocity	m/s		10 (max.) 3 (max.)	10 (max.) 0.9 (max.)
operating pressure	N/mm^2	10	14-18	18
surface roughness	µm Ra	0.03-0.3	~0.2	0.3-0.8
sliding distance	km	0.01-120	—	—
lubricant	—	distilled water/dry	mine water	

Table 4.2: The test operating variables and those typically encountered in a rockdrill and an impact hammer. [After refs. 2,4,164].

4.3 EXPERIMENTAL PROCEDURES

To study the development of the steady-state film of UHMWPE, each test used a new clean counterface and wear pin and was subjected to the same velocity and load. UHMWPE absorbs less than 0.1% water (see also Appendix B), and to correct for any moisture absorption, the pins were soaked in water until they were saturated, blow dried and weighed, before being mounted. Material removed by wear was monitored at set intervals by measuring the weight of the pins accurately on a Sartorius 2474 microbalance having a sensitivity of 0.01 mg.

The following operating procedure was carried out for all the tests:

(i) The polymer pins were placed in the specimen holder, with the chamfered side oriented to the sliding direction.

(ii) The pin protrudes beneath the holder by 1.5 mm and it is then secured with an aluminium T-clamp.

(iii) A pre-calibrated steel spring was placed in the plunger and the load screw placed onto the lid of the spring, ensuring that no load is applied. The fastening screws of the cylinder lid were then tightened.

(iv) The load screw was turned such that the required pressure was applied.

(v) The LVDT was set such that it will trigger off when a safety limit is exceeded.

(vi) Since the sliding velocity is kept constant at 0.25 $m.s^{-1}$, the desired sliding distances were set on a preset counter.

(vii) Finally, the rig was switched on and the friction force is monitored periodically on a digital storage oscilloscope.

After each run, the pin was ultra-sonically cleaned in ethanol, blow dried and weighed. The counterfaces were also cleaned in ethanol before roughness measurements were made. The pins were placed in exactly the same positions after weighing and the test is restarted. After the completion of a test, the pins and counterfaces were stored in a desiccator for optical and scanning electron microscopy.

4.3.1 Experimental Measurements

4.3.1.1 Measurement of specific wear rate

Changes in weight loss were preferred to recording dimensional changes as the latter

method showed greater scatter in results [4]. Dimensional changes also combine the effects of creep and weight loss which could lead to larger experimental errors. Polymer mass loss was converted to volume loss *(V)* and plotted against sliding distance *(S)*. The the slope of the steady-state linear portion divided by the normal load *(P)* gives the specific wear rate *(K_o), i.e.*,

$$K_o = V/PS \ (mm^3/N.m)$$

4.3.1.2 Measurement of counterface roughness

Counterface roughnesses were measured at the start of the tests and as the tests progressed, measurements of the surface roughness were taken to coincide with the weight loss measurements. The roughness traces across the counterface wear tracks were useful in revealing the extent of transfer film formation and also the general nature of the film.

4.3.1.3 Measurement of frictional forces

Frictional forces generated at the sliding interface were measured by a friction force transducer shown schematically in figure 4.7. The clamped counterface is mounted on a freely moving trolley running on several rows of stainless steel ball bearings within machine grooves parallel to the sliding direction. The entire specimen holder can be considered as a nominally "frictionless" trolley. The trolley is connected via a rigid steel beam, to a vertically mounted bending beam load cell. Frictional forces that are generated, produce horizontal displacements of the trolley which are transmitted directly to the load cell. The friction force signal is then monitored at regular intervals and displayed on a digital storage oscilloscope.

The mean static and kinetic friction coefficients were calculated at the end of each test period, *i.e.*, prior to stopping the test for weight measurements of the polymer pins. Figure 4.8 illustrates a friction plot obtained during a test and shows how both the static and kinetic friction forces are obtained from the friction force *vs.* time curve. The frictional coefficients were obtained by dividing the horizontal frictional force by the applied normal load.

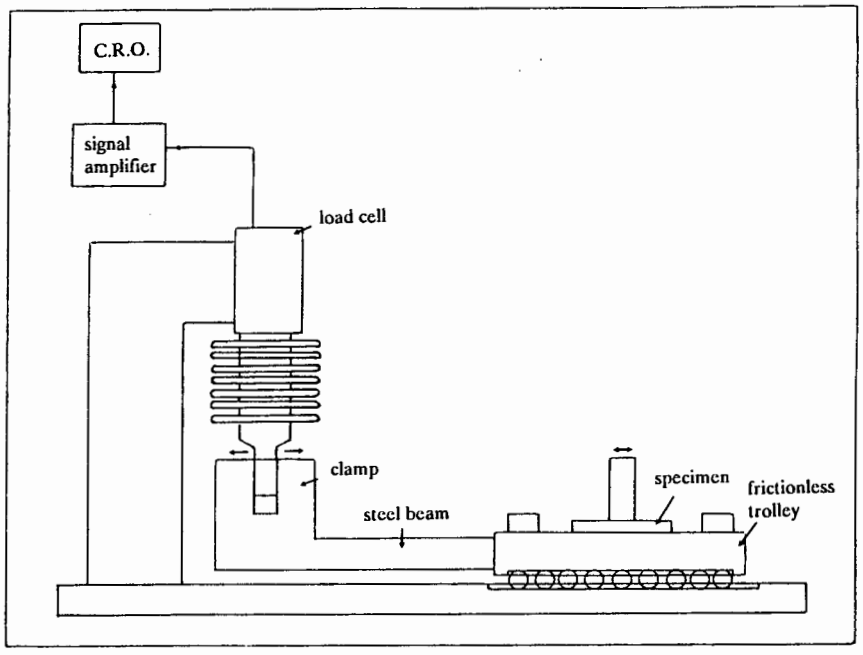

Figure 4.7: A schematic representation of the friction force transducer for friction measurements.

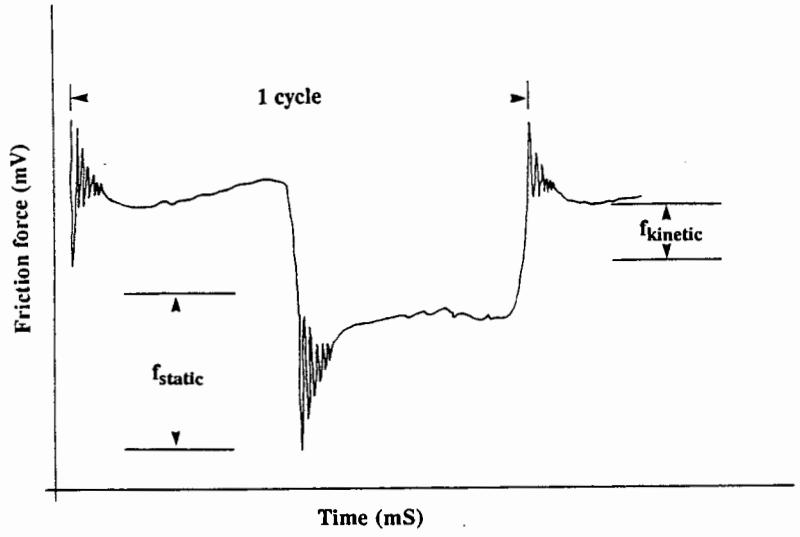

Figure 4.8: A typical variation of friction force *vs.* time curve in a reciprocating contact, recorded during a water-lubricated test, showing how the friction coefficients are derived.

4.3.1.4 Measurement of surface temperature

The average surface temperature at the sliding interface resulting from frictional heating, was obtained by inserting a calibrated iron-constantan thermocouple in a hole drilled 0.5 mm below the wearing surface of the metal counterface. A recording of the interfacial

temperature rise was obtained on a chart recorder.

4.3.2 Test Reproducibility

The reproducibility of the test rig was determined from a series of three individual tests shown in figure 4.9. In figure 4.9, volume loss *vs.* sliding distance curves are shown for three UHMWPE samples, tested at 0.25 $m.s^{-1}$ under a pressure of 10 MPa in distilled water. All the tests followed the general trend of high wear followed by a region of lower wear with increasing sliding distance. Although the initial stages (bedding-in) were quite variable, all the curves showed similar slopes at longer sliding distances. The steady-state wear rates were thus calculated from sliding distances between 10 and 40 km and are shown in table 4.3. The reproducibility of the wear rates were deemed acceptable. Any variability in wear rates may be ascribed to the viscoelastic nature of the polymeric material and more importantly, to small variations in counterface roughness for a particular set of tests. The majority of the subsequent sliding wear tests were triplicated to derive mean specific wear rates and it was found that counterface roughness, which cannot be reproduced very accurately, had the largest influence on reproducible results. (See also section 5.3.1.1).

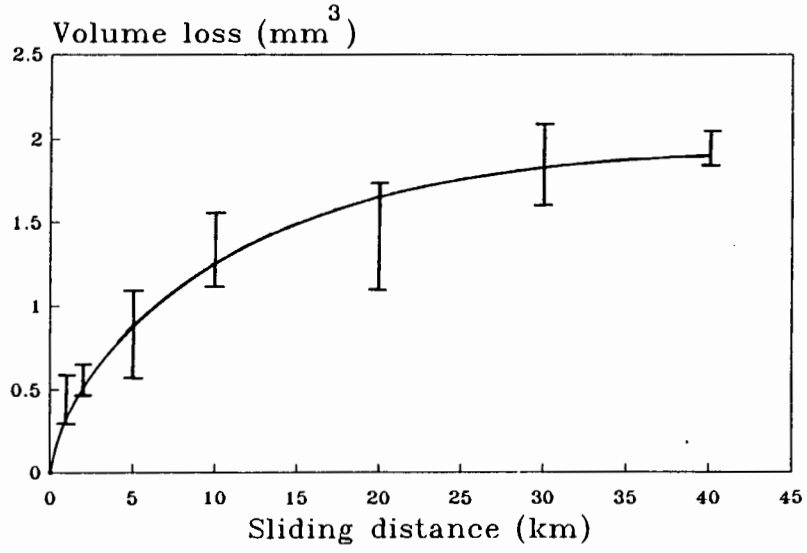

Figure 4.9: The average volume loss *vs.* sliding distance curve for three tests with UHMWPE (grade B 15) in distilled water, showing the reproducibility of the sliding wear rig.

test	key	surface roughness μm Ra	steady-state wear rate $mm^3/N.m$	correlation coefficient
1	■	0.284 ± 0.016	1.42×10^{-6}	0.739
2	◆	0.317 ± 0.033	2.98×10^{-6}	0.749
3	●	0.287 ± 0.021	1.66×10^{-6}	0.808
ave.		0.296	2.02×10^{-6}	–
std. dev.		0.018	0.84	–

Table 4.3: The results of the reproducibility tests. pressure: 10 MPa; sliding velocity: 0.25 $m.s^{-1}$.

4.3.3 Polymer Characterization

4.3.3.1 Optical microscopy

Light microscopy was used in both the incident and transmitted modes to study the worn surfaces, transfer films and wear particles formed during the period of experimentation. For these purposes a Nikon Optiphot and a Reichert projection optical microscope were used. At very high magnifications, the build-up of polymer films on the metal counterface was observed by using the depth of focus of the optical microscope. For optical microscopy studies of the polymeric material, 10 - 15 μm thick films were microtomed using a sledge microtome. The films were then mounted between a glass slide and coverslip using Canada Balsam as a fixative, before viewing under polarized light. Birefringent studies were also made of the worn surfaces of UHMWPE pins taken from the reciprocating sliding wear tests. For these purposes, the specimens were microtomed normal to the wear surface and parallel to the sliding direction.

Method used to detect birefringency

The organization of the long-chain molecules of a polymer has a profound effect on its physical, mechanical and optical properties. Due to the fact that the polymer chain is highly anisotropic with respect to its dimensions, the polarizability parallel to the chain will

differ from that perpendicular to it. The refractive index with respect to a light wave with its electric vector parallel to the chain will differ from that for a wave with its electric vector perpendicular to it, *i.e.*, the polymer chains are intrinsically birefringent, the birefringence being the difference between the refractive indices in the two orthogonal directions. Light microscopy applied to an ideal homogeneous and isotropic specimen would yield no useful information, as the difference in refractive index will average out and the sample will show no residual birefringence. For polymer molecules that are aligned, the orientation manifests itself as a visible detectable birefringence [165,166].

Consider a stressed specimen in a state of plane stress between a polarizer and analyzer as shown in figure 4.10. Light from source *S* passes through the polarizer and analyzer in crossed orientation so that no light is transmitted. The plane polarized light enters the stressed specimen and is then resolved into two components, one vibrating parallel to the major axis and the other parallel to the minor axis. The analyzer reduces these two components along the axis of polarization. The transmitted intensity is a maximum when the polarized beam of light is at 45° to the major axis of the specimen. If the specimen is plastically deformed, the resultant strain birefringence is a function of the permanent deformations or strains [165].

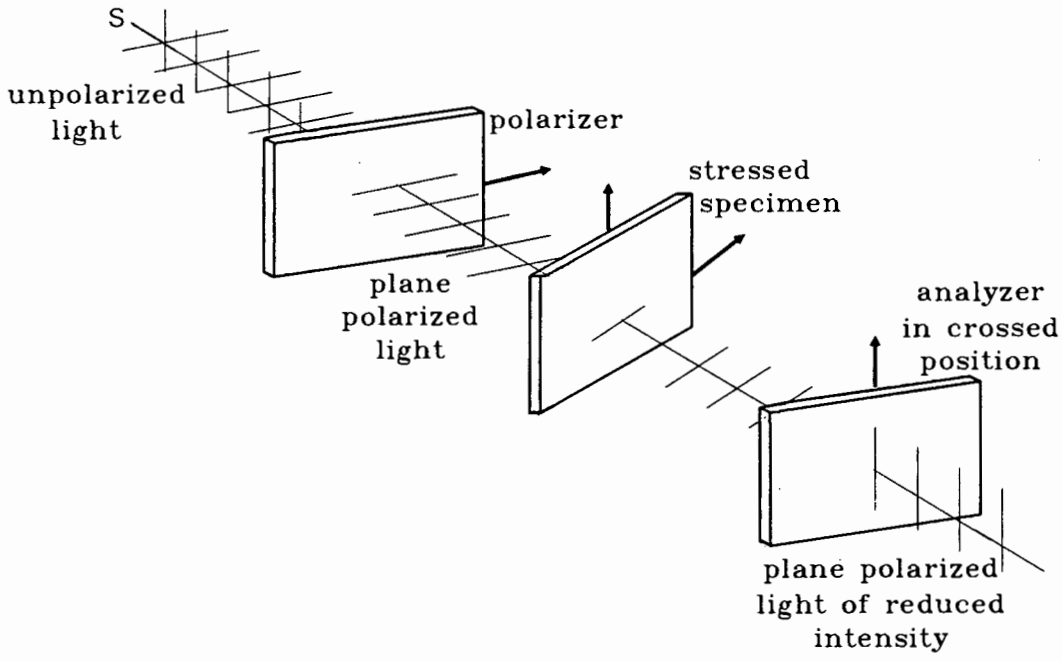

Figure 4.10: An illustration of the method used to detect birefringence.

4.3.3.2 Scanning electron microscopy (SEM)

After completion of a particular test, the worn surfaces of the polymer pins and steel counterfaces were ultrasonically cleaned in alcohol. The polymer pins were mounted on aluminium stubs and a conductive paint was applied to the sides of the pins to form a conducting path between the polymer and the stub. The worn surfaces were then sputtered with a gold/palladium coating to prevent charging and to render them electrically conducting, prior to examination in Cambridge Stereoscan 200 scanning electron microscope. Polymer wear debris which was recovered from the wear pins and lubricant were also examined by SEM. An accelerating voltage of between 10-15 kV was used to minimize radiation damage.

Energy dispersive X-ray analysis (EDX)

The semi-quantitative composition of any transferred material was determined by using a TRACOR NORTHERN TN 5400 energy dispersive X-ray microanalyser attached to the SEM.

4.3.3.3 Transmission electron microscopy (TEM)

Transmission electron microscopy of replicas of the worn surfaces were carried out. For replication, the worn counterfaces were shadowed with Au/Pd and sputter coated with carbon. A thin layer of gelatin was deposited onto the surface, and when this had dried, it was dissolved away by flotation on distilled water. The replica then consisted of shadowed Au/Pd with a carbon backing. Another replication technique was also tried. This consisted of sputtering carbon onto the wear surface and depositing a concentrated layer of gelatin onto the surface. When the gelatin solidified, the carbon film with the gelatin was peeled off from the counterface and floated upside down onto an aqueous solution of potassium thiocyanate (KSCN) to dissolve away the gelatin and then floated on distilled water to wash the remaining gelatin away. The carbon films were then carefully collected with copper grids between a fine tweezer. Selected area electron diffraction (SAED) were carried out in a JEOL 200 transmission electron microscope on thin layers of polymer still attached to the carbon film. The procedure used, was followed by Komoto *et al.* and is summarized in Appendix B.

4.3.3.4 X-ray diffraction (XRD)

The x-ray diffraction data were obtained using nickel filtered CuKα radiation in a Philips diffractometer. The diffraction studies were conducted on 1.2 mm slices from the tips of worn and unworn polymer specimens as well as on powdered debris collected from the wear process. The scanning rate was 2° min^{-1} and the diffraction angle 2θ varied between 10° and 50°. An accelerating voltage of 40 kV and a current of 20 mA was used. The crystallinity of UHMWPE was found by calculating the areas under the amorphous and crystalline peaks. The crystallinity and crystallite sizes of the UHMWPE were determined from the D_{110} and D_{200} peaks [167]. The crystallinity of PTFE was obtained from the ratio of the crystalline and amorphous peaks [168].

4.3.3.5 Differential scanning calorimetry (DSC)

Theory

The differential scanning calorimeter (DSC) measures the change in power to the heaters of the sample and the reference cells, required to maintain a constant temperature, in response to any thermal event occurring in the sample. The change in the power requirements of the sample with temperature *(T)* through the polymer melting range allows calculation of the enthalpy of the transition from the area under the dq/dT *vs.* temperature traces [169].

Differential thermal analysis has already been shown to be a very versatile technique for the rapid characterization of several aspects of polymer melting. Determinations of the degree of crystallinities are obtained from the heats of fusion *(ΔH_f)* based on measuring the area of a DSC melting peak above a predetermined baseline. The scans for HDPE and higher molecular weight polyethylenes, eliminate difficulties in obtaining the degree of crystallinity, in that the melting peaks are usually sharp and well-defined [170].

Analysis of DSC traces

Microtomed films from the bulk polymer as well as wear debris were heated in a Perkin-Elmer DSC 2 to detect any likely internal changes in the material as a result of sliding. The weight of the samples was kept constant at 5 mg, since it is known that the amount of

material can affect the results. A heating rate of 10 °C.min^{-1} and 20 °C.min^{-1} was used for the UHMWPE and PTFE respectively. At least three scans were made per test.

The degree of crystallinity of UHMWPE can be calculated by assuming the heats of fusion of 100% crystalline polyethylene (ΔH_f^*) to be 293 J.g^{-1} [171]. For PTFE ΔH_f^* = 61.17 J.g^{-1} [168]. The percentage crystallinity is then calculated from the formula:

$$\text{percentage crystallinity} = (\Delta H_f/\Delta H_f^*) \times 100$$

where ΔH_f is the heat of fusion of the sample.

From the heat of fusion data, the number average molecular weight, M_n, of PTFE can also be calculated from the empirical relationship:

$$M_n = 2.1 \times 10^{10}(\Delta H_f)^{-5.16}$$

where ΔH_f is in calories per gram [172].

4.3.3.6 Infrared spectroscopy (IR)

Theory

Infrared spectroscopy can be used for the identification of compounds, structural determination of unknown molecules and also for a quantitative determination of a given compound in a mixture [173]. The energy of most molecular vibrations, except homonuclear diatomic molecules, correspond to that of the infrared region of the electromagnetic spectrum. The vibrational motion of the bonds is detected and measured in an infrared spectrum or indirectly in a Raman spectrum. The most useful vibrations may be found in the 2.5 μ or 15 μ (wavelength) range. The position of an absorption may be expressed in microns (μ) or more commonly in wavenumbers (cm^{-1}). The usual range of an infrared spectrum is thus between 4000 and 667 cm^{-1}.

The spectrometer consists of a source of infrared light emitting radiation throughout the desired frequency range. The light is split into two beams of equal intensity, one of which passes through the sample to be examined. If the frequency of a vibration falls within this

range, the molecule absorbs the energy of this frequency and an absorption peak is recorded on a chart. Infrared spectroscopy may be used in the field of frictional transfer studies. This may be done by comparing the initial spectra with the spectra taken from samples after the test [118,174].

Sample preparation and examination in the infrared spectrometer

The polymer samples were prepared in the following manner and scans were made in a Perkin-Elmer 983 Spectrophotometer.

(i) Very thin films ($\approx 20\ \mu m$) were microtomed off the unworn polymer pin and the polymer was sellotaped over the circular hole of the spectrometer.

(ii) The above technique was not possible for the wear debris. About 1 mg of solid debris was mixed in a small agate mortar and a few drops of either liquid hydrocarbon (Nujol) or hexachlorobutadiene (HCBD or C_4Cl_6) were added and mixed. The mull was then pressed between the flat plates of sodium chloride and the scans were made. Separate cells, containing pure solvent were used to subtract the peaks due to the solvent alone. The Nujol sample was run between the range 1400 - 600 cm^{-1}, while the HCBD sample was run between 4000 and 1400 cm^{-1}, since peaks only due the sample are obtained in these regions.

4.3.3.7 Mass spectrometry

The mass spectrometer

The conventional mass spectrometer can be considered as an apparatus that produces a supply of gaseous ions from a sample. Ions are separated according to the mass to charge ratios (m/e) and a record of the intensities of the ions from the solid surface may be displayed on a chart. In the mass spectrometer, positively charged molecular ions are produced as follows:

$$[M] \xrightarrow{-e} [M]^+$$

by the electron bombardment of the molecules of the vapour (70 eV). The energy of an

electron beam which is required to remove an electron from organic molecules is usually of the order 10 eV, so that the additional energy of the electrons may be dissipated in breaking bonds in the molecular ion. Molecular ions are odd-electron species $[AB]^{\ddagger}$, which fragment into a carbonium ion and a radical as follows:

$$[AB]^{\ddagger} \rightarrow A^{+} + B\cdot \quad \text{or} \quad A\cdot + B^{+}$$

The ions are accelerated by an electric field and deflected by a magnetic field. The amount they are deflected depends on their (m/e) ratios and different ions thus separate into different beams which are unique to every element [174].

Mass spectra representation and its use in frictional transfer

A representation of the main features is obtained by plotting m/e values against relative abundance *(%I)*, arbitrarily assigning the most abundant ion (base peak) in the mass spectrum as 100%. The structures of the charged fragments, formed from the molecular ion, can be related to the structure of the intact molecule [174].

Mechanical stresses and high contact temperatures create conditions which may induce mechanical and thermal degradation of the polymer. The polymer transferred onto the counterface may be formed by heavy non-volatile molecular fragments which may adhere mechanically to the counterface or the chains may break down by a synthesis reaction on transfer. This type of information occurring at the contact region may be provided by the method involving the use of the mass spectrometer, by analysis of the volatile products formed when the transferred layer and the wear particles become thermally dissociated [118].

It has already been shown that the mass spectra obtained for the volatile products of certain polymers formed by thermal and mechanical degradation coincide, thus proving that there exist some common elements in the mechanism by which polymers disintegrate [77,118,131].

4.3.3.8 X-ray fluorescence (XRF)

X-ray measurements on both the polymer and counterface was used to determine the

composition of the material and that of the transfer film. The x-ray fluorescent measurements were made in vacuum with a wavelength dispersive spectrometer with a Cr tube operating at 60 kV and 45 mA using a LiF (200) crystal and fine collimators.

CHAPTER 5

RESULTS

5.1 GENERAL INTRODUCTION

This chapter presents a systematic analysis of the tribological behaviour of ultra-high molecular weight polyethylene (UHMWPE). The wear behaviour of a commonly used bearing material, polytetrafluoroethylene (PTFE), has also been included for comparison with that of UHMWPE under similar testing conditions. In order to present the results clearly, it was necessary to include some discussion in certain instances. The experimental results are presented in the following order:

(i) Polymer Characterization

(ii) Friction and Wear

(iii) The Transfer Film

(iv) The Nature of the Worn Material

(v) The Effect of Water Lubrication

(v) The Friction and Wear Behaviour of PTFE

5.2 POLYMER CHARACTERIZATION

5.2.1 The Structure of the Bulk UHMWPE

Figure 5.1 shows an infrared scan of a 20 μm film microtomed from the bulk polymer. It is clear from figure 5.1 that the molecular structure of the UHMWPE used in this investigation shows no evidence for chain branching or double-bond formation. The absorption bands occurring at 720, 1460 and 2800 - 3000 cm^{-1} are due to C-H out-of-plane bends in $C-(CH_2)_n-C$ (for $n \rightarrow \infty$), C-H deformation frequencies and C-H stretching frequencies, respectively. Thus, considering only singly bonded chains, the average molecular chain length is calculated to lie between 40 and 72 μm for the different grades of UHMWPE whose molecular weights ranged from 4.5 to 8 x 10^6 $g.mol^{-1}$, respectively.

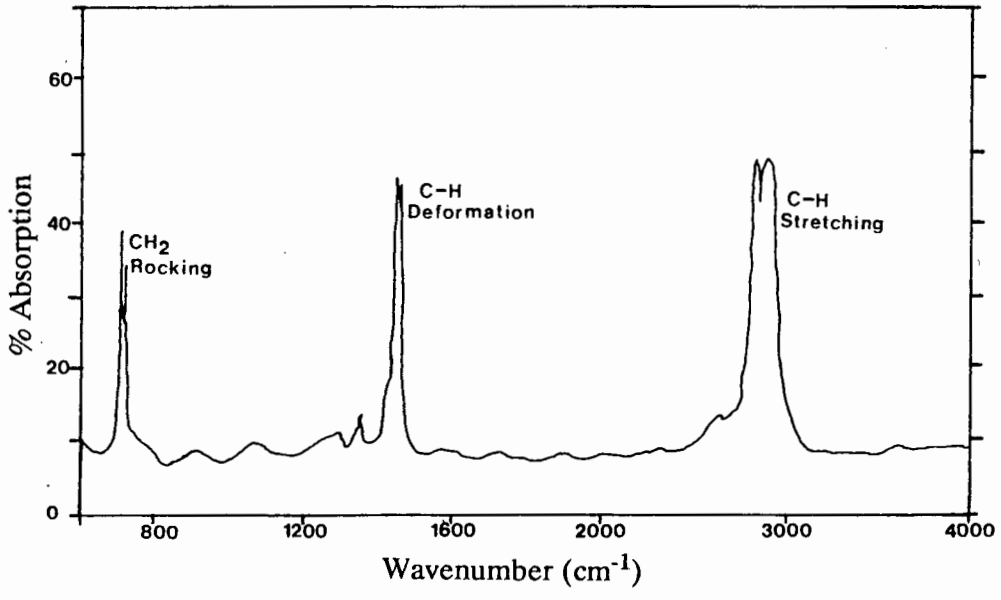

Figure 5.1: An infrared spectrum of UHMWPE film.

When examined under polarized light, these microtomed films show that the predominant morphology of the polymer is not fully spherulitic. Large areas of non-spherulitic material can be observed in figure 5.2. The ordered regions consist of plate-like lamellae which consist of regularly folded chains perpendicular to the lamellae surface and interspersed in a highly coiled amorphous matrix [14]. (See also section 2.5). The Maltese crosses attest to the prevalence of birefringent units.

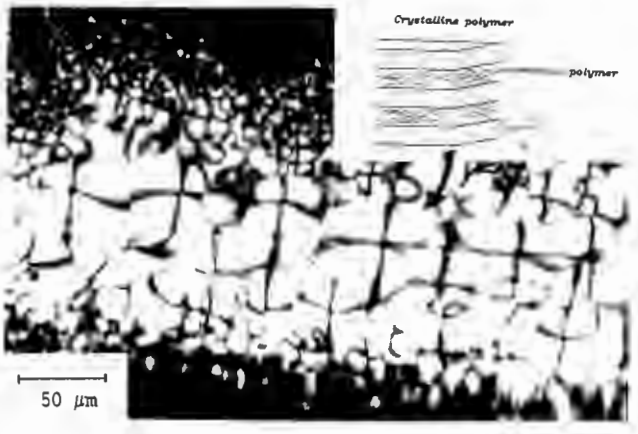

Figure 5.2: The 'semi'-spherulitic structure of semicrystalline UHMWPE as observed in polarized light. Inset: A model of the lamellar nature of a fibril with regular chain-folded structure.

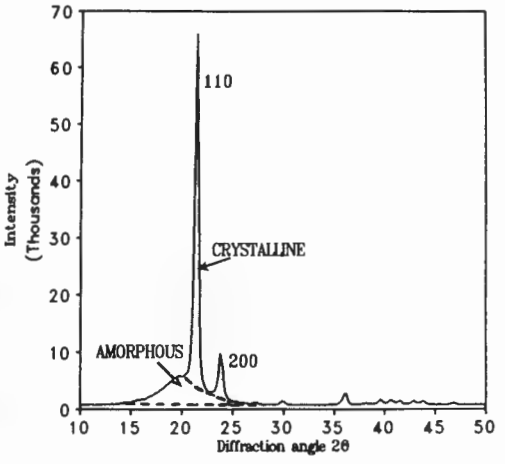

Figure 5.3: An X-ray diffraction trace of bulk UHMWPE showing the crystalline peaks.

X-ray studies also confirm that highly ordered regions, as shown by the intensity and sharpness of the peaks in figure 5.3, are found in the bulk polymer. From these data it has been calculated that the dimensions of the polyethylene unit cell are a = 0.748 nm, b = 0.499 nm and c = 0.255 nm (chain axis). The lamellae are estimated to be about 16 nm thick. The crystallinity of the bulk polymer was found to be 41.7 and 42% by XRD and DSC, respectively. (See table 5.3, p. 136).

5.2.2 Filler Characterization of UHMWPE

Figure 5.4 shows the fracture surface of Ceram P after it has been fractured at liquid nitrogen temperature. The measured diameters of the glass beads ranged from 16 to 60 μm and their concentration was found to be approximately 10 vol. %. A typical x-ray spectrum obtained from a glass bead is shown in figure 5.5. Because of the limitation of EDS, only silicon, calcium and traces of magnesium and aluminium were detected.

An EDS scan of the Special DS grade failed to identify the filler compound because of the low level of filler concentration. Figure 5.6 shows a micrograph of a thin film of this filled material when examined under the optical microscope. The particulate structure is obtained through sintering a mixture of powdered polyethylene with the filler.

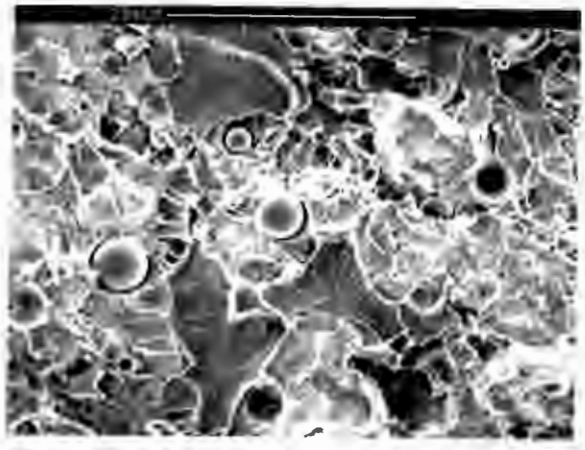

Figure 5.4: A SEM image of the fractured surface of glass bead filled UHMWPE, showing the variation in the sizes of the glass beads in the UHMWPE.

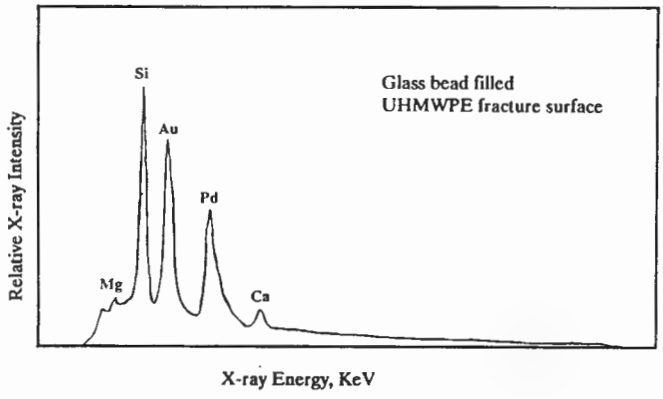

Figure 5.5: An X-ray spectrum of a glass bead inclusion in UHMWPE (vertical full scale = 1024 counts).

An XRF scan of the Special DS UHMWPE is given in figure 5.7. The XRF scan shows that elements such as barium, sulphur, zinc, cadmium, titanium and vanadium were present in the UHMWPE. The yellow colour of the polymeric material was probably due to $ZnSO_4$ and the filler, titanium based. The Special DS UHMWPE will henceforth be termed the *"inorganically filled UHMWPE"*, while the Ceram P material will be termed the *"glass bead filled UHMWPE"*.

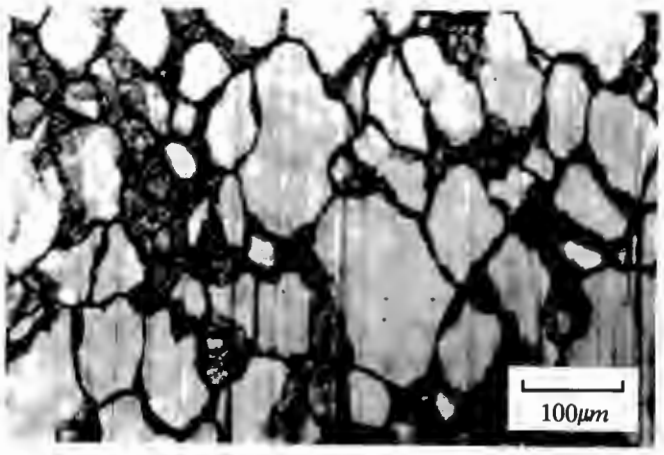

Figure 5.6: An optical micrograph of a thin film of the inorganically filled UHMWPE showing the particulate structure of the polymer. The dark mottled areas are associated with the filler.

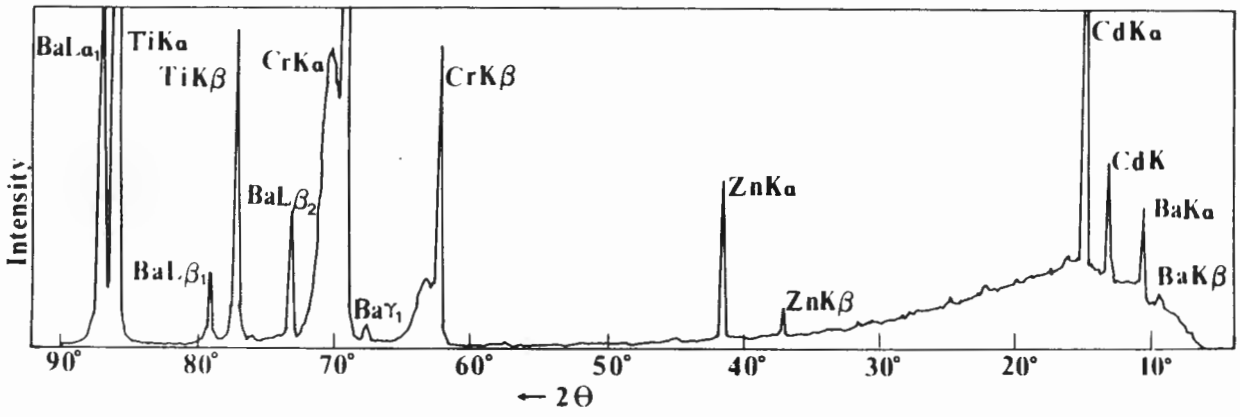

Figure 5.7: A portion of a typical XRF trace of the inorganically filled UHMWPE in fig. 5.6, showing the elements present in the filler.

5.3 FRICTION AND WEAR

5.3.1 Wear Studies on 0.3 μm R_a Counterfaces

The variation in volume loss for all the UHMWPE materials together with the variation of counterface roughness with sliding distance is shown in figures 5.8 (a), (b), (c), (d) and (e). The tests were conducted in distilled water at 0.25 $m.s^{-1}$ under a pressure of 10 MPa, with the sliding direction perpendicular to the grinding direction on the metal counterface.

Each data point represents the average of three tests and the data for these tests and other tests conducted to different sliding distances are all tabulated in Appendix A.

The graphs show that the variations found were typical for all the polymers tested. In all cases, the graphs show an initial high wear rate regime or *"bedding-in"* stage, followed by a reduction in the wear rate when sliding perpendicular to the grinding marks of the counterface. The value of counterface roughness, R_a, decreases rapidly during the early stages of sliding, due to a build-up of transferred polymer, before levelling off during steady-state polymer wear.

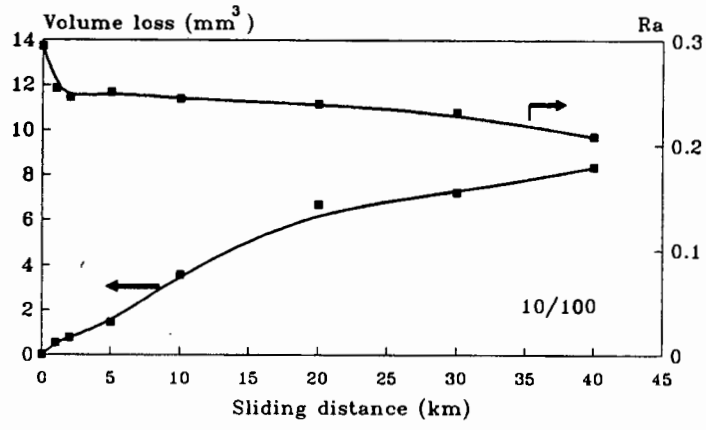

Fig. 5.8(a)

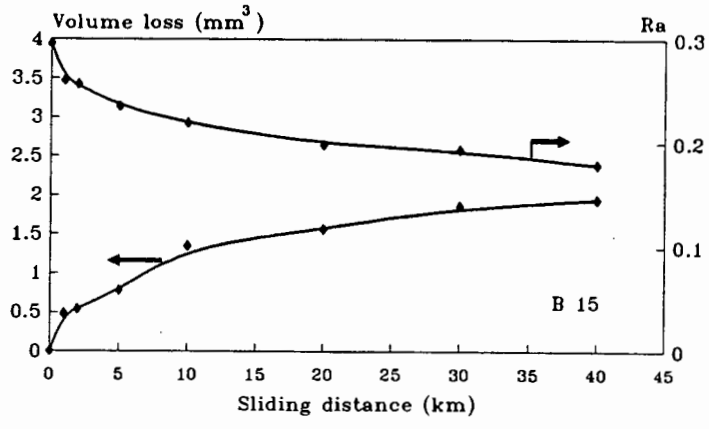

Fig. 5.8(b)

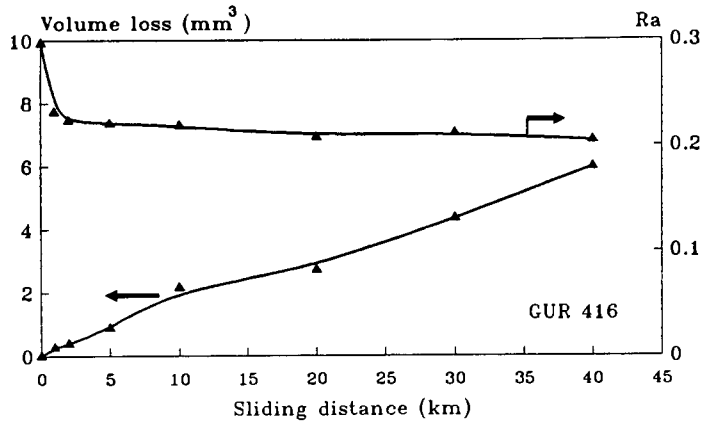

Fig. 5.8(c)

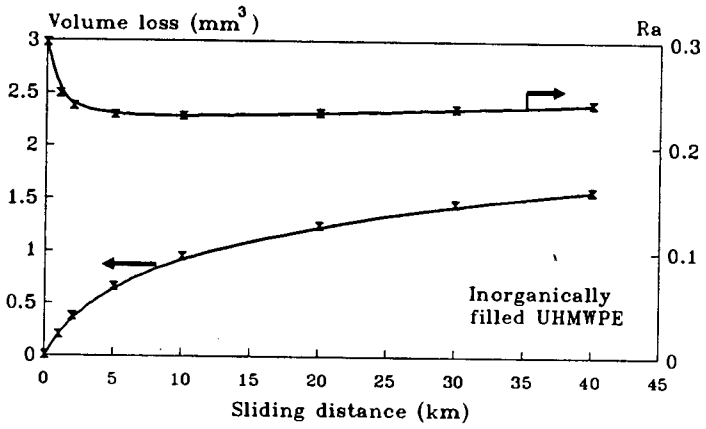

Fig. 5.8(d)

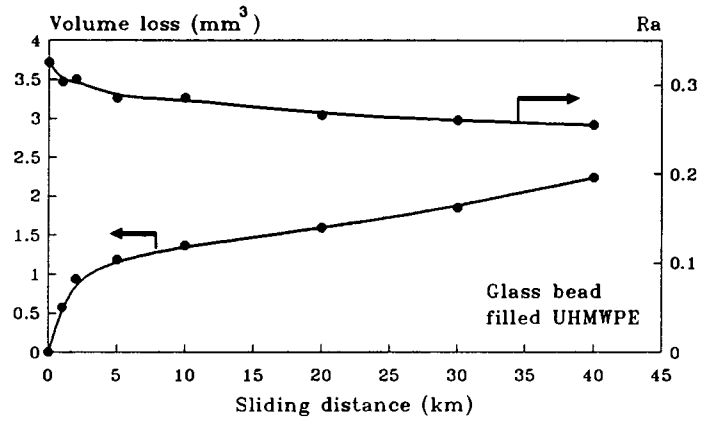

Fig. 5.8(e)

Figures 5.8 (a) - (e): The variation in volume loss of the UHMWPE and counterface roughness, R_a, with sliding distance. (a) 10/100; (b) B 15; (c) GUR 416; (d) Inorganically filled UHMWPE (Special DS); (e) Glass bead filled UHMWPE (Ceram P).

In figure 5.9, the results of all the UHMWPE materials tested have been plotted on a single curve. Each point thus represents the average of 15 data points. From this figure, the two regions of wear can clearly be distinguished and it is seen that the *"bedding-in"* period corresponds to approximately 10 km of sliding. The specific wear rate in the *"bedding-in"* stage was found to be 1.76 x 10^{-7} $mm^3.N^{-1}.m^{-1}$, while that for the steady-state wear regime was 7.07 x 10^{-8} $mm^3.N^{-1}.m^{-1}$ This means that wear on the initial, unblemished metal counterfaces was about 2.5 times greater than that found during the latter stages of *"steady-state"* wear.

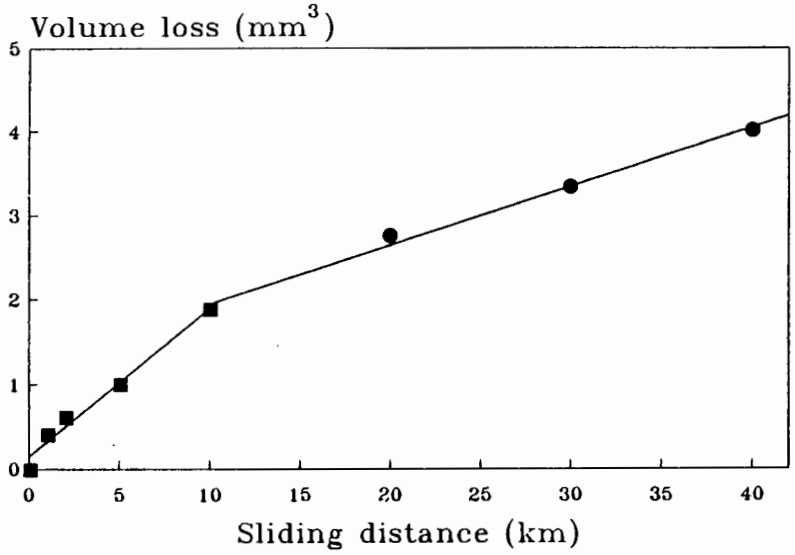

Figure 5.9: The variation in volume loss against sliding distance for all the UHMWPE examined plotted on a single curve. The graph shows that a *"bedding-in"* region of high wear can be differentiated from a lower steady-state wear regime. ■ bedding-in stage, k_a = 1.76x10^{-7} $mm^3.N^{-1}m^{-1}$; ● steady-state wear stage, k_b = 7.07x10^{-8} $mm^3.N^{-1}m^{-1}$.

The reason for this behaviour is believed to be due to the process of transfer film formation in the early stages of sliding wear and a subsequent decrease in the abrasive component of the asperities of the metal counterface. During *"steady-state"* polymer wear, a transfer film completely covers the metal counterface as shown in figure 5.10.

The counterface roughness values decrease by up to 85% in the *"bedding-in"* region corresponding to sliding distances of 10 km. Between 36 and 71% of the total volume is lost from the polymer wear pins during the *"bedding-in"* region, for total sliding distances of 40 km. Thus the decrease in counterface roughness results in an effective decrease in wear

rates. The steady-state wear rates of the UHMWPE materials were approximated from the latter stages of these curves.

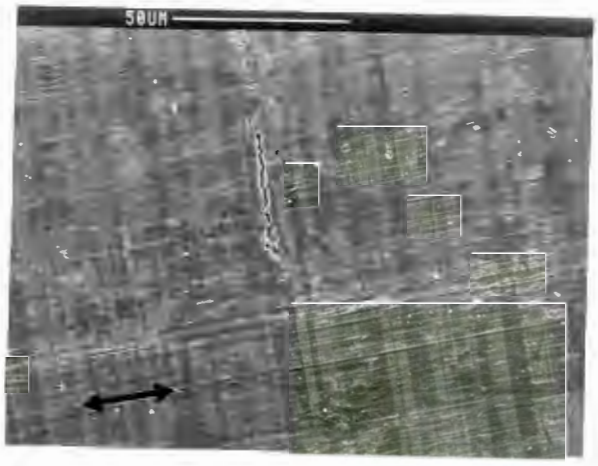

Figure 5.10: A SEM image of the worn metal counterface of unfilled UHMWPE (B 15) after 40 km of sliding showing a uniform transfer film. The arrow indicates the sliding direction.

The specific wear rates for all the UHMWPE materials, as well as the operating conditions for these tests are shown in table 5.1.

Polymeric Material	Specific Wear Rate ($mm^3/N.m$)	Steady-State Kinetic Friction Coefficients	Test Conditions
10/100	9.6×10^{-8}	0.044	test on 0.3 μm R_a
B 15	1.9×10^{-8}	---	perpendicular to grinding direction on metal counterface
GUR 416	5.7×10^{-8}	---	
Ceram P	2.9×10^{-8}	0.033	distilled water
Special DS	1.7×10^{-8}	0.035	0.25 $m.s^{-1}$; 10 MPa

Table 5.1: A summary of the sliding wear results of the UHMWPE materials against the 0.3 μm R_a counterfaces. The % standard deviation was within 15% for all cases.

From table 5.1, a significant difference can be seen between the steady-state wear rate values for the different UHMWPE grades. The significance of the test results can also be seen more clearly in figure 5.11, when the wear performance of these polymers are shown relative to that for the inorganically filled UHMWPE *i.e.* the Special DS grade. The wear resistance of this material was almost 6 times better than that for the unfilled 10/100 grade. Furthermore, large increases in molecular weight of the UHMWPE did not necessarily lead to corresponding large decreases in wear rates (tables 4.1 and 5.1).

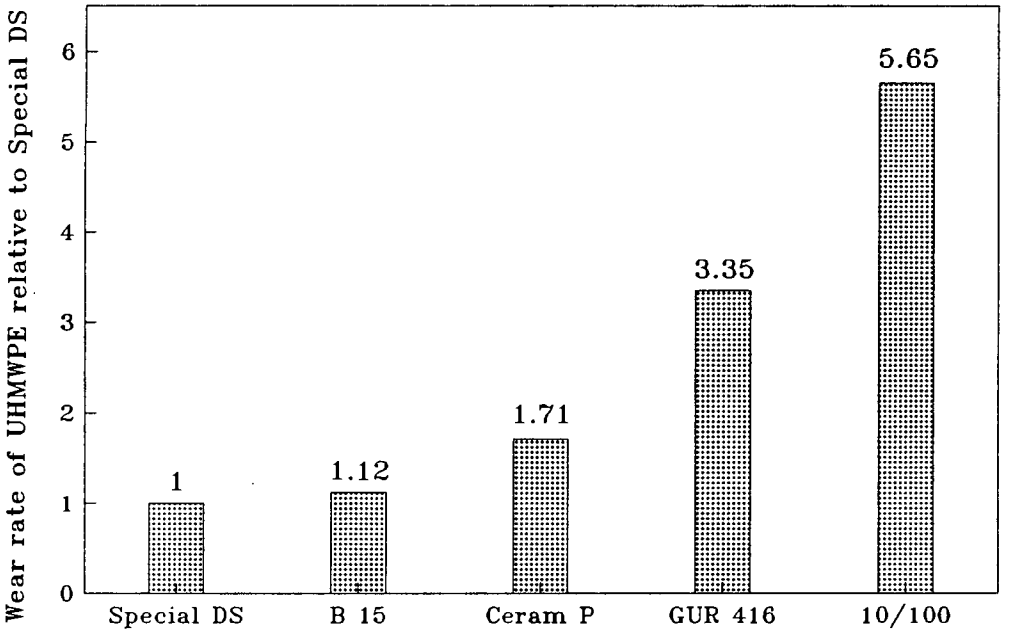

Figure 5.11: The sliding wear performance of UHMWPE grades listed in table 5.1 relative to that of the Special DS grade.

Figure 5.12 shows the relationship between the coefficient of friction and sliding distance for various UHMWPE materials. The initial friction represents the friction of the polymer against the metal counterfaces when no or little material has been transferred. The initial, unsteady-state friction is about 20-30% higher than the steady-state values. The polymer fills the crevices between the metal asperities and modifies the metal surface topography (figure 5.10) to the extent that the friction coefficients are reduced to a stable value. From figure 5.12, it is also clear that the filled UHMWPE displayed much lower friction coefficients than the unfilled UHMWPE, 0.033-0.035 compared with 0.044 as shown in table 5.1. The average surface temperature increased by about 3 °C during the water-lubricated wear tests.

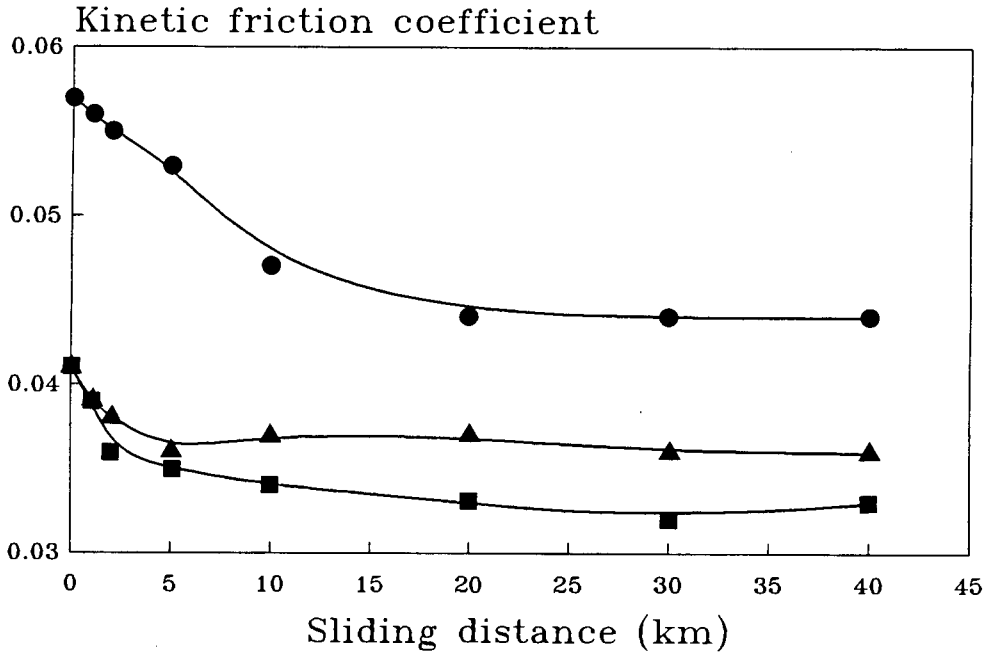

Figure 5.12: The variation of coefficient of friction with sliding distance for filled and unfilled UHMWPE on counterfaces of 0.3 μm R_a roughnesses. ● unfilled UHMWPE, ■ glass bead filled UHMWPE, ▲inorganically filled UHMWPE.

5.3.1.1 The effect of small changes in counterface roughness, R_a, on wear rates

In order to determine the effect of relatively small changes in counterface roughness, R_a, tests were conducted on counterfaces of controlled R_a values both rougher and smoother than the 0.3 μm R_a initially selected for the wear tests. A tolerance of approximately 0.05 μm R_a was chosen for these tests, conducted on UHMWPE grade B 15 under water lubrication at 0.25 $m.s^{-1}$ under a pressure of 10 MPa. The results of these tests are shown in figure 5.13. In figure 5.13(a), the average volume loss of polymer of two tests for each value of R_a, is plotted against sliding distance. During the *"bedding-in"* period, the wear rate is higher for the rougher counterface as more polymer is lost due to the greater abrasivity of the metal asperities. The wear rates during *"steady-state"* also appear to be a function of the initial counterface roughness, even though the metal counterface is completely covered with a transfer film. Thus, higher initial counterface roughnesses gave higher *"steady-state"* wear rates. The counterface roughness for all the tests were found to decrease steadily during the wear tests as shown in figure 5.13(b). The specific wear rates of these tests are plotted on a log-linear scale in figure 5.14. Test results obtained by Lloyd on UHMWPE grade 10/100 obtained under the same operating conditions are also included for comparison [4]. The specific wear for UHMWPE grade 10/100, correlates

closely to the results by Lloyd, but grade B 15 produced lower wear rates for the counterface roughnesses examined. At low counterface roughness the wear rate varies little with R_a, but increases rapidly as the metal roughness is increased.

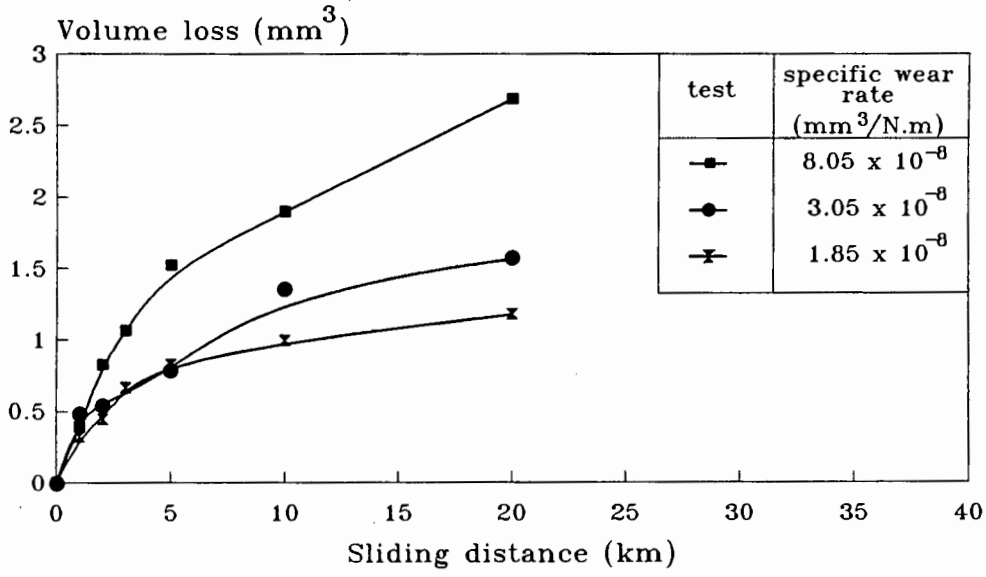

Figure 5.13(a): The variation in volume loss of UHMWPE (B 15) with sliding distance for different values of counterface roughness, R_a. The values of R_a are tabled in fig. 5.13(b).

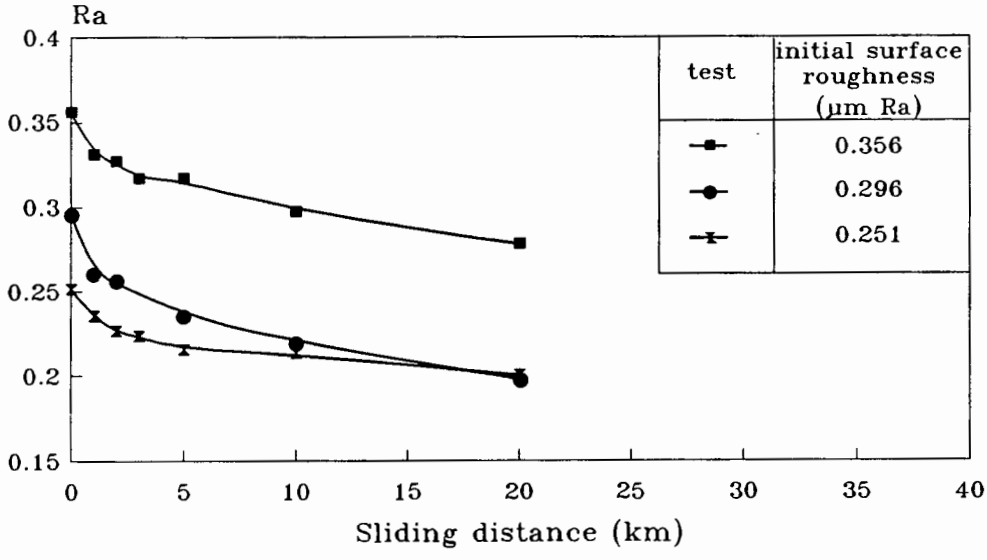

Figure 5.13(b): The variation in counterface roughness, R_a, for three different initial roughnesses, with sliding distance.

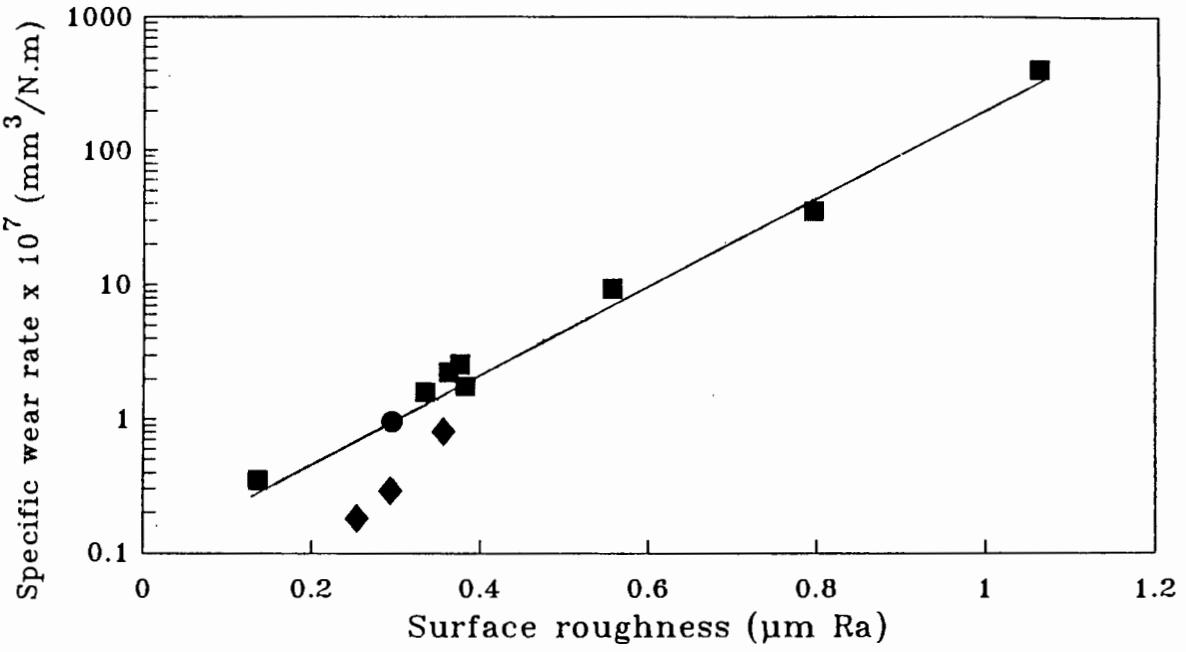

Figure 5.14: The variation of specific wear rate for UHMWPE grades 10/100 and B 15 with counterface roughness R_a. The results obtained are compared with those Lloyd [ref. 4]. ■ Lloyd (10/100), ● Marcus (10/100), ◆ Marcus (B 15).

5.3.1.2 Extended wear studies on rough counterfaces (0.3 μm R_a)

These studies were conducted on the 0.3 μm R_a counterfaces to investigate the long term sliding wear behaviour of filled UHMWPE. The variation of volume loss with sliding distance for the filled UHMWPE materials are shown in figure 5.15. The inorganically filled UHMWPE exhibited low wear rates even after 120 km of sliding. The specific wear rate for this material dropped even further than that obtained in the 0-40 km tests. The wear rate of 7.3 x 10^{-9} $mm^3.N^{-1}.m^{-1}$ is about 2.3 times less than that for the 0-40 km range.

Both the static and kinetic friction coefficients are found to decrease rapidly initially and then more gradually throughout the entire sliding distance examined as shown in figure 5.16.

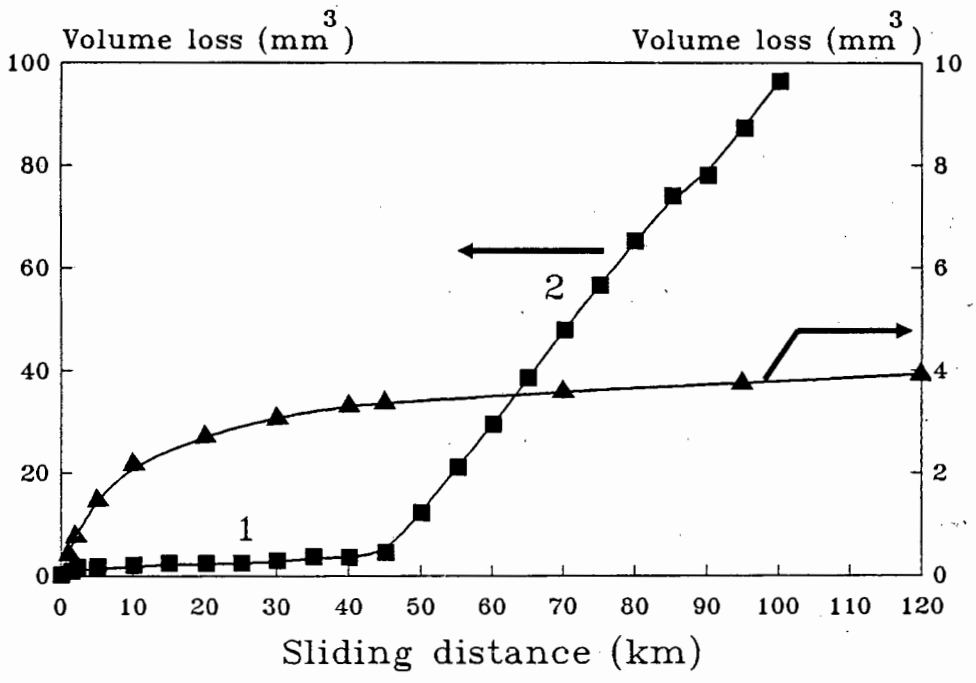

Figure 5.15: The variation in volume loss with sliding distance for filled UHMWPE on the rough (0.3 μm R_a) counterface. ■ glass bead filled UHMWPE, ▲ inorganically filled UHMWPE.

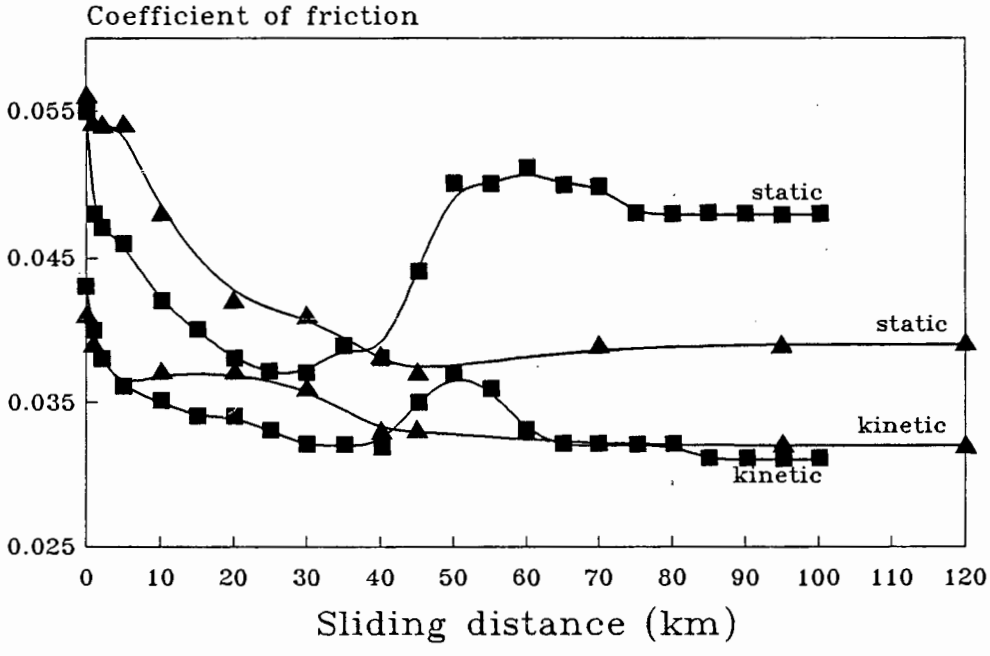

Figure 5.16: The variation in static and kinetic friction coefficients for filled UHMWPE on the rough counterface. Key in fig. 5.15.

A SEM examination of the metal counterface (figure 5.17) shows a heavy build-up of transferred material on the counterface during the closing stages of such a test.

It would appear that the final surface roughness at the end of the test is significantly smaller than that of the initial 0.3 μm R_a (table 5.2, p.119), but this could not be established quantitatively due to the hard stylus partially penetrating the soft transferred material. Nevertheless, the profile of the inorganically filled UHMWPE on the metal counterface is different from that of the initial clean metal surface. Figure 5.18(a) shows a typical profile of the unworn surface, while that of the worn surface covered with a transfer film is shown in figure 5.18(b). The worn profile shows smaller irregularities than the initial profile, due to material being transferred onto the counterface.

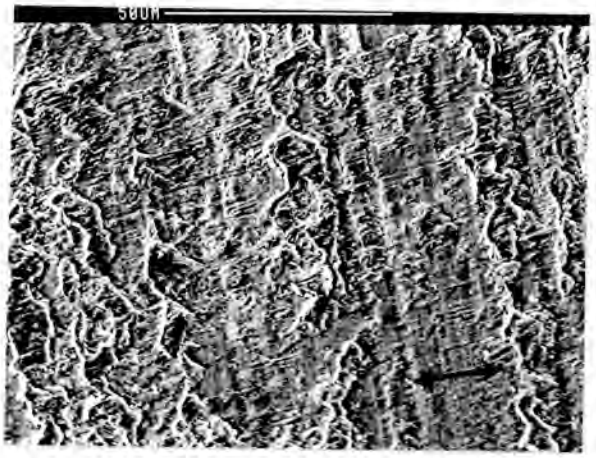

Figure 5.17: A SEM image of the worn metal counterface after 75 km following sliding against the inorganically filled UHMWPE. The arrow indicates sliding direction.

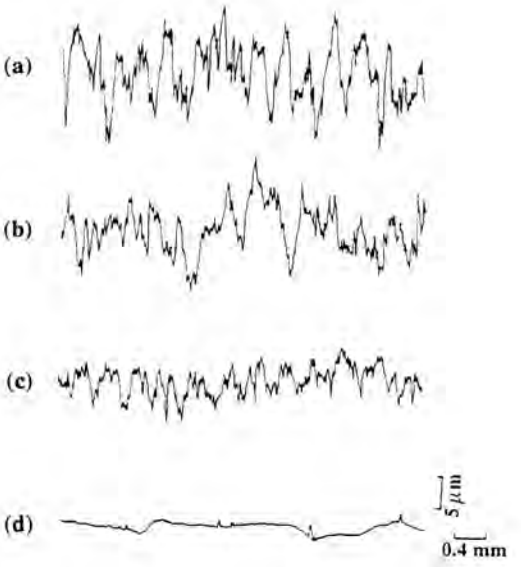

Figure 5.18: Talysurf profiles of the unworn and worn metal plates after sliding against filled UHMWPE on the rough counterface. *(a)* unworn plate. *(b)* inorganically filled UHMWPE after 60 km. *(c)* glass bead filled UHMWPE after 30 km. *(d)* glass bead filled UHMWPE after 100 km.

The glass bead filled UHMWPE showed an abrupt increase in wear after about 45 km of sliding. It was noticed that the counterface surface had become polished prior to this high wear regime. The initial low wear rate region is labelled *"1"*, and the high wear rate region is labelled *"2"* in figure 5.15. The wear rate of region 1 is approximately 33 times lower than that obtained for region 2. These wear rates are also given in table 5.2. At the onset of high wear, there is a slight increase in kinetic friction (figure 5.16) before the friction decreases to a constant value. The static friction coefficient, however, shows a dramatic 30% increase in friction during this transition period. The counterface roughness profile

was found to be altered when measured after 30 km of sliding (figure 5.18(c)) and completely polished and devoid of a transfer film at the end of the test *i.e.* after 100 km. Figure 5.18(d) shows that very few irregularities are found on the mirror-like finish at the end of 100 km sliding. The surface roughness of the metal surface has decreased to 0.05 μm R_a, as shown in table 5.2 (p 119). Very little polymer remains attached to the counterface and it is only near the end of the stroke that a build-up of patchy transferred material was detected as shown in figure 5.19. This micrograph shows evidence that the initial striations are completely polished away by the glass beads in the UHMWPE.

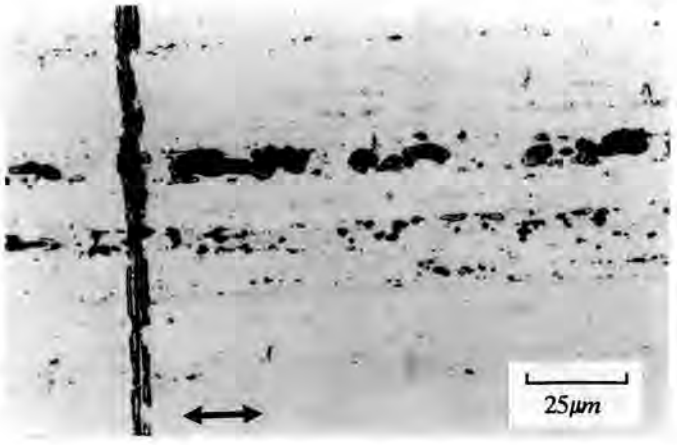

Figure 5.19: An optical micrograph of the worn metallic counterface after 100 km following sliding against glass bead filled UHMWPE. Most of the polymer on the glass bead abraded surface are found near the end of the stroke. The arrow indicates sliding direction.

5.3.2 Wear Studies on Surfaces Ground Parallel to the Sliding Direction

Sliding wear tests were conducted on metal counterfaces ground parallel to the sliding direction in order to compare the wear behaviour of UHMWPE with the tests conducted on counterfaces ground perpendicular to the sliding direction. The operating conditions are listed in table 5.1, but the values of R_a measured in the direction of sliding were lower than those measured across the grinding marks (0.212 ± 0.015 compared with 0.313 ± 0.015 μm R_a). When the polymer pin is worn in a direction parallel to the grinding direction of the metal counterface, a high *"bedding-in"* region followed by a region of *"steady-state"* wear, similar to that found when wear studies are conducted perpendicular to

the striations on the metal counterface, are found. In figure 5.20, the results of three tests on UHMWPE grade GUR 416, conducted parallel to the grinding marks on the counterface, are compared with the average result of three tests when the polymer was worn perpendicular to the grinding direction. It can be seen from figure 5.20 and table 5.2, that the wear rates obtained were approximately 1.9 times higher for the period of experimentation, when sliding is conducted parallel to the grinding direction.

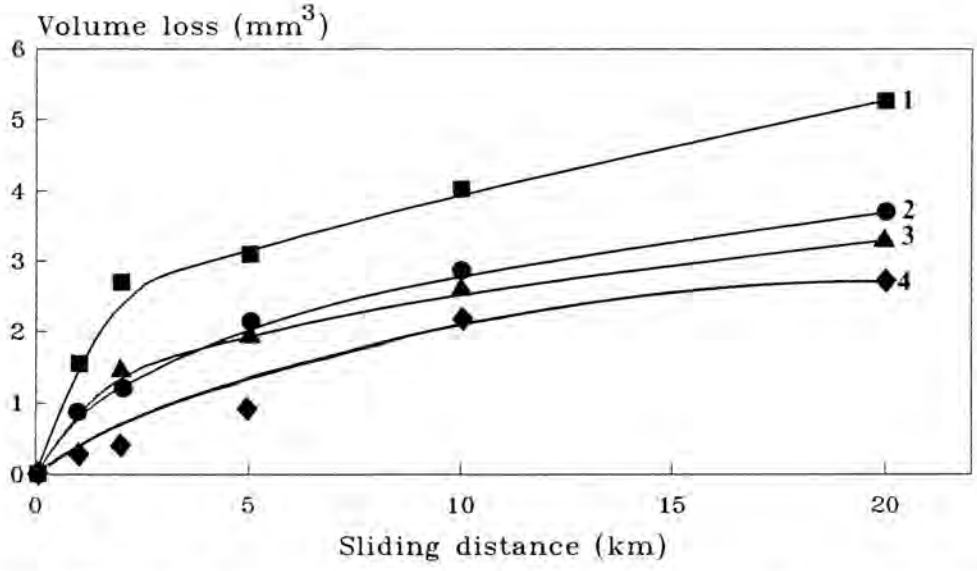

Figure 5.20: Volume loss *vs.* sliding distance curves for UHMWPE grade GUR 416, sliding both parallel and perpendicular to the grinding direction of the metal counterface. 1,2,3 parallel; 4, perpendicular.

When the polymer is worn in a direction parallel to the grinding direction on the counterface, a stable and coherent transfer film is not formed on the counterface. Figure 5.21(a) shows optical micrographs of the worn metal counterface after 2, 10 and 20 km when the polymer is worn parallel to the grinding direction. The optical micrographs of figure 5.21(a) shows that polymer particles are found on the counterface and these particles increase in number as the wear process continues. Optical micrographs in figure 5.21(b) show the worn metal counterface with the grinding direction perpendicular to the counterface, after being subjected to the same amount of sliding. In figure 5.21(b), the transferred polymer bands grow towards each other and a complete and highly adherent transfer film is formed after 20 km. In contrast, the amount of polymer transferred after 20 km when sliding parallel to the grinding direction, resembles that found in the first 100 m when sliding perpendicular to it.

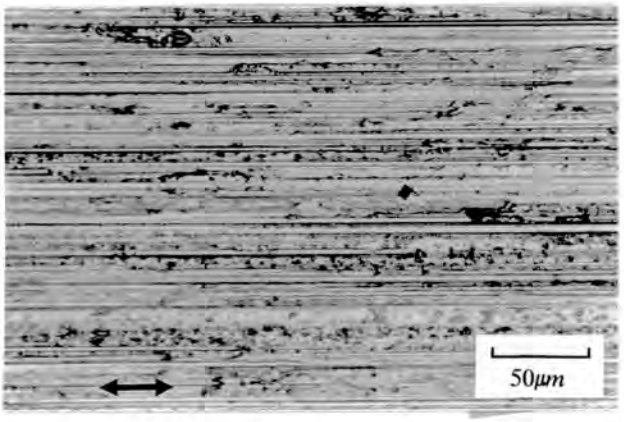

(i)

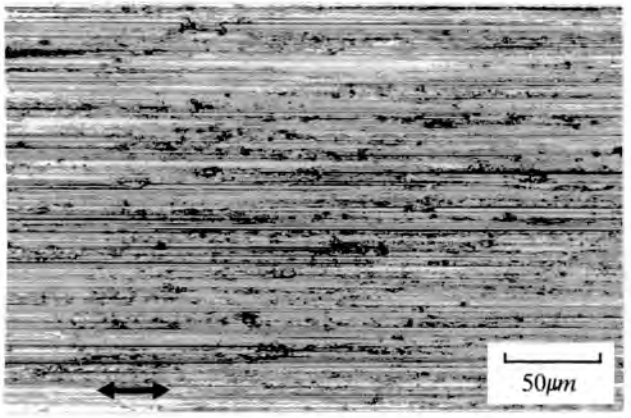

(ii)

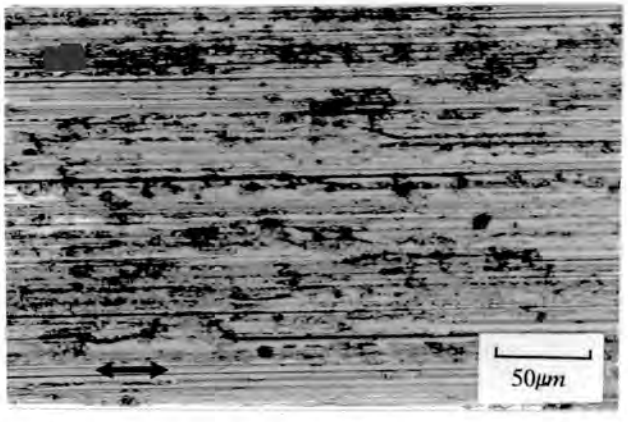

(iii)

Figure 5.21(a): Optical micrographs of the worn metallic counterface after *(i)* 2 km *(ii)* 10 km and *(iii)* 20 km of sliding wear. Sliding is parallel to the grinding direction showing polymer particles which do not form a coherent film on the metal counterfaces. The arrows indicate the sliding direction.

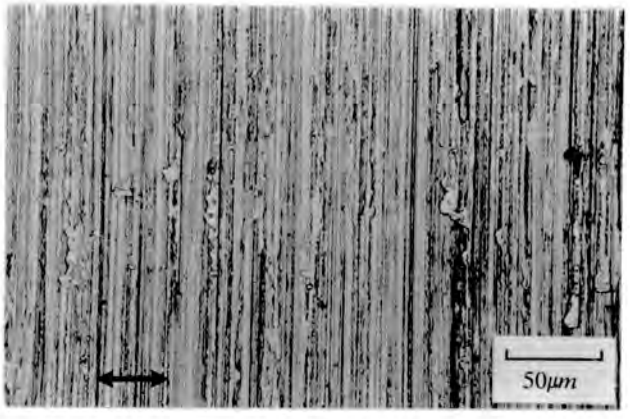

(i)

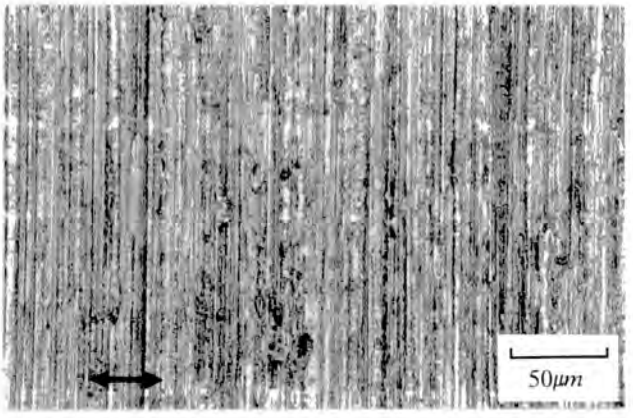

(ii)

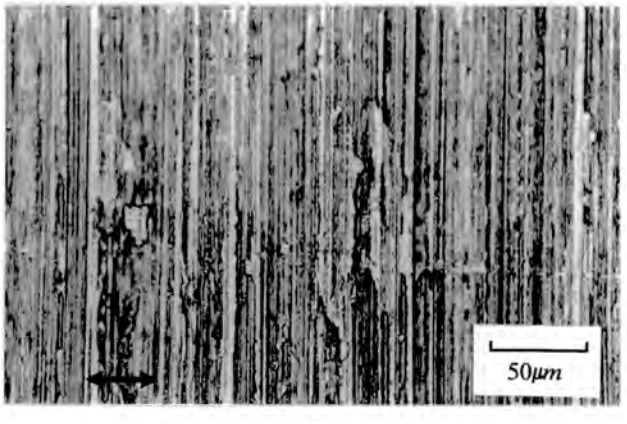

(iii)

Figure 5.21(b): Optical micrographs of the worn metallic counterface after *(i)* 2 km *(ii)* 10 km and *(iii)* 20 km of sliding wear. Sliding is perpendicular to the grinding direction and a stable and adherent transfer film is formed over the metal surface. The arrows indicate the sliding direction.

Wear tests on UHMWPE grades GUR 416 and B 15 showed that the wear behaviour on surfaces ground parallel to the sliding direction becomes very erratic when the wear tests are performed over extended periods. The wear of the UHMWPE was found to increase dramatically over the period of experimentation as shown in figure 5.22. The values of R_a, measured in the direction of sliding, do not decrease steadily but are found to fluctuate due to the agglomeration of relatively large polymer particles on the metal counterface. In figure 5.23, both the static and kinetic friction coefficients decrease initially but then increase rapidly as the wear rate increases. These friction coefficients are similar to those found during the initial periods on sliding wear tests conducted perpendicular to the ground surface (see figures 5.12 and 5.16), but are higher over the major part of the test. The higher friction are associated with the inability of the polymer to form a coherent film on the metal counterface.

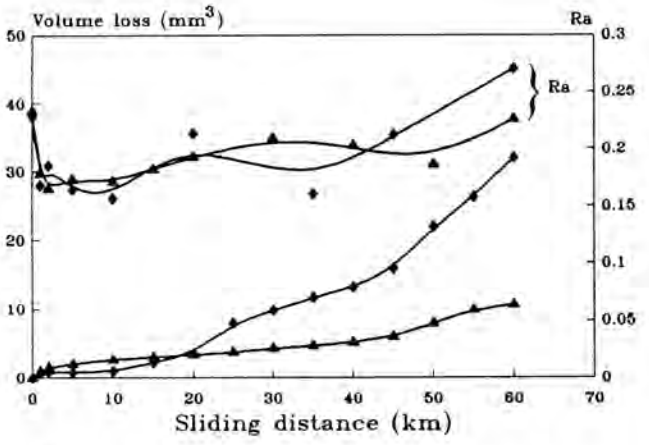

Figure 5.22: Volume loss *vs.* sliding distance curves for UHMWPE grades B 15 and GUR 416 on surfaces ground parallel to the sliding direction. ◆B 15, ▲GUR 416.

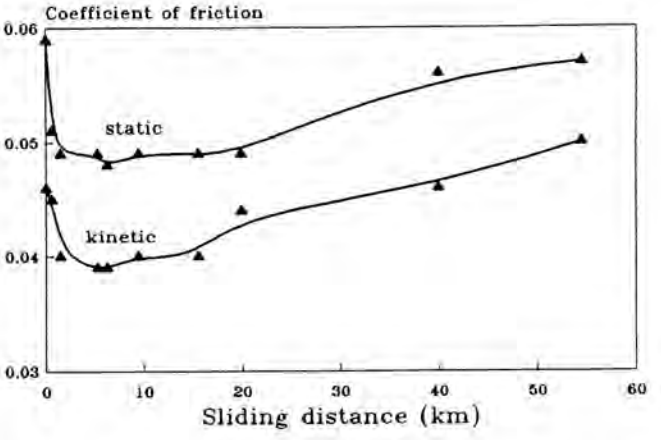

Figure 5.23: Static and kinetic friction coefficients *vs.* sliding distance of UHMWPE grade GUR 416 on a surface ground parallel to the sliding direction. ▲GUR 416.

Figure 5.24 shows an optical micrograph of the worn metal surface covered with patchy polymer, during an extended test with the grinding direction parallel to the sliding direction. Relatively large patchy polymer particles which do not form a coherent transfer film, leads to the higher wear rates on these counterfaces.

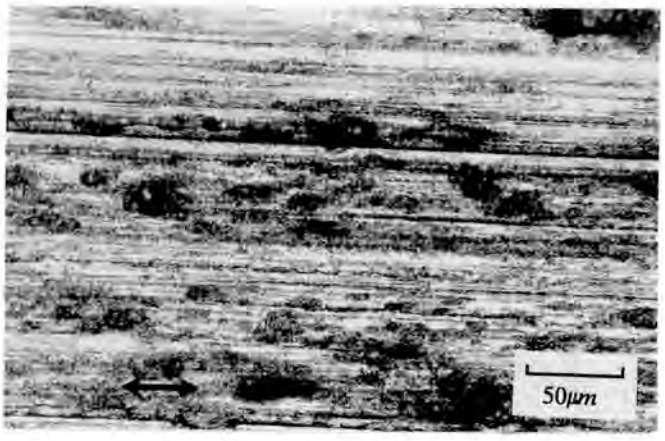

Figure 5.24: An optical micrograph of the worn metal counterface after 50 km of sliding wear on a surface ground parallel to the sliding direction. Relatively large polymer particles responsible for the high wear rates are found on the surface. The arrow indicates sliding direction.

Counterface roughness traces taken across these steel sliders, both parallel and perpendicular to the grinding direction, do not show the characteristic sharp decrease in R_a when sliding is conducted perpendicular to the ground surface (figure 5.25). The traces taken parallel (*i.e.* along BB in figure 5.25) are erratic and the effective R_a values are increased slightly. The polymer particles present on the surface (figure 5.21(a)) are responsible for the small increase in R_a.

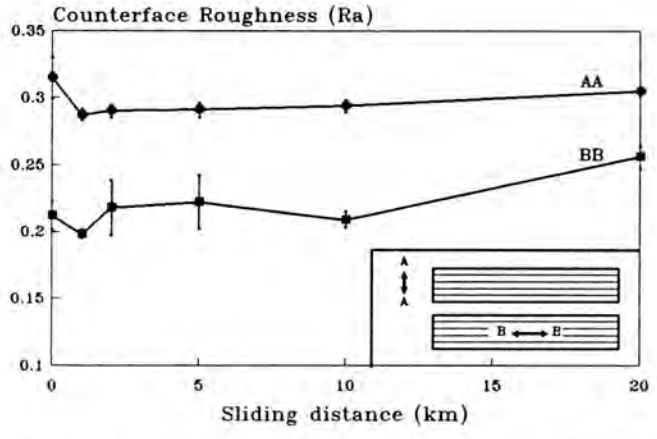

Figure 5.25: Counterface roughness (R_a) traces *vs.* sliding distance when sliding parallel to the grinding direction: (AA) roughness measurements taken perpendicular to the grain; (BB) roughness measurements taken parallel to the grain.

Figure 5.26 shows the Talysurf profiles of the unworn and worn counterface taken in the direction of sliding. The highly irregular profile of the worn surface are due to the discrete lumps of polymer found on these metal counterfaces.

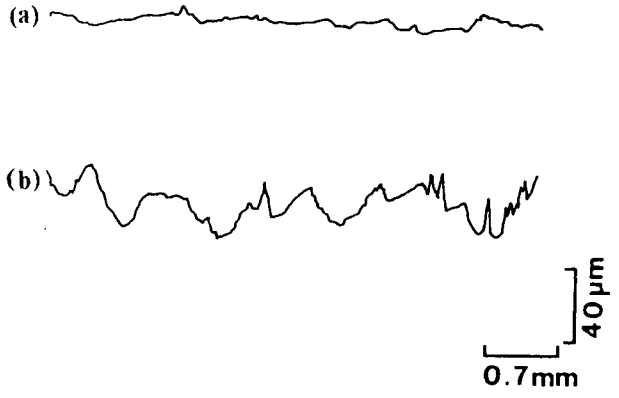

Figure 5.26: Talysurf profiles of the unworn and worn metal counterfaces ground parallel to the sliding direction and taken in the sliding direction. *(a)* a trace of the unworn counterface. *(b)* a trace of the worn counterface after 20 km.

5.3.3 Wear Studies on Smooth Counterfaces (0.03 μm R_a)

The variation in volume loss of polymer with sliding distance for the filled UHMWPE (grades Special DS and Ceram P) and an unfilled UHMWPE (grade B 15) on the smooth counterfaces (0.03 μm R_a) is shown in figure 5.27. The characteristic high initial wear of the UHMWPE materials sliding against counterface roughnesses of 0.3 μm R_a was absent on these smooth counterfaces. For the inorganically filled UHMWPE, *test 1* refers to the test on a counterface which was abraded on SiC paper, while *test 2* refers to a test of the inorganically filled UHMWPE on a counterface that has previously been smoothly polished by the glass bead filled UHMWPE. Since no steady-state wear rates were apparent on the smooth counterfaces, the total volume losses after 20 km sliding were used for comparing the different materials (table 5.2). The filled UHMWPE showed the highest volume losses on the smooth counterfaces. It was also apparent that the wear of the inorganically filled UHMWPE on the surface polished by the glass beads was much higher when compared to those tests performed on the SiC abraded surfaces with similar R_a values (table 5.2).

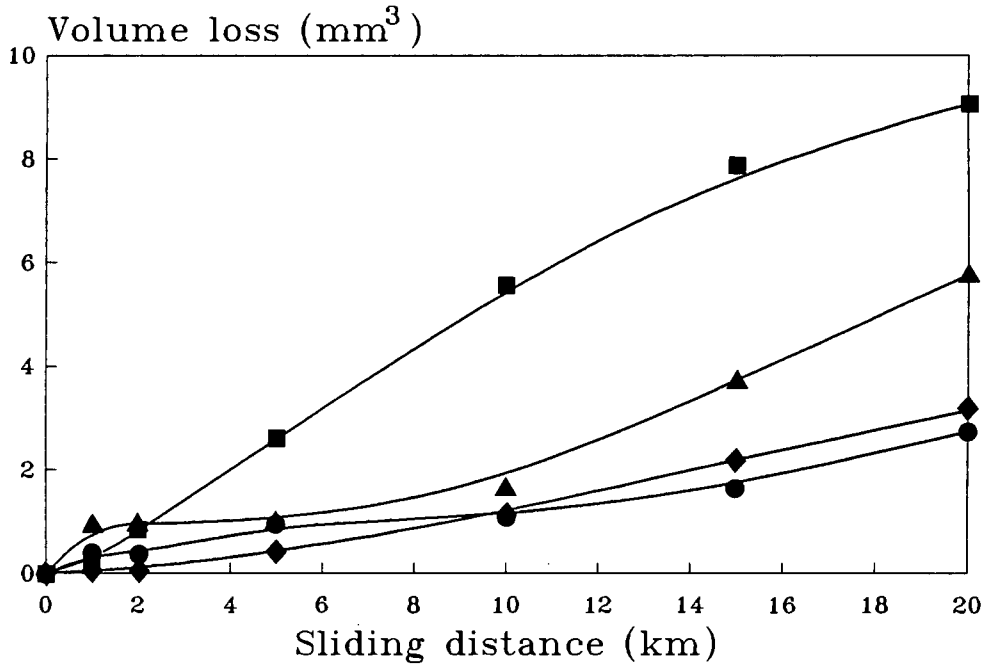

Figure 5.27: Volume loss *vs.* sliding distance curves for filled UHMWPE (grades Special DS and Ceram P) and unfilled UHMWPE (grade B 15) on 0.03 μm R_a counterfaces. ◆ unfilled UHMWPE, ▲ glass bead filled UHMWPE, ● inorganically filled UHMWPE (test 1), ■ inorganically filled UHMWPE (test 2).

Figures 5.28(a), (b) and (c) shows optical micrographs of the surfaces for the three different UHMWPE materials on the smooth counterfaces after a total sliding distance of 20 km. For the unfilled UHMWPE (figure 5.28(a)), thin discontinuous polymer films covered the metal counterface, while little transfer was observed on the glass bead polished counterface (figure 5.28(b)). Figure 5.28(b) shows that glass beads are mobile at the interface and abrade the metal counterface. Both the unfilled and glass bead filled UHMWPE exhibited little wear when compared with that of the inorganically filled UHMWPE (table 5.2). Transfer for the inorganically filled material occurred in the form of patchy, discontinuous lumps of polymer, as shown in figure 5.28(c), and even thicker lumps of polymer were observed on the surface polished by the glass beads *i.e. test 2.*

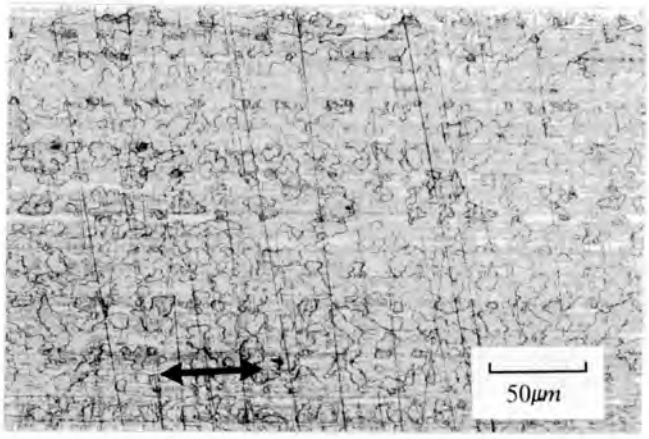

Fig. 5.28(a)

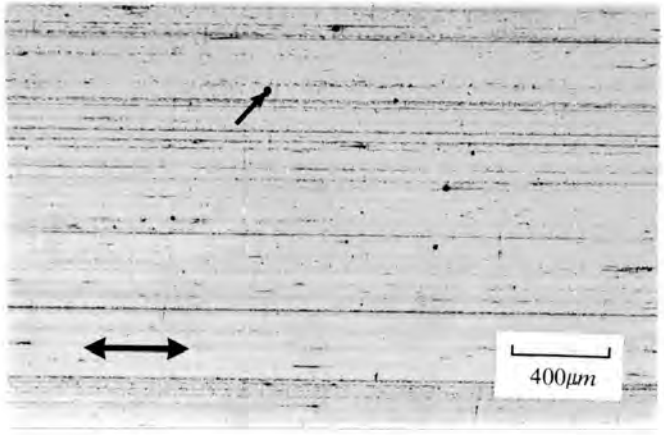

Fig. 5.28(b)

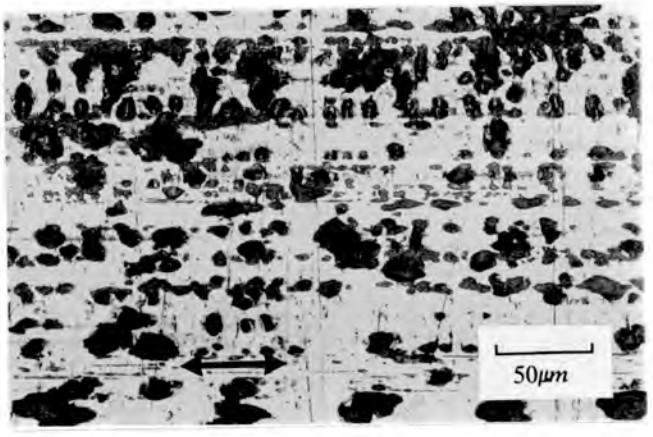

Fig. 5.28(c)

Figures 5.28 (a), (b) and (c): Optical micrographs of the worn smooth metal counterfaces of UHMWPE after 20 km. The arrow indicates sliding direction. (a) unfilled UHMWPE (B 15); (b) glass bead filled UHMWPE, showing a mobile glass bead on the metal counterface - arrowed; (c) inorganically filled UHMWPE showing patchy lumps of polymer on the metal counterface.

The friction coefficients of the sliding couples on these smoother counterfaces did not show the rapid initial decreases observed on the rougher counterfaces, but either increased slightly or remained constant throughout the test as shown in figure 5.29. These friction coefficients are comparable to those obtained on the rougher counterfaces during the steady-state wear regime. The only anomaly occurred for the unfilled UHMWPE friction coefficient. Its coefficient of friction was much lower than that obtained during steady-state wear on the rougher counterfaces (0.032 compared with 0.044).

When the values of R_a, at the end of the tests, are compared with the initial R_a for the smooth counterfaces, the glass bead abraded surfaces show a slight increase in R_a as shown in figure 5.29 and table 5.2. The R_a for the inorganically filled UHMWPE is, however, greatly increased due to the patchy polymer lumps on the metal counterfaces (figure 5.29). The final values of R_a at the end the tests are also shown in table 5.2.

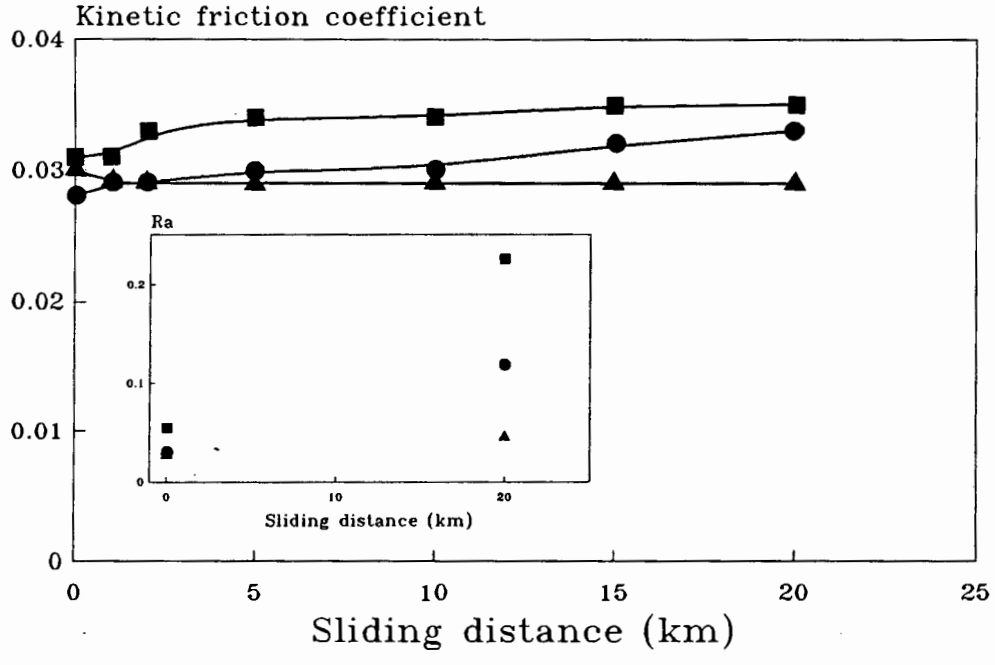

Figure 5.29: The variation of friction coefficient with sliding distance for UHMWPE on the smooth counterface. The inset shows the initial and final values of R_a obtained on these surfaces. ▲ glass bead filled UHMWPE, ● inorganically filled UHMWPE (test 1), ■ inorganically filled UHMWPE (test 2).

Figure 5.30 shows the Talysurf profiles of the unworn and worn frictional tracks. These Talysurf traces show that the initially smooth frictional tracks become rougher with time due to the build-up of transferred material. Although the values of R_a for the SiC abraded surface is similar to that of the glass bead polished surface, their surface profiles are found to be quite different. The surface profile of the unworn steel counterface in figure 5.30(a) shows that there are small irregularities due to the surface preparation, whereas a smoother profile is obtained for the glass bead polished surface after 100 km of sliding wear (see figure 5.18(d)). The glass bead abraded surface profile after 20 km of sliding (figure 5.30(b)) does not show a marked difference to the initial SiC abraded surface profile (figure 5.30(a)). Following sliding wear studies against the inorganically filled polymer, the counterface roughness profiles were found to be highly irregular (figure 5.30(c)) due to discrete polymer lumps adhering to the metal surface. The extent of lumpy transfer occurring on the original glass bead polished surface is even more irregular, as shown in figure 5.30(d), compared to the SiC abraded surface.

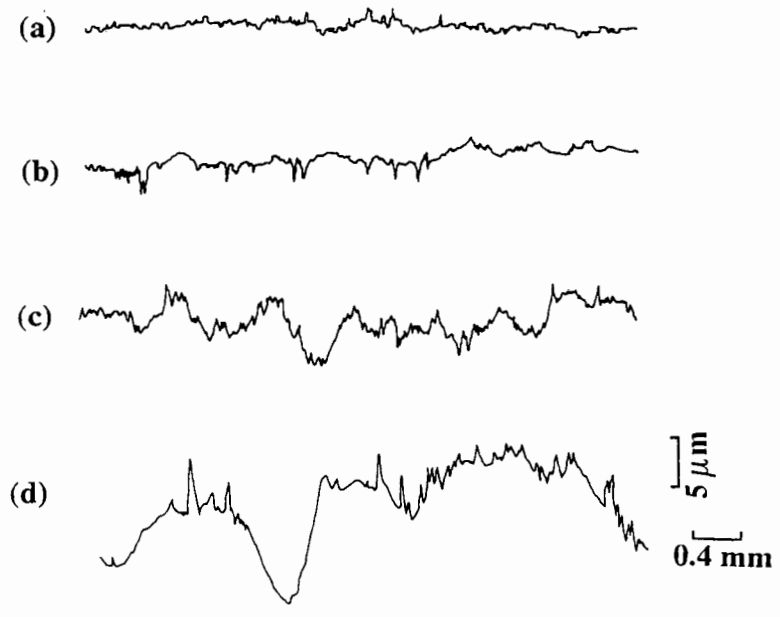

Figure 5.30: Profiles of the unworn and worn metal plates after sliding against filled UHMWPE on the smooth (0.03 μm R_a) counterface for 20 km. (a) unworn SiC abraded plate; (b) glass bead filled UHMWPE on SiC abraded plate; (c) inorganically filled UHMWPE on SiC abraded plates; (d) inorganically filled UHMWPE on glass bead polished plate.

Test	Polymeric Material	Initial Ra	Sliding distance	Wear rate/ volume loss	Friction static/kinetic	Ra at the end of the test
extended tests on 0.3 μm Ra metal counterfaces for filled UHMWPE	Ceram P	0.313	100-120 km	wear rate ($mm^3/N.m$) $6.1x10^{-8}$ (region 1) $2.0x10^{-6}$ (region 2)	0.031 (kin.) 0.05 (stat.)	0.05 (100 km)
	Solidur DS	0.294		$7.3x10^{-9}$	0.03 (kin.) 0.04 (stat.)	0.25 (120 km)
test on surfaces ground parallel to the sliding direction	GUR 416	0.212	20 km	wear rate ($mm^3/N.m$) $1.1x10^{-7}$	0.045 (kin.)	0.256
extended tests on surfaces ground parallel to the sliding direction	GUR 416	0.233	60 km	volume loss (mm^3) 10.65	~ 0.05 (kin.)	0.226
	B 15	0.228		31.95		0.27
test on polished or abraded smooth metal counterfaces	B 15	0.03 (polished)	20 km	volume loss (mm^3) 3.14	0.03 (kin.)	—
	Ceram P	0.028 (polished)		5.76	0.03 (kin.)	0.046
	Solidur DS	0.03 (polished)		2.34	0.03 (kin.)	0.119
	Solidur DS	0.053 (abraded)		9.05	0.034 (kin.)	0.226

Table 5.2: A summary of sliding wear results of UHMWPE materials under different operating conditions.

5.3.4 Wear Studies of UHMWPE Sliding Against UHMWPE

Sliding wear studies conducted of UHMWPE reciprocating against itself showed that no bedding-in periods are obtained for polymer/polymer sliding couples. All polymer/polymer wear tests conducted under water lubrication, showed linear relationships between polymer wear and sliding distance. Figure 5.31 shows the results of wear tests conducted on UHMWPE grades Special DS and B 15 sliding against themselves. The polymer counterfaces generally showed higher wear than their corresponding wear pins. This is attributed to the ease with which any loosely attached polymer can be removed from the counterface once the pin has moved away from that position. Conversely, potential polymer debris still attached to the pin remains in the contact zone and preferentially gets compacted on the pin wear surface. The worn polymer surfaces show signs of severe adhesive damage (figure 5.32) and flaky debris readily aggregate on the pin surface as shown in figure 5.33. The wear rates of approximately 10^{-4} $mm^3.N^{-1}.m^{-1}$ obtained, were of the order of three magnitudes greater than that for UHMWPE sliding against stainless steel under water lubrication. Figure 5.34, shows the results of tests conducted at different loads for two UHMWPE grades. The relatively high coefficients of friction of approximately 0.14 (figure 5.31) can be attributed to the high adhesive forces at the interface or a greater deformation component of friction.

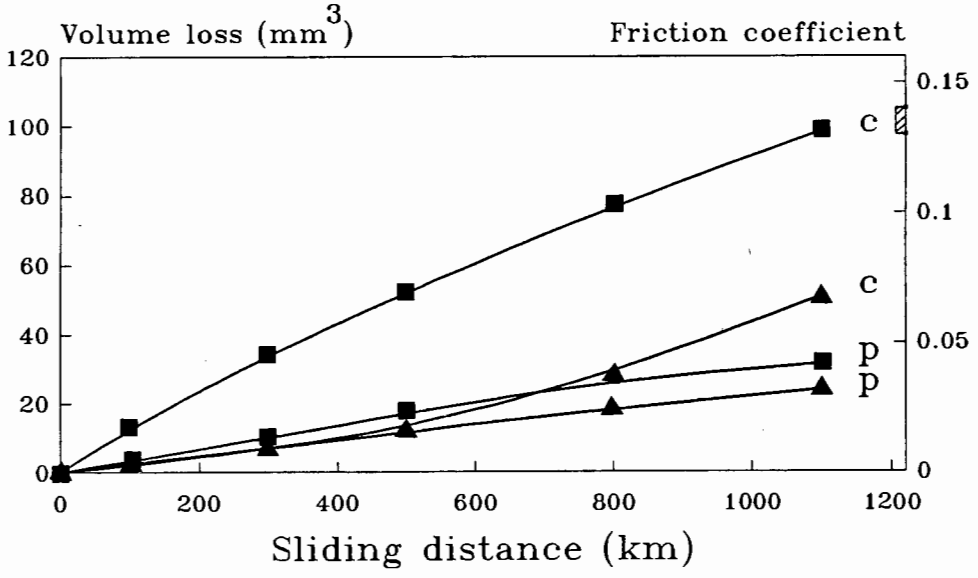

Figure 5.31: Volume loss and friction coefficient *vs.* sliding distance curves for UHMWPE (grades Special DS and B 15) sliding against themselves. ■ inorganically filled UHMWPE, ▲ B 15. p = pin, c = counterface, pressure: 2.5 MPa, velocity: 0.25 $m.s^{-1}$.

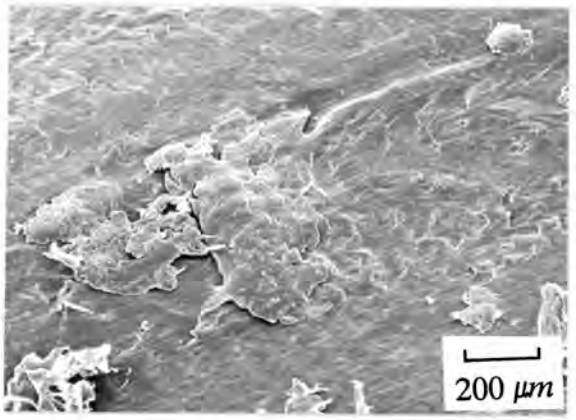

Figure 5.32: A SEM image of the worn surface of an UHMWPE/UHMWPE sliding couple showing signs of severe plastic deformation.

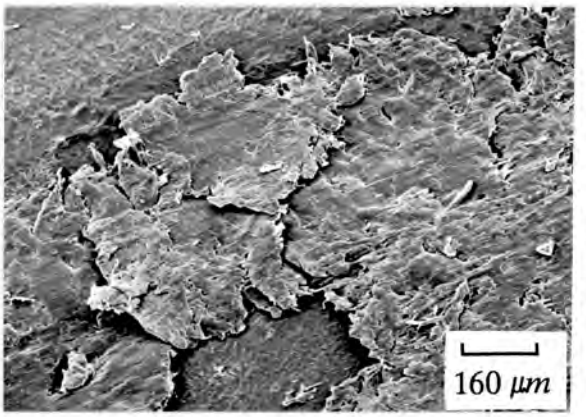

Figure 5.33: Debris flakes agglomerate and become compacted on the polymer pin surface during the reciprocating sliding wear process of UHMWPE on UHMWPE.

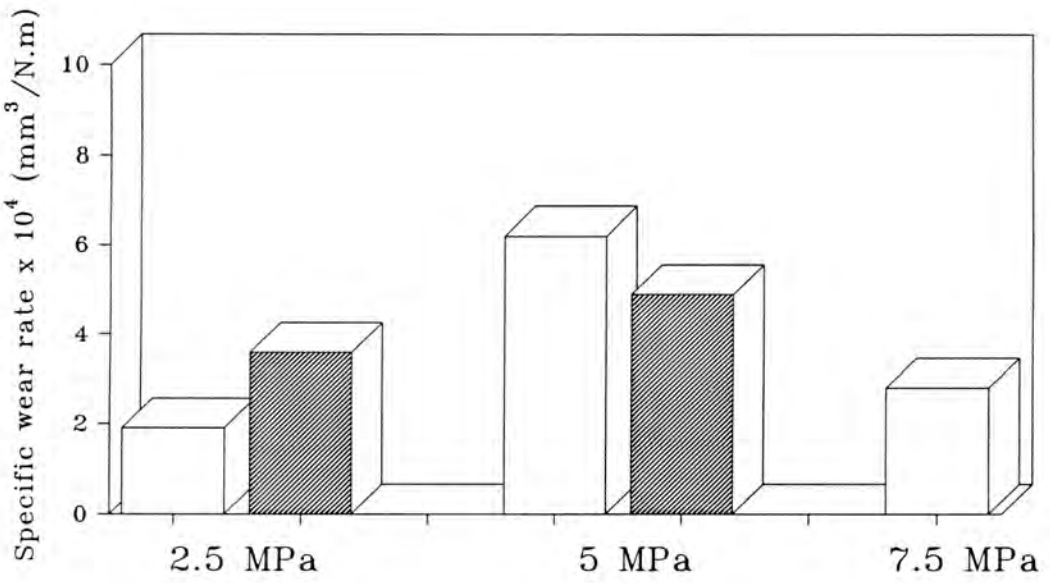

Figure 5.34: A summary of UHMWPE on UHMWPE sliding wear results. □ inorganically filled UHMWPE, ▨ B 15.

5.4 THE TRANSFER FILM

5.4.1 The Build-up of the Transfer Film on the Metal Counterface

Optical and scanning electron micrograph figures 5.35(a) and 5.35(b) reveal that small patches of polymer films of approximately 10 μm in size and 1 μm thick adhere initially to the asperity ridges of the metal counterface. An examination of the adhered films between crossed Polaroids showed that, even after relatively small sliding distances, the particles were anisotropically crystalline in structure. The initial transfer process occurs at isolated ridges on the counterface and results from both abrasive and adhesive wear mechanisms. The films that adhere initially to the asperity ridges appear to be smeared from the right to the left in figure 5.35(b). Thus, the initial contact of these thin films occur at discreet points on the asperities and are initially smeared to and fro from these anchors during reciprocating motion. As the pin moves across the metal counterface, the polymeric material is forced into the valleys between the ridges of the asperities and mechanically interlocks with the metal counterface. Figure 5.36 shows a thin film of polymer being smeared across the asperities of the metal counterface. In this way the abrasive action of the metal asperities are reduced and the real area of contact and adhesion between the polymer pin and the metal surface is increased. The cummulative effect results in an effective decrease in the coefficient of friction. The decrease in friction is also attributed to the contact changing from an abrasive UHMWPE/metal couple to an UHMWPE/transfer film, coupled with an increased adhesive component of friction.

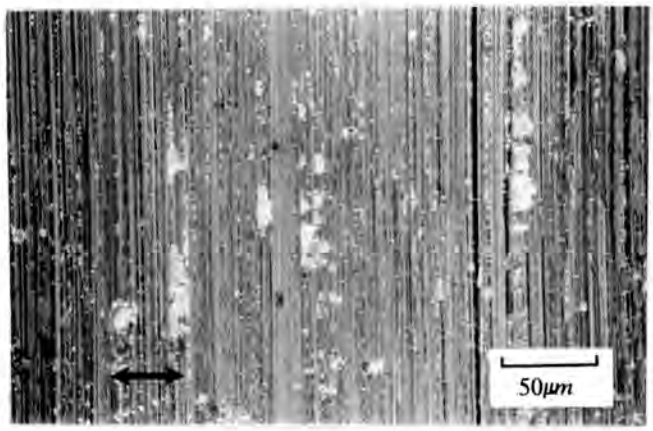

Figure 5.35(a): An optical micrograph (crossed Polaroids) of the metal counterface showing isolated polymer patches after 50 m of sliding wear. The arrow indicates the sliding direction.

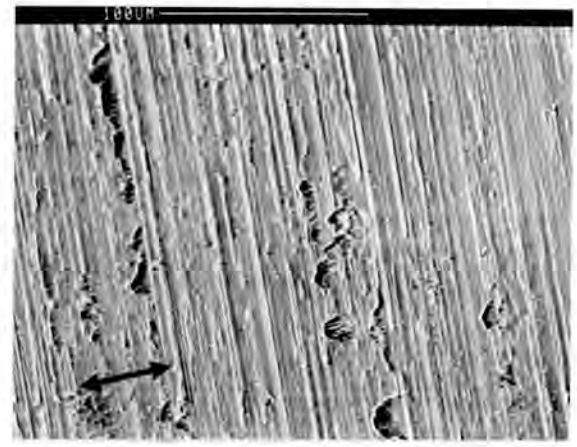

Figure 5.35(b): A SEM micrograph of polymer films about 10 μm in diameter adhering on the asperity ridges of the metal counterface after 50 m of sliding. The arrow indicates the sliding direction.

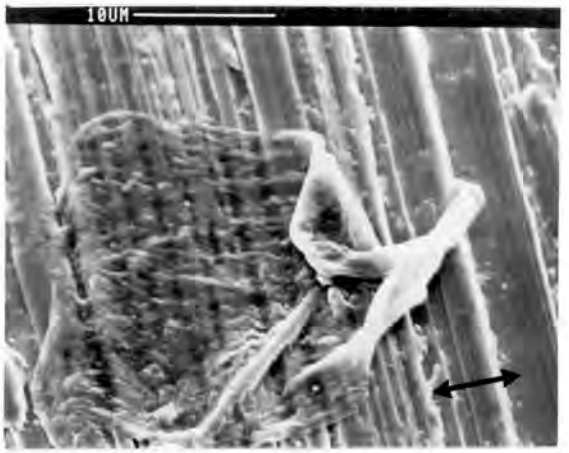

Figure 5.36: A SEM image showing a thin film of polymer smeared across the asperities of the metal counterface. The arrow indicates the sliding direction.

The loss of small patches of polymer from the pin takes place by chain scission, as inferred from the mass spectral data in section 5.5.1. Adherence of theses particles to oxide film of the metal counterface can thus occur through chemical bonding in addition to the van der Waals, Coulombic and hydrogen bonds. The initially transferred polymer appear to be the sites for further transfer since the film particles are found to increase in size at greater sliding distances as shown in figure 5.37.

Figure 5.37(a): A SEM micrograph showing large film patches on the metal counterface after 500 m of sliding wear. The arrow indicates the sliding direction.

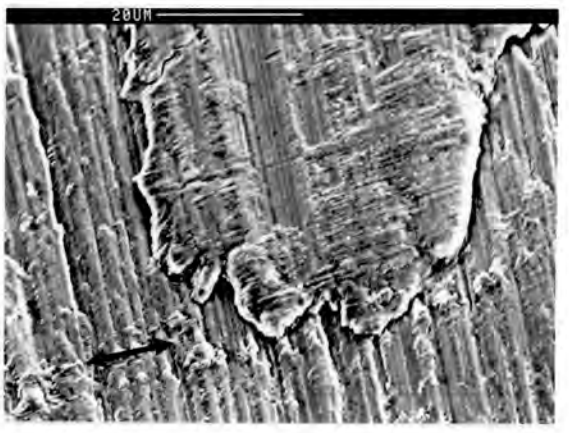

Figure 5.37(b): A magnified view of a particle in fig. 5.37(a).

The build-up of these layers on the metal counterface was studied by using the depth of focus of the optical microscope. It was found that the transfer film eventually consisted of consisted of several of these layers. Figure 5.38(a) shows that thin layers of polymer films (focussed and arrowed) are found below other layers (unfocussed area). Bands of transferred polymer grow from the asperity ridges towards each (figure 5.38(b)) other and a coherent and highly adherent film is eventually formed across the metal surface.

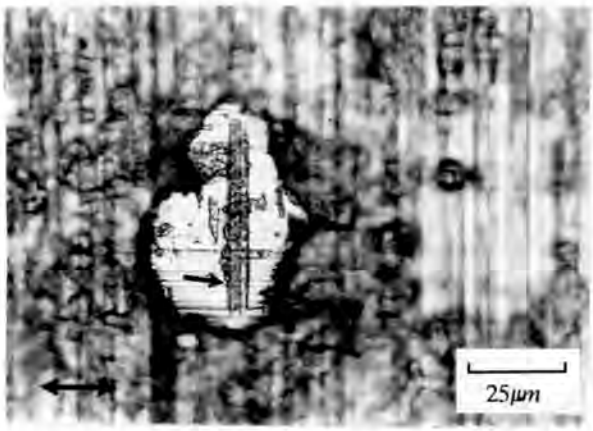

Figure 5.38(a): An optical micrograph showing the underlying film (arrowed) by using the depth of focus of the optical microscope. Several layers of polymer films are found to grow over the films initially laid down. The arrow indicates the sliding direction.

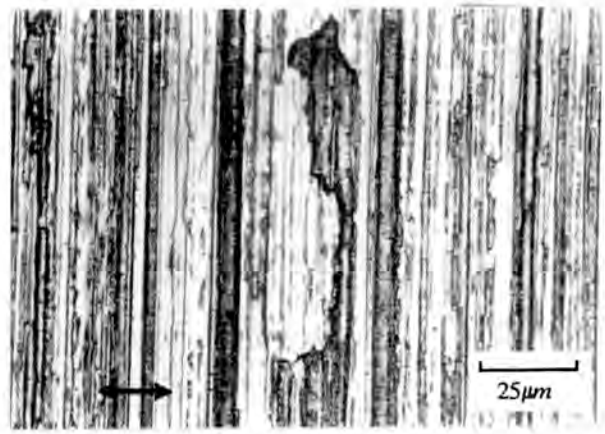

Figure 5.38(b): The layered nature of the transfer film is seen in this optical micrograph after 5 km of sliding. The arrow indicates the direction of sliding.

Figure 5.39(a) shows a SEM image of polymer that is being smeared into the valleys between the metal asperities until the surface is uniformly covered with transferred polymer. Partially filled valleys becomes completely filled as the build-up of the transfer film takes place. In figure 5.39(b) many features found on the counterface after 25 km of sliding wear are shown. This micrograph shows valleys that are completely filled by the lateral growth process as well as partially filled valleys. During the process of lateral growth a smooth transfer film covers the metal counterface (see figure 5.10) and the sliding couple now consists essentially of an UHMWPE/UHMWPE transfer film couple. Adhesive wear is the dominant mode of wear and the wear rate and friction coefficients are very low (see figures 5.12 and 5.16).

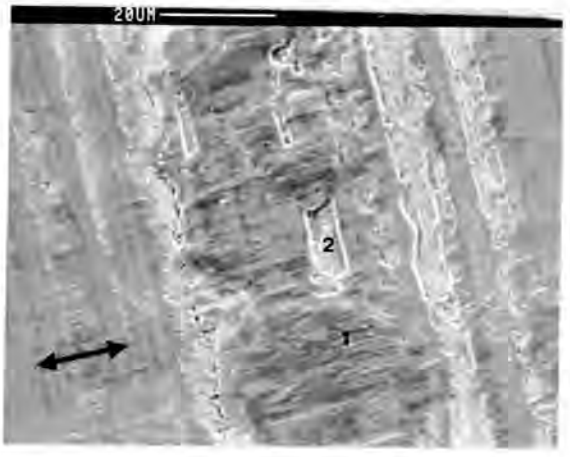

Figure 5.39(a): A SEM image showing polymer adhering initially to the metal asperity being smeared across an asperity valley *(1)*. Part of the valley that is unfilled *(2)* can also be seen. The arrow indicates sliding direction.

Figure 5.39(b): A SEM image of the worn metal counterface after 20 km showing a uniform transfer film. The following features can be distinguished: *(1)* a polymer filled asperity valley; *(2)* a polymer covered asperity ridge; *(3)* an unfilled or partially filled valley; *(4)* an abrasive track caused by entrapped metallic particles.

Figure 5.40 shows an optical micrograph of the worn metal counterface after 75 km of sliding wear. This figure shows that ridges of polymer were formed on a film already laid down during steady-state wear. During steady-state wear, transfer occurs preferentially on *"hidden"* asperities (figure 5.40) and these raised bands of polymer appear to be worn away and replaced during continued sliding wear. An examination of the counterface at higher magnification (figure 5.41) shows that cracks form along the ridges of polymeric material. The transfer film also appear to suffer from a fatigue spallation process, as shown in figure 5.42, giving rise to wear particles which contribute to the vast majority of debris formed. A delamination of polymer flakes results from crack growth on the transfer film. It is possible that the cracks result from the absorbtion of water and a subsequent embrittlement of the film on drying. However, this was considered unlikely as cracking of the transfer film was not noticed during the earlier periods of sliding wear. In the steady-state region wear particles, less than 1 μm thick, similar to that shown in figure 5.42, are plucked from the transfer film and leave the contact area as wear debris or are deposited elsewhere on the steel counterface. Craters in the transfer film are then filled with fresh transferred polymer (figure 5.43). It is clear that during the process of debris formation, only the top layer is removed and an underlying film is always present.

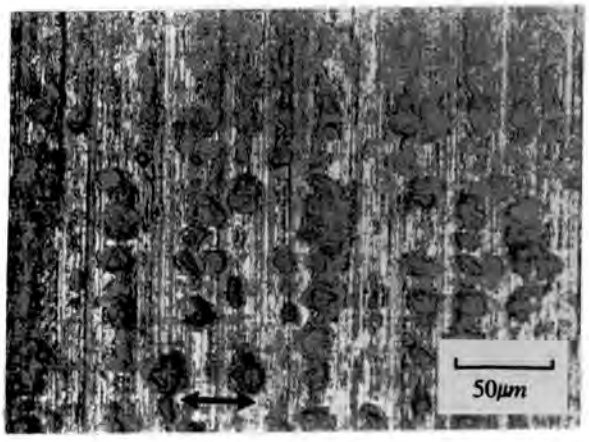

Figure 5.40: An optical micrograph of the metal counterface after 75 km of sliding, showing preferential transfer at asperity regions. The arrow shows the sliding direction.

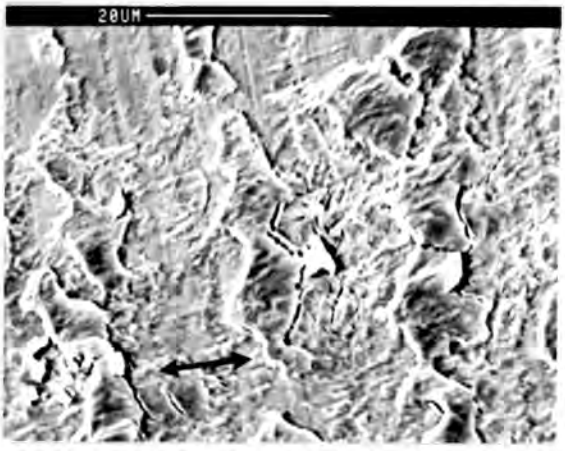

Figure 5.41: A SEM image shows that the transferred layers on the metal counterface shows signs of fatigue failure after 75 km and the raised polymer may then be easily knocked off by the polymer pin.

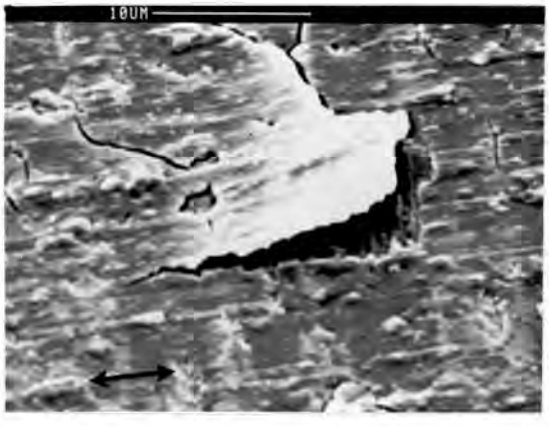

Figure 5.42: A SEM photograph of a fatigue debris particle in the process of being spalled off the metallic counterface as a result of crack growth. The arrow indicates the sliding direction.

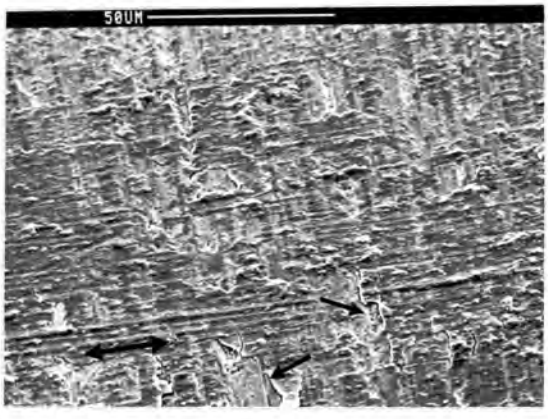

Figure 5.43: The transfer film shows craters (arrowed) after the removal of debris particles. Notice the underlying film when these particles are removed. The double arrow indicates the sliding direction.

When sliding wear tests are performed in a direction parallel to the grinding direction of the metal counterface, any transferred material formed on the metal counterface appear as

patches which are easily dislodged from the counterface. Figures 5.44 and 5.45 show SEM micrographs of the worn surfaces after 60 km of sliding wear. In figure 5.44 large patches of polymer are scattered over the counterface and the original grinding marks of the metal can be identified. This lumpy form of transfer is responsible for the high wear rates found in figure 5.22. Figure 5.45 shows that very little mechanical interlocking can occur with the metal counterface and transferred material is discharged more easily from these interfaces than on surfaces ground perpendicular to the grinding direction.

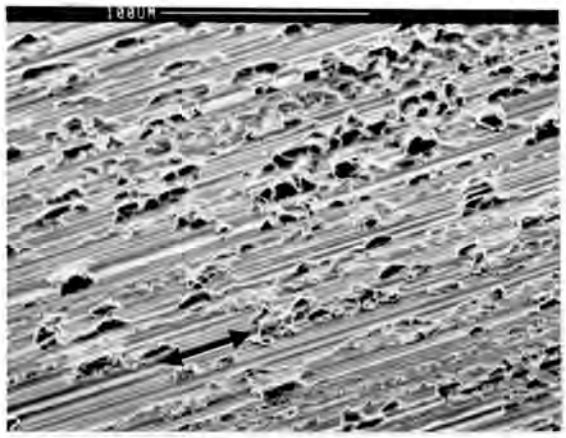

Figure 5.44: A SEM image shows that lumpy transfer is found on surfaces ground parallel to the sliding direction even after 60 km of sliding. The arrow indicates the sliding direction.

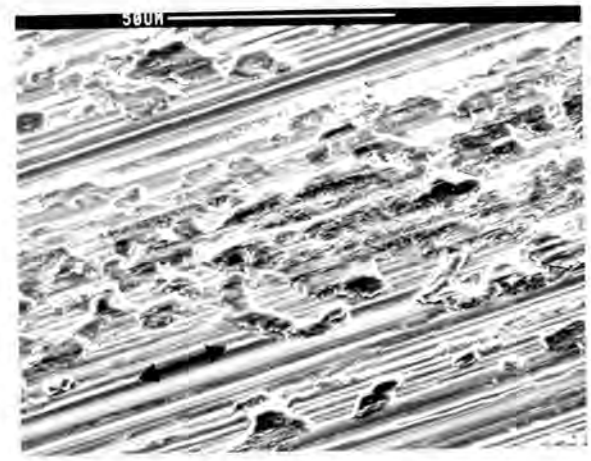

Figure 5.45: Very little mechanical interlocking is afforded to the polymer and transferred material is easily dislodged from the worn counterface, leading to relatively high wear rates.

5.4.2 The Shear Process on the Polymer Pin Surface

The transfer film that is built up on the metal counterface during water-lubricated reciprocating sliding wear is believed to arise initially from a ductile shear process occurring on the polymer pin surface as shown in figure 5.46. A typical sheared layer may be about 5 μm thick as indicated in figure 5.47. Since the initial transferred particles were about 10 μm in diameter and 1 μm thick, a sheared film, such as those shown in figures 5.46 and 5.47, must have broken down further during the transfer process. The outer sheared surface layers on the worn polymer pin surface are very smooth and relatively featureless and debonding takes place approximately 3 - 5 μm below the outer surface. Figures 5.48 and 5.49 show the different characteristics of the fracture surface compared with the worn

surface. The characteristics of the exposed polymer surface following the loss of a sheared layer is quite different to the worn surface (figure 5.49). Bands approximately 2.8 μm wide and 42 μm long which appear to consist of crystallites aligned in the sliding direction, could be distinguished between larger amorphous areas in figure 5.49. The crystallites were measured to be approximately 16 nm thick. Further sliding results in the smoothing of the surface through plastic deformation of the polymer and eventual debonding of this material.

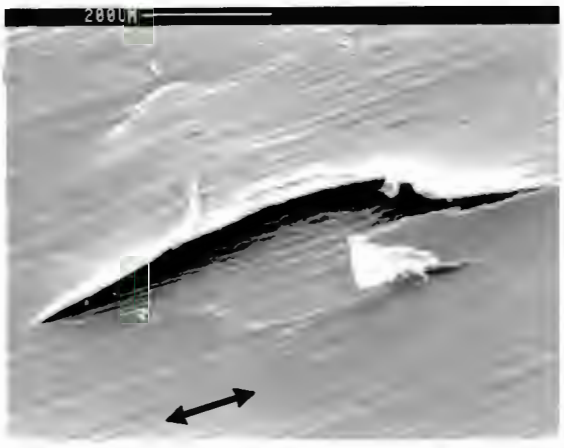

Figure 5.46: A SEM micrograph of the worn surface of an UHMWPE pin showing the polymer being sheared off the surface. The arrow indicates the sliding direction.

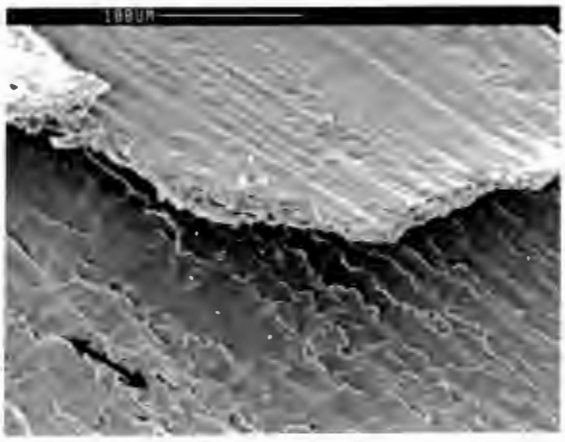

Figure 5.47: Highly deformed layers, typically a few micrometres thick are easily sheared off the pin surface. The arrow indicates the sliding direction.

Figure 5.48: A SEM micrograph of the worn pin surface showing a variation in features in the surface layers. The arrow indicates the sliding direction.

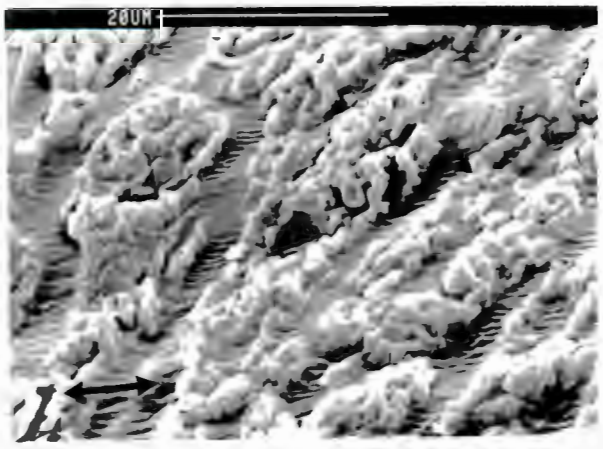

Figure 5.49: A SEM micrograph of the surface beneath a sheared layer showing lamellar features after the top layer has been sheared off. The arrow indicates the sliding direction.

Optical micrographs of thin polymer films taken under polarized light, show that the depth of subsurface deformation of the polymer pin arising from a combination of normal and tangential stresses may extend up to 45 μm below the wear surface as shown in figure 5.50. Figure 5.50 shows a section cut from the polymer pin, both parallel and perpendicular to the sliding direction. The highly deformed region is blue in colour and this subsurface deformation appears to be uniform.

When the film is rotated so that the sliding direction is at 45° to the crossed Polaroids, a bright surface layer is seen (figure 5.51(a)). The bright layer changes to a dark layer when the specimen is rotated through another 45° (figure 5.51(b)). This is most evident in a narrow band approximately 5-10 μm below the wear surface, indicating that orientation of the polymer molecules in the surface has become parallel to the sliding direction. Such an acute change in structure and thus physical and mechanical properties at an interface of a few micrometres below the wearing surface allows the easy shear at the interface observed in figure 5.46, since there is less mechanical interlocking between the molecular chains.

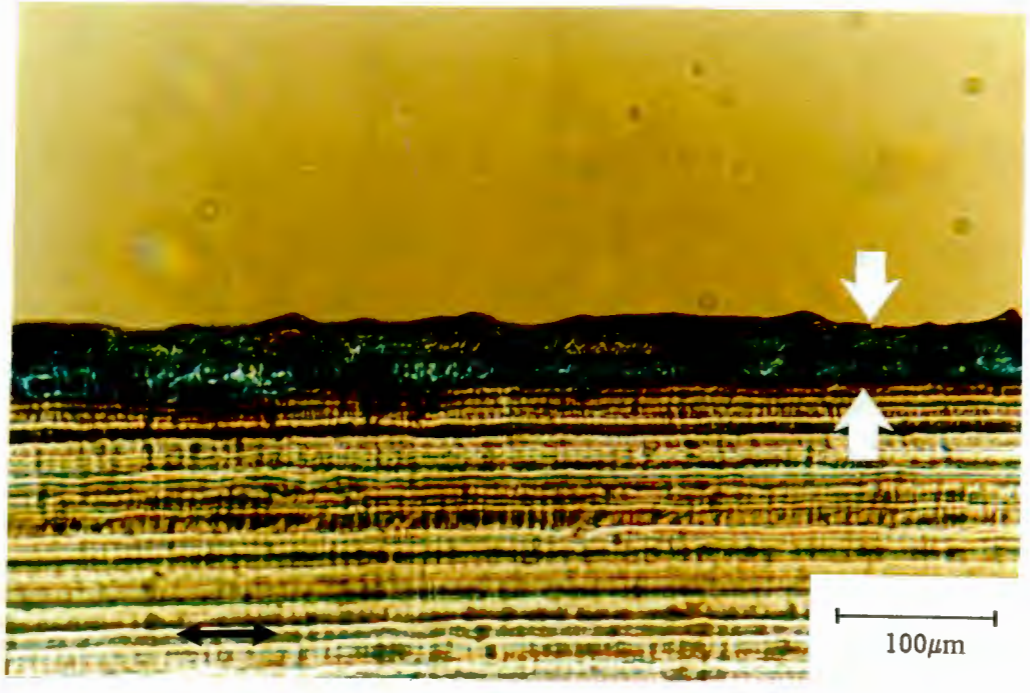

Figure 5.50: An optical micrograph of a 15 μm section cut from the worn polymer pin. The worn surface shows appreciable birefringence and residual strain below the wear interface. The white arrows show the depth of the highly deformed region, while the black arrow shows the sliding direction.

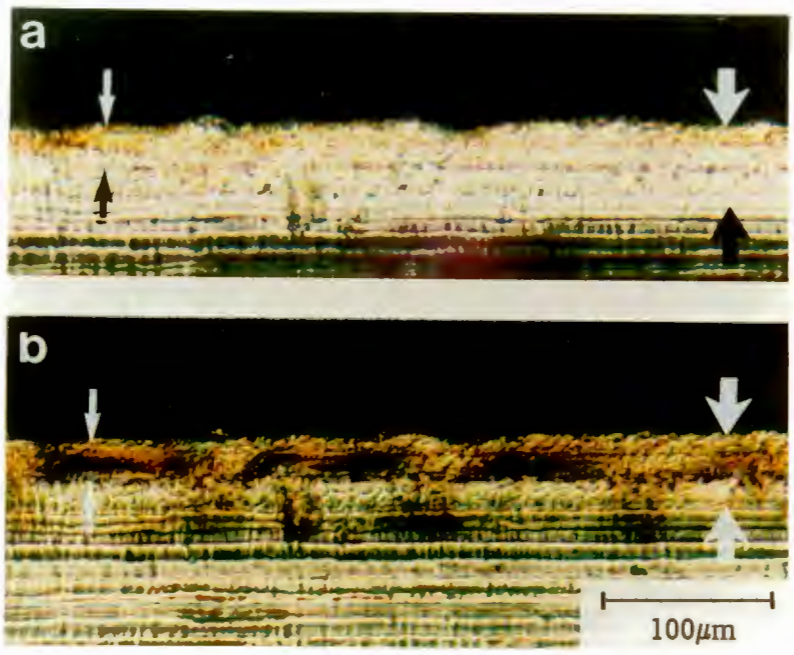

Figure 5.51: Polarized optical micrographs showing a section of the worn polymer pin between crossed Polaroids. A bright surface layer (fig. 5.51(a)) changes to a dark layer (fig. 5.51(b)) when the specimen is rotated 45 degrees. The small arrows indicate the depth of the highly oriented portion of the deformed surface layer.

5.4.3 Interfacial Wear Features

During the course of studying the operative wear mechanisms, several features, in addition to those already shown, can be identified on both the worn metal counterface and polymer pin surface.

5.4.3.1 Features observed on the worn metal counterface

Any metallic particles which become dislodged from the counterface during sliding wear may become entrapped at the sliding interface and severely abrade the metal counterface by a microploughing action, causing *wear grooves* or furrows of varying widths parallel to the direction of sliding as shown in figure 5.52(a). These work hardened steel particles assist in polishing the original surface grinding marks. The abraded grooves may be up to 120 μm wide, as shown in figure 5.52(b) of a Talysurf trace taken at 4° across an abrasive groove. The wear grooves formed on the counterface conformed to similar grooves on the

corresponding pin surface and ran across the entire stroke length, indicating that many of these metallic particles moved freely at the interface, giving rise to three-body abrasive wear. Particles at the interface which become embedded in the polymer surface act as miniature cutting tools, giving rise to two-body abrasive wear. Figure 5.52(a) also shows that *fatigue cracks* are found on the counterfaces after long sliding distances.

Large amounts of *polymer deposits* are found at the end of the stroke as the sliding velocity decreases to zero, allowing for greater adhesion between the transferred polymer and the metal counterface. Figure 5.53 shows the large patches of polymer found at the end of an abrasive wear groove.

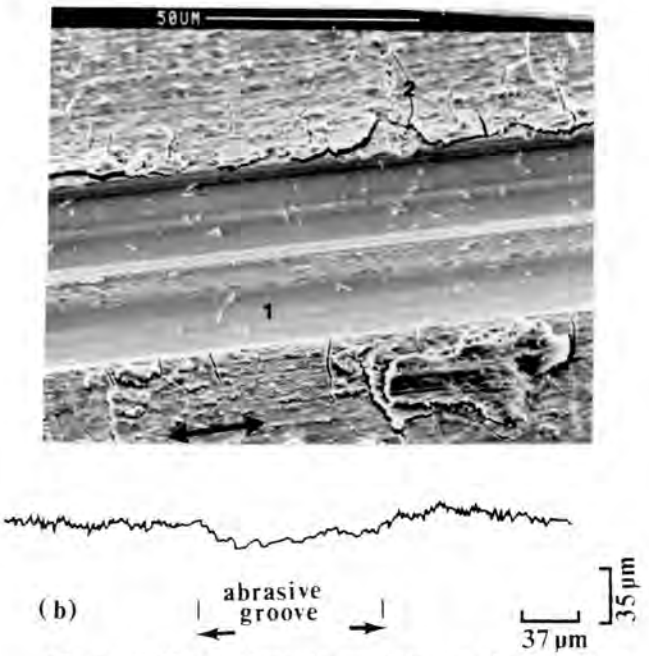

Figure 5.52(a): Metallic particles at the interface cause the formation of abrasive wear grooves (*1*) to form on the metal counterface. Fatigue cracks (*2*) are also shown after 60 km of sliding wear. The arrow indicates the sliding direction. **(b):** A Talysurf trace taken at 4° across an abrasive groove.

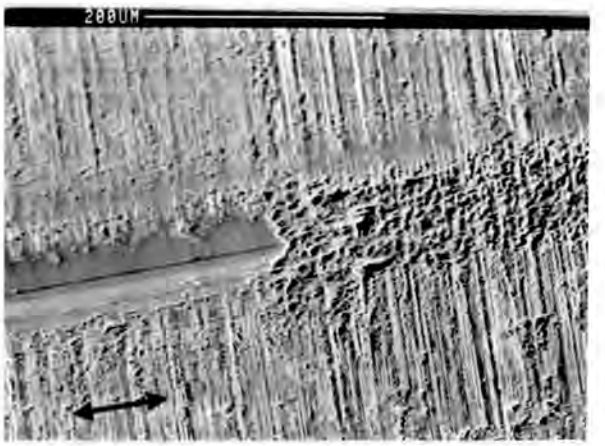

Figure 5.53: A SEM image showing large amounts of polymer that are piled up at the end of an abrasive groove as the pin's velocity is decreased to zero.

5.4.3.2 Features observed on the polymer pin wear surface

A number of features observed on the surface of wear pins, have also been observed by other workers [80]. Figure 5.54 shows typical *abrasion marks* caused by sharp edged

metallic particles. *Striations* could also be observed perpendicular to the sliding direction in figure 5.54 (area 2). These striations occur at regular intervals of 6 μm and may be due to elastic tearing of the polymer by sharp asperities or metallic particles and a subsequent elastic recovery by the polymer molecules.

Surface tractions also cause the formation of *raised crescents* (figure 5.55) aligned in the direction of sliding. These wavy features probably arise from a partial softening of the polymer surface during sliding wear. The softened polymer is then pulled out of the surface and smeared in the direction of sliding. The effect of the softened polymer being pulled out of the surface is even more evident from observations on the polymer pin following dry wear tests (see figure 5.71).

During steady-state wear, *back transfer* of polymer detached from the counterface occurred. Figure 5.56 shows similar markings on the surface of the back transferred polymer to those found on the polymer wear surface. Rotation of these particles during the sliding wear process probably account for the non-alignment of these markings with the sliding direction in figure 5.56.

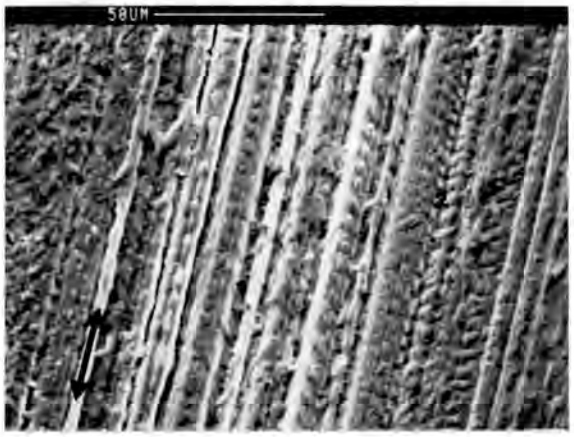

Figure 5.54: A SEM micrograph of the worn polymer pin surface after 25 km of sliding in a water lubricated test showing abrasion marks (*1*) with striations (*2*) running perpendicular to the sliding direction. The arrow indicates the sliding direction.

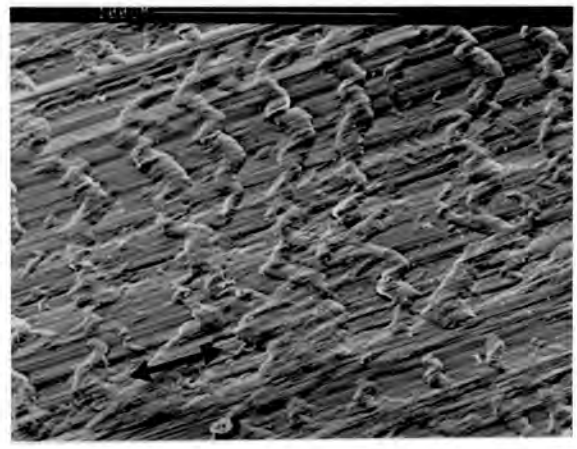

Figure 5.55: Wavy raised crescents of polymer shows evidence of localized melting in this SEM micrograph. The ductile polymer is smeared in the sliding direction. The arrow indicates the sliding direction.

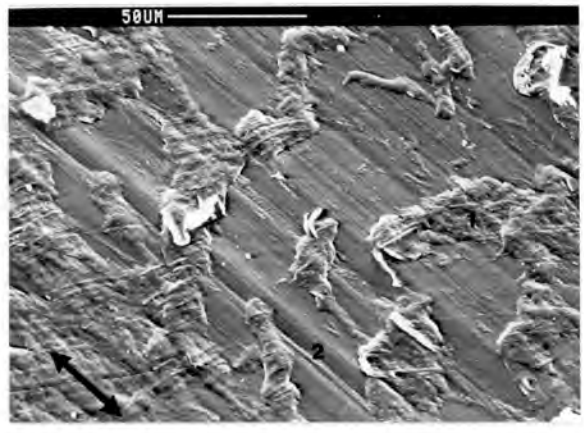

Figure 5.56: Back transferred particles (*1*) and abrasion grooves (*2*) are shown in this SEM micrograph after 95 km of sliding wear. The arrow indicates the sliding direction.

5.5 THE NATURE OF THE WORN UHMWPE MATERIAL

5.5.1 The Nature of the Debris

Debris arises from a fatigue spallation process (see figure 5.42) and debonds at a distinct depth below the transfer film surface when sliding perpendicular to the ground surface of the metal counterface. This debris is formed primarily in the steady-state region and is plate-like in appearance as shown in figure 5.57. Conversely, when the polymer is worn in a direction parallel to the grinding direction of the metal counterface, debris arises in the form of polymer stringers of about 5-10 mm long (figure 5.58). It is also interesting to note that more debris particles are obtained during the initial bedding-in stages when sliding is conducted parallel to the grinding direction, when compared with sliding perpendicular to the grinding direction.

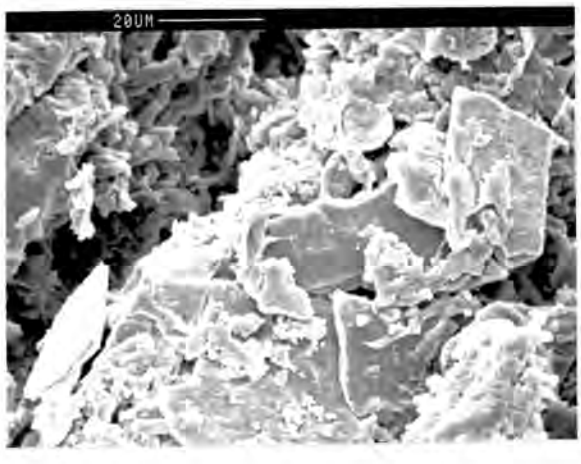

Figure 5.57: A SEM image showing plate-like debris formed when sliding perpendicular to the grinding direction of the metal counterface.

Figure 5.58: A SEM image showing stringer-like debris formed when sliding parallel to the grinding direction of the metal counterface.

DSC results show that the initial crystallinity of debris formed when sliding perpendicular to the ground surface is significantly higher than the unworn material, 72.8% compared with 42.1% respectively (figure 5.59(a)) and in table 5.3 indicated by (1)). The crystallinity of debris formed in sliding studies conducted parallel to the grinding direction is initially about 14% less than that formed when sliding takes place perpendicular to the grinding marks of the counterface. The crystallinity of the debris formed when sliding parallel to

the grinding direction is shown in figure 5.59(b) as well as in table 5.3 by (2). Figure 5.60 shows that debris formed when sliding perpendicular to the grinding direction increased rapidly in crystallinity during the bedding-in stages, whereas the crystallinity of the debris formed when sliding parallel to the grinding direction increases more slowly.

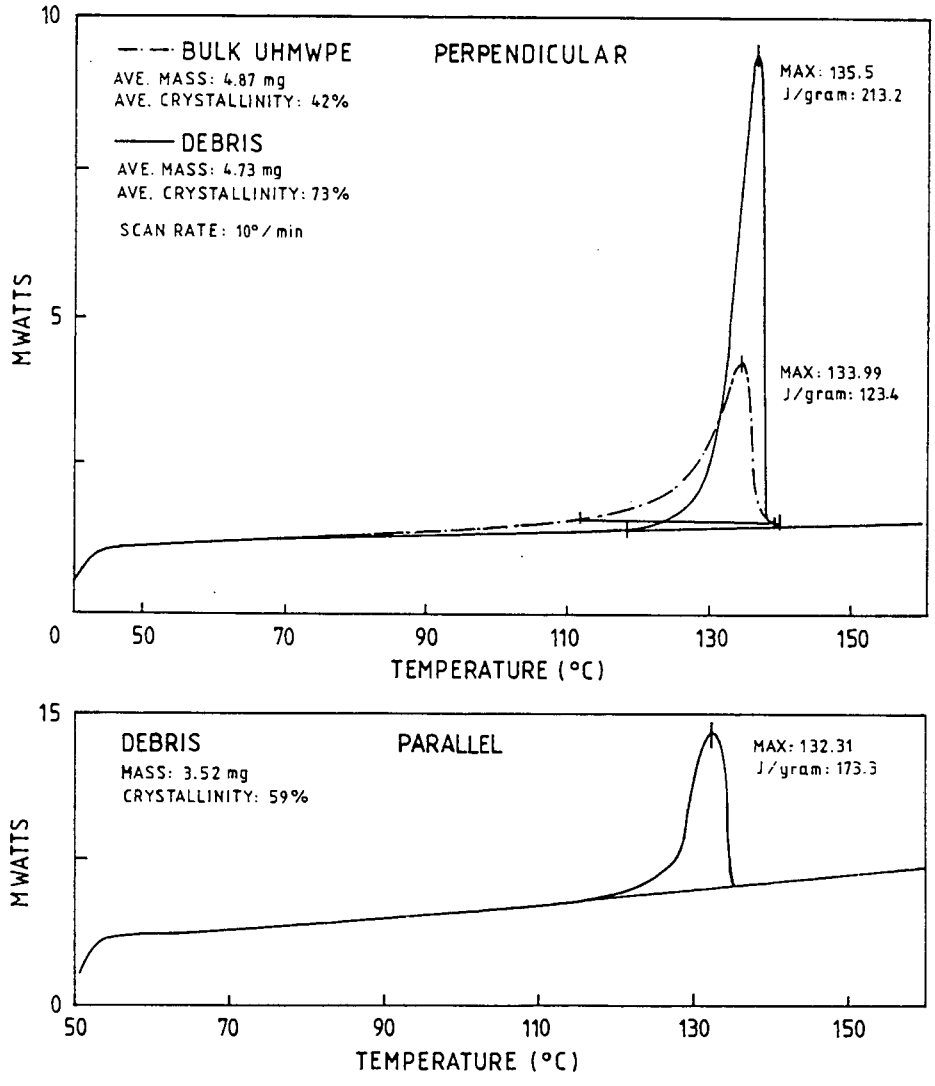

Figure 5.59: DSC analysis of UHMWPE. (a) Normalized DSC scan of unworn polymer and debris when sliding perpendicular to the grinding direction. (b) Normalized DSC scan of the debris formed when sliding parallel to the grinding direction.

Technique	Material			Number of samples	Crystallinity (%)	Standard deviation (%)
	unworn bulk polymer	worn surface	debris			
X-ray analysis	X			5	41.7	3
		X		5	46.5	4.5
			X	1	73	0
DSC	X			3	42.1	6.2
			X(1)	4	72.8	4.8
			X(2)	1	59.2	0

Table 5.3: X-ray and DSC analysis of UHMWPE. X(1): worn debris when sliding perpendicular to the ground surface. X(2): worn debris when sliding parallel to the ground surface.

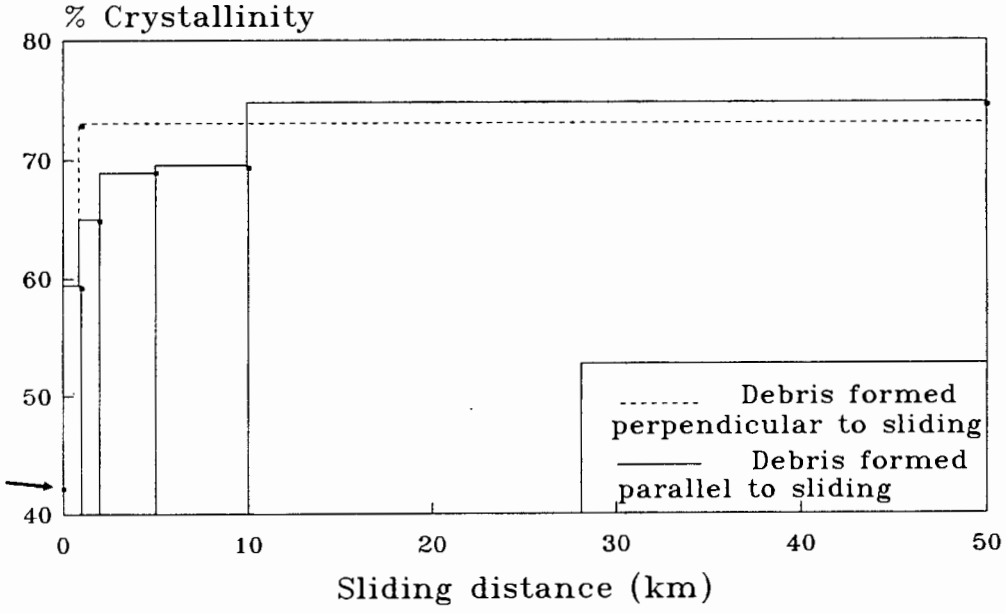

Figure 5.60: The crystallinity of the debris *vs.* sliding distance determined by DSC. The arrow indicates the crystallinity of the unworn material at 42.1%. Full curve: debris were collected between the intervals 0-1, 1-2, 2-5, 5-10 and 10-50 km. Broken curve: debris were collected between 1 and 50 km.

An IR scan of the worn debris is shown in figure 5.61. The splitting of the band at 2800-3000 cm^{-1} is due to CH_2 asymmetric stretches (2920 cm^{-1}) and CH_2 symmetric stretches (2840 cm^{-1}) of methylene groups. This splitting suggests that there is an increase in interchain forces of the debris compared with the bulk polymer [173]. No splitting of the CH_2 rocking band occurred in the debris as was the case with the UHMWPE film (see figure 5.1). The relative intensity of the C-H rocking mode at 720 cm^{-1} is lower for the debris than for the original UHMWPE film (*cf.* figures 5.1 and 5.61), indicating a reduced molecular chain length. It should be noted that the intensities of the bands in the debris may be influenced by moisture, as indicated by the O-H stretching frequency.

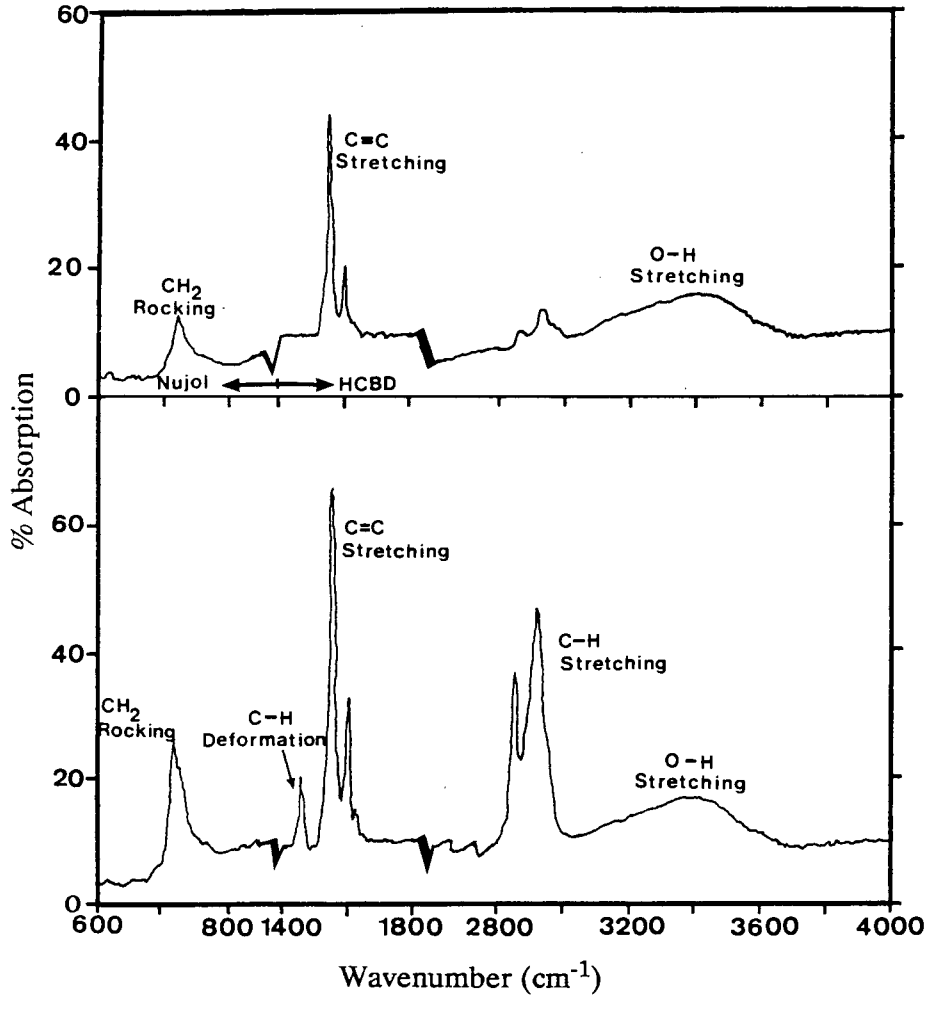

Figure 5.61: An IR scan of the solvents (top) and debris + solvents (bottom).

Wear debris obtained from region *2* in figure 5.15, when glass bead filled UHMWPE was abraded against the metal counterface, consisted of powdered polymer interspersed with pulverized glass beads. Figure 5.62 shows a SEM image of the glass bead filled UHMWPE wear debris. A corresponding EDS scan of the debris (figure 5.63) indicates the presence of the main constituent of the glass namely silicon. The Au and Pd peaks are due to the coating.

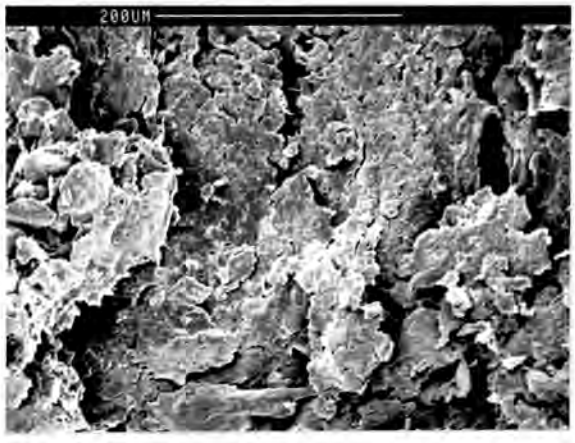

Figure 5.62: A SEM image of the pulverized wear debris of the glass bead filled UHMWPE.

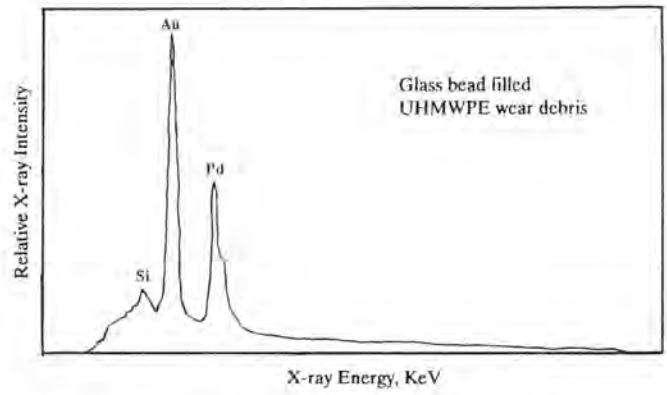

Figure 5.63: An x-ray spectrum of the debris in fig. 5.62 shows that silicon associated with the glass fragments are present (vertical full scale = 1024 counts).

The x-ray diffraction data have been used to calculate the crystallinity and crystallite size of the worn and unworn materials (see tables 5.3 and 5.4). An XRD trace of the worn debris is shown in figure 5.64. The values of the intensities are lower than those obtained for the bulk material and this is due to the intensity being proportional to the product of the density ρ and the thickness t of a given sample [35]. In addition to the (110) and (200) reflections from orthorhombic polyethylene, a peak appears at $2\theta = 19.2°$. This peak is due to scattering by the amorphous material. The crystallinity of the debris was calculated by XRD to be approximately 73%. A large percentage of amorphous material is assumed to be orientated, contributing to the high enthalpy value obtained by DSC. This contribution is shown in figure 5.64. The crystallite sizes in the debris are significantly smaller than those calculated for the unworn material, 8 nm compared with 16 nm as shown by the XRD data in table 5.4. The crystallite sizes of the highly deformed UHMWPE by a rolling process are similar to that of the wear debris.

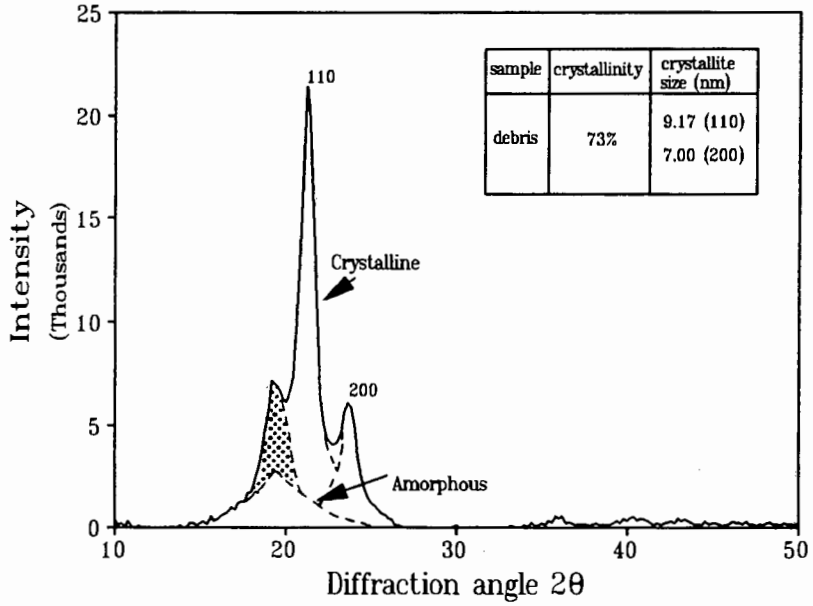

Figure 5.64: An XRD trace of worn debris after subtraction due to the Perspex holder. The shaded region indicates the contribution by the oriented amorphous polymer.

Polymeric material	Average crystallite size (nm)	Crystallinity (%)	Number of samples
debris	8.1	73	1
unworn surface	15.2 ± 2.1	41.7	5
worn surface	15.5 ± 2.2	46.5	5
deformed UHMWPE			
i) 66 %	9.7 ± 1.0	78	1
ii) 77 %	9.4 ± 0.6	74	1
iii) 83%	8.7 ± 0.5	77	2

Table 5.4: X-ray analysis of worn and unworn UHMWPE. The crystallite sizes of UHMWPE by mechanical rolling deformation are also shown.

Figures 5.65(a) and 5.65(b) illustrate the thermal decomposition of the unworn polymer and wear debris respectively. The mass spectrum of the wear debris shows lower molecular weight fractions owing to decomposition, than the initial (unworn) polymer. This supports the postulate that the polymer in the surface layers fragment during transfer.

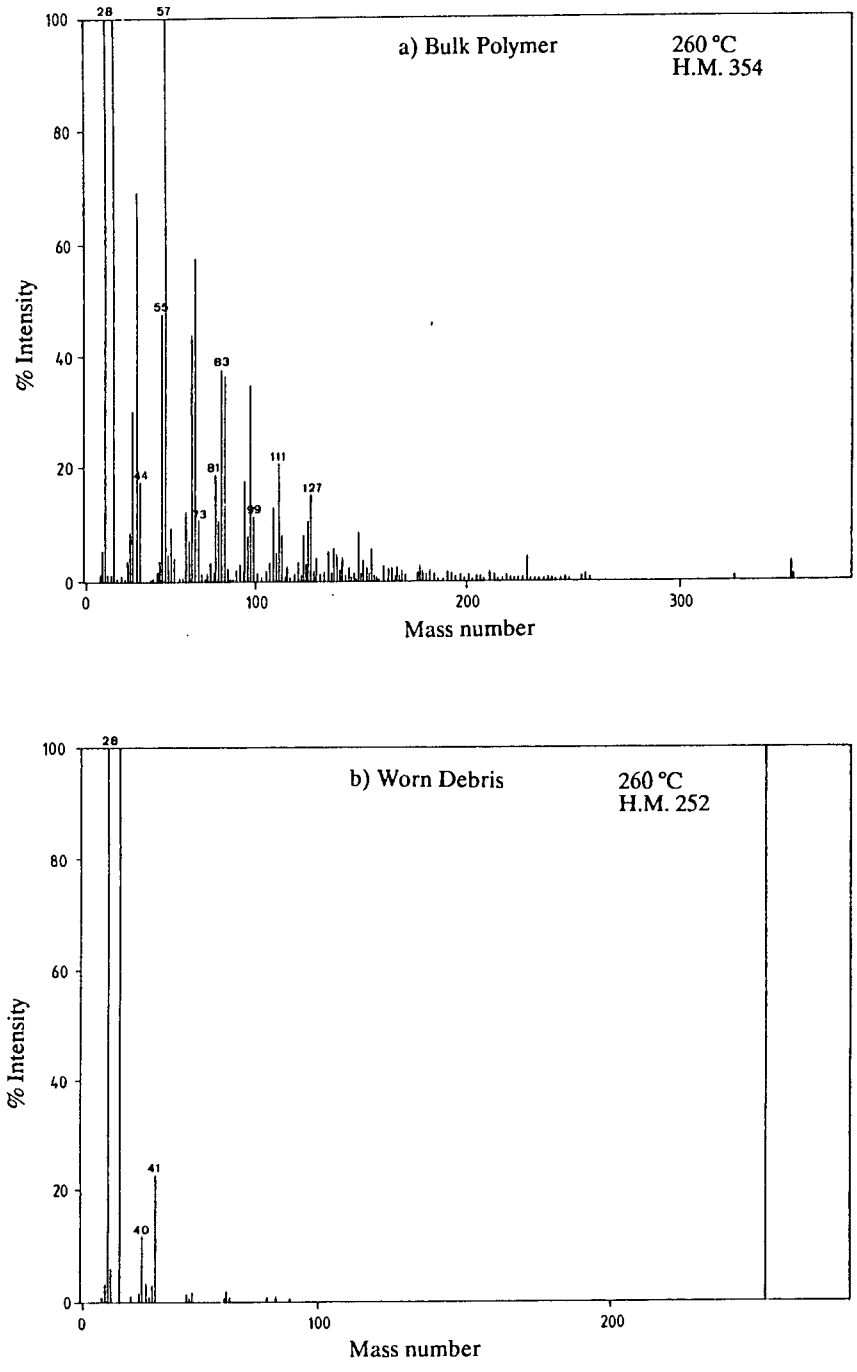

Figure 5.65: Mass spectra of volatile products liberated during the thermal decomposition of wear products and unworn UHMWPE: (a) unworn polymer; (b) worn debris.

5.5.2 The Nature of the Worn Surfaces

5.5.2.1 The nature of the worn polymer wear surface

The crystallite sizes of the worn and unworn polymer surfaces are not very different, but the crystallinity of the worn polymer surfaces increased from 41.7 to 46.5% during this process (tables 5.3 and 5.4). Table 5.4 also shows the changes in crystallite sizes in UHMWPE due to different degrees of plastic deformation. The crystallite sizes in the plastically deformed UHMWPE are similar to that found in the wear debris, hence any material removed from the polymer wear surface is subjected to similar degrees of deformation found in the bulk deformation process. Figure 5.66 shows infrared scans taken from film microtomed off the worn polymer pins after water-lubricated tests. The broad peaks appearing at 3100 - 3600 cm^{-1} are due to an O-H stretch. The peaks may be due to free H_2O molecules entrapped in the amorphous regions of the UHMWPE as it was shown that water is absorbed by the UHMWPE (Appendix B). However, the band could also be due to an O-H band as ROH (where R is an alkyl group). Active free radicals formed during chain scission may react with the water lubricant to form the hydroxyl bond. Oxidation of the polymer may lead to the carbonyl absorbtion band at 1600-1700 cm^{-1} in the worn polymer. The process of oxidation may embrittle the surface layers and hence affect the wear properties of the polymer.

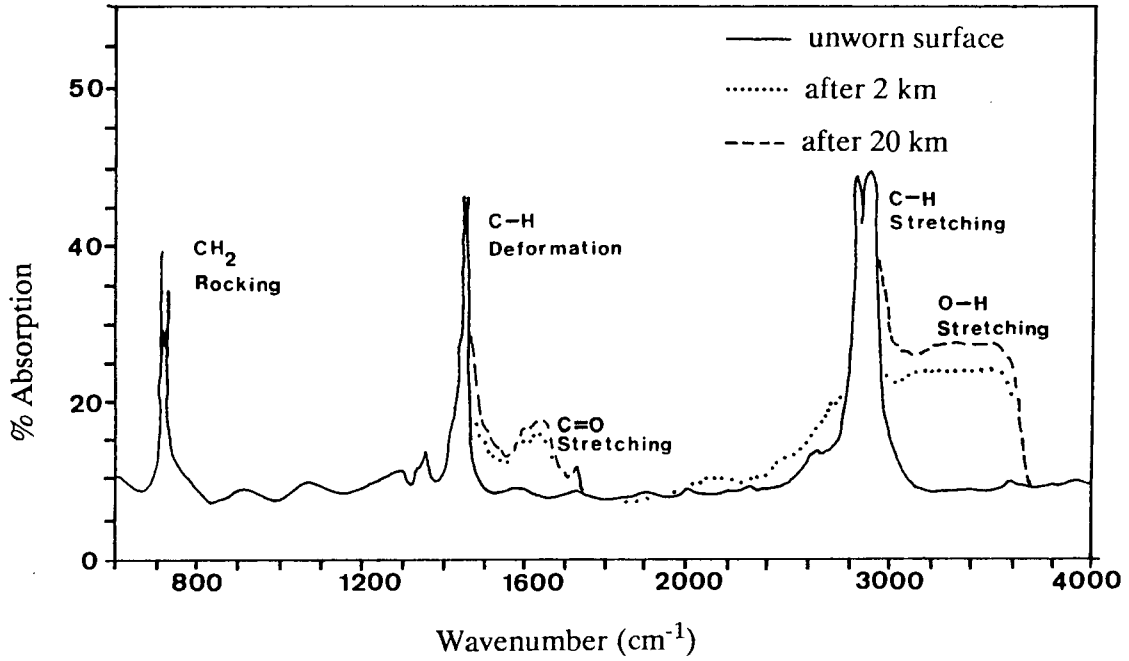

Figure 5.66: IR scans of microtomed films from the worn polymer pin surfaces after two different sliding distances.

5.5.2.2 The nature of the transfer film

Figure 5.67 shows a portion of an XRF scan of both the unworn and worn metal counterface following sliding against the inorganically filled UHMWPE. Only titanium can be identified as a constituent that was transferred with the polyethylene to the metal counterface.

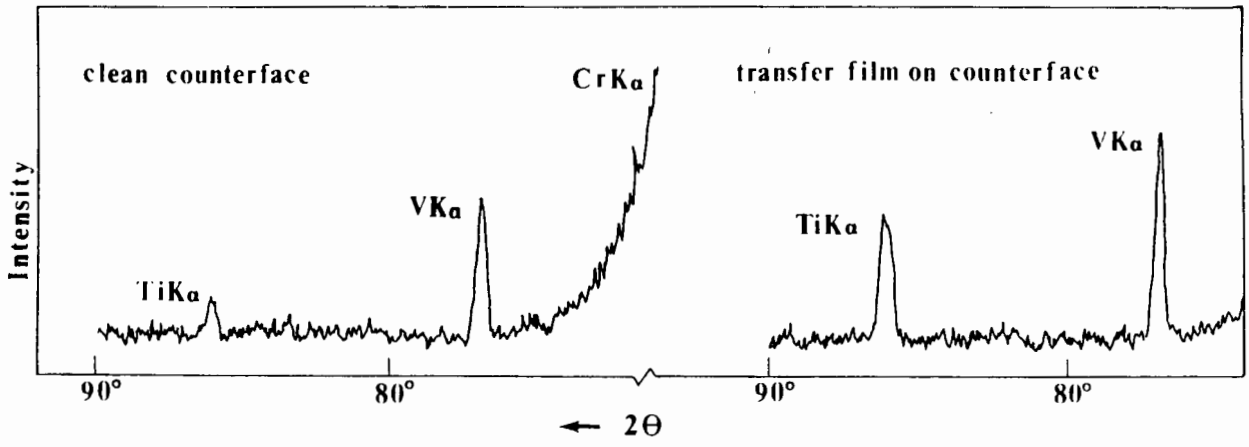

Figure 5.67: A portion of an XRF scan of both the unworn and the metal counterface worn by the inorganically filled UHMWPE.

During the course of the transmission electron spectroscopy studies, an attempt was made to obtain selected area electron diffraction patterns of thin polyethylene films still attached to the carbon replica. We were unable, however, to optimize the conditions for diffraction and hence get an acceptable diffraction pattern due to melting of the polyethylene under the electron beam. In order to accurately determine orientation relationships of the polyethylene crystallites relative to the sliding direction, it would be necessary to obtain several zone axes from the crystallites.

5.6 DRY SLIDING WEAR

5.6.1 Dry Reciprocating Sliding Wear

Dry reciprocating sliding wear studies were conducted on two UHMWPE grades *viz.*, the Special DS grade and the 10/100 grade. These tests were conducted in order to compare the wear performance of the UHMWPE with that observed during the lubricated wear tests. Although the average sliding velocity was kept constant at 0.25 $m.s^{-1}$, the contact pressures for the dry tests were reduced to 5 MPa to avoid the possibility of gross polymer degradation. The wear tests were conducted on counterface surface roughnesses of 0.25 ± 0.012 μm R_a, which were similar to those used for the water-lubricated tests.

5.6.1.1 Friction and wear

The variation in volume loss together with the variation in kinetic friction coefficient of the average of two tests is shown in figure 5.68. The wear behaviour of the UHMWPE did not follow the characteristic trend of high initial wear observed during the lubricated tests on the ground metal counterfaces. Rather, an incubation period of low wear preceded a high wear regime. The specific wear rate of the filled grade *i.e.* the Special DS grade, was approximately two times lower than that of the unfilled grade, as shown in table 5.5. The dry wear rates were also found to be approximately an order of magnitude higher than the wear rates found from tests in water lubrication under the same operating conditions (table 5.5).

Figure 5.68 also shows the friction coefficients obtained during the dry wear tests. The friction coefficients either increased slightly, or remained constant throughout the tests. This frictional behaviour was different to that observed during lubricated tests, where higher friction coefficients were recorded during the running-in stages (*cf.* figures 5.68 and 5.12).

This apparent anomaly in friction behaviour between the two types of testing can be explained as follows. In dry wear testing, the adhesive component of friction increases as the contact area between the two mating surfaces increases with transference of polymer to the metal counterface. In water-lubricated sliding, this adhesive component is lowered by the interposed water film. The decreasing contribution of the deformation component of

friction during water-lubricated sliding wear, due to the build-up of a transfer layer, leads to a total reduction of friction force with sliding distance.

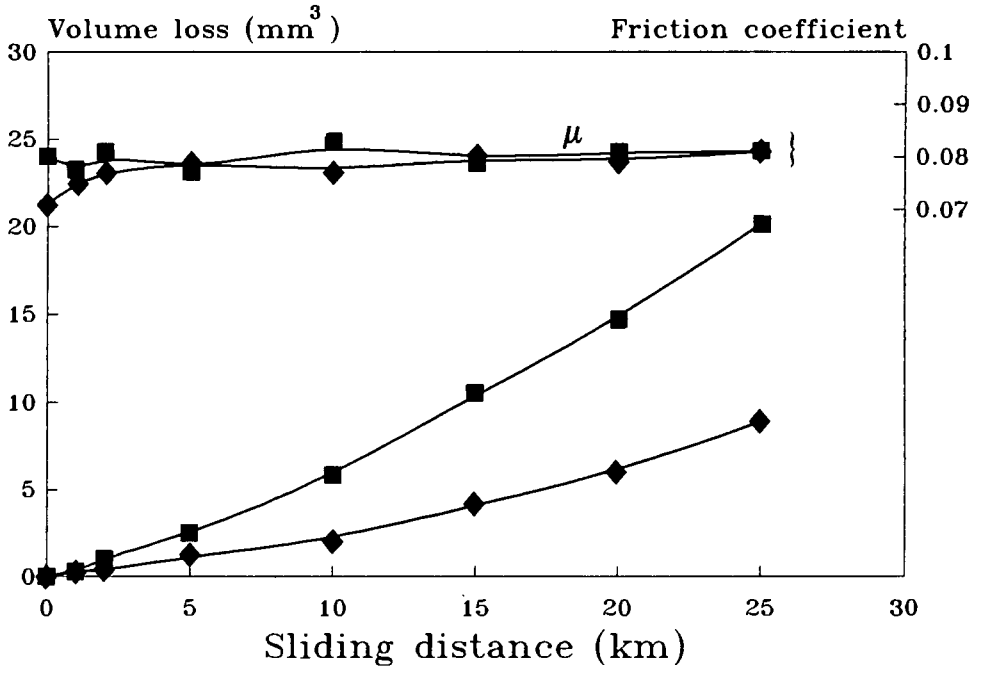

Figure 5.68: The variation in volume loss and friction coefficient with sliding distance for two UHMWPE grades, ■10/100 and ◆Special DS. The reciprocating wear tests were run dry at 0.25 $m.s^{-1}$ and pressures of 5 MPa.

5.6.1.2 An examination of the worn surfaces

Optical and scanning electron microscopy shows that the process of transfer film formation is similar to that described in section 5.4.1 for water-lubricated reciprocating sliding wear. Figure 5.69 shows a SEM micrograph of a counterface after a dry wear test. Abrasive wear is the predominant mode of wear initially, and as the polymer fills up the valleys between the metal asperities, high adhesive forces between the UHMWPE transfer film and the polymer wear pins and the subsequent shear of welding surfaces and debris formation of the mating surfaces is responsible for the high wear rates found for these sliding couples. This seems to indicate that the boundary water film in water-lubricated tests serve mainly to lower the effect of these adhesive forces and hence lower the wear rate.

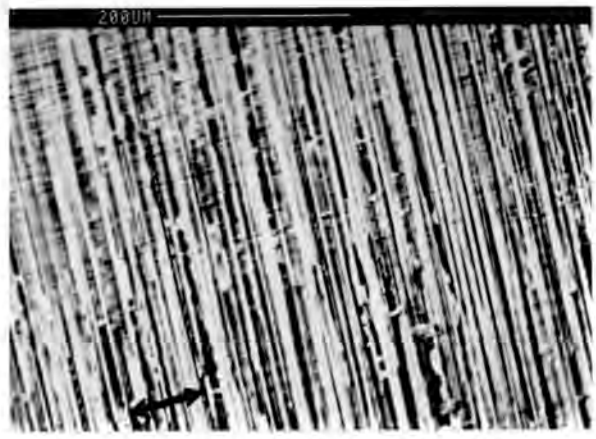

Figure 5.69: A SEM micrograph of the worn metal counterface following a dry wear test. The polymer appears dark due to damage by the electron beam. The arrow indicates the sliding direction.

It is evident that the temperature at the interface plays an important role in the mechanism of material removal during dry sliding wear. The subsurface thermocouple shows that temperatures of approximately 60 °C (figure 5.70) are experienced near the wear surface of the steel counterfaces. These temperatures, along with features found on the polymer wear pins, indicate that the melting temperature of the polymer is reached at the interface during such wear tests.

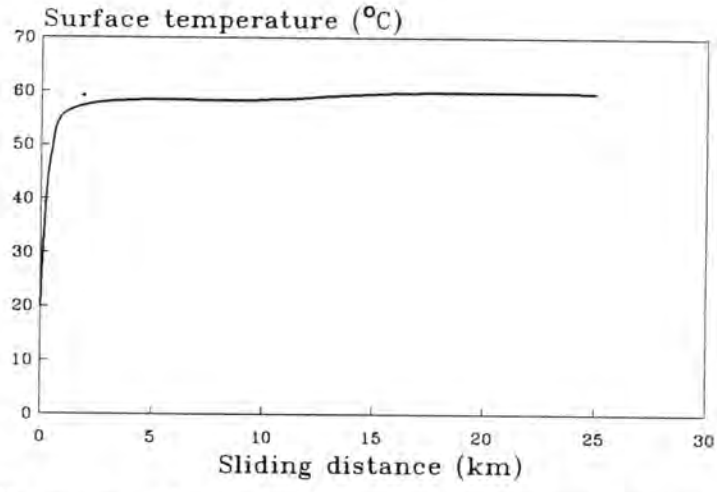

Figure 5.70: A plot of the rise in surface temperature during dry reciprocating sliding wear. Average sliding velocity: 0.25 $m.s^{-1}$; Normal pressure: 5 MPa.

The polymer wear pins show wavy surface undulations indicative of localized melting and smearing of polymer in the sliding direction. Large cracks were also observed perpendicular to the sliding direction. These cracks probably originate from a fatigue mechanism arising from the repeated stress cycles coupled to the high adhesion between the two mating surfaces. Figure 5.71 shows the typical morphology of the worn polymer surfaces during dry sliding wear. This micrograph shows evidence that polymeric material is plucked out of the surface by the high adhesive forces. Wear debris formed during dry sliding had the appearance of thin streamers, several millimeters in length, compared to the powdered debris found in lubricated wear tests (*cf.* figures 5.72 and 5.57). From figure 5.72, it would appear that the streamer debris consist of fused aggregates of polymer approximately 100-200 μm that were sheared from the polymer pin and fused together during subsequent cooling as the material is extruded from the wear interface.

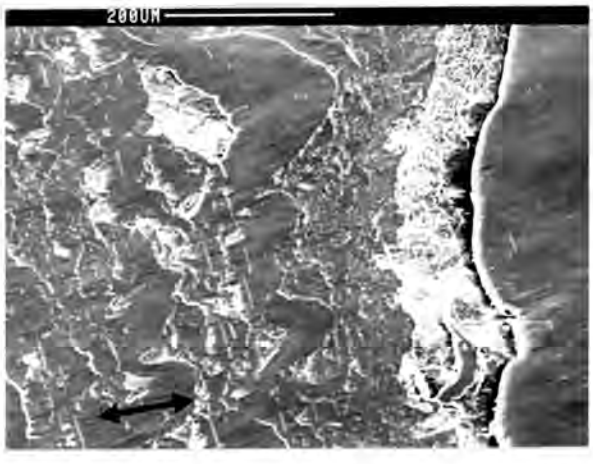

Figure 5.71: A SEM micrograph of the worn polymer pin surface after 25 km of dry reciprocating sliding wear. The surface shows signs of localized melting and polymeric material is plucked from the worn surface. Large cracks can be seen perpendicular to the sliding direction. The arrow indicates the sliding direction.

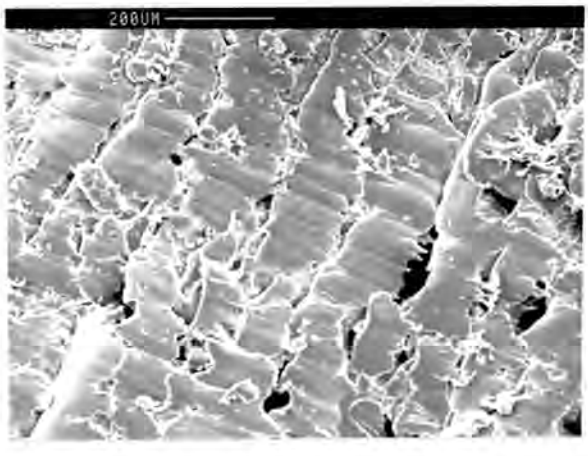

Figure 5.72: A SEM micrograph of streamer type polymer wear debris formed during dry reciprocating sliding wear.

When distilled water was introduced into the sliding configuration, the wear rate dropped by an order of magnitude. When the lubricant is removed, the initial high wear is restored. The results of these dramatic changes are shown between dashed lines in figure 5.73. Tests which were conducted under water lubrication only, are also shown for comparison. No

apparent changes in the transfer film could be detected visually, due to the introduction of the distilled water.

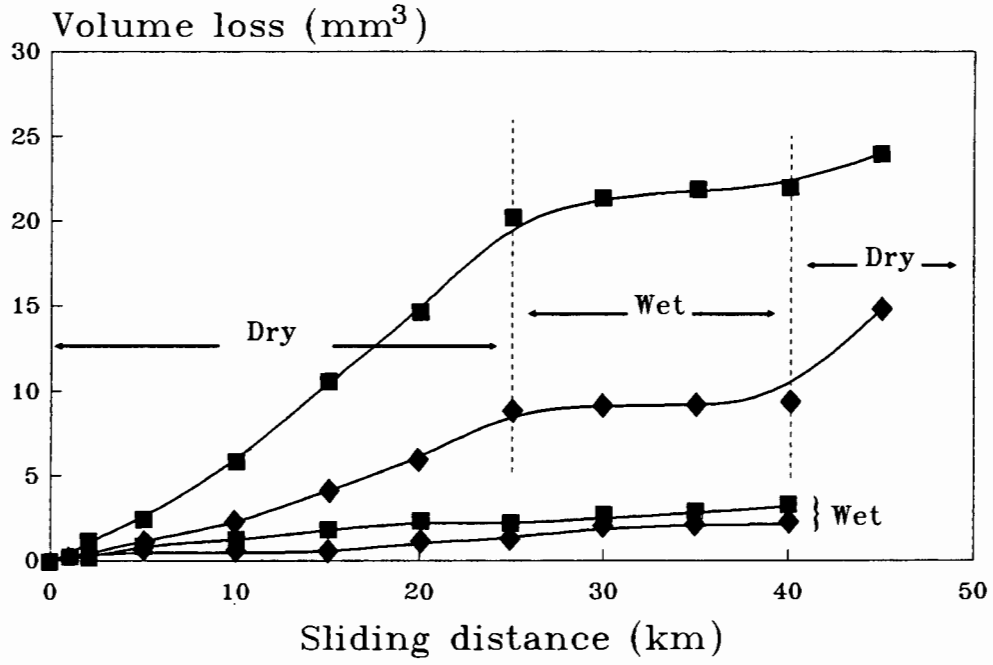

Figure 5.73: Volume loss of polymer *vs.* sliding distance under dry and wet (distilled water) reciprocating sliding wear conditions. All the tests were run at 0.25 $m.s^{-1}$ and 5 MPa. Tests conducted under water lubrication only, are also shown. ■ 10/100; ◆ Special DS.

The corresponding changes in kinetic friction coefficients and surface temperatures due to the distilled water is shown in figure 5.74. The temperature dropped to about 2-3 °C above ambient when the tests are conducted under distilled water, while the friction also dropped dramatically during this period (table 5.5). The friction coefficients were also found to increase to the previous higher values when the lubricant was removed.

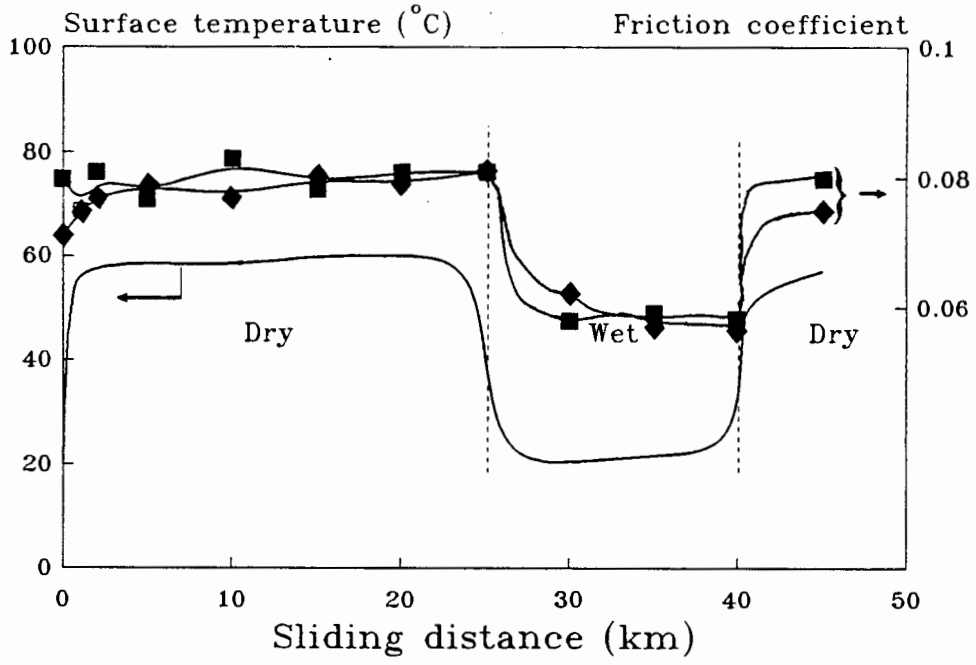

Figure 5.74: The variation in surface temperature and friction coefficient with sliding distance under dry and wet conditions. ■ 10/100; ◆Special DS.

Polymer	Test	Wear rate ($mm^3/N.m$)	Kinetic friction coefficient	Wear ratio of 10/100:Special DS
10/100	dry	1.62×10^{-6}	0.08	2.2
Special DS		7.45×10^{-7}	0.08	
10/100	wet	1.44×10^{-7}	0.06	1.4
Special DS		1.05×10^{-7}	0.06	
10/100	wet following	1.66×10^{-7}	0.06	1.4
Special DS	dry	1.14×10^{-7}	0.06	

Table 5.5: Specific wear rates and friction coefficients for UHMWPE during reciprocating sliding wear. Average sliding velocity: 0.25 $m.s^{-1}$; Normal pressure: 5 MPa.

5.6.2 Dry Pin-on-Disk Sliding Wear

A pin-on-disk wear testing machine was used to compare the unidirectional wear behaviour of UHMWPE to that observed under dry reciprocating sliding wear. The pin-on-disk wear rig employed for this study has previously been described [175]. The experiments were carried out using 3.2 mm diameter UHMWPE grade 10/100 pins, sliding on hardened stainless steel counterfaces similar to those used in the reciprocating wear tests. Loads ranging between 46.9 N and 165 N were applied to the wear pins via a cantilever system. The 90 mm diameter counterfaces were ground to a unidirectional lay with surface roughnesses of 0.32 ± 0.02 μm R_a. A sliding velocity of 0.25 m.s^{-1} was employed and tests were carried out at a mean wear diameter of 80 millimeters.

5.6.2.1 Friction and wear

Figure 5.75 shows the variation in friction and volume loss with sliding distance for two different pressures. A steady-state region of low wear, which followed an incubation period of high wear, was observed for all the tests.

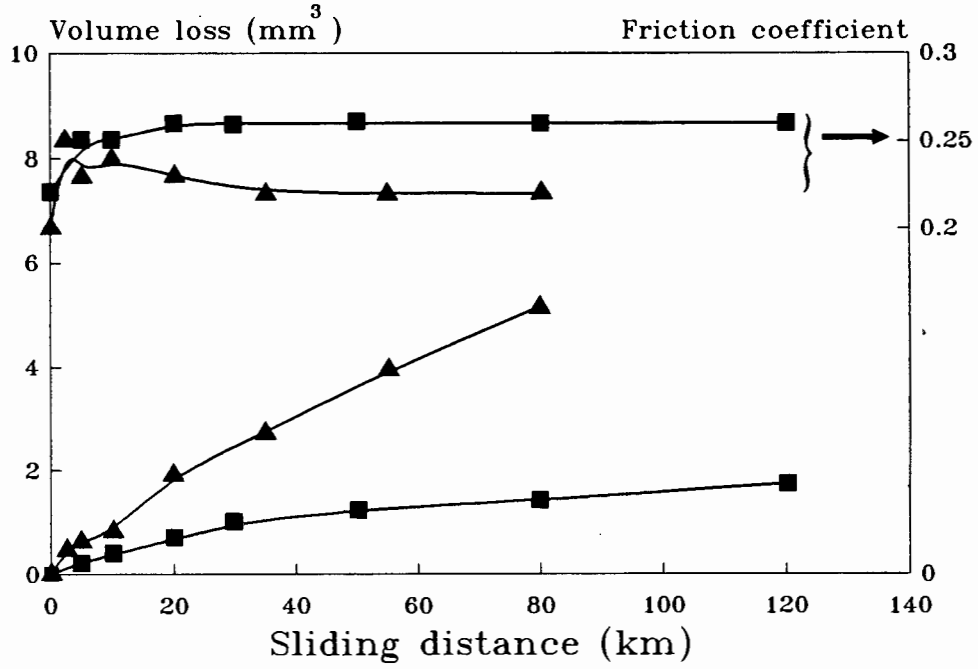

Figure 5.75: The variation in volume loss and friction coefficient with sliding distance for UHMWPE grade 10/100 during dry unidirectional sliding wear. The tests were conducted at sliding speeds of 0.25 m.s^{-1} and normal pressure of ▲5.14 MPa and ■1.46 MPa.

The wear rate for the higher pressure (5.14 MPa) was approximately two times greater than that of the lower pressure (1.46 MPa) and these results are tabulated in table 5.6. The wear rate obtained using the higher pressure can be compared with that obtained for UHMWPE grade 10/100 under dry reciprocating sliding wear in table 5.5. The specific wear rate in reciprocating sliding wear is then found to be approximately five times greater than that found for unidirectional sliding wear.

The friction coefficients appear to decrease as the pressure is increased. This decrease in friction is associated with a viscoelastic response where A_r increases less rapidly than proportionately with load.

Polymer	Pressure (MPa)	Wear rate ($mm^3/N.m$)	Friction coefficient
10/100	1.46	1.71×10^{-7}	0.26
10/100	2.27	5.5×10^{-7}	0.22
10/100	5.14	3.3×10^{-7}	0.22

Table 5.6: Specific wear rates and friction coefficients of UHMWPE obtained from dry pin-on-disk wear tests. Sliding velocity: 0.25 $m.s^{-1}$.

5.6.2.2 An examination of the worn surfaces

An optical microscopic examination of the counterfaces indicated that the surface topography was also modified by transferred polymeric material. A SEM examination of the worn polymer pins showed that a shear process, similar to that found during reciprocating sliding wear, occurs on these polymer pins (*cf.* figures 5.76 and 5.46). It is evident from figure 5.76 that shear occurs at a distinct depth below the wearing surface of the polymer material. The depth of these layers are estimated to be several micrometers thick. The streamer debris (figure 5.77) that is extruded at the rear end of the polymer pins also appear to be agglomerates of smaller polymer films that were fused together during extrusion as wear debris.

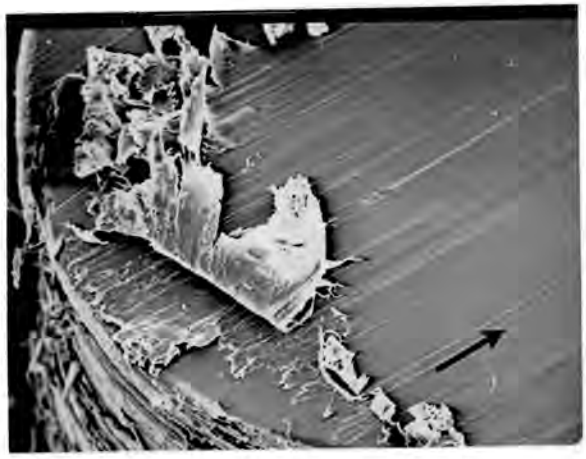

Figure 5.76: A SEM micrograph showing the shear process on the polymer wear pin during dry unidirectional sliding wear. The micrograph shows the trailing edge of the wear pin after 120 km of sliding wear. The trailing wear debris have been removed prior to SEM examination. The arrow shows the sliding direction.

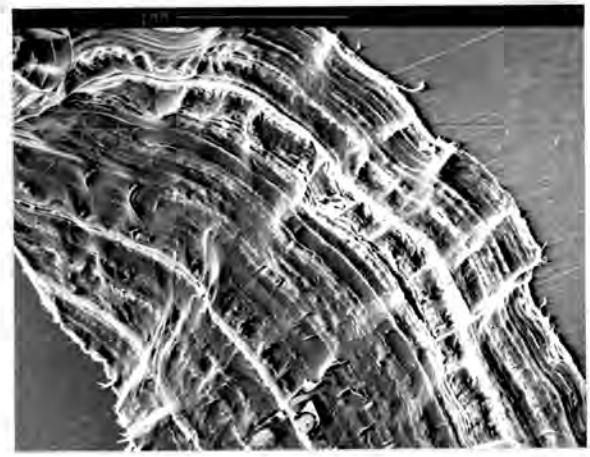

Figure 5.77: A SEM image of the streamer type wear debris produced during unidirectional sliding wear.

5.7 THE FRICTION AND WEAR BEHAVIOUR OF PTFE

5.7.1 The PTFE Composites

The commercially produced PTFE had the same compositions as those used by Tanaka *et al.* and Blanchet *et al.* [177,178]. The compositions of all the PTFE composites used in this investigation are given in table 5.7. Figures 5.78a, c and d show SEM micrographs of the fractured surfaces of the unfilled-, glass fibre filled- and bronze filled PTFE, respectively, impacted at liquid nitrogen temperature. A TEM replica of the surface of unfilled PTFE is shown in figure 5.78b. The unfilled PTFE fracture surface exhibited several cracks as a result of the fracture process (figure 5.78a), but TEM reveals a banded structure, with the bands being approximately 0.2-0.3 μm apart. Tanaka *et al.*, Speerscheider *et al.* and Makinson *et al.* observed finer striations approximately 20 nm thick, perpendicular to these bands [12,33,123].

The bronze particles in bronze filled PTFE ranged from 10 to 100 μm in size. The glass fibres had diameters of about 10 μm and their lengths ranged from 100 to 200 μm.

The molecular weight and crystallinity of the unfilled PTFE was calculated to be approximately 7.4 x 10^6 g.mol^{-1} and 33.5% by DSC, respectively (table 5.7).

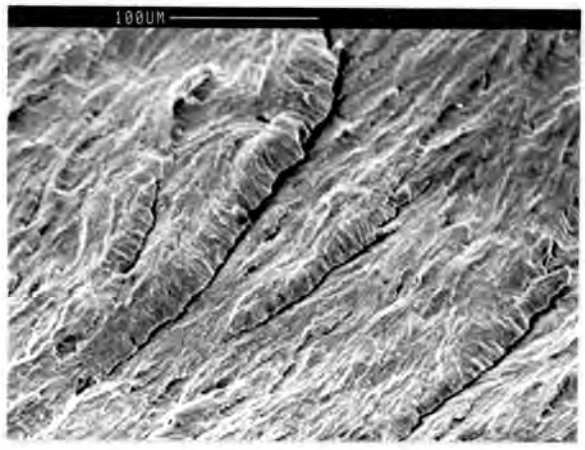

Figure 5.78a: A SEM image of the fracture surface of unfilled PTFE. The cracks are due to the fracture process.

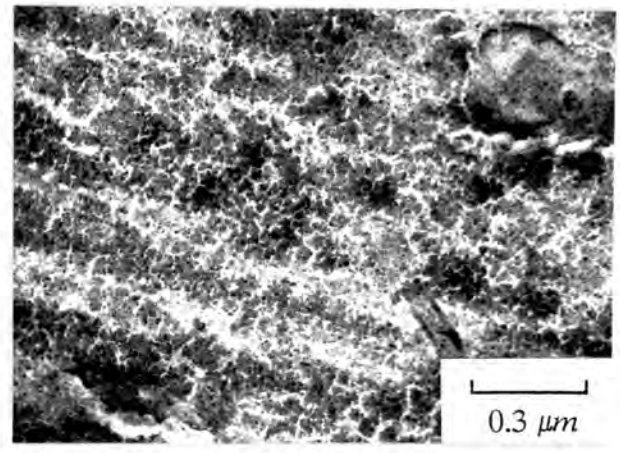

Figure 5.78b: A TEM micrograph of the unfilled PTFE fracture surface showing the banded nature of this polymer.

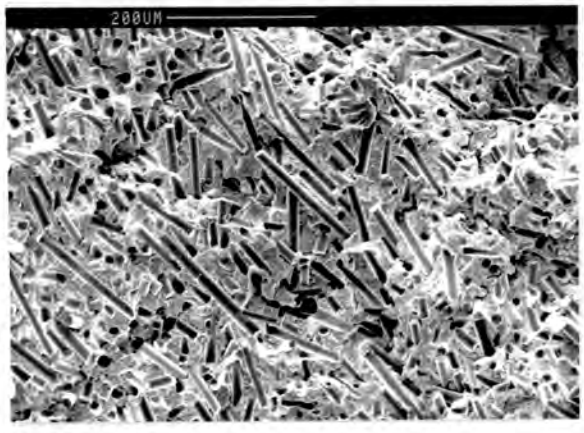

Figure 5.78c: A SEM image of the glass fibre filled PTFE fracture surface.

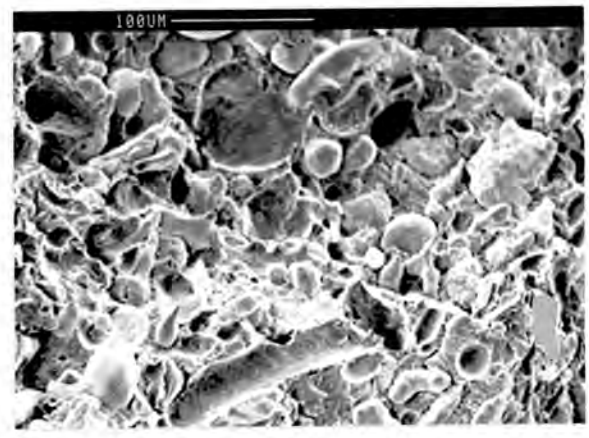

Figure 5.78d: A SEM image of the bronze filled PTFE fracture surface.

Polymer	Trade name	Filler		Shape and size of filler	Crystallinity (%)	Molecular weight (g/mol)
		type	%			
unfilled PTFE	Teflon	—	—	—	33.5 (DSC)	7.4×10^6 (DSC)
bronze filled PTFE		bronze	40	particles 10 - 100 μm in size	—	—
glass fibre filled PTFE		glass fibres	25	fibres 10 μm in diameter and 100 - 200 μm in length		

Table 5.7: The compositions of the PTFE

5.7.2 The Friction and Wear Behaviour of PTFE under Water Lubrication

5.7.2.1 Wear rates

Figure 5.79 shows the typical variation of volume loss and friction coefficient with sliding distance for both filled and unfilled PTFE, under nominal pressures of 5 MPa. The trends in volumetric wear and friction with sliding distance, were similar to those obtained at higher pressures of 10 MPa. Although the wear rates for all the grades did not vary significantly with an increase in pressure, the friction coefficients tended to be slightly lower (table 5.8). Figure 5.79 shows that linear relationships between volume loss and sliding distance are found for all the PTFE composites from the onset of the wear test. The unfilled grade showed wear rates that were approximately an order of magnitude higher than the filled PTFE. Furthermore, the unfilled PTFE also showed an appreciable degree of cold flow, especially at the higher pressure of 10 MPa. The glass fibre filled PTFE shows a lower wear resistance than the bronze filled PTFE under the imposed test conditions.

The lowest coefficient of friction was obtained for the unfilled PTFE, which showed a small decrease before reducing to a low steady-state value. The friction coefficients for glass fibre filled PTFE, however, showed initial increases before decreasing to lower values. No significant differences in friction coefficient could be found for the filled grades at both 5 and 10 MPa.

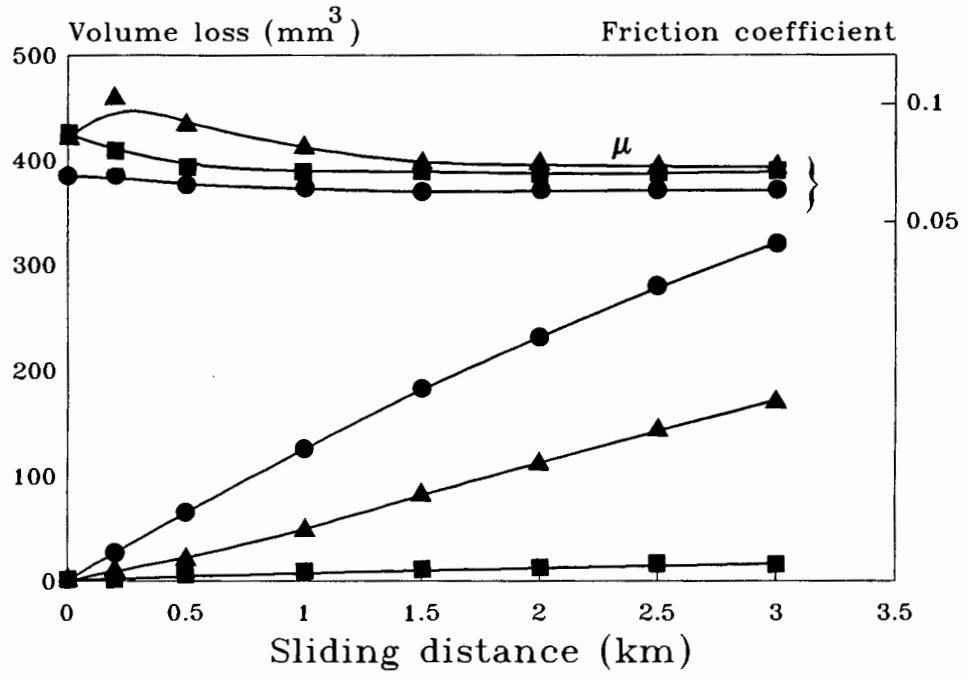

Figure 5.79: Volume loss and friction coefficient *vs.* sliding distance for PTFE. The tests were conducted in distilled water under nominal pressures of 5 MPa; ● unfilled PTFE, ■ bronze filled PTFE, ▲ glass fibre filled PTFE.

5.7.2.2 An examination of the worn surfaces

The wear and friction behaviour of the PTFE composites can be explained more clearly when the worn counterfaces are examined in the SEM. The counterface worn by the unfilled PTFE was completely devoid of a transfer film and relatively large amounts of polymer was observed at the ends of the wear stroke.

The counterface worn by the glass fibre filled composite, however, showed small lumps of polymer scattered across the metal surface as depicted schematically in figure 5.80a. These lumps of polymer were approximately a few millimeters in size and were poorly adhered to the metal substrate. Figure 5.80b shows a SEM micrograph of such a lump and the film is clearly seen to be in the process of peeling off the counterface as a result of the reciprocating action of the polymer pin. It would also appear that the glass fibres in the matrix inhibit the shearing action of large volumes of polymer from the pin as observed for the unfilled grade. The glass fragments give rise to high pressure areas which effectively "weld" portions of the polymer onto the metal surface.

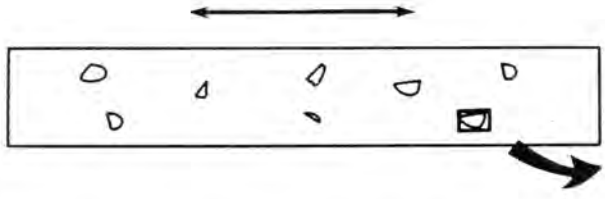

Figure 5.80a: A schematic of the worn metal counterface following sliding against the glass fibre filled PTFE under water lubrication. The double arrow shows the sliding direction.

Figure 5.80b: Lumpy and weakly adhered transfer films, several millimeters in size, can be observed on the counterface depicted in fig. 5.81a. The arrow shows the sliding direction.

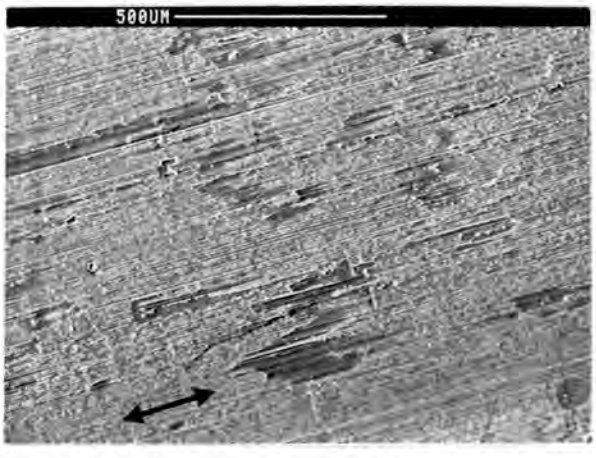

Figure 5.81a: Small plate-like particles are uniformly distributed across the metal counterface when worn against bronze filled PTFE under distilled water. The arrow shows the sliding direction.

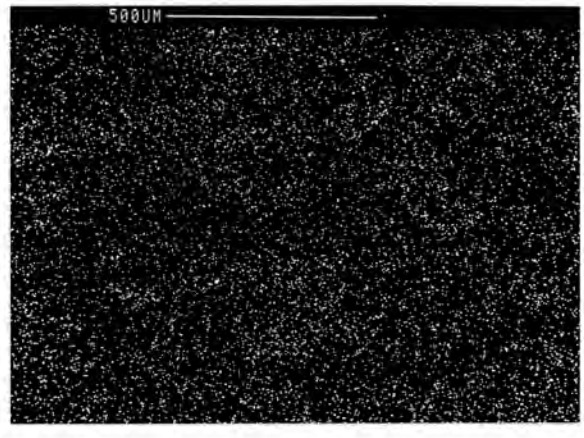

Figure 5.81b: A Cu x-ray map of the corresponding area in fig. 5.82a.

The counterface worn by the bronze filled PTFE, showed small plate-like particles more evenly distributed across the metal surface (figure 5.81a). The bronze filler is also more effective in breaking up the PTFE film into smaller fragments, than that observed for glass

fibre filled PTFE. A Cu x-ray map of the counterface (figure 5.81b), confirms the fact that the filler is more uniformly spread across the metal surface. Any material that was transferred, however, did not adhere firmly to the counterface. When unfilled PTFE was subsequently worn against a surface covered with a PTFE/bronze transfer film, high wear rates found for unfilled PTFE on unblemished surfaces, are again obtained. Any transferred material by the bronze filled composite was removed by the unfilled PTFE.

5.7.3 The Dry Friction and Wear Behaviour of PTFE

5.7.3.1 Wear rates

The volume loss of polymer and friction coefficient *vs.* sliding distance for filled and unfilled PTFE under dry reciprocating sliding wear conditions is shown in figure 5.82. The wear rates for the unfilled PTFE were approximately three times higher than those obtained under water lubrication, while the same level of frictional work was maintained (table 5.8). The wear rates for the bronze- and glass fibre filled PTFE were reduced by one and almost three orders of magnitude respectively, when compared to tests performed under water lubrication. No significant differences in wear rate could be found for the two filled grades under dry sliding wear conditions (table 5.8).

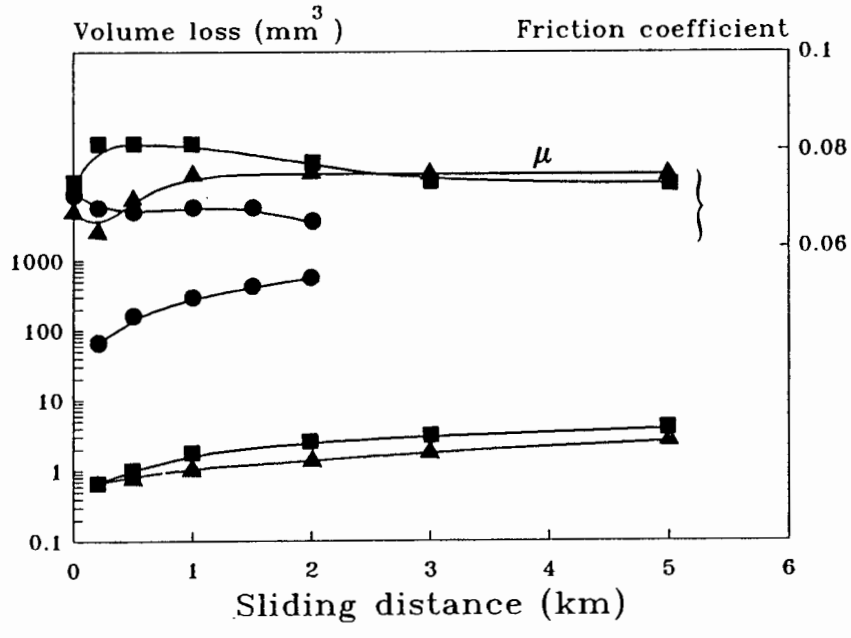

Figure 5.82: Volume loss and friction coefficient *vs.* sliding distance for PTFE under dry reciprocating sliding wear. The nominal contact pressure was 5 MPa. ● unfilled PTFE, ▲glass fibre filled PTFE, ■ bronze filled PTFE.

Figure 5.82 also shows that the coefficient of friction for the unfilled PTFE was lower than that for the filled grades. The friction for unfilled PTFE was slightly lower during the test than the friction measured at the onset of the test. The friction coefficients for the filled grades were very similar and both appeared to increase initially before reaching a steady-state value, as shown in figure 5.82. These friction coefficients were the same as those obtained in the water-lubricated wear tests (table 5.8).

5.7.3.2 An examination of the worn surfaces

The worn metal counterfaces were examined using both optical and scanning electron microscopy. It is clear that the wear process for PTFE is dictated by the formation of transfer films formed on the metal substrates. The transfer film for unfilled PTFE completely covered the metal counterface. These films appeared as large sheets which were not very adherent to the metal counterface and were subsequently easily peeled off. Fresh material is continuously sheared off the pin surface as the transferred polymer is removed from the contact zone as wear debris. Figure 5.83 shows a SEM micrograph of the appearance of weakly adhered PTFE films on the metal counterface.

The bronze- and glass fibre filled PTFE, however, showed transfer films that were more stable on the metal counterfaces. In the case of bronze filled PTFE, the metal counterface was very smooth due to small films of material being mechanically worked into the asperity valleys. It would thus appear that the fillers are effectively breaking down the polymer into small fragments which can easily be forced into the valleys by the shearing action of the polymer pin. The transfer film does, however, appear to suffer from a spallation process as shown in figure 5.84.

Figure 5.85 shows that the glass fibres in the worn polymer pin surface fragment and debond from the polymer matrix. These glass fragments are further broken down and subsequently abrade the transfer film into small pieces which are easily forced into the valleys of the counterface by the pin until the surface is uniformly covered with polymeric material as shown in figure 5.86. It is also conceivable that the high pressures created at the contacts between the glass fragments and the metal surface create the opportunity for "localized welding" of the polymer film to the metal substrate.

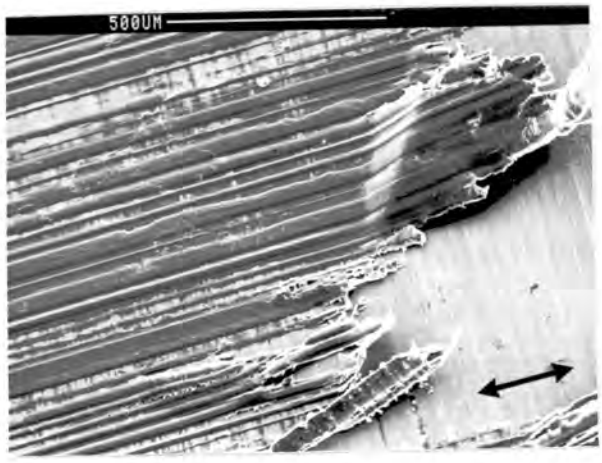

Figure 5.83: A SEM image showing how thin, weakly adhered polymer films found for unfilled PTFE are easily peeled off the metal counterface during dry sliding wear. The arrow shows the sliding direction.

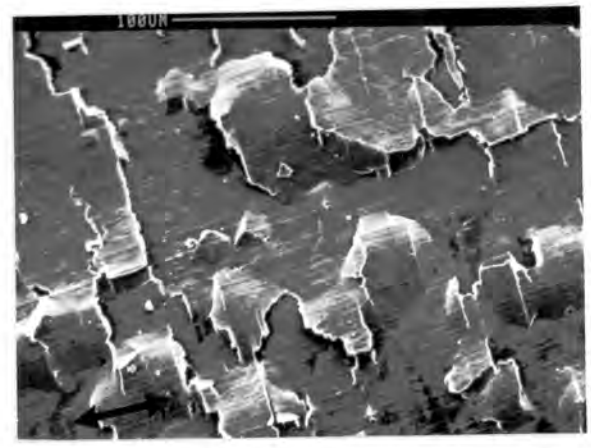

Figure 5.84: A SEM image of the worn counterface following sliding against bronze filled PTFE. The transfer film appears to be spalled off the surface during the dry wear process. The arrow shows the sliding direction.

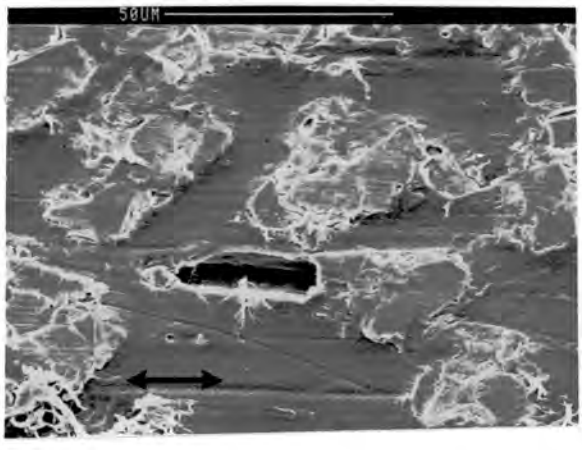

Figure 5.85: A SEM image of the worn surface of the glass fibre filled PTFE wear pin. The micrograph shows that glass fibres may debond from the worn surface. The arrow shows the sliding direction.

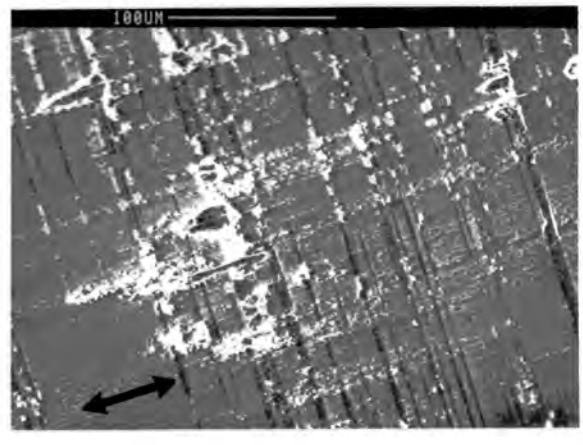

Figure 5.86: A SEM image showing a uniform transfer film following dry sliding against glass fibre filled PTFE. Glass fragments are scattered across the metal surface. The arrow shows the sliding direction.

Polymer			Test conditions			Wear rate	Friction
unfilled PTFE	bronze filled PTFE	glass fibre filled PTFE	pressure (MPa)	distilled water	dry	(mm^3/N.m)	coefficient
X			10	X		2.36×10^{-4}	0.03
	X					6.13×10^{-6}	0.043
		X				9.93×10^{-5}	0.042
X			5	X		1.95×10^{-4}	0.063
	X					9.8×10^{-6}	0.071
		X				1.21×10^{-4}	0.073
X			5		X	5.36×10^{-4}	0.066
	X					9.1×10^{-7}	0.074
		X				8.3×10^{-7}	0.075

Table 5.8: Specific wear rates and friction coefficients for the PTFE under various operating conditions. All the tests were conducted at 0.25 $m.s^{-1}$. The X indicates the testing condition.

5.7.4 The Nature of the Worn PTFE Material

5.7.4.1 The worn wear pin surfaces

XRD data of the worn wear pin surfaces are tabulated in table 5.9. Although the crystallinity of the worn wear surfaces is shown to be less than that of the bulk polymer, it cannot conclusively be said that the wear pins showed signs of amorphisation.

5.7.4.2 The nature of the polymer wear debris

The PTFE debris have been analyzed using both XRD and DSC. Debris formed during the dry reciprocating wear process are designated type 1 and those obtained from water-lubricated tests are referred to as type 2 in table 5.9. Figures 5.89a and 5.89b show SEM micrographs of these two types. Type 1 is sheet-like in appearance, whereas type 2 debris was powdery.

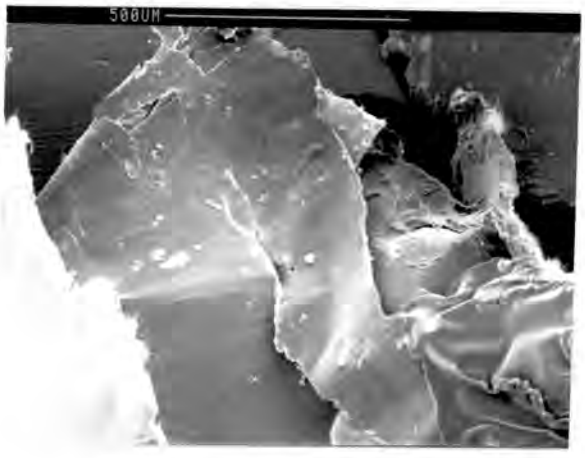

Figure 5.89a: Sheet-like debris (type 1) formed during dry reciprocating sliding wear of PTFE against stainless steel.

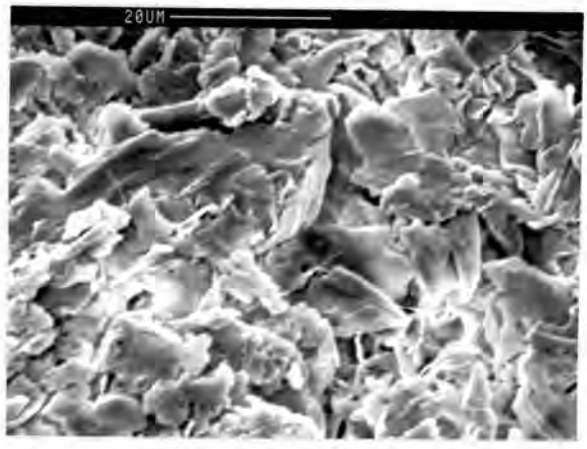

Figure 5.89b: Powdery PTFE debris (type 2) is formed when the wear tests are conducted in distilled water.

Table 5.9 shows that the crystallinity of the debris is higher than that of the bulk polymer and that the crystallinity of type 2 debris can be attributed to the fact that, although material is not transferred to the metal counterface during water-lubricated sliding wear of the unfilled PTFE, the polymer sheets remain in the contact zone before being expelled as powder-like wear debris. A XRD trace of both the unfilled PTFE and powder-like debris is shown in figure 5.90. It would appear that the amorphous peak at 16.4° is absent in the debris. The crystalline peak was also found to be much more pronounced than that of the unworn PTFE. The molecular weight of the unfilled PTFE was calculated to be approximately 7.4×10^6 g.mol^{-1}. The molecular weights of type 1 and type 2 debris were calculated to be about 1.3×10^5 g.mol^{-1} and 3.2×10^4 g.mol^{-1}, respectively (table 5.9). This shows that material that remained within the contact zone, is systematically broken down by the shearing forces experienced at the polymer/metal interface.

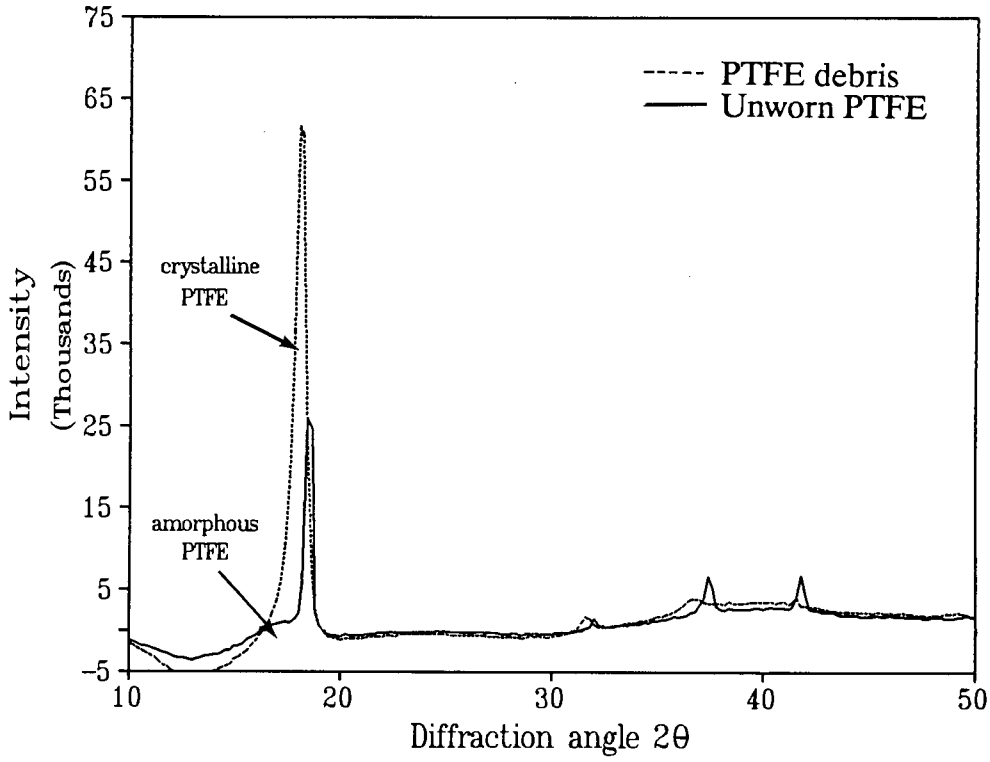

Figure 5.90: XRD traces of unworn PTFE and powder-like (type 2) wear debris. The crystallinity of the wear debris is substantially higher than that of the unworn bulk polymer.

Polymer	Technique	Material			Number of samples	Crystallinity	Standard deviation (%)	Molecular weight (g/mol)
		unworn bulk polymer	worn surface	debris				
unfilled PTFE	X-ray analysis	X			3	60.3	9	
			X		2	55.5	0.9	
				X	1	>95	0	
	DSC	X			2	33.5	6	7.4×10^6
				X (type1)	3	69.7	4.9	1.3×10^5
				X (type2)	3	91	5.1	3.2×10^4

Table 5.9: X-ray and DSC analysis of unfilled PTFE. X (type1) and X (type 2) refers to debris obtained under dry and wet sliding conditions, respectively.

CHAPTER 6

DISCUSSION

6.1 INTRODUCTION

It is well known that in practical tribology, many parameters operate simultaneously and affect the friction and wear processes in complex and often unpredictable ways. It is not true to assume that friction and wear are interrelated surface phenomena. Thus, the acquisition of any new information of the tribological pair at the contacting interface can lead to valuable contributions to our overall understanding of friction and wear. An individual consideration of the factors governing the wear process may be useful from the point of view of materials selection.

The following discussion describes systematically how parameters and factors such as counterface roughness, distilled water lubrication, bearing pressure, polymer molecular weight and fillers influence the tribological behaviour of an UHMWPE/stainless steel sliding couple. It was deemed necessary to repeat certain concepts in the various sections in the discussion because of the interplay between the factors governing the wear process. Details of morphological changes in the polymer surface layers and modifications of the metal counterface by transferred material during the sliding wear process are also described. Finally, the discussion concludes with a comparison between the wear behaviour of UHMWPE and PTFE.

6.2 THE FRICTION AND WEAR BEHAVIOUR OF UHMWPE

6.2.1 Basic Wear Mechanisms

6.2.1.1 Water-lubricated sliding wear

The variation in volume loss of polymer with sliding distance for all the UHMWPE examined showed that initially, high wear was followed by reductions in the wear rate on

the rough counterfaces under water lubricated sliding wear. Polymer that is worn from the polymeric pin is either ejected from the sliding interface as wear debris or adheres to the steel surface as transfer films.

Two distinct wear stages were identified from the volume loss *vs.* sliding distance curves on relatively rough counterfaces of 0.3 μm R_a surface values, *viz.* a high wearing-in or bedding-in stage and a lower steady-state wear regime. During the bedding-in stage, abrasion and adhesion are the operative wear mechanisms. The hard metal asperities partially penetrate the softer surface of the polymer and shallow abrasive grooves, due to the ploughing action of the asperities, were observed on the wear pin surfaces (see figure 5.54). The abrasive grooves were accompanied by striation marks formed perpendicular to the sliding direction. These features suggests that any material removed by the metal asperities occurred either via. a tensile tearing or a microcutting action. It is, however, postulated that adhesive wear is the dominant wear mode during the early stages of the sliding wear process.

The high pressures created at the contact between the initial relatively clean metal counterface and the wear pin effectively squeezes away the water film and creates the opportunity for adhesive wear between the two mating surfaces. The size, shape and thickness of the initially transferred films suggest that most of the polymer is worn from the pin by a shearing action. The ease with which the polymeric material is sheared, is aided by orientation of the polymer molecules in the surface layers in the sliding direction. As the polymeric films are gradually worked into the asperity valleys, better load support by the water film leads to a reduction in the wear rate. Adhesive wear, by shearing of polymeric films, continues to operate during the steady-state wear regime and material may be back transferred to the wear pin. TEM reveals evidence of the severe ductile deformation process as the polymeric transfer film is smeared across the metal asperities in the sliding direction (figure 6.1). The contribution of abrasive wear to the total wear process appears to be negligible during the steady-state wear regime. Hollander and Lancaster contend that the elastic modulus of the polymeric transfer films is similar to that of the bulk polymer and in consequence, the localized stresses are reduced as the real area of contact is increased [74].

Discussion: page 164

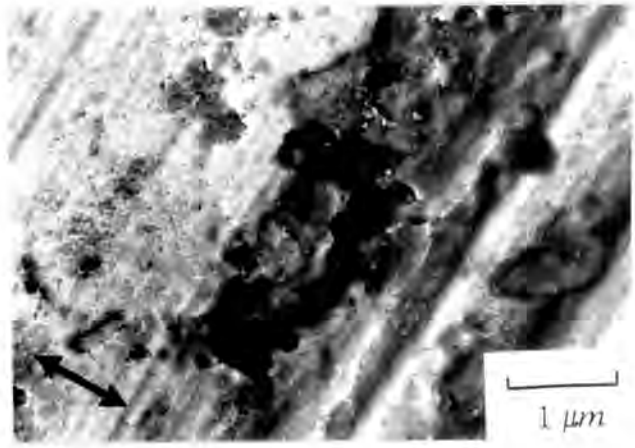

Figure 6.1: A TEM image of the worn metal counterface following sliding against UHMWPE. The micrograph shows evidence of microductile deformation indicative of adhesive wear. The undulations due to the metal asperities can be seen. The arrow indicates the sliding direction.

The friction of polymers against metallic counterfaces can be considered to involve two main process [41,46]. The first is the shearing of adhesive bonds at the regions of real contact, and the second is the ploughing of the metallic asperities through the surface of the polymer. These separate contributions can be added together to obtain a frictional force which excludes other contributions *e.g.* fatigue,

$$F = F_{adhesion} + F_{deformation}$$

It is difficult to quantify exact values for these components of friction. The friction coefficients were found to follow the same trend as the decrease in volume loss curves on the rough counterfaces (see figure 6.3). With continued sliding, the initial high energy losses due to the abrasive component of friction are reduced as the polymer fills up the valleys between the metal asperities. This reduction in "abrasive wear" is clearly not compensated for by an increase in total contact surface area. Thus, lower values of friction are obtained when the polymer fills up the valleys between the metal asperities forming a coherent transfer film. The friction coefficient values obtained during steady-state wear are also dependent on a lowering of the adhesive component of friction by the interposed water film being sustained by the smoother wearing surfaces. Specific characteristics of the transfer film and surface layer layers of the wear pin may also affect the friction coefficient.

Polymers such as PTFE and HDPE have been shown to exhibit low friction coefficients once the polymer molecules in the transfer film are aligned in the sliding direction [55,78]. This orientation of polymer molecules in the sliding have also been shown in this work for unfilled UHMWPE. Absorbed water into the surface of the wear pins may also affect the friction, but this was thought to be negligible due to the continual removal of the surface material.

6.2.1.2 Dry sliding wear

The variation of volume loss of polymer with sliding distance during dry sliding wear was distinctively different from that observed during the water-lubricated tests. An incubation period of low wear was followed by a high wear rate regime. During the early stages of the wear process, the same initial wear mechanisms described for the water-lubricated tests, are true for dry sliding wear on relatively rough counterfaces. As the counterfaces become smoother with transferred polymer, sliding wear takes place between the polymer wear pin and the transfer film covered metal counterface. In addition, the adhesive wear mechanism was also found to be further influenced by thermal softening of the polymer. The dry wear rates were approximately an order of magnitude higher than that observed for the water-lubricated tests.

The friction coefficients for the UHMWPE were also significantly higher in dry sliding than in water-lubricated environments. These higher values of friction can be attributed to the increase in adhesion with increases in surface temperature. By interposing a water film between the rubbing surfaces, the friction coefficients immediately drops from 0.08 to 0.06, by a lowering of the adhesion between the polymer and the polymer transfer film (see figure 5.74).

6.2.2 Transfer Film Formation of UHMWPE

Extensive optical and scanning electron microscopy has shown that the transfer film of UHMWPE which forms on a hardened stainless steel counterface during reciprocating sliding wear under water lubrication is built up of thin films that are sheared off the polymer wear pin (see figure 5.46). It is believed that shear occurs in interlamellar regions of the unworn polymer. These films accumulate preferentially on the asperity ridges, *i.e.*

the site of the highest localized adhesion, and a transfer film that is essentially layered is eventually built up. Wear will be minimal if this film is smooth across the metal counterface and some of the load is carried by the water lubricant. SEM shows that the outermost layer on the polymer wear surface is smooth and thin films, between 1 and 3 μm thick debond from the surface. "Fibrils" of about 0.29 μm wide are aligned in the sliding direction beneath a sheared layer (see figure 5.49). These fibrils consists of lamellae with the chain axis of the molecules tilting towards the sliding direction.

It was also shown from polarized light microscopy studies, that substantial subsurface deformation arising from normal and tangential shear stresses play a major role in aiding the shearing process. Polymer molecules were shown to be substantially orientated in the sliding direction in a narrow band of approximately 5 - 10 μm below the polymer wearing surface, allowing for the easy shear of the surface layers observed in figure 5.46. The polarized microscopy studies are thus consistent with SEM observations which showed layers of approximately 3 - 5 μm thick being sheared off the UHMWPE wear pins. Recent studies by Cooper *et al.* also showed residual strains at depths ranging from 30 to 60 μm below UHMWPE pin surfaces after prolonged sliding against stainless steel in deionized water [180].

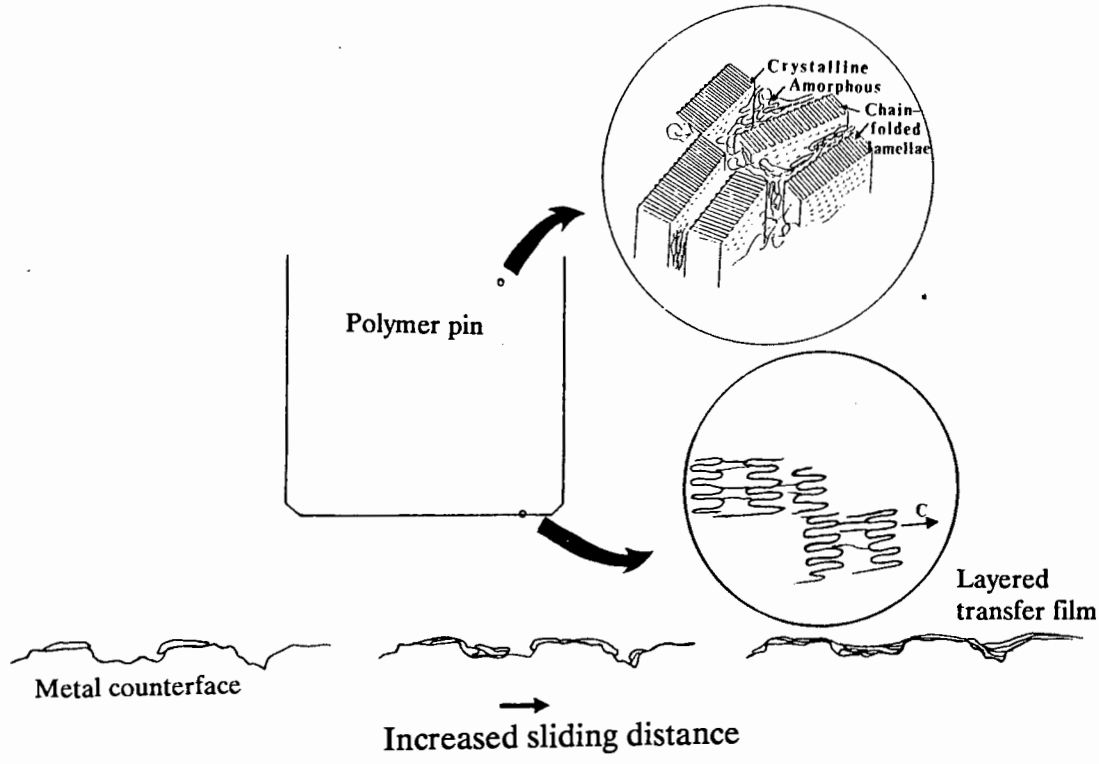

Figure 6.2: A schematic illustration of the formation of transfer films on relatively rough metal counterfaces (0.3 μm R_a) during water lubricated sliding wear.

Polymer films that are not transferred to the metal counterface tend to remain in the contact zone for some time before being ejected as highly crystalline wear debris. The debris was also shown to have a smaller crystallite size and lower molecular weight than the bulk polymer due to the interfacial deformation process. The process of transfer film formation under water lubrication is schematically illustrated in figure 6.2 above.

6.3 FACTORS THAT INFLUENCE THE FRICTION AND WEAR OF UHMWPE

6.3.1 The Influence of Counterface Roughness on the Friction and Wear of UHMWPE

6.3.1.1 The effect of a small change in counterface roughness, R_a

Investigations into the effects of changes in surface roughness alone was complicated by a modification of the metal counterface by transferred polymer. Studies of the effect of changing the counterface roughness from 0.25 to 0.35 μm R_a, however, showed that the magnitude of both the initial bedding-in and steady-state wear regimes are affected by the initial surface roughness (see figure 5.13(a)). During the initial bedding-in period, in particular, any variation in wear rate can be ascribed to small differences in R_a. Rougher surfaces generally exhibited higher wear rates in the bedding-in period. Abrasion and microploughing of the sharp metal asperities coupled with adhesion are the principle operative wear mechanisms. Mechanical interlocking of the polymeric films with the counterface is enhanced by an increase in surface roughness. An examination of the surface topography by stylus profilometry also showed a sharp decrease in R_a during the bedding-in period. The values of R_a cannot, however, be taken as representative values, as the softer transfer film cannot fully resist penetration by the stylus ball. The effect of surface roughness parameters such as the shape, slopes, height distribution and radii of curvature of the metal asperities are expected to play a role in mechanical interlocking in the early stages of sliding wear, but their influence would decrease as polymer fills up the depressions between the metal asperities.

The steady-state wear rates were also found to be dependent on the initial counterface roughness. A log-linear relationship between specific wear rate and counterface roughness for UHMWPE under water lubrication was obtained by Lloyd: [4]

$$K_o = 1.1 \times 10^{-8} e^{7.7R_a}$$

where K_o is the specific wear rate in $mm^3/N.m$

Lloyd's equation was obtained over a large range of counterface roughness, R_a, and although the author used a much smaller range, the wear data appeared to correlate well with the equation above. Generally the wear rate varies exponentially with counterface roughness [135,139]. Dowson *et al.*, for example, showed that the wear rate of UHMWPE is proportional to $R_a^{1.2}$ in tests conducted under water lubrication [139].

6.3.1.2 Wear studies on very smooth counterfaces

Linear relationships between volume loss and sliding distance from the onset of sliding were obtained on the very smooth metal counterfaces. Patchy lumps and discontinuous transfer films were characteristic of sliding against the smooth counterfaces. These patchy films are associated with adhesive wear between the polymer wear pin and the relatively smooth counterfaces. The wear rates, which varied between 1.6- and 4.5 x 10^7 $mm^3/N.m$, were approximately an order of magnitude greater than the steady-state wear rates on the rougher counterfaces. The inorganically filled UHMWPE showed the highest wear rates. It would appear that any initial lumps that formed were preferential sites for further transfer of polymer. This type of lumpy transfer, leading to increased wear rates, was observed by several authors for "normal" polymers such as LDPE on smooth counterfaces [60,78].

Conversely, the unfilled UHMWPE did not show this lumpy transfer on the smoother counterfaces. Rather, thin discontinuous films eventually formed on the smooth metal surfaces. This is presumably so, because an initial site of transferred polymer is not a preferential site for further transfer, as displayed by the inorganically filled UHMWPE. Thus, it would appear that some form of mechanical interlocking, particularly with rougher counterfaces, is imperative for long term low wear rates. It was also interesting to note that higher wear rates for the inorganically filled polymer are obtained when sliding against a glass bead polished surface than on a surface abraded by SiC paper with similar R_a values. The reason for this behaviour is believed to be due to a greater degree of mechanical interlocking provided by the SiC abraded counterfaces compared to the smoother profile of

the glass bead abraded surface, leading to the establishment of a more adherent transfer film. The profiles for these surfaces were shown to be quite different (*cf.* figures 5.18(d) and 5.30(a))

A direct correlation exists between the coefficient of friction and the wear rate on the smoother metal counterfaces. The observed steady trends in friction coefficient are attributed to the fact that adhesive wear predominates throughout the test.

6.3.1.3 Wear studies of polymer sliding on polymer

The wear rates for a polymer/polymer sliding couples are approximately three orders of magnitude higher than that of polymer/steel sliding couples and the results can be explained by a distinct increase in adhesion at the sliding interface. The friction coefficient were more than two times higher than that obtained for UHMWPE sliding on stainless steel. Scanning electron microscopy studies confirmed that the relatively high frictional values are due to severe adhesive wear. In this regard, Czichos also showed that there is a correlation between the frictional work and the work of adhesion (a measure of the surface energies of the contacting materials) for a number of polymer/polymer sliding pairs [140].

6.3.1.4 The effect of grinding direction on the metal counterface

The influence of mechanical interlocking of the polymer with the metal counterfaces is also seen from sliding wear studies conducted on counterfaces ground parallel to the sliding direction. A uniform, coherent transfer film is formed relatively quickly when sliding takes place normal to the grinding direction on the metal counterface. However, no uniform transfer film was found when sliding was conducted parallel to the steel surface grinding direction. Rather, the form of the polymer transfer was patchy and increased in amount very slowly over the period of experimentation in this study. The reason for this difference in behaviour is believed to be primarily a result of mechanical interlocking aiding polymer build-up on the surface when sliding takes perpendicular to the corrugated ground surface of the stainless steel. Any material which would normally be lost as debris, due to the shearing forces experienced at the interface of the reciprocating couple, can be accommodated in the valleys between the asperities on the metal surface. Conversely, such particles are more easily discharged when sliding takes place parallel to the grinding

direction. This interpretation also explains why the amount of debris found during the bedding-in stage of the total wear process is greater when sliding parallel to the grinding direction.

Although these transfer characteristics are quite different, in the two cases mentioned for equal sliding distances, the steady-state wear are seen to be similar initially (table 5.2). This similarity in wear rates is believed to be linked additionally to the counterface surface roughness. When wear studies are conducted normal to the grinding direction, the value of R_a decreases quite sharply as the build-up of a fully coherent transfer film takes place and then remains essentially constant with further sliding distance. This decrease in the value of R_a is parallelled by a decrease in the wear rate. When wear occurs parallel to the sliding direction, the measured initial value of R_a is lower and remains relatively constant during the period of experimentation. Figures 5.8 and 5.25 show that the value of R_a in both cases is similar during the steady-state regime. Such results imply that both transfer films and surface roughness values have an important influence on the total wear process.

The higher friction and wear rates found over extended sliding distances can be attributed to similar mechanisms observed from studies on smooth counterfaces. Polymeric material already found on the counterfaces appear to be preferential sites for the further transference of polymer, and hence the increase in size of polymer lumps. In the design of components, the factor of grinding direction has to be taken into consideration. The results indicate that grinding ought to be carried out perpendicular to the sliding direction for metal/UHMWPE couples which are operating over long periods of time in water-lubricated environments. Since coherent transfer films are a prerequisite for low wear rates, it would be interesting to see if low wear rates are obtained when the wear pin slides parallel to the grinding over a uniform transfer film. We may speculate that wear will be low initially, but will increase due to the material being more easily sheared from the sliding interface.

6.3.2 The Role of Fillers and Molecular Weight on the Friction and Wear of UHMWPE

The steady-state wear rates for the inorganically filled UHMWPE material are significantly lower than that for the unfilled UHMWPE (figure 6.3). The lower wear rates obtained for the inorganically filled UHMWPE may be explained by an increase in chemical activity between the transfer film and the metal counterface due to the presence of increased

amounts of titanium in the transferred UHMWPE. Only titanium was clearly detected in the transfer film on the metal counterface which suggests that titanium forms a chemical bond with the metal and enhances the adhesion of the transfer film thus lowering the wear rate. The increase in chemical activity and enhanced adhesion may also explain why this polymer forms patchy lumps on the smooth counterfaces. Thus, the influence of both the filler and some form of mechanical interlocking, particularly with rougher counterfaces, is imperative for long term low wear rates. In figure 6.4, the wear rates of both filled and unfilled polymers tested under the same operating conditions are compared with that of the UHMWPE. The polymers used for comparison are also commonly employed as bearing materials in mining equipment. This figure clearly shows the superior wear resistance of the UHMWPE under the imposed operating conditions. Mechanical and physical data of these polymers are tabulated in Appendix C.

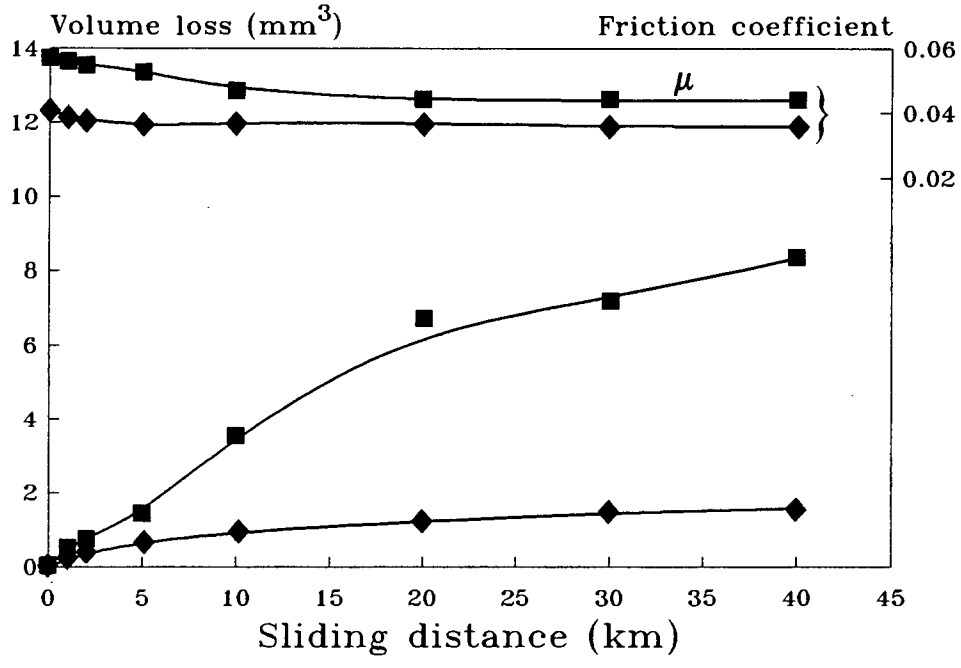

Figure 6.3: The variation in volume loss and friction coefficient, μ, with sliding distance for two UHMWPE grades, ■ unfilled UHMWPE (grade 10/100) and ◆ inorganically filled UHMWPE. The reciprocating tests were performed in distilled water at 0.25 $m.s^{-1}$ and 10 MPa.

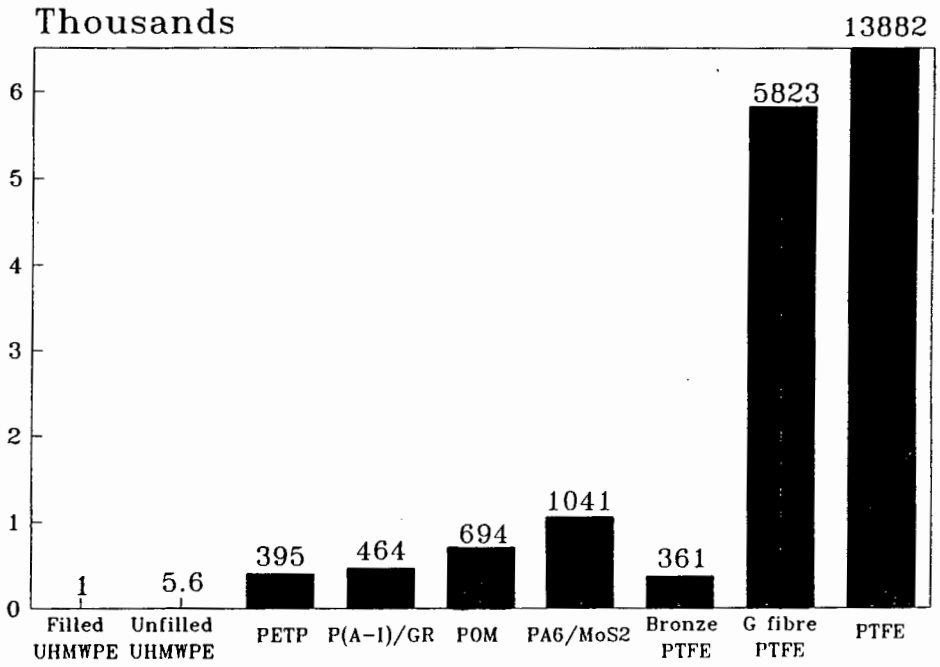

Figure 6.4: A comparison of the wear rates of UHMWPE with that of other commonly used bearing polymers. The tests were carried out under distilled water lubrication at 0.25 $m.s^{-1}$ and 10 MPa. Data on these polymers appear in Appendix C

During sliding wear with glass bead filled UHMWPE, the transfer film is initially securely attached to the rougher counterface. According to Briscoe and Steward, glass beads may act as stress intensifiers in the interfacial contact region which could provide suitable mechanical and chemical interactions to allow the polymer transfer to adhere strongly to the metal counterface [143]. Thus it would appear that the glass beads in the UHMWPE aid the initial mechanical interlocking process by forcing the material during sliding into the asperity valleys on the metal counterface. With continued sliding, however, the harder glass beads abrade the steel counterface until the polished surface is smooth and devoid of a transfer film. When this stage is reached, relatively high wear rates are obtained. Recent studies using different concentrations of glass beads in UHMWPE in pin-on-disk tests, show a decrease in wear rates with increasing concentration. At a concentration of 20%, however, the wear rate of the filled composite was found to be greater than that of the unfilled matrix [181].

The steady-state friction coefficients obtained from the filled material when using a contact pressure of 10 MPa on the rough counterfaces all lie in the range 0.032 ± 0.03. The unfilled UHMWPE did, however, show friction values that were higher (see table 5.1). These low friction values for the filled UHMWPE indicate that less energy is expended in shearing material at the interface when fillers are present.

Although the kinetic friction coefficient is found to decrease steadily after the transition from low to high wear for the glass bead filled UHMWPE, the static friction coefficient increases dramatically (see figure 5.16). It is possible that the increase in kinetic friction at the transition represents a stage at which an optimum surface roughness is reached for low wear. This phenomenon was observed by Briscoe and Steward when graphite filled PTFE were run against counterfaces of increasing roughness [143]. The corresponding large increase in the static coefficient of friction can be explained by the fact that large amounts of debris containing pulverized glass beads are now deposited at the ends of the wear track and more energy needs to be dissipated in these regions due to enhanced adhesive and abrasive contact between the polymer wear pin and the debris.

Large increases in molecular weight do not lead to corresponding large decreases in wear rates. This agrees with the work of Anderson who has shown that the specific wear rates will decrease exponentially with an increase in molecular weight and that only small decreases in specific wear rates are expected within the UHMWPE [83].

6.3.3 The Effect of Water Lubrication on the Friction and Wear of UHMWPE: A Comparison of Dry and Water-Lubricated Sliding Wear

6.3.3.1 The lubrication ability of water under boundary conditions

The coefficients of friction recorded at the start of the tests for dry (μ_d') and water-lubricated (μ_w') conditions are not very different, 0.08 compared with 0.07 , respectively (figure 6.5). These friction coefficients are assumed to represent the friction without the transference of polymer to the metal counterface. Wet (μ_w) and dry (μ_d) friction coefficients during steady-state, are also shown in figure 6.5.

Discussion: page 174

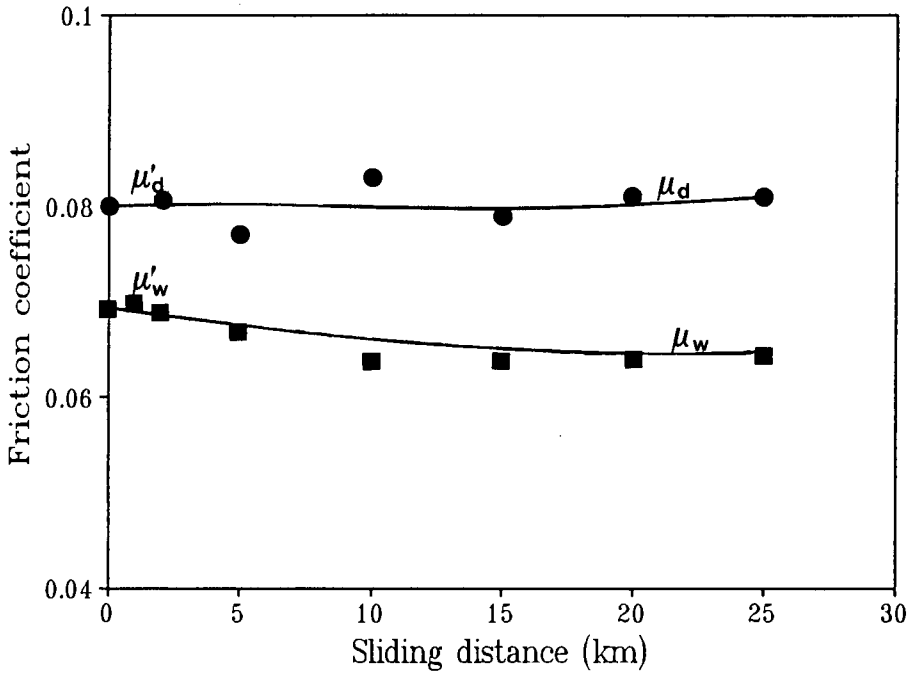

Figure 6.5: The variation of coefficient of friction, μ, with sliding distance under dry and water-lubricated sliding wear. ● dry, ■ water-lubricated. Pressure: 5 MPa; velocity: 0.25 $m.s^{-1}$.

Under water lubrication, the water film initially offers negligible support at the high contact pressures between the metal asperities and the polymer pin as the water film is effectively squeezed out from these pressure points. As more polymer is transferred to the metal counterface, the real area of contact increases and more load support by the water film leads to a decrease in friction. IR data (see figure 5.66) shows that when tests are carried out under water lubrication, water molecules penetrate the surface of the polymer and can thus alter the mechanical properties of the surface layers. The distilled water did not, however, appear to change the morphology of the transferred material. The hydrophilic nature of the steel counterface may allow the formation of a weakly held film, but as more polymer is transferred to the steel counterface, this effect would diminish due to the hydrophobic nature of the polyethylene.

The mechanism of boundary lubrication for polyethylene on the steel counterface can be summarized as follows:

Discussion: page 175

$$F = A_r \tau_e$$
$$= A_r\{\alpha\tau_o + (1-\alpha)\tau_l\} \quad (6.1)$$

where

F = the frictional force
τ_e = the effective shear strength
A_r = the true area of contact
α = the fraction of the true area at which polymer/metal contact occurs
τ_o = the shear strength of the junctions at the polymer/metal contact in dry friction
τ_l = the shear strength of the lubricant film

The area of contact is related to the normal load W by the equation:

$$W = P_o A_r \quad (3.9)$$

where P_o is the hardness pressure of the softer material.

From equation (6.1), the coefficient of friction under boundary lubrication, μ, is expressed as:

$$\mu = F/W$$
$$= \alpha\tau_o/P_o + (1-\alpha)\tau_l/P_o$$
$$= \alpha\mu_d + (1-\alpha)\tau_l/P_o \quad (6.2)$$

where μ_d is the coefficient of friction under dry conditions.

By using equation (6.2) and a value of 0.53 MN/m^2 obtained by Tanaka for τ_l, it can be shown that α decreases from an initial value of 0.86 (α') to a steady-state value of 0.77 (α) during water-lubricated sliding [103]. These calculations also support the view that the water lubricant film supports the load more effectively as the metal counterface becomes smoother with transferred polymer. In deriving the values of α' and α, it was assumed that τ_o and P_o are not significantly affected by the water penetrating the surface during the sliding wear process. In particular, if it is assumed that τ_o is reduced to τ and P_o to P, it is not expected that the ratio τ/P will be very different from τ_o/P_o as τ and P are interrelated strength properties [104].

6.3.3.2 The role of stable transfer films under water lubrication

It is evident that the stability of polyethylene transfer films on the metal counterface under water lubrication plays a role in determining the wear behaviour of UHMWPE. Optical and scanning electron microscopy shows that stable transfer films are found under both dry and water-lubricated conditions. The stable transfer films found in the water-lubricated reciprocating sliding wear tests can be attributed primarily to mechanical interlocking of polymeric material on the relatively rough counterfaces of 0.3 μm R_a surface roughness. Several authors, however, reported higher wear rates for UHMWPE in distilled water than in dry sliding conditions [116,139,182]. Tetreault *et al.*, for example, reported wear rates for UHMWPE on very smooth counterfaces (0.05 - 0.09 μm R_a) to be significantly higher than those found in dry conditions and attributed this to a smoother morphology of the transferred material in the dry wear tests [182]. They also reported that the polyethylene adhered more easily to the counterface in dry conditions than under water lubrication. According to these studies, the friction of UHMWPE sliding against steel surfaces decreases under boundary lubrication while the wear rates increase. In our studies, however, both the friction and wear rates decrease in distilled water.

6.3.3.3 The influence of temperature increases at the sliding interface

As a result of the low thermal conductivity of the UHMWPE, a high temperature rise at the interface, due to the frictional heating process, can significantly affect the properties and hence the mode of material removal from the polymer wear surface. Temperature readings of the order of 60 °C were recorded by using a thermocouple placed below the metal wearing surface. DSC results indicate that the UHMWPE starts to melt at about 115 °C and, although there is evidence that these temperatures are attained during dry sliding, the dry steady-state friction coefficients are not significantly higher than those measured in distilled water (figure 6.5). This is be partly due to the fact that the "molten" surface layer is virtually solid as a result of the material's high viscosity. As a result, penetration of metal asperities into less viscous polymers would lead to lower friction coefficients.

The *pv* limit for UHMWPE under dry sliding is normally quoted to lie between 0.1 and 0.4 MPa.m.s^{-1} and the *pv* value of 1.25 MPa.ms.$^{-1}$ used in the dry tests, is thus well above the recommended *pv* limit for UHMWPE [80,99]. Tanaka *et al.* also attributed the high wear rate found for HDPE, using a similar *pv* of 1.41 MPa.m.s^{-1}, to melting of the polymer

surface by frictional heating. They measured a molten layer of approximately 7 μm in the HDPE pin and found the layer to be devoid of the polymer's spherulitic structure [135]. Scanning electron microscopy showed features indicative of localized softening of the UHMWPE. Relatively large portions of the viscous polymer are plucked from the polymer wearing surface and the polymeric material is smeared in the direction of sliding (see figure 5.71). This evidence support the views of Barret *et al.* that, at temperatures approaching the melting point of UHMWPE, the wear mode is a non-linear discontinuous progression by discrete steps [183]. Their wear measurements were made by LVDT and it would appear that the same mechanism of chunks of polymer being intermittently removed, is operative in our studies. Mass loss wear measurements over large intervals, however, show an overall linear wear behaviour and cannot sense small stepped variations in the wear process.

By using a modification of Jaeger's equation for calculating the temperature rise at a single asperity contact, Lancaster derived an equation to calculate the flash temperature for the case of a polymer sliding against steel. By substituting the appropriate variables, a simplification leads to the equation:[84]

$$\theta = 2.86 \times 10^{-2} \mu_d P_m^{0.5} W^{0.5} v \qquad (6.3)$$

where

θ = the flash temperature
μ_d = the dry friction coefficient
W = the normal load
v = the sliding velocity
P_m = the indentation hardness

The flash temperature is calculated to be approximately 85 °C, and a total surface temperature of 145 °C is obtained by adding the measured subsurface temperature to the calculated flash temperature. Factors which lead to an overestimation of the temperature include:

(i) An assumption that the load was supported on a single plastically deformed asperity contact. In practice there is more than one contact and hence the real area of contact will be greater. The real contact area will also be greater for a partially elastic contact.

(ii) Another source of error in the calculation of the flash temperature is that the hardness was assumed to be independent of temperature. Lancaster showed that the hardness decreases almost exponentially with temperature and thus the contact area would increase with temperature [117].

The above calculations therefore confirm that temperatures close to the melting point of the UHMWPE are reached in dry sliding wear under the imposed operating conditions. Wear debris and transfer films, however, lower the ability of the counterface to conduct heat away from the sliding interface and this leads to an underestimation of the flash temperature.

6.3.4 The Effect of Bearing Pressure

The volumetric polymer loss for both the filled and unfilled UHMWPE were found to decrease with a decrease in nominal pressure under water-lubricated environments. The reason for this behaviour is believed to be due to the water film supporting the load more effectively at the lower pressures. By taking the load into account, however, the specific wear rate for the UHMWPE was found to decrease by between 1.5 and 6 times when the pressure is increased from 5 to 10 MPa (see tables 5.1 and 5.5). The decrease in friction is expected as the deformation is partly elastic and for an elastic contact, the real area of contact $A_r \propto W^n$ where $n < 1$. Thus the friction coefficient μ, is proportional to W^{-n}.

6.4 AN ANALYSIS OF THE WORN UHMWPE MATERIAL

6.4.1 The Worn Polymer Pin Surface

XRD data has shown that the crystallinity of the worn polymer pin surface is increased slightly owing to increased structural alignment of the molecules as a result of the deformation process at the sliding interface. Polarized optical microscopy studies have also indicated that orientation of the polymer molecules in the surface has become parallel to the sliding direction. This orientation of the polymer molecules allows for the easy shearing of thin films from the surface layers of the worn pins. The sizes of the crystallites in the worn and unworn polymer surfaces are very similar. However, the sizes of the crystallites in the worn debris are reduced drastically from 16 to 8 nm (table 5.4). It can

therefore be deduced that the crystallites in the surface layers of the polymer may be reduced substantially, but was not possible to detect by XRD. Krimm and Tobolsky also noted that the crystallite sizes in polyethylene are reduced from about 14 to 5.9 nm when the material is stretched to 500% and attributed this to the crystallites being torn apart in the process of achieving these high elongations [35]. Although these tensile tests were conducted under low strain rates and the strain rates encountered in the wear tests are much higher, large elongations are expected in the transferred material.

6.4.2 The Debris and Transfer Film

The debris analyzed in this work was found to be significantly more crystalline, approximately 31%, than the original bulk polymer (table 5.4). The DSC results show that when the pin is slid perpendicular to the to the ground surface, the crystallinity of the initial debris increases quite sharply to a value of approximately 75% during the early stages of the sliding wear process. The crystallinity of the debris appears to reach an equilibrium of approximately 75%. Since the crystallites are broken down during the wear process, the high enthalpy value obtained by DSC seems to have arisen from an increased structural alignment of the molecules. A concurrent alignment in the transfer film seems to be responsible for the high adhesion to the metal counterface because of the increase in the number of van der Waals secondary bonding.

When the polymer pin is worn perpendicular to the ground surface, the polymer is accommodated more easily in the valleys and is deformed more easily. This also suggests that during the build-up of the transfer layer, substantial deformation takes place which leads to significant orientation of the polymer molecules. This increase in crystallinity is aided by the structural breakdown of the polymer as indicated from the results of the mass spectra. The original "semi-spherulitic" structure of the UHMWPE is destroyed giving rise to highly oriented transfer films.

When the pin is slid in a direction parallel to the ground surface, most of the initial material cannot be accommodated in the valleys of the asperities on the metal surface and is lost as debris. It is interesting to note that the crystallinity of the wear debris collected when sliding parallel to the grinding marks is less crystalline that of debris formed from studies conducted on wear pins perpendicular to the grinding marks of the counterface. Clearly such debris is not subjected to the same intensity of deformation since it is removed

from the sliding interface much sooner. As the build-up of larger patchy films continue on these counterfaces, the "retention time" of loose polymer at the interface increases and the debris increases in crystallinity. Thus, the appearance and crystallinity of the debris by DSC gives an indication of the degree of deformation suffered by the wear particles.

From the above results, the following assertions can be made when sliding is conducted perpendicular to the ground surface:

(i) The polymer that is lost from the wear surface is more crystalline than the bulk polymer when it is transferred to the metal counterface and increases in crystallinity during continued sliding. It is assumed that the increase in crystallinity of the debris reflects this change.

(ii) The polymer lost as debris probably consists of a mixture of some polymer lost from the pin surface, as well as the major contribution from polymer that has been in the contact area for some time.

Komoto *et al.* used electron diffraction patterns obtained from carbon replicas for HDPE transfer films to show that the molecular chains (the crystallographic c-axis) of HDPE were highly oriented along the sliding direction [184]. They postulated that wear in water for this polymer takes place along the crystallographic a-c plane. It is envisaged that the same mechanism would apply for UHMWPE, but this would have to be clarified by TEM.

6.5 THE FRICTION AND WEAR BEHAVIOUR OF PTFE

The friction and wear behaviour of PTFE is also controlled by the adhesion of polymeric transfer films formed onto the metal counterface. The filled PTFE grades showed a higher wear resistance than the unfilled PTFE under both dry and water-lubricated environments (figure 6.6a).

Water lubrication was found to be detrimental to the stability of transfer PTFE films on the metal substrates. This behaviour was different to that of the UHMWPE which showed stable transfer films under water lubrication and much lower wear rates (figure 6.6a). Water does not wet the surface of PTFE and the highly polar water molecules effectively prevent the formation of a transfer film onto the metal substrate. The wear rates were also

found to be independent of pressure in water-lubricated environments. Again, it would appear that, because water does not wet the surface, any lowering in pressure does not significantly affect the wear rate as found in the case of UHMWPE. Relatively large sheets of polymeric films, which do not adhere to the metal counterface, move freely at the interface where they are subsequently broken down in the contact zone before being expelled as wear debris.

Fillers inhibit the formation of these large sheets and mechanically assist in breaking down the material into small wear fragments. In this regard, smaller wear fragments are formed from bronze filled PTFE. Fragments that do become attached to the metal counterface are, however, only weakly adhered in water-lubricated environments and are easily removed as wear debris. It would appear that high pressures created at the contact points of the fillers with these particles create the opportunity for localized "welding" of fragmented films onto the metal counterface. Briscoe and Steward contend that abrasive fillers act as stress intensifiers in the contact region, thus allowing suitable mechanical and chemical interactions between the transfer film and the counterface to take place, which support this view [143].

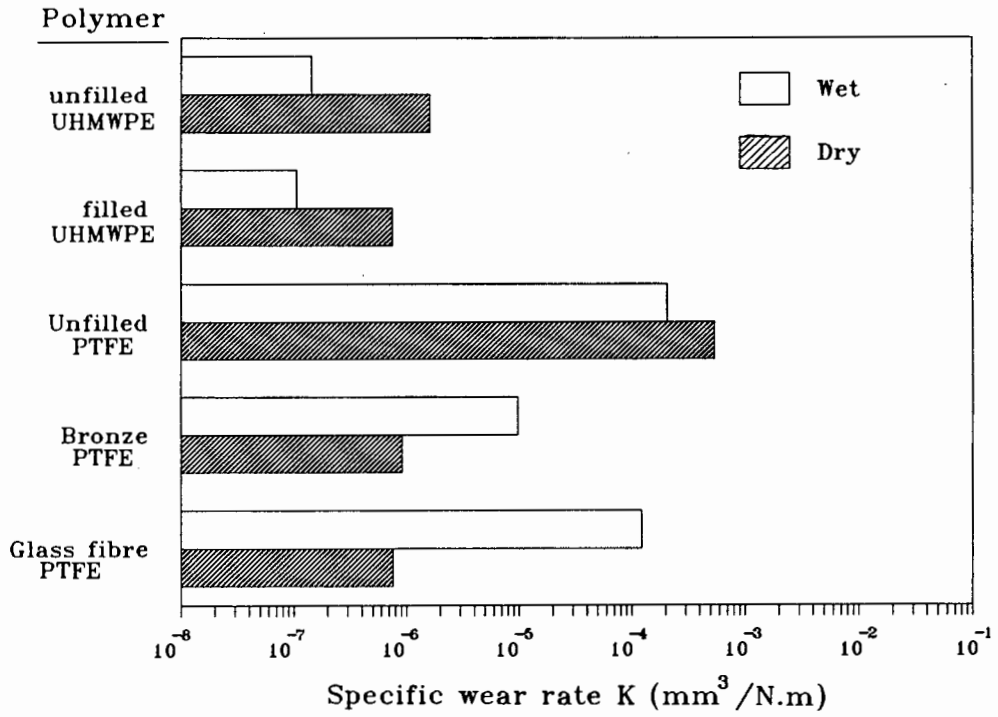

Figure 6.6a: A summary of the dry and water-lubricated wear rates of UHMWPE and PTFE. Pressure: 5 MPa; velocity: 0.25 $m.s^{-1}$.

Discussion: page 182

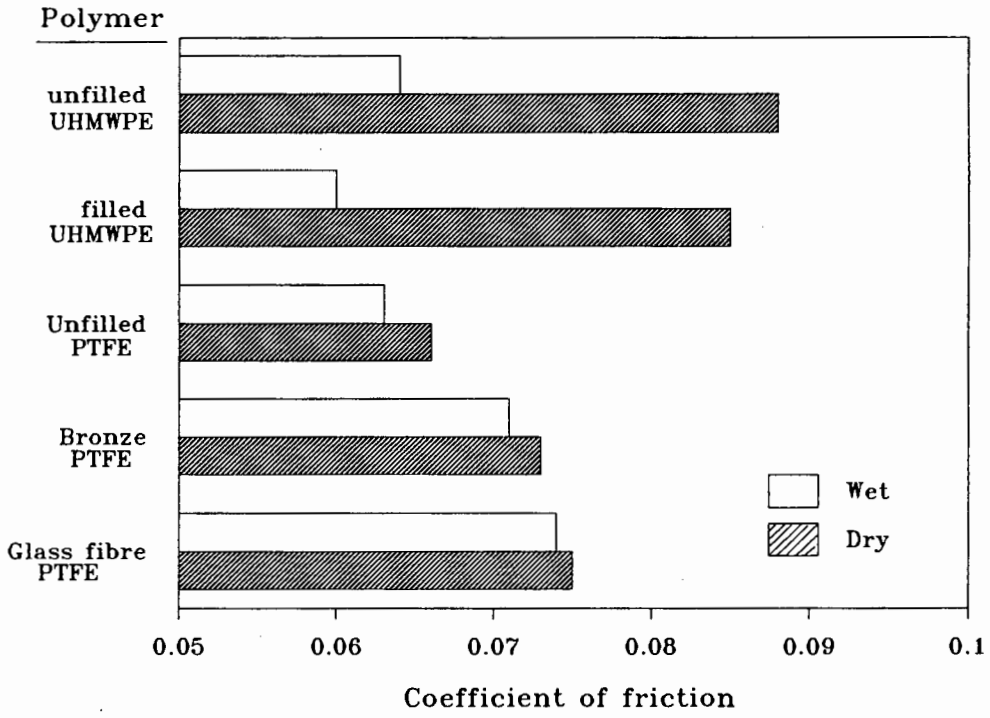

Figure 6.6b: The dry and water-lubricated friction coefficients for UHMWPE and PTFE. Pressure: 5 MPa; velocity: 0.25 $m.s^{-1}$.

The wear rate of unfilled PTFE under dry reciprocating sliding is about three times higher than that found under water lubrication. This can be attributed to the fact that the weakly bonded transfer film is easily peeled off the counterface, leading to a continuing loss of material. These polymer sheets were shown to be less crystalline than the powdery debris material found in water-lubricated tests. By using XRD on the worn PTFE surface and wear debris, it has been postulated that crystallites in the surface layers of the wear pin grow in size before being detached as a sheet of wear debris [185-187]. It is therefore proposed that the same mechanism prevails in this investigation, as sheets of debris of the order of about 1 μm thick are considered to be composed of up to fifty 20 μm thick crystalline sheets.

No direct correlation between friction and wear could be found for PTFE. Although the coefficients of friction for unfilled PTFE was lower than that for filled PTFE, the wear rate of the filled grades were approximately three orders of magnitude lower than the unfilled grade under dry sliding wear (figures 6.6a and 6.6b). The lower wear rates for filled PTFE can be attributed to the formation of coherent transfer films on the counterface surface.

The fillers break down the polymer film into small fragments which are subsequently worked into the valleys of the asperities.

Although different wear mechanisms are operative, the wear rates for the filled PTFE are very similar to those obtained for filled UHMWPE under dry reciprocating sliding wear (figure 6.6a). The friction coefficients for filled PTFE are, however, slightly lower. At these operating conditions, the UHMWPE already starts to melt and it would therefore be preferable to use filled PTFE if more severe conditions of velocity or pressure are imposed on the system.

Blanchet and Kennedy also showed that similar reductions in wear rates, due to the incorporation of glass fibre and bronze fillers into the PTFE, can be obtained under dry oscillating sliding, as shown in this study [179,188]. Their tests were carried out under similar conditions of velocity and load but with very smooth steel counterfaces of 0.02 μm R_a surface roughnesses where adhesive wear is expected to predominate throughout the test. It is interesting to note that these authors also noted that the fillers reduce the wear rate by preventing the formation of large wear sheets. It would seem that the transferred material formed on these smooth counterfaces, forms patchy layers rather than a more evenly distribution of polymeric material as observed on the rougher surfaces of 0.3 μm R_a in our investigations.

Tanaka *et al.* showed that similar reductions in wear rate are obtained in dry pin-on-disk experiments when glass fibres and bronze fillers are added to the PTFE matrix [177,189]. They propose that the wear reducing action of fillers on very smooth steel surfaces ($\approx$ 0.03 μm R_a), is related to the fillers preventing the destruction of the polymer's banded morphology. Yamada and Tanaka then proceeded to study the effect of fillers under water lubrication using speeds and pressures of 0.01 $m.s^{-1}$ and 1.4 MPa, respectively [190]. They found that wear rates of certain PTFE composites were much higher than that obtained under dry conditions, a result which was exactly the opposite to that found from testing in our sliding configuration. On the other hand their glass fibre filled- and bronze filled composites showed similar reductions in wear, under both dry and water-lubricated environments, to our studies.

6.6 OVERVIEW

It is evident that a knowledge of the transfer and wear process can by no means be treated in a simplistic manner. Research emphasis has mainly been focussed on PTFE and HDPE systems, but more recently UHMWPE has emerged as the front runner in the South African mining and metallurgical industries where sliding wear applications are concerned. The exceptionally low wear of polymers like UHMWPE is controlled by a transfer film that is highly adherent on relatively rough counterfaces, even under water lubrication. It is also evident that the chemistry of the polymer, its mechanical properties as well as that of the base metal can be correlated to that of the transfer phenomenon.

The transfer behaviour and hence the frictional properties of the "smooth molecular profile" polymers is determined by the peculiarities in their molecular structure. The differences in the transfer and wear behaviour within the polyethylenes may well be found in polymer properties such as density, chain length, crystallinity and the number of side branches. This work has found, however, that the counterface preparation plays a more important role than chain length within the UHMWPE in determining wear rates. The fact that large elongations can be achieved by the UHMWPE enables the transfer films to be easily deformed and mechanically interlocked with asperity valleys of the counterface.

CHAPTER 7

CONCLUSIONS

The work carried out during the course of this thesis has lead to a substantial contribution to our understanding of the water-lubricated sliding wear of UHMWPE against hardened stainless steel counterfaces. In particular, the following conclusions are noteworthy:

Wear Mechanisms and Transfer Film Morphology

1) Abrasive and adhesive wear were found to be the principal operative wear mechanisms under water-lubricated reciprocating sliding wear on relatively rough counterfaces of 0.3 μm R_a surface roughness. Although some material is initially removed by a microploughing and microcutting wear mechanism, adhesive wear was prominent throughout the wear test. The thin films that are laid down on the metal counterface arise from a shear process on the polymer pin surface. As the thin films of polymeric material are plastically deformed into the asperity valleys, adhesive wear continues by the shearing of material from the wear pins. Some load support by a thin water film between the two relatively smooth wearing surfaces leads to a reduction in friction coefficient and wear rate.

2) On very smooth counterfaces ($\approx$ 0.03 μm R_a), adhesive wear predominates throughout the test. The inorganically filled UHMWPE showed the highest wear rates and transfer for this material occurred in the form of lumpy polymer patches.

3) Polymer molecules that are aligned in the sliding direction in the surface layers of the wearing pins aid the shearing process. The transfer films are highly adherent to the relatively rough metal counterfaces. The transfer film formed during the reciprocating sliding wear process was also shown to be oriented in the sliding direction.

4) The wear debris of the UHMWPE is significantly more crystalline than the bulk polymer. The degree of crystallinity of the debris is determined by the amount of deformation suffered by the transferred material during the transfer process.

The Effect of Fillers and Molecular Weight on Wear Rates

5) The wear rates of UHMWPE are reduced when a proprietary non-abrasive inorganic filler is incorporated into the polymer matrix. The transferred polymer mechanically interlocks with the metal counterface and the titanium in the filler increases the adhesion of the transfer film to the metal substrate through chemical bonding.

6) The glass bead filled UHMWPE exhibited low wear rates provided polishing of the metal counterface did not take place.

7) An increase in molecular weight of the UHMWPE did not show a marked improvement in wear rates. Small changes in counterface roughness, R_a, were found to have a bigger influence on the wear rate.

The Effect of Counterface Roughness

8) Counterface roughness, in addition to aiding the formation of a transfer film, plays a role in determining wear rates.

9) The formation of a uniform stable transfer film of UHMWPE is influenced by the grinding direction on the stainless steel counterface. When sliding is conducted parallel to the grinding direction only patchy films are observed. The relatively low wear rates obtained initially on these counterfaces are attributed primarily to the lower value of R_a in the direction of sliding. Over longer sliding distances high wear rates are obtained.

10) Non-abrasive fillers are sensitive to a change in surface roughness R_a and polymer transfer to smooth polished counterfaces was patchy and resembled that observed for "normal" polymers such as LDPE, and showed relatively high wear rates. The type of counterface preparation is important for these materials, as mechanical interlocking

with the metal substrate aids the adhesion of the transfer film.

11) The unfilled and glass bead filled UHMWPE are less sensitive to R_a provided that polishing of the surface does not take place which results in much increased wear.

Dry Sliding Wear of UHMWPE

12) The dry sliding wear behaviour of UHMWPE is dominated by temperature effects and wear rates were approximately an order of magnitude higher than those obtained in water-lubricated environments.

13) Dry pin-on-disk tests under similar operating conditions as those in reciprocating tests, shows lower wear rates than the latter and may be attributed to better heat dissipation in the pin-on-disk configuration.

The Wear Behaviour of PTFE

14) Unfilled PTFE shows very high wear rates, compared to the UHMWPE, under both dry and water-lubricated environments. When fillers are incorporated into the matrix, the dry wear rates were shown to drop by up to three orders of magnitude. The fillers appear to effectively break down large transferred wear sheets into small fragments which are subsequently mechanically worked into the valleys on relatively rough (0.3 μm R_a) metal counterfaces.

15) The wear rates for filled PTFE showed similar wear rates to filled UHMWPE under dry sliding conditions, but are not adversely affected by the high surface temperatures generated under the imposed testing conditions.

RECOMMENDATIONS FOR FUTURE WORK

The present work served to enhance our understanding of the wear mechanisms occurring during the water-lubricated reciprocating sliding wear of UHMWPE on a stainless steel counterface. Future research in this field should include the following studies:

i) A detailed study of the wear-reducing action of fillers incorporated into the UHMWPE. In this regard a variety of inorganic and organic fillers at different percentage levels can be added to the UHMWPE. We already know that mechanical interlocking aids the adhesion of the transfer film to the metal counterface. The study should therefore ideally include the combined effect of counterface roughness with these fillers on the friction and wear behaviour of the UHMWPE.

ii) Single traversals should be run over a much bigger range of counterface roughness, R_a. It would also be interesting to study the effect of counterface topographical parameters such as the slopes and radii of curvature of the metal asperities during the bedding-in wear regime.

iii) We have explored the possibility of using the transmission electron microscope to obtain diffraction patterns of thin polymeric transfer films of the UHMWPE. A detailed study on in this aspect seems seems feasible.

REFERENCES

1. Wagner H. and Joughin N.C., *"The use of research in management"*, **J. South African Inst. Mining and Metallurgy**, Vol. 89, No. 11, pp. 333-340.

2. COMRO Information leaflet, No. 12, **Hydro-Power**, Nov. 1986.

3. Thomas R.H., *"Sliding and Wear Characteristics of Plastics in the Mineral Processing Industry"*, Solidur Plastics.

4. Lloyd A.I.G., **The Sliding Wear of UHMWPE Against Stainless Steel**, MSc Thesis, University of Cape Town, 1986.

5. Flory P.J. and Yoon D.Y., *"Molecular Morphology in Semicrystalline Polymers"*, **Nature**, Vol. 272, 16 March, 1978.

6. Moore G.R. and Kline D.E., **Properties and Processing of Polymers for Engineers**, Soc. Plastic Engnrs. Inc., Prentice Hall, London, 1984.

7. McCrum N.G., Buckley C.P. and Bucknall C.B., **Principles of Polymer Engineering**, Oxford Sci. Publ., 1988.

8. Meares P., **Polymers: Structure and Bulk Properties**, D. Van Nostrand Company Ltd., London, 1965.

9. Crowie J.M.G., **Polymers: Chemistry and Physics of Modern Materials,** 2nd edn., Blackie and Son Ltd., Chapman and Hall, Inc., N.Y., 1991.

10. Bunn C.W., *"The Crystal Structure of Long-Chain Normal Paraffin Hydrocarbons. The "Shape" of the >CH2 Group"*, **Trans. Faraday Soc.,** Vol. 35, 1939, pp. 482-491.

11. Alexander L.E., **X-Ray Diffraction Methods in Polymer Science,** John Wiley and Sons Inc., N.Y., 1985.

12. Makinson K.R., and Tabor D. *"The friction and transfer of polytetrafluoroethylene"*, **Proc. Roy. Soc. London**, Series A, Vol. 281, 1964, pp. 49-61.

13. Renecker D.H. and Geil P.H., *"Morphology of Polymer Single Crystals"*, **J. of Appl. Physics,** Vol. 31, No. 11, 1960, pp. 1916-1925.

14. Williams D.J., **Polymer Science and Engineering,** Prentice-Hall Inc., London, 1971.

15. Rodriguez F., **Principles of Polymer Systems,** McGraw-Hill Book Company, N.Y., 1970.

16. Rees D.V. and Basset D.C., *"The Texture of Crystalline Polymers: A Brief Review"*, **J. Mater. Sci.,** Vol. 6, 1971, pp. 1021-1035.

17. Hay J.N., *"Recent developments in polymer materials"*, **Engineering Plastics, Metals and Materials,** May 1989, pp. 275-279.

18. Solidur Pamphlet., Pty. (Ltd.) S.A.,

19. Small P.A., *"Some Factors Affecting the Solubility of Polymers"*, **J. Appl. Chemistry,** Vol. 3, 1953, pp. 71-80.

20. Evans D.G. and Lancaster J.K., *"The Wear of Polymers"*, **Treatise on Materials Science and Technology,** Scott D. (ed.), Vol. 13, Academic Press Inc., 1979, pp. 85-140.

21. Lancaster J.K., *"Introduction to Bearing Materials"*, **Non-Metallic Bearings in Engineering,** NCT Notes, 23 May 1989, pp. 1-38.

22. Bowden P.B. and Young R.J., *"Review: Deformation Mechanisms in Crystalline Polymers"*, **J. Mater. Sci.,** Vol. 9, 1974, pp. 2034-2051.

23. Peterlin A., *"Molecular Model of Drawing Polyethylene and Polypropylene"* ibid, Vol. 6, 1971, pp. 470 - 508.

24. Allan P. and Bevis P., *"Deformation processes in thin melt-cast films of high density polyethylene I: Experimental methods and deformation processes in the equatorial regions of spherulites"*, **Phil. Mag.**, Vol. 335, No. 2, 1977, pp. 405-430.

25. Idem, ibid, *"II: Deformation processes in non-equitorial regions of spherulites"*, Vol. 41, No. 4, 1980, pp. 555-572.

26. Keller A. and Pope D.P., *"Identification of Structural Processes in Deformation of Oriented Polyethylene"*, **J. Mater. Sci.**, Vol. 6, 1971, pp. 453-473.

27. Geil P.M., **Chem. Eng. News**, 1965, Vol. 16, pp. 72-83.

28. Petermann J. and Gleiter H., *"Plastic Deformation of polyethylene crystals by dislocation motion"*, **J. Mater Sci.**, Vol. 8, 1973, pp. 673-675.

29. Suehiro K., Terashima T and Takayanagi M., *"Change of mosaic block size of bulk polyethylene in drawing processes"*, **J. Mater Sci.**, Vol. 9, 1974, pp. 1563-1568.

30. Billmeyer F.W. (Jr.), **Textbook of Polymer Science**, John Wiley and Sons, 3rd edn., 1957.

31. Peterlin A., *"Structure of Drawn Polymers"*, Technical Report, AFML - TR - 67-6, U.S. Air Force Materials Lab., Wright-Patterson, AFB., Ohio, 1966

32. Zum Gahr K.H., **Microstructure and Wear of Materials**, Tribology Series, Vol. 10, Elsevier, Amsterdam, 1987.

33. Speerscheider C.J. and Li C.H., *"Some Observations on the Structure of Polytetraflouroethylene"*, **J. Appl. Phys.**, Vol. 33, No. 5, 1962, pp. 1871-1875.

34. Krimm S., *"X-Ray Studies of Crystalline and Amorphous Order in High Polymers"*, **J. Phys. Chem.**, Vol. 57, 1953, pp. 22-25.

35. Krimm S. and Tobolsky A.V., *"Quantitative X-Ray Studies of Order in Amorphous and Crystalline Polymers. Quantitative X-Ray Determination of Crystallinity in Polyethylene"*, **J. Polym. Sci.**, Vol. 7, No. 1, pp. 57-76, 1951.

36. Tobin M.C. and Carrano M.J., *"Infrared Determination of Orientation, Orientation Distribution and Crystallinity in Polyethylene Films"*, **J. of Polym. Sci.**, Vol. 14, 1957, pp. 93-104,

37. Jahanmir S., *"Future Directions in Tribology Research"*, **J. Tribology**, ASME Trans., 1987, Vol. 709, pp. 207-214.

38. Briscoe B.J., *"Fundamentals of Friction and Wear"*, Paper 2, **Non-Metallic Bearings in Engineering**, NCT Notes, 23 May 1989, pp. 1-45.

39. Briscoe B.J. and Tabor D., *"Friction and Wear of Polymers: The Role of Mechanical Properties"*, **Br. Polym. Journal**, Vol. 10, March 1978, pp. 74-78.

40. Briscoe B.J., *"Wear of Polymers: An Essay on Fundamental Aspects"*, **Trib. Int.**, Vol. 14, No. 4, August 1981, pp. 231-243.

41. Halling J. (ed.), **Principles of Tribology**, MacMillan Press Ltd., 2nd. edn., London, 1983.

42. Hondros E.D., **Tribology**, Mills and Boon Ltd., London, 1971.

43. Frees N, *"Characterizing and Solving Industrial Wear Problems"*, **Wear**, Vol. 115, 1987, pp. 193-202.

44. Quinn T.F.S., **The Application of Modern Physical Techniques to Tribology**, Butterworth and Co. Ltd., 1971.

45. Tabor D., *"Friction - The Present State of Our Understanding"*, **J. of Lub. Tech.**, ASME Trans., 1981, Vol. 103, pp. 169-179.

46. Bowden F.P. and Tabor D, **The Friction and Lubrication of Solids**, Part II: Oxford University Press, 1964.

47. Halling J., **Introduction to Tribology**, Wykenham Publ., London, 1976.

48. Greenwood J.A. and Williamson J.B.P., *"Contact of Nominally Flat Surfaces"*, **Proc. R. Soc. London**, Vol. A 295, 1966, pp. 300-319.

49. Tabor D., *"Friction and Wear - developments over the last fifty years"*, **Tribology - Friction and Lubrication and Wear Fifty Years on**, Proc. IMechE, Vol. 1, 1987, pp. 157-172.

50. Czichos H., *"Introduction to Friction and Wear"*, in **Friction and Wear of Polymer Composites**, K. Friedrich (ed.), Ch. 1, Vol. 1, Composite Materials Series, Amsterdam, Elsevier, 1986, pp. 1-23.

51. Timoshenko S. and Goodier J.N., **Theory of Elasticity**, McGraw-Hill inc., 3rd. edn., N.Y, 1970.

52. Archard J.F., *"Elastic deformation and the laws of friction"*, **Proc. R. Soc. London**, No. 1233, Series A, Vol. 243, 1957, pp. 190-205.

53. Briscoe B.J. and Tweedale P.J., *"A View of Polymer Composite Tribology"*, **Tribology of Composite Materials**, ASM Int. Conf. Proc., Rohatgi P.K., Blau P.J. and Yust C.S. (eds.), 1990, pp. 15-23.

54. Briscoe B.J., *"Interfacial Friction of Polymer Composites, General Fundamental Principles"*, in **Friction and Wear of Polymer Composites**, Friedrich K. (ed.), Vol. 1, Ch. 2, Composite Materials Series, Vol. 1, Amsterdam, Elsevier, 1986, pp. 25-59.

55. Pooley C.M. and Tabor D., *"Friction and Molecular Structure : The behaviour of some thermoplastics"*, **Proc. R. Soc. London**, Series A, Vol. 329, 1972, pp. 251-274.

56. Makinson K.R. and Tabor D., *"The Friction and transfer of polytetrafluoroethylene"*, **Proc. R. Soc. London**, Series A, Vol. 281, 1964, pp. 49-61.

57. Briscoe B.J., Scruton B. and Willis F.R., *"The Shear Strength of Thin Lubricant Films"*, **Proc. R. Soc. London**, Series A, Vol. 333, 1973, pp. 99-114.

58. Briscoe B.J. and Tabor D., *"Shear Properties of Thin Polymeric Films"*, **J. Adhesion**, Vol. 9, 1978, pp. 145-155.

59. Amuzu J.K.A., Briscoe B.J. and Chaudri M.M., *"Frictional Properties of Explosives"*, **J. Physics, D : Appl. Phys.**, Vol. 9, 1976, pp. 133-143.

60. Amuzu J.K.A., Briscoe B.J. and Tabor D., *"Polymers as Bearings and Lubricants : Aspects of Fundamental Research"*, **Advances in Tribology**, Proc. IMechE, 1978, pp. 59-62.

61. Summers-Smith D, **An Introduction to Tribology in Industry**, The Machinery Publishing Co. Ltd., London, 1969.

62. Pascoe M.W. and Tabor D., *"Friction and deformation of polymers"*, **Proc. R. Soc. London**, Series A, Vol. 235, 1956, pp. 210-224.

63. Tabor D, *"Friction, Adhesion and Boundary Lubrication of Polymers"*, in **Advances in Polymer Friction and Wear**, Lee L.H. (ed.), Polymer Science and Technology Symposium Series, Plenum Press, N.Y., Vol. 5A, 1974, pp. 5-28.

64. Eiss N.S. (Jr.) and Milloy S.C., *"The Effect of Asperity Curvature on Polymer Wear"*, in **Proc. Conf. Wear of Materials**, Ludema K.C. (ed.), ASME Trans., N.Y., 1983, pp. 650-656.

65. Sin H.C., Saka N. and Suh N.P., **Wear**, Vol. 55, 1979, p. 163.

66. Buckley D.H., **Surface Effects in Adhesion, Friction, Wear and Lubrication**, Tribology Series 5, Elsevier, N.Y., 1981.

67. O.E.C.D (Organization for Economic Co-operation and Development), *"Friction, Lubrication, Wear Terms and Definitions"*, **Research Group on the Wear of Engineering Materials**, Paris, 1968.

68. Misra A. and Finnie I., *"An Experimental Study of 3-Body Abrasive Wear"*, **Wear**, Vol. 85, pp. 57-68.

69. Lancaster J.K., *"Abrasive Wear of Polymers"*, **Wear**, Vol. 14, 1969, pp. 223-239.

70. Rowe C.N., *"Lubricated Wear"*, **Wear Control Handbook**, pp. 143-146.

71. Lancaster J.K., *"Friction and Wear"*, in **Polymer Science**, Jenkins A.D. (ed.), A Materials Science Handbook, Ch. 14, North-Holland Publ. Co., Elsevier, N.Y., 1972.

72. Ratner S.B., Farberova I.I., Radyukevich O.V. and Lure E.G., *"Connection between the wear resistance of plastics and other mechanical properties"*, **Soviet Plastics**, 1964, Vol. 7, pp. 37-45.

73. Giltrow J.P., *"A Relationship Between Abrasive Wear and the Cohesive Energy of Materials"*, **Wear**, Vol. 15, 1970, pp. 71-78.

74. Hollander A.E. and Lancaster J.K., *"An Application of Topographical Analysis to the Wear of Polymers"*, **Wear**, Vol. 25, No. 2, 1973, pp. 155-170.

75. Tabor D., *"A Simplified Account of Surface Topography and Contact Between Solids"*, **Wear**, Vol. 32, 1975, pp. 269-271.

76. Rabinowicz E., *"The Wear Coefficient - Magnitude, Scatter, Uses"*, **J. Lub. Tech.**, ASME Trans., Vol. 103, 1981, pp. 188-194.

77. Belyi V.A., Sviridyonok A.I., Smurugov V.A. and Nevzorov V.V., *"Adhesive Wear of Polymers"*, **J. Lub. Tech.**, ASME Trans., Vol. 99, 1977, pp. 396-400.

78. Tabor D., *"The wear of non-metallic materials: a brief review"* in **The Wear of Non-Metallic Materials**, Proc. 3rd Leeds-Lyon Symposium on Tribology, Dowson D., Godet M. and Taylor C.M. (eds.), 1976, London, MEP, Paper 1, pp. 3-8.

79. Brown K.J., Atkinson J.R., Dowson D. and Wright V., *"The wear of UHMWPE and a preliminary study of its relation to the in vivo behaviour of replacement hip joints"*, **Wear**, Vol. 40, 1976, pp. 255-264.

80. Atkinson J.R., Brown K.J. and Dowson D. *"The Wear of High Molecular Weight Polyethylene, Part 1: The Wear of Isotropic Polyethylene against Dry Stainless Steel in Undirectional Motion"*, **J. Lub. Tech.**, ASME Trans., Vol. 100, 1978, pp. 208-218.

81. Ratner S.B. and Lure E.G., **Abrasion of Rubber**, D.I James (ed), MacLaren and Sons Ltd., London., 1967 pp. 155 .

82. Schaper H., Engel G.L., Klingele H. and Ehrenstein G.W. (eds.), **An Atlas of Polymer Damage**, Wolfe Publ. Ltd, 1981.

83. Anderson J.C., *"High density and ultra-high molecular weight polyethenes: their wear properties and bearing applications"*, **Trib. Int.**, Vol. 15, No. 1, 1982, pp. 43-47.

84. Shen C. and Dumbleton J.H., *"The Friction and Wear Behaviour of Irradiated Very High Molecular Weight Polyethylene"*, **Wear**, Vol. 30, 1974, pp. 349-364.

85. Rose R. M., Cimino W.R., Ellis E. and Grugnola A.N., *"Exploratory Investigation on the Structure Dependence of the Wear Resistance of Polyethylene"*, **Wear**, Vol. 77, 1982, pp. 89-104.

86. Jones W.R. (Jr.), Hady W.F. and Grugnola A.N., *"Effect of γ-Irradiation on the Friction and Wear of Ultrahigh Molecular Weight Polyethylene"*, **Wear**, Vol. 70, 1981, pp. 77-92.

87. Briscoe B.J. and Zhilong N.I., *"The Friction and Wear of γ-Irradiated Polytetrafluoroethylene"*, **Wear**, Vol. 100, 1984, pp. 221-242

88. Brown K.J., Atkinson J.R. and Dowson D., *"The Wear of High Molecular Weight Polyethylene - Part II: The Effects of Reciprocating Motion, Orientation in the Polyethylene, and a Preliminary Study of the Wear of Polyethylene Against Itself"*, **J. Lub. Tech.**, ASME Trans., 1982, Vol. 104, pp. 17-22

89. Wineman A., *"Mechanical Response of Linear Viscoelastic Solids"*, M.R.S. Bulletin, May 1991, pp. 19-23.

90. McLaren K.G. and Tabor D., *"Visco-elastic Properties and the Friction of Solids. Friction of Polymers: Influence of Speed and Temperature"*, **Nature**, Vol. 197, 1963, pp. 856-858.

91. Grosch K.A., *"The relation between the friction and visco-elastic properties of rubber"*, **Proc. Roy. Soc. London**, Series A, Vol. 274, 1963, pp. 21-27.

92. Ludema K.C. and Tabor D., *"The Friction and Visco-elastic Properties of Polymeric Solids"*, **Wear**, Vol. 9, 1966, pp. 329-348.

93. Lancaster J.K., *"Relationships Between the Wear of Polymers and their Mechanical Properties"*, **Tribology Convention**, Proc. IMechE, Paper 12, Vol. 183, Part 3P, 1968-1969, London, pp. 98-106.

94. Czichos H., **Tribology: a systems approach to the science and technology of friction, lubrication and wear**, Vol. 1, Elsevier, Amsterdam, 1978.

95. Tabor D., *"The Role of Surface and Intermolecular Forces in Thin Film Lubrication"*, **Microscopic Aspects of Adhesion and Lubrication**, Georges J.M. (ed.), Amsterdam, Elsevier, Tribology Series, Vol. 7, 1982, pp. 651-679.

96. **Lubrication Theory and its Application**, BP Trading Ltd., London, 1969.

97. Davies C.B., *"A Review of Boundary Lubrication"*, **Wear**, Vol. 1, 1957/8, pp. 244-253.

98. Kapsa Ph. and Martin J.M., *"Boundary lubricant films: a review"*, **Trib. Int.**, Vol. 15, No. 1, 1982.

99. Clauss F.J., **Solid Lubricants and Self-Lubricating Solids**, Academic Press Inc., N.Y., 1972.

100. Sviridyonok A.I., *"Self-lubrication mechanisms in polymer composites"*, **Trib. Int.**, 1991, Vol. 24, No. 1, pp. 37-42.

101. Lancaster J.K., *"Transfer Lubrication for High Temperatures: A Review"* **J. of Trib.**, 1985, Vol. 107, pp. 437-443.

102. Evans D.C., *"Polymer-fluid interactions in relation to wear"*, in **The Wear of Non-Metallic Materials**, Paper III, Proc. of the 3rd Leeds-Lyon Symp. on Tribology, Dowson D, Godet M., Taylor C.M. (eds.), 1976, MEP, pp. 47-55.

103. Tanaka K., *"Friction and Wear of Semicrystalline Polymers Sliding Against Steel Under Water Lubrication"*, **J. Lub. Tech.**, ASME Trans., Vol. 102, 1980, pp. 526-533.

104. Rubenstein C., *"Lubrication of Polymers"*, **J. Appl. Phys.**, Vol. 32, No. 8, 1961, pp. 1445-1450.

105. Fort T. (Jr.), *"Adsorption and Boundary Friction on Polymer Surfaces"*, **J. Phys. Chemistry**, Vol. 66, No. 5, 1962, pp. 1136-1143.

106. Cohen S.C. and Tabor D., *"The Friction and Lubrication of Polymers"*, **Proc. Roy. Soc. London**, Series A, Vol. 291, No. 1425, 1966, pp. 186-207.

107. Senior J.M. and West G.H., *"Interaction Between Lubricants and Plastic Bearing Surfaces"*, **Wear**, Vol. 18, 1971, pp. 311-323.

108. Lagally P. and Nagy R., *"Steric Factors Affecting Friction and Wear of Polyalkenes"*, **ASLE Trans.**, Vol. 14, No. 1, 1971, pp. 12-22.

109. Pascoe M.W., Ph.D dissertation, Cambridge, England, 1954, in ref 105.

110. Anderson J.C., *"Wear of commercially available plastic materials"*, **Trib. Int.**, Vol. 15, No. 5, 1982, pp. 255-263.

111. Anderson J.C. and Robbins E.J., *"The Role of Wear Debris in the Wear of Some Polymer Composites at High Loads"*, in **Proc. Conf. Wear of Materials**, Ludema K.C. (ed.), ASME Trans., N.Y, 1981, pp. 539-543.

112. Dowson D., Atkinson J.R. and Brown K., *"The Wear of High Molecular Weight Polyethylene with Particular Reference to its Use in Artificial Joints"*, in **Advances in Polymer Friction and Wear**, Lee L.H. (ed.), Polymer Science and Technology Symposium Series, Vol. 5B, Plenum Press, N.Y, 1974, pp. 533-551.

113. Challen J.M. and Dowson D., *"The calculation of interfacial temperatures in a pin-on-disc machine"*, in **The Wear of Non-Metallic Materials**, Proc. 3rd Leeds-Lyon Symp. on Tribology, Dowson D., Godet M. and Taylor C.M. (eds.), Paper (iv), MEP, London, 1976, pp. 87-93.

114. Faber K., Atkinson J.R. and Dowson D., *"Wear Mechanisms of Nylon 66"*, **The Wear of Non-Metallic Materials**, Proc. 3rd Leeds-Lyon Symposium on Tribology, Dowson D., Godet M. and Taylor C.M. (eds.), MEP, London, 1976, pp. 25-31.

115. Dumbleton J.H. and Shen C., *"The Wear Behaviour of Ultrahigh Molecular Weight Polyethylene"*, **Wear**, Vol. 37, 1976, pp. 279-289.

116. Anderson J.C., *"The Wear and Friction of Commercial Polymers and Composites"* in **Friction and Wear of Polymer Composites**, Friedrich K. (ed.), Vol. 1, Ch. 10, Composite Materials Series, Amsterdam, Elsevier, 1986, pp. 329-362.

117. Lancaster J.K., *"Estimation of the limiting PV relationships for thermoplastic bearing materials"*, **Tribology**, Vol. 4, No. 2, 1971, pp. 82-86.

118. Bely V.A., Sviridenok A.I., Petrokovets M.I. and Savkin V.G., **Friction and Wear in Polymer-Based Materials**, Pergamon Press, 1982.

119. Dickens P.M., Sullivan J.L. and Lancaster J.K., *"Speed Effects on the Dry and Lubricated Wear of Polymers"*, **Wear**, Vol. 112, 1986, pp. 273-289.

120. Bartenev G.M. and Lavrentev V.V., **Friction and Wear of Polymers**, Tribology Series 6, Lee L.H. and Ludema K.C. (eds.), Elsevier, N.Y., 1981.

121. Vaziri M., Stott F.H. and Spurr R.T., *"Studies of the Friction of Polymeric Materials"*, **Wear**, Vol. 122, 1988, pp. 313-327.

122. Watanabe M. and Yamaguchi H., *"The Friction and Wear Properties of Nylon"*, **Wear**, Vol. 110, 1986, pp. 379-388.

123. Tanaka K., Uchiyama Y. and Toyooka S., *"The Mechanism of Wear of Polytetrafluoroethylene"*, **Wear**, Vol. 23, No. 2, 1973, pp. 153-172.

124. Tanaka K. and Yamada Y., *"The Effect of Sliding Speed on Transfer and Wear of Semicrystalline Polymers Sliding Against Smooth Steel Surfaces"*, in **Proc. Conf. Wear of Materials**, Ludema K.C. (ed.), ASME Trans., 1983, pp. 617-624.

125. Jaeger J.C., *"Moving sources of heat and temperature at sliding contacts"*, **Proc. Roy. Soc. New South Wales**, Vol. 76, 1942, p 203.

126. Kar M.K. and Bahadur S., *"An Investigation of the Temperature Rise in Polymer-Metal Sliding"*, **Wear**, Vol. 82, 1982, pp. 81-92.

127. Kuhlman-Wilsdorf D., *"Temperatures at Interfacial Contact Spots: Dependence on Velocity and on Role Reversal of Two Materials in Sliding Contact"*, **J. Tribology**, ASME Trans., Vol. 109, 1987, pp. 321-329.

128. Glascott J., Stott F.H. and Wood G.C., *"Thermoelectric voltage measurements and the determination of surface flash temperatures during sliding contact"*, **Phil. Mag. A**, Vol. 152, No. 6, 1985, pp. 811-832.

129. Anderson J.C. and Robbins E.J., *"The influence of temperature generation on the wear of some polymers"*, in **The Wear of Non-Metallic Materials**, Proc. 3rd. Leeds-Lyon Symp. on Tribology, Dowson D, Godet M and Taylor C.M. (eds.), MEP, London, 1976, pp. 94-98.

130. Evans D.C. and Lancaster J.K., General discussion on papers II(i), IV(ii), (iii) and X(i), in **The Wear of Non-Metallic Materials,** Proc. Leeds-Lyon Symp. on Tribology, Dowson D., Godet M. and Taylor C.M. (eds.), MEP, London, 1976, pp. 288-290.

131. Rhee S.H. and Ludema K.C., *"Transfer Films and Severe Wear of Polymers"*, in **The Wear of Non-Metallic Materials**, Dowson D., Godet M. and Taylor C.M. (eds.), Proc. 3rd. Leeds-Lyon Symp. on Tribology, MEP, London, 1976, pp. 11-17.

132. Uetz H., Richter K. and Wiedemeyer J., *"System Temperature and Tribological Behaviour of Polymer-Metal Sliding Couples in Pin-on-Disk Model Testing"*, **Wear**, Vol. 88, 1983, pp. 103-114.

133. Evans V.R. and Kennedy F.E., *"The Effects of Temperature on Friction and Wear in Oscillatory Motion of Polyethylene Against Stainless Steel"*, **Proc. Conf. on Wear of Materials**, ASME Trans., Vol. 1, Houston, 1987, pp. 427-434.

134. Blanchet T.A. and Kennedy F.E., *"The Development of Transfer Films in Ultra-High Molecular Weight Polyethylene / Stainless Steel Oscillatory Sliding"*, **Tribology Trans.**, Vol. 32, No. 3, 1989, pp. 371-379.

135. Tanaka K. and Yamada Y, *"Effect of Counterface Roughness on the Friction and Wear of Polyethylene Under a Sliding Condition Involving Surface Melting"*, in **Proc. Conf. on Wear of Materials**, Ludema K.C. (ed.), ASME Trans., Vol. 1, Houston, 1987, pp. 407-414.

136. Eiss N.S. (Jr.), Wood K.C., Herold J.A. and Smyth K.A., *"Model for the Transfer of Polymer to Rough Hard Surfaces"*, **J. Lub. Tech.**, ASME Trans. , Vol. 101, No. 2, 1979, pp. 212-219.

137. Tanaka K and Nagai T., *"Effect of Counterface Roughness on the Friction and Wear of Polytetrafluoroethylene and Polyethylene"*, in **Proc. Conf. Wear of Materials**, Ludema K.C. (ed.), ASME Trans., 1985, pp. 394-404.

138. Dowson D., Challen J. M., Holmes K. and Atkinson J.R., *"The influence of counterface roughness on the wear rate of polyethylene"*, in **The Wear of Non-Metallic Materials**, Dowson D., Godet M and Taylor C.M. (eds.), Proc. 3rd. Leeds-Lyon Symp. on Tribology, MEP, London, 1976, Paper IV (iv), pp. 99-102.

139. Dowson D., El-Hady Diab M.M., Gillis B.J. and Atkinson J.R., *"The Influence of Counterface Topography upon the Wear of Ultra-high Molecular Weight Polyethylene under Wet or Dry Conditions"* in **Polymer Wear and its Control**, Lee L.H. (ed.), ACS Series 287, Ch. 12, 1985, pp. 171-187.

140. Czichos H., *"Influence of Adhesive and Abrasive Mechanisms on the Tribological Behaviour of Thermoplastic Polymers"*, **Wear**, Vol. 88, 1983, pp. 27-43.

141. Buckley D.H., *"Introductory Remarks - Friction and Wear of Polymeric Composites"*, in **Advances in Polymer Friction and Wear**, Lee L.H. (ed.), Polymer Science and Technology Symposium Series, Vol. 5B, Plenum Press, N.Y., 1974, pp. 601-603.

142. Giltrow J.P. and Lancaster J.K., *"The role of the counterface in the friction and wear of carbon fibre reinforced thermosetting resins"*, **Wear**, Vol. 16, 1970, pp. 359-374.

143. Briscoe B.J. and Steward M.D., *"The Effect of Carbon and Glass Fillers on the Transfer Film Behaviour of PTFE Composites"*, **Tribology 1978**, Materials Performance and Conservation, IMechE Conf. Publications, 1978, pp. 17-22.

144. Greenwood J.A. and Williamson J.B.P., *"Developments in the Theory of Surface Roughness"* in **Surface Roughness Effects in Lubrication**, Proc. 4th Leeds-Lyon Symp. on Tribology, Dowson D., Taylor C.M., Godet M. and Berthe D (eds.), MEP, London, 1977, pp. 167-177.

145. Bahadur S. and Stiglich A.J., *"The Wear of High Density Polyethylene Sliding Against Steel Surfaces"*, **Wear**, Vol. 68, 1981, pp. 85-95.

146. Jain V.K. and Bahadur S., *"Surface Topography Changes in Polymer Metal Sliding I"*, **J. Lub. Tech.**, ASME Trans., Vol. 102, 1980, pp 520-525.

147. Jain V.K. and Bahadur S., *"Surface Topography Changes in Polymer Metal Sliding II"*, **J. Lub. Tech.**, ASME Trans., Vol. 105, 1983, pp. 526-533.

148. Dowson D., Taheri S. and Wallbridge N.C., *"The Role of Counterface Imperfections in the Wear of Polyethylene"*, **Wear**, Vol. 119, 1987, pp. 277-293.

149. Friedrich K., Karger-Kocsis J. and Lu Z., *"Effects of steel counterface roughness and temperature on the friction and wear of PEEK composites under dry sliding conditions"*, **Wear**, Vol. 148, 1991, pp. 235-247.

150. Giltrow J.P. and Lancaster J.K., *"Carbon-Fibre Reinforced Polymers as Self-Lubricating Materials"*, **Tribology Convention 15-17 May 1968**, Proc. IMechE, Part 3N, Vol. 182, London, pp. 147-157.

151. Gansheimer J., *"A Review on Chemical Reactions of Solid Lubricants During Friction"*, **ASLE Trans.**, Vol. 15, No. 4, pp. 244-251.

152. Briscoe B.J., Pogosian A.K. and Tabor D., *"The Friction and Wear of High Density Polyethylene: The Action of Lead Oxide and Copper Oxide Fillers"*, **Wear**, Vol. 27, 1974, pp. 19-34.

153. Rhee S.K. and Ludema K.C., *"Mechanisms of Formation of Polymeric Transfer Films"*, **Wear**, Vol. 46, 1978, pp. 231-240.

154. Kar M.K. and Bahadur S., *"Micro-mechanism of Wear at Polymer-Metal Sliding Interface"*, **Wear**, Vol. 82, 1978, pp. 189-202.

155. Briscoe B.J. and Tabor D., *"Self-Lubricating Polymers"*, in **Polymers and Lubrication**, CNRS, International Colloquium Series, 1974, pp. 425-432.

156. Tanaka K., *"Transfer of Semi-Crystalline Polymers Sliding Against Smooth Stainless Steel Surfaces"*, in **Proc. Conf. Wear of Materials**, Rhee S.K., Ruff A.W. and Ludema K.C. (eds.), ASME Trans., N.Y., 1981, pp. 98-106.

157. Karpe S.A., *"The Frictional Behaviour of Unlubricated Polyethylene"*, **ASLE Trans.**, Vol. 25, No. 4, 1982, pp. 537-545.

158. Kar M.K. and Bahadur S., *"Estimation of Wear Particle Thickness in Polymer Metal Sliding"*, **Wear**, Vol. 63, 1980, pp. 105-112.

159. Madakson P.B., *"The Frictional Behaviour of Materials"*, **Wear**, Vol. 87, 1983, pp. 191-206.

160. Sviridenok A.I., Nevzorov V.V. and Pleskachevskii Yu M., *"On the role of friction transfer in the wear of some thermoplastics"*, **Inst. of Mechanics of Metal-Polymer Systems**, Academy of Sciences, USSR, pp. 439-443.

161. Martinella R., Giovanardi S. and Palombarini P., *"Wear of Ultrahigh Molecular Weight Polyethylene Sliding Against Surface-treated Ti6 Al 4V, AISI 316 Stainless Steel and Vitallium"*, **Wear**, Vol. 133, 1989, pp. 267-279.

162. Clarke C.G., **The Sliding Wear of Polymers Against Steel**, MSc Thesis, University of Cape Town, 1988.

163. Play D., *"Mutual Overlap Coefficient and Wear Debris Motion in Dry Oscillatory Friction and Wear Tests"*, **ASLE Trans.**, Vol. 28, No. 4, 1985, pp 527-535.

164. COMRO Information Pamphlet: **The Emulsion Hydraulic Rockdrill.**

165. R.A. Fava (ed.), **Methods of Experimental Physics, Polymers: Physical Properties,** Vol. 16, Part C, Academic Press, N.Y., 1980, p 162.

166. Hemsley D.A., **The light microscopy of synthetic polymers,** Roy. Microscopy Soc., Oxford Science Publ., 1984.

167. Campbell D. and White R.J., **Polymer Characterization: Physical Techniques,** Chapman and Hall, London, 1989.

168. Hu T.Y., *"Characterization of the crystallinity of ptfe by X-ray and IR spectroscopy, DSC, viscoelastic spectroscopy and the use of a density gradient tube",* **Wear,** Vol. 82, 1982, pp. 369-376.

169. Hoffman D.M. and McKinley B.M., *"Crystallinity as a Selection Criterion for Engineering Properties for High Density Polyethylene",* **Polymer Engineering and Science,** Vol. 25, No. 9, 1985, pp. 562-569.

170. Blandell D.J., Beckett D.R. and Willcocks P.H., *"Routine Crystallinity Measurements of Polymers by D.S.C.",* **Polymer,** Vol. 22, 1981, pp. 704-707.

171. Msuya W.F. and Yue C.Y., *"The correlation between lamellar thickness and the degree of crystallinity in semicrystalline polymers",* **J. Mater. Sci. Lett.,** Vol. 8, No. 11, 1989, pp. 1266-1268.

172. Sawa T., Takehisa M. and Machi S., **J. Appl. Polym. Sci.,** Vol. 17, 1973, p 3253.

173. Bellamy L.J., **The Infrared Spectra of Complex Molecules,** Vol. 2, Advances in infrared Group Frequencies, 2nd edn., London, Chapman and Hall, 1980.

174. Williams and Fleming, **Spectroscopic Methods in Organic Chemistry,** McGraw-Hill

175. Fordyce E.P., **The Unlubricated Sliding Wear Behaviour of Austempered Ductile Irons,** MSc Thesis, University of Cape Town, 1988.

176. Tanaka K. and Yamada Y., *Influence of counterface roughness on the friction and wear of polytetrafluoroethylene- and polyacetal-based composites"*, **Proc. IMechE**, Vol. 1, MEP, 1987, pp. 219-226.

177. Tanaka K., *"Effects of Various Fillers on the Friction and Wear of PTFE-Based Composites"*, in **Friction and Wear of Polymer Composites**, Friedrich K. (ed.), Composite Materials Series, Vol. 1, Amsterdam, Elsevier, 1986, pp. 137-174.

178. Gong D., Zhang B., Xue Q. and Wang H., *Investigation of Adhesion Wear of Filled Polytetrafluoroethylene by ESCA, AES and XRD"*, **Wear**, Vol. 137, 1990, pp. 25-39.

179. Blanchet T.A. and Kennedy F.E., *"Effects of Oscillatory Speed and Mutual Overlap on the Tribological Behaviour of PTFE and Selected PTFE-based Self-Lubricating Composites"*, **Trib. Trans.**, Vol. 34, No. 3, 1991, pp. 327-334.

180. Cooper J.R., Dowson D. and Fisher J., *"Birefringent Studies of Polyethylene Wear Specimens and Acetabular Cups"*, in **Proc. Conf. Wear of Materials**, Ludema K.C. and Bayer R.G. (eds.), ASME Trans., Vol. 1, Orlando, 1991, pp. 345-351.

181. Speck J.B., **The effect of counterface roughness and glass content on the wear of glass bead filled ultrahigh molecular weight polyethylene (UHMWPE) under dry sliding contact conditions**, Thesis Project, Dept. of Materials Engineering, Univ. of Cape Town, 1992.

182. Tetreault D.M. and Kennedy F.E., *"Friction and Wear Behaviour of Ultrahigh Molecular Weight Polyethylene on Co-Cr and Titanium Alloys in Dry and Lubricated Environments"*, **Wear**, Vol. 133, 1989, pp. 295-307.

183. Barret T.S., Stachowiak G.W. and Batchelor A.W., *Effect of roughness and sliding speed on the wear and friction of ultra-high molecular weight polyethylene"*, **Wear**, Vol. 153, 1992, pp. 331-350.

184. Komoto T., Tanaka K., Hironaka S., Matsumoto T. and Takano N., *"Morphological Study on Wear of Crystalline Polymers I. High Density Polyethylene"*, in **Proc. Conf. Wear of Materials**, Ludema K.C., Ruff A.W. and Rhee S.K. (eds.), ASME Trans., San Francisco, 1981, pp. 120-124.

185. Biswas S.K. and Vijayan K., *"Changes to near-surface region of PTFE during dry sliding against steel"*, **J. Mater. Sci.**, Vol. 23, 1988, pp. 1877-1885.

186. Biswas S.K. and Vijayan K., *Wear of polytetrafluoroethylene: some crystallographic observations"*, Wear, Vol. 150, 1991, pp. 267-273.

187. Biswas S.K. and Vijayan K., *"Friction and wear of PTFE - a review"*, **Wear**, Vol. 158, 1992, pp. 193-211.

188. Blanchet T.A. and Kennedy F.E., *"Sliding wear mechanism of polytetrafluoroethylene (PTFE) and PTFE composites"*, **Wear**, Vol. 153, 1992, pp. 229-243.

189. Tanaka K. and Kawakami, *"Effect of Various Fillers on the Friction and Wear of Polytetrafluoroethylene-Based Composites"*, **Wear**, Vol. 79, 1982, pp. 221-234.

190. Yamada Y. and Tanaka K., **Junkatsu**, Vol. 29, 1984, pp. 209 (in ref. 177).

APPENDIX A

A1:
Wear data for figures 5.8, 5.9,5.12. Testing conditions: reciprocating sliding, distilled water, 0.25 m/s, 10 MPa. Average of three tests.

sliding distance (km)	Polymer: 10/100				
	volume loss (mm^3)	min/max vol. loss	Ra (um Ra)	friction coeff.	
				stat.	kin.
0	0	0	0.294	0.087	0.057
1	0.52	0.41/0.64	0.254	0.083	0.056
2	0.76	0.49/1.01	0.245	0.082	0.055
5	1.45	1.01/1.69	0.25	0.081	0.053
10	3.57	1.69/6.68	0.244	0.077	0.047
20	6.68	2.32/12.10	0.239	0.075	0.044
30	7.21	2.54/12.64	0.231	0.074	0.044
40	8.34	2.95/13.26	0.208	0.072	0.044

sliding distance (km)	Polymer: Ceram P				
	volume loss (mm^3)	min/max vol. loss	Ra (um Ra)	friction coefficient	
				stat.	kin.
0	0	0	0.325	0.056	0.041
1	0.57	0.47/0.71	0.303	0.049	0.039
2	0.93	0.69/1.14	0.306	0.047	0.036
5	1.18	0.76/1.50	0.285	0.045	0.035
10	1.36	0.76/1.78	0.285	0.042	0.034
20	1.59	1.06/2.27	0.266	0.039	0.033
30	1.85	1.11/2.72	0.26	0.039	0.032
40	2.24	1.18/3.63	0.255	0.039	0.033

sliding distance (km)	Polymer: Solidur DS				
	volume loss (mm^3)	min/max vol. loss	Ra (um Ra)	friction coefficient	
				stat.	kin.
0	0	0	0.298	0.056	0.041
1	0.2	0.03/0.44	0.249	0.054	0.039
2	0.37	0.05/0.78	0.237	0.054	0.038
5	0.66	0.16/1.49	0.229	0.054	0.036
10	0.95	0.25/2.18	0.228	0.048	0.037
20	1.24	0.42/2.73	0.231	0.042	0.037
30	1.45	0.42/3.1	0.235	0.041	0.036
40	1.57	0.42/3.3	0.24	0.038	0.036

sliding distance (km)	Polymer: GUR 416		
	volume loss (mm^3)	min/max vol. loss	Ra (um Ra)
0	0	0	0.298
1	0.28	0.05/0.41	0.232
2	0.39	0.09/0.62	0.224
5	0.89	0.11/1.87	0.221
10	2.17	0.46/1.58	0.219
20	2.72	0.46/4.97	0.208
30	4.35	0.54/8.16	0.212
40	5.99	1.49//10.47	0.205

sliding distance (km)	Polymer: B 15		
	volume loss (mm^3)	min/max vol. loss	Ra (um Ra)
0	0	0	0.296
1	0.48	0.34/0.61	0.26
2	0.54	0.48/0.64	0.256
5	0.78	0.57/1.13	0.235
10	1.35	1.10/1.58	0.219
20	1.56	1.08/1.83	0.198
30	1.86	1.60/2.10	0.193
40	1.94	1.84/2.04	0.179

Wear data for figure 5.16. Testing conditions: reciprocating sliding, distilled water, 0.25 m/s, 10 MPa.

sliding distance (km)	polymer : Ceram P			polymer : Solidur DS		
	volume loss (mm^3)	friction coefficient		volume loss (mm^3)	friction coefficient	
		static	kinetic		static	kinetic
0	0	0.055	0.043	0	0.056	0.041
1	0.71	0.048	0.04	0.44	0.054	0.039
2	1.14	0.047	0.038	0.78	0.054	0.038
5	1.5	0.046	0.036	1.49	0.054	0.036
10	1.78	0.042	0.035	2.18	0.048	0.037
15	2.34	0.04	0.034			
20	2.27	0.038	0.034	2.73	0.042	0.037
25	2.54	0.037	0.033			
30	2.72	0.037	0.032	3.1	0.041	0.036
35	3.54	0.039	0.032			
40	3.63	0.038	0.032	3.3	0.038	0.033
45	4.31	0.044	0.035	3.37	0.037	0.033
50	12.21	0.05	0.037			
55	21.07	0.05	0.036			
60	29.22	0.051	0.033			
65	38.2	0.05	0.032			
70	47.72	0.05	0.032	3.58	0.039	0.032
75	56.57	0.048	0.032			
80	64.9	0.048	0.032			
85	73.63	0.048	0.031			
90	78	0.048	0.031			
95	87.32	0.048	0.031	3.76	0.039	0.032
100	96.48	0.048	0.031			
120				3.92	0.039	0.032

Wear data for figures 5.13, 5.25. Testing conditions: reciprocating sliding, distilled water, 0.25 m/s, 10 MPa.

sliding distance (km)	volume loss (mm^3) [Ra] effect of small changes in Ra, B15 10 MPa, d/w			Ra values perpendicular (AA) and parallel (BB) to the grinding marks. Sliding is parallel to the grinding direction.					
	0.356 um Ra	0.296 um Ra	0.251 um Ra	AA	min.	max.	BB	min.	max.
0	0 [0.356]	0 [0.296]	0 [0.251]	0.315	0.299	0.33	0.212	0.201	0.222
1	0.39 [0.331]	0.48 [0.26]	0.32 [0.235]	0.287	0.283	0.291	0.198	0.195	0.201
2	0.82 [0.327]	0.54 [0.256]	0.44 [0.226]	0.29	0.285	0.294	0.218	0.197	0.238
3	1.06 [0.317]		0.66 [0.223]						
5	1.52 [0.317]	0.78 [0.235]	0.82 [0.215]	0.291	0.285	0.296	0.222	0.202	0.242
10	1.89 [0.297]	1.35 [0.219]	0.99 [0.213]	0.294	0.289	0.298	0.209	0.203	0.215
20	2.68 [0.278]	1.56 [0.198]	1.17 [0.200]	0.305	0.305	0.307	0.256	0.247	0.264

Wear data for figures 5.22, 5.23. Testing conditions: reciprocating sliding parallel to the grinding direction, distilled water, 0.25 m/s, 10 MPa.

sliding distance	volume loss (mm^3)		Ra parallel to sliding		Ra perpendicular to sliding	
(km)	GUR 416	B 15	GUR 416	B 15	GUR 416	B 15
0	0	0	0.233	0.228	0.31	0.314
1	0.91	0.6	0.178	0.168	0.271	0.251
2	1.48	0.82	0.165	0.185	0.256	0.239
5	1.95	0.78	0.173	0.164	0.276	0.244
10	2.6	0.9	0.171	0.156	0.259	0.248
15	2.98	2.12	0.182		0.276	
20	3.3	3.57	0.193	0.213	0.274	0.252
25	3.68	7.87				
30	4.27	9.81	0.209		0.273	
35	4.62	11.67		0.16		0.245
40	5.13	13.14	0.203		0.27	
45	5.92	15.8		0.212		0.259
50	7.89	21.89	0.186		0.277	0.25
55	9.89	26.15				
60	10.65	31.95	0.226	0.275	0.272	0.235

sliding distance	GUR 416 friction coefficient	
(km)	kinetic	static
0	0.046	0.059
0.6	0.045	0.051
1.44	0.04	0.049
5.2	0.039	0.049
6.2	0.039	0.048
9.4	0.04	0.049
15.5	0.04	0.049
19.9	0.044	0.049
40	0.046	0.056
54.5	0.05	0.057

Wear data for figures 5.27, 5.29, 5.68, 4.9. Testing conditions: reciprocating sliding, distilled water (d/w) and dry, 0.25 m/s, 5 and 10 MPa, average of two and three tests.

sliding distance	volume loss (mm^3) [kinetic friction]								
	10 MPa, 0.03 um Ra, d/w				5 MPa, dry		reproducibility tests, B15		
(km)	Special DS test 1	Special DS test 2	B 15	g/bead UHMWPE	10/100	Special DS	10 MPa, d/w, (um Ra) (0.284)	(0.317)	(0.287)
0	0 [0.028]	0 [0.031]	0	0 [0.03]	0 [0.08]	0 [0.071]	0	0	0
1	0.38 [0.029]	0.23 [0.031]	0.05	0.94 [0.029]	0.25 [0.077]	0.3 [0.075]	0.48	0.61	0.34
2	0.34 [0.029]	0.81 [0.033]	0.1	0.94 [0.029]	1.11 [0.081]	0.32 [0.077]	0.53	0.65	0.48
5	0.97 [0.03]	2.57 [0.034]	0.4	1.01 [0.029]	2.43 [0.077]	1.17 [0.079]	1.13	0.57	0.65
10	1.07 [0.03]	5.55 [0.034]	1.15	1.64 [0.029]	5.75 [0.083]	2.11 [0.077]	1.38	1.1	1.58
15	1.64 [0.032]	7.86 [0.035]	2.2	3.7 [0.029]	10.5 [0.079]	4.13 [0.08]			
20	2.73 [0.033]	9.05 [0.035]	3.14	5.76 [0.029]	14.6 [0.081]	5.98 [0.079]	1.76	1.08	1.83
25					20.15 [0.081]	8.89 [0.081]			
30							1.8	1.6	2.11
40							1.84	1.91	2.04

Wear data for figure 5.31. Testing conditions: reciprocating sliding, distilled water, 0.25 m/s, 5 MPa, polymer on polymer, average of two tests.

sliding distance	counterface		pin	
(km)	Special DS	B 15	Special DS	B 15
0	0	0	0	0
0.1	13.19	1.88	3.38	2.89
0.3	34	6.97	10	6.69
0.5	52.27	12.42	17.06	11.8
0.8	77.23	27.83	26.74	18.38
1.1	98.58	51.05	31.33	23.83

Wear data for figures 5.73, 5.74. Testing conditions: reciprocating sliding, distilled water (d/w) and dry, 0.25 m/s, 5 MPa, average of two tests.

sliding distance (km)	testing condition	volume loss (mm^3)		kinetic friction		Temperature	testing condition	volume loss (mm^3)	
		10/100	Special DS	10/100	Special DS			10/100	Special DS
0		0	0	0.08	0.071	20		0	0
0.2						43			
0.4						46.3			
0.6						53			
0.8						55			
1	dry	0.25	0.3	0.075	0.075	56	wet	0.11	0.26
2		1.11	0.32	0.081	0.077	57.9		0.12	0.28
5		2.43	1.17	0.077	0.079	58.7		0.9	0.51
10		5.75	2.11	0.083	0.077	58		1.16	0.48
15		10.5	4.13	0.079	0.08	60		1.79	0.47
20		14.6	5.98	0.081	0.079	60		2.31	1.04
25		20.15	8.89	0.081	0.081	59.8		2.13	1.3
25.1				0.081	0.081	20.8			
30		21.35	9.15	0.058	0.062	20		2.5	1.95
35	wet	21.86	9.19	0.059	0.057	22		2.78	2.1
40		21.96	9.38	0.058	0.057	22		3.19	2.14
40.2						43			
40.4	dry					46			
40.6						53			
45		23.98	14.77	0.08	0.075	57			

Wear data for figures 5.79, 5.82 for PTFE. Testing conditions: reciprocating sliding, distilled water (d/w) and dry, 0.25 m/s, 5 MPa and 10 MPa, average of two tests.

sliding distance (km)	volume loss (mm^3) [kinetic friction]								
	5 MPa, d/w			10 MPa, d/w			5 MPa, dry		
	unfilled	bronze	g/fibre	unfilled	bronze	g/fibre	unfilled	bronze	g/fibre
0	0 [0.069]	0 [0.087]	0 [0.085]	0 [0.032]	0 [0.042]	0 [0.053]	0 [0.071]	0 [0.073]	0 [0.067]
0.2	27.79 [0.069]	2.03 [0.08]	9.7 [0.102]	81.35 [0.031]	1.82 [0.048]	11.27 [0.047]	66.1 [0.068]	0.65 [0.081]	0.66 [0.063]
0.5	65.24 [0.065]	4.49 [0.073]	21.25 [0.091]	165.45 [0.030]	4.1 [0.044]	39.25 [0.044]	156.1 [0.067]	1.03 [0.081]	0.82 [0.070]
1	126.12 [0.064]	7.34 [0.071]	48.57 [0.081]	279.05 [0.030]	7.38 [0.044]	91.87 [0.042]	283.9 [0.068]	1.73 [0.081]	1.08 [0.075]
1.5	183.03 [0.062]	9.86 [0.071]	82.32 [0.074]	397.95 [0.030]	10.42 [0.043]	140.67 [0.042]	421.7 [0.068]		
2	231.98 [0.063]	12.15 [0.070]	112.58 [0.074]	519.72 [0.030]	13.3 [0.043]	188.15 [0.042]	558.4 [0.065]	2.51 [0.077]	1.34 [0.075]
2.5	279.5 [0.063]	14.51 [0.070]	143.24 [0.073]						
3	320.84 [0.063]	16.72 [0.071]	172.04 [0.073]					3.05 [0.073]	1.82 [0.075]
5								3.88 [0.073]	2.59 [0.075]

Material	Specific heat (J/kg.K)	Thermal conductivity (W/m.K)	Flexural modulus (MPa)	Cohesive energy density x 10^8 (N/m^2)	hardness (kgf/mm^2)	Compressive strength (MPa)	Melting point (°C)	Max. service temperature	Specific gravity (g/cm^2)	water absorbtion (%)
UHMWPE	1883	0.42	680-890	2.68	4.9 0.7	20-25	137	-140-85	0.93-0.94	<0.1
HDPE	1855	0.33	850	2.68		19-25	120-140	-140-80	0.94-0.97	
PTFE	938	0.25	700	1.6	3.6	12	320-340	-200-260	2.16-2.2	<0.05
LDPE	2315	0.33					110-130			
Nylon6	1599	0.24					225			9
Aluminium	900	237								
Iron	444	80								
S/Steel	500	90			200			750	7.8	
E/Glass		1.04			550-750		730		2.5	

APPENDIX B

B1:

TEM technique by Prof. Tadashi Komoto for obtaining a diffraction pattern from polyethylene films. Dept. Materials Engineering, Gunma University, 1-5-1 Tenjin-cho, Kiryu, Gunma 376, Japan, Tel. 0277-22-3181, Fax. 0277-44-4599.

i) use 75 - 120 kV. Minimize the beam intensity by decreasing the filament current and by diffusing the beam to the lowest brightness.

ii) make a focus at ca. 10000, take the objective lens aperture out of the beam path, put selected area aperture into the path, make a selected area diffraction by changing the intermediate lens current, where the direct beam changes from a beam spot to a diffused circle.

iii) depending on the beam current, the life time of the electron diffraction spots from polyethylene is ca. 10 - 30 seconds at room temperature.

B2:

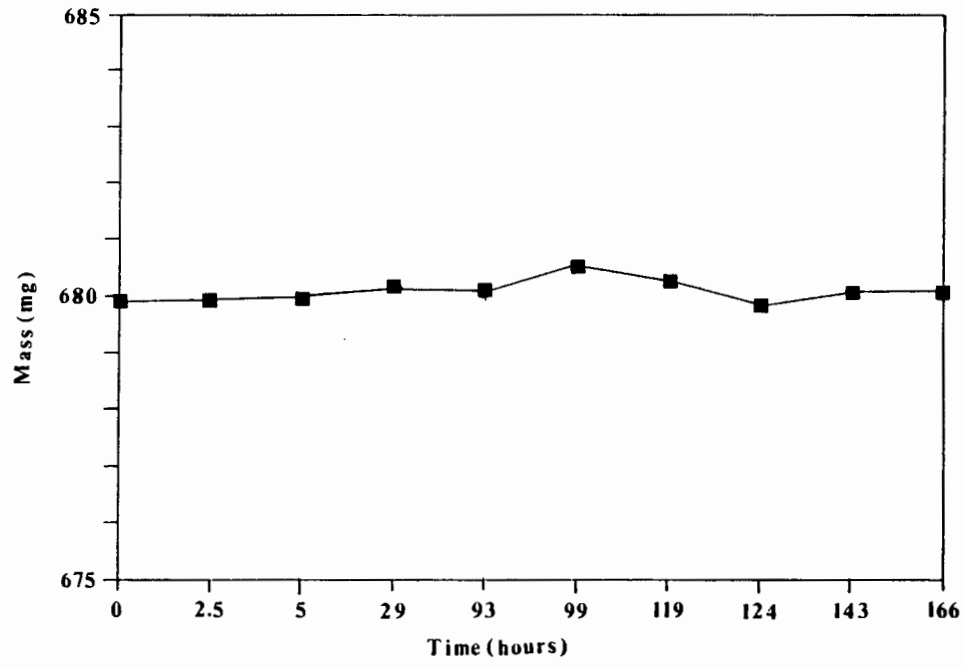

Figure B1: Weight gain of UHMWPE in water as a function of time. The weight gain of the UHMWPE was less than 0.02% at the end of 166 hrs.

APPENDIX C

C1:

Polymer	Trade name	Repeat unit	Maximum useful temp.	Tribological applications	environment	
					abrasive	water
unfilled ultrahigh molecular weight polyethylene (UHMWPE)	10/100		80℃	wear strips chute liners	✓	✓
filled UHMWPE	Special DS			bearings, seals	✓	✓
unfilled poly-tetrafluoroethylene (PTFE)	Teflon		275℃	seals, gaskets	✗	✗
PTFE - Glass				bearing cages	✗	✗
PTFE - Bronze				piston rings	✗	✗
Polyoxymethylene (POM)	Delrin 500		125℃	seals, bushings	✗	✓
Polyethylene-terepthalate (PETP)	Ertalyte		200℃	bearings	✗	✗
Polyamide 6 + MoS2 (PA6/MoS2)	Nyaltron GSM		130-150℃	gears, cams	✓	✗
Polyamide-imide + 12% graphite + 3% PTFE P(A-I)/Gr	Torlon 4301		220-240℃	gears	✗	✗

Figure C1: Structure and uses of various polymers commonly used in the South African mining industry.

Polymer	Trade name	Density (g/cm^3)	Molecular weight ($g/mol \times 10^6$)	UTS (N/mm^2)	Elastic modulus (N/mm^2)	Shore "D" hardness	Melting point (°C)	Thermal conductivity (W/m.K)	Izod impact toughness (J/m)	Elong-ation %
UHMWPE	10/100	0.94	4.5	44	232	66	137	↑ 0.42 ↓	↑ No break ↓	450
	Special DS	0.96	6	43		67	139			450
	B 15	0.93	7.3	40		61	136			> 350
	GUR 416	0.93	8.0	40		61	136			> 350
POM	Delrin 500	1.42	—	78	927	81	175	0.37	55	38
PETP	Ertalyte	1.38	—	78	1049	86	255	0.29	29	34
P(A-I)/GR	Torlon 4301	1.45	—	83	2230	91	260	0.54	32	5
PA6/MoS_2	Nyaltron GSM	1.16	—	58	743	75	220	0.36	—	69

Figure C2: Mechanical and physical properties of polymers in fig. C1.

PUBLICATIONS

1) Marcus K., Ball A. and Allen C., *"On the Nature of Transfer Films Formed During the Sliding Wear of UHMWPE Against Steel"*, in **Proc. Conf. Electron Microscopy Soc. of Southern Africa**, Vol. 20, 1990, pp. 21-22.

2) Marcus K., Ball A. and Allen C., *"The effect of grinding direction on the nature of the transfer film formed during the sliding wear of ultrahigh molecular weight polyethylene against stainless steel"*, **Wear**, Vol. 151, 1991, pp. 323-336.

3) Marcus K., Ball A. and Allen C., *"Birefringent Studies of the Wear Mechanism During the Sliding Wear of UHMWPE Against Steel"*, in **Proc. Conf. Electron Microscopy Soc. of Southern Africa**, Vol. 21, 1991, pp. 289-290.

4) Marcus K., Ball A. and Allen C., *"On the nature of the transfer film at the interface of a water-lubricated sliding polymer-metal couple"*, **J. Phys. D: Appl. Phys.**, "Frontiers of Tribology", Vol. 25, 1992, pp. 57-64.

5) Marcus K. and Allen C., *"The Effect of Fillers on the Friction and Wear Behaviour of UHMWPE- and PTFE Composites During Sliding Wear"*, in **Proc. Joint Soviet / American Conf. on Tribology**, "New Materials and Technologies in Tribology", Minsk, 1992. (in press)

6) Marcus K. and Allen C., *"Engineering Polymers for Sliding Wear Applications in the South African Mining Industry"*, in **Tribology '92**, Int. Symp. on Tribology in Mining, SAIT, Pretoria, Sept. 1992.

7) Marcus K. and Allen C., *"The effect of fillers on the friction and wear behaviour of UHMWPE during water-lubricated reciprocating sliding wear"*, in **Proc. Conf. Wear of Materials**, Ludema K.C. (ed.), ASME Trans., San Francisco, 1993. (in press).